SANDIA REPORT

SAND84-8189 • Unlimited Release

Printed January 1985

Small Central Receiver Brayton Cycle Study Final Technical Report December 1, 1982 — June 30, 1983

Boeing Aerospace Company Energy Systems

When printing a copy of any digitized SAND Report, you are required to update the markings to current standards.

Prepared by
Sandia National Laboratories
Albuquerque, New Mexico 87185 and Livermore, California 94550
for the United States Department of Energy
under Contract DE-AC04-76DP00789

SF 2900-Q(6-82)

Issued by Sandia National Laboratories, operated for the United States Department of Energy by Sandia Corporation.
NOTICE: This report was prepared as an account of work sponsored by an agency of the United States Government. Neither the United States Government nor any agency thereof, nor any of their employees, nor any of the contractors, subcontractors, or their employees, makes any warranty, express or implied, or assumes any legal liability or responsibility for the accuracy, completeness, or usefulness of any information, apparatus, product, or process disclosed, or represents that its use would not infringe privately owned rights. Reference herein to any specific commercial product, process, or service by trade name, trademark, manufacturer, or otherwise, does not necessarily constitute or imply its endorsement, recommendation, or favoring by the United States Government, any agency thereof or any of their contractors or subconractors. The views and opinions expressed herein do not necessarily state or reflect those of the United States Government, any agency thereof or any of their contractors or subcontractors.

Printed in the United States of America
Available from
National Technical Information Service
5285 Port Royal Road
Springfield, VA 22161

NTIS price codes
Printed copy: **A15**
Microfiche copy: A01

SAND 84-8189
Unlimited Distribution
Printed January 1985

SMALL CENTRAL RECEIVER BRAYTON CYCLE STUDY
FINAL TECHNICAL REPORT
DECEMBER 1, 1982 - JUNE 30, 1983

Prepared by
Boeing Aerospace Company
Energy Systems

Prepared for
Sandia National Laboratories
Livermore, California
Contract No. 81-7415

ABSTRACT

The Small Central Receiver Brayton Cycle Study was initiated to investigate the potential of small scale, central receiver Brayton cycle systems to provide simple, highly reliable, low-maintenance electrical generating systems. The study objectives were to identify Brayton cycle configurations suited for high-reliability central receiver systems generating electricity in the 2- and 25-MW_e power ranges and to identify and recommend high-temperature receiver designs most appropriate to the preferred cycle configurations.

The Brayton cycle configurations task involved a definition of a baseline system configuration and system-level requirements, selection of cycle alternatives, survey of available turbomachinery, analysis of cost and performance sensitivities, and selection of preferred cycle configurations. The cycle configurations considered were open and closed cycles with and without regeneration and/or intercooling. The configurations were assessed in terms of required machine design modifications, component availability turbomachinery location, costs and performance. Design point performance was studied as a function of system pressure, turbine inlet temperature and receiver pressure loss. An open cycle regenerated and intercooled configuration was selected for the 25-MW_e plant size because of its high cycle efficiency, reduced heliostat field costs, reduced capital and energy costs, and turbomachinery availability. At the 2-MW_e size, an open simple cycle was chosen because of its low capital and energy costs, reduced complexity, and turbomachinery availability.

The high temperature receiver study involved the identification of heat exchange concepts, survey of high-temperature materials, and selection of preferred concepts. Thirteen high-temperature (1093°C = 2000°F) receiver concepts were identified as potentially aplicable to the air-heating requirements. An initial screening process was used to reduce the number of concepts. Thermal and mechanical design analyses were completed on the receiver concepts. After consideration of the thermal analysis results, the design analysis considerations, and a high-temperature materials assessment, a preferred receiver concept was developed for each plant size.

The ceramic tube receiver concept was selected as the preferred concept for the 25-MW_e plant size. This concept has reasonable performance and cost through the use of a simple, straight forward design. The small particle receiver concept was selected for the 2-MW_e plant size. This concept has superior performance and cost and reasonable reliability, maintainability and operability.

The preferred receiver designs were combined with the preferred cycle data to produce system level designs. System performance and cost data were generated for each plant size. The results of this study show that small-scale, remotely-sited solar Brayton central receiver systems are technically feasible and economically attractive through the use of simple, passive receiver designs and low-maintenance, high-reliability gas turbomachinery. Relatively straight forward development will be required to implement these solar central receiver designs.

TABLE OF CONTENTS

	Page No.
Abstract	i
Table of Contents	iii
List of Figures	vi
List of Tables	xi
Acknowledgements	xiv
1.0 INTRODUCTION AND SUMMARY	1-1
1.1 Study Objectives	1-2
1.2 Study Ground Rules	1-2
1.3 Program Work Flow	1-4
1.4 Summary of Results	1-4
1.4.1 System Level Requirements	1-4
1.4.2 Baseline System Definition	1-4
1.4.3 Brayton Cycle Configuration Study	1-6
1.4.4 High-Temperature Receiver Study	1-10
2.0 BRAYTON CYCLE CONFIGURATION STUDY	2-1
2.1 System Requirements Definition	2-1
2.2 Baseline System Definition	2-4
2.3 Configuration Alternative Definition	2-4
2.4 Cycle Performance Analyses	2-8
2.4.1 Cycle Performance Model	2-9
2.4.2 Performance Analysis Results	2-12
2.5 Turbomachinery Survey	2-27
2.5.1 Turbomachinery Performance Data	2-32
2.5.2 Turbomachinery Cost Data	2-35
2.5.3 External Firing Assessment	2-37
2.5.4 Maintenance and Durability	2-39
2.5.5 Solar Applications Modifications	2-39
2.5.6 Turbomachinery Control	2-42

Page No.

2.6 Cycle Configuration Cost Analysis 2-43
2.6.1 Component Unit Cost Assumptions 2-44
2.6.2 Component Capital Cost Results 2-44
2.6.3 System Capital Cost Comparison 2-52
2.6.4 Off-Design Performance Assessment 2-59
2.6.5 Busbar Energy Cost Comparison 2-63
2.6.6 Turbine Location Trade Results 2-63
2.7 Preferred Cycle Configuration Selection 2-66
2.8 Alternative Closed Cycle Working Fluids Assessment 2-69

3.0 HIGH-TEMPERATURE RECEIVER STUDY 3-1
3.1 High-Temperature Heat Exchange Concept Identification 3-1
3.1.1 Receiver Design Requirements 3-1
3.1.2 Classification of Receiver Concepts 3-3
3.2 Receiver Concept Initial Screening 3-20
3.2.1 Preliminary Screening 3-20
3.2.2 Cavity Thermal Analysis 3-25
3.2.3 Design Analysis 3-34
3.3 High-Temperature Materials Candidate Selection 3-60
3.3.1 Materials Survey and Initial Screening 3-62
3.3.2 Fabrication and Design Considerations 3-74
3.4 Preferred Receiver Concept Selection 3-91
3.4.1 25-MW_e Plant Receiver 3-91
3.4.2 2-MW_e Plant Receiver 3-94
3.5 Preferred Receiver Concept Definition 3-95
3.5.1 Materials Assessment 3-96
3.5.2 Concept Design Definition 3-96
3.5.3 Receiver Concept Performance 3-110
3.5.4 Receiver Concept Cost Estimate 3-116

Page No.

4.0 SYSTEM DESCRIPTION 4-1

4.1 System Design Description 4-1

4.1.1 25-MWe Plant 4-1

4.1.2 2-MW_e Plant 4-6

4.2 System Performance 4-6

4.3 System Cost Estimates 4-6

4.3.1 Direct Capital Cost Estimates 4-6

4.3.2 Busbar Energy Costs 4-6

5.0 DEVELOPMENT PLANS 5-1

5.1 Technology Assessment 5-1

5.1.1 Turbomachinery Technology Assessment 5-1

5.1.2 Piping Technology Assessment 5-6

5.1.3 Receiver Technology Assessment 5-6

5.2 Critical Technology Issues 5-8

5.3 Plan to Reduce Technical Risk 5-9

5.3.1 System Level Studies 5-9

5.3.2 Critical Technology Areas 5-10

6.0 REFERENCES 6-1

APPENDICES

Appendix A: Turbomachinery Survey Cost Data Base A-1

Appendix B: Receiver, Recuperator, Intercooler, and Precooler and Thermal Scale Modeling Methods B-1

Appendix C: Preliminary Structural Analysis of the 25-MW_e Ceramic Tube Receiver C-1

Appendix D: Detailed Receiver Subsystem Cost Data D-1

LIST OF FIGURES

Figure No.	Title	Page No.
1-1	Work Flow Plan	1-5
1-2	Cycle Efficiency Versus Pressure Ratio	1-7
1-3	Cycle Efficiency Versus Pressure Ratio	1-8
1-4	Relative Capital and Busbar Cost Results	1-9
1-5	System Design Requirements - 2-MW_e Plant	1-11
1-6	System Design Requirements - 25-MW_e Plant	1-12
1-7	Plan and Elevation Views of 25-MW_e Ceramic Tube Receiver	1-17
1-8	Heat Exchanger Tube Assembly	1-18
1-9	2-MW_e Small Particle Receiver	1-20
1-10	3.0-m Diameter Fused Quartz Window Design	1-21
1-11	3.0-m Diameter Window/Shell Interface Design	1-22
1-12	25-MW_e Plant Tower Arrangement	1-24
1-13	Design Point 2-MW_e System Performance	1-28
1-14	Design Point 25-MW_e System Performance	1-28
1-15	Program Development Plan	1-32
1-16	Preliminary Design Process	1-33
2-1	Brayton Cycle Configuration Study	2-2
2-2	Baseline System Performance - 2-MW_e Plant	2-6
2-3	Baseline System Performance - 25-MW_e Plant	2-7
2-4	Cycle Configuration Alternatives	2-8
2-5	Cycle Model Configuration Diagram	2-11
2-6	Component Polytropic Efficiencies Versus Pressure Ratio	2-13
2-7	Cycle Efficiency Versus Pressure Ratio - 25-MW_e, Open Simple Configuration	2-14
2-8	Cycle Efficiency Versus Pressure Ratio - 25-MW_e, Open Regenerated Configuration	2-15
2-9	Cycle Efficiency Versus Pressure Ratio - 25-MW_e, Closed Regenerated and Intercooled Configuration	2-16

LIST OF FIGURES

Figure No.	Title	Page No.
2-10	Cycle Efficiency Versus Pressure Ratio - 25-MW_e, Open Regenerated and Intercooled Configuration	2-17
2-11	Cycle Efficiency Versus Pressure Ratio - 25-MW_e Cycle Configurations Comparison	2-19
2-12	Cycle Efficiency Versus Pressure Ratio - 2-MW_e Cycle Configurations Comparison	2-20
2-13	Energy Flow for an Intercooled and Regenerated Cycle	2-22
2-14	Energy Flow for a Simple Cycle	2-23
2-15	Off-Design Performance Effects	2-28
2-16	Comparison of Off-Design Performance Predictions with Five Real Engines	2-29
2-17	Pressure Ratio Versus Output Power	2-33
2-18	Turbine Inlet Temperature Versus Output Power	2-33
2-19	Cycle Efficiency Versus Output Power	2-34
2-20	Gas Turbine Electricity Generator Bids for One Job	2-37
2-21	Relative Variation of Field Costs with Cycle and Receiver Efficiency	2-46
2-22	Downcomer Cost Data (11)	2-54
2-23	Direct Capital Cost Comparison - 25-MW_e	2-58
2-24	Direct Capital Cost Comparison - 2-MW_e	2-60
2-25	Off-Design Daily Electric Generation Comparison	2-62
2-26	Relative Capital and Busbar Cost Results	2-64
2-27	2-MW_e Preferred Cycle Configuration Flow Schematic	2-67
2-28	25-MW_e Preferred Cycle Configuration Flow Schematic	2-68
3-1	High-Temperature Receiver Study	3-2
3-2	Atmospheric Pressure Receiver Flow Schematic - Option 1	3-6
3-3	Atmospheric Pressure Receiver Flow Schematic - Option 2	3-7
3-4	Atmospheric Pressure Receiver Flow Schematic - Option 3	3-7

LIST OF FIGURES

Figure No.	Title	Page No.
3-5	Ceramic Matrix Receiver Concept	3-8
3-6	Volumetric Receiver	3-8
3-7	Pressurized Receiver Flow Schematic	3-10
3-8	Ceramic Tube Receiver Concepts	3-11
3-9	Ceramic Dome Receiver Concepts	3-12
3-10	Transparent Tube Receiver Concepts	3-13
3-11	Small Particle Receiver Concept	3-14
3-12	Intermediate Fluid Heat Exchange Flow Schematic	3-15
3-13	Falling Particle Receiver Concepts	3-16
3-14	Phase Change Falling Particle Receiver Concept	3-17
3-15	High-Temperature Molten Salt Concept	3-17
3-16	Liquid Metal Heat Pipe Receiver Concept	3-18
3-17	Boiling Metal Receiver Concept	3-19
3-18	Liquid Metal Bath Receiver Concept	3-19
3-19	Generalized 25-MW_e Receiver Cavity Configuration	3-26
3-20	First Incident Solar Flux Map	3-28
3-21	Adjustment of Cavity Size for Peak Flux	3-29
3-22	Radiative Interchange Model	3-30
3-23	Receiver Temperature Distribution	3-32
3-24	Ceramic Tube Receiver Temperature Distribution	3-33
3-25	Plan and Section Views of Falling Particle Receiver Concept	3-37
3-26	Falling Particle Receiver Flow Diagram	3-38
3-27	High-Temperature Molten Salt Receiver Flow Diagram	3-43
3-28	Plan and Elevation Views of Molten Salt Receiver Concept	3-44
3-29	Molten Salt Receiver Collector and Downcomer Piping Concept	3-45
3-30	Molten Salt Heat Exchange Concept	3-46
3-31	Molten Salt Second Stage Centrifugal Pump and Distributor Concept	3-48

LIST OF FIGURES

Figure No.	Title	Page No.
3-32	Plan and Elevation Views of Transparent Tube Receiver Concept	3-52
3-33	Transparent Tube Receiver Alternative Flow Concepts	3-53
3-34	Plan and Elevation Views of Ceramic Tube Receiver Concept	3-54
3-35	Ceramic Tube Heat Exchanger	3-55
3-36	Small Particle Receiver Concept	3-56
3-37	3.0-m Diameter Fused Quartz Window Design	3-58
3-38	3.0-m Diameter Window/Shell Interface Design	3-59
3-39	Multiple Facet Windowed Aperture Concept	3-61
3-40	Cavity Insulation Material Design	3-70
3-41	Effect of Component Size and Complexity on Fracture Strength and Variability (64)	3-75
3-42	Elevation View of 25-MW_e Receiver, Turbine Room and Tower	3-97
3-43	25-MW_e Ceramic Tube Receiver	3-98
3-44	Receiver Interior Insulation Concept	3-99
3-45	Heat Exchanger Tube Assembly	3-100
3-46	Heat Exchanger Tube-to-Manifold Assembly	3-101
3-47	Manifold Design	3-103
3-48	Receiver Structural Design	3-104
3-49	Aperture Structural Design	3-105
3-50	Turbine Room Structural Design	3-106
3-51	Steel Tower and Concrete Base Design	3-107
3-52	2-MW_e Plant Tower Arrangement	3-111
3-53	2-MW_e Small Particle Receiver	3-112
3-54	3.0-m Diameter Fused Quartz Window Design	3-113
3-55	Window-to-Shell Interface Design	3-114
4-1	25-MW_e Plant Tower Arrangement	4-4
4-2	Control Room Design	4-5
4-3	Design Point 25-MW_e Plant System Performance	4-8

LIST OF FIGURES

Figure No.	Title	Page No.
4-4	Annual Average 25-MW_e Plant System Performance	4-8
4-5	Design Point 2-MW_e Plant System Performance	4-9
4-6	Annual Average 2-MW_e Plant System Performance	4-9
5-1	Thomassen TF-10 Gas Turbine	5-3
5-2	Comparison Between Recuperator Types	5-5
5-3	Preliminary Design Process	5-11
5-4	Program Development Plan	5-13

LIST OF TABLES

Table No.	Title	Page No.
1-1	Small Central Receiver Brayton Cycle Study Ground Rules	1-3
1-2	Receiver Concept Candidates	1-13
1-3	25-MW_e Receiver Energy Balance	1-15
1-4	2-MW_e Receiver Energy Balance	1-16
1-5	Receiver Concept Performance	1-23
1-6	Receiver Cost Estimates	1-23
1-7	25-MW_e System Definition	1-25
1-8	2-MW_e System Definition	1-27
1-9	System Direct Capital Cost Estimates (1983 $)	1-29
1-10	Busbar Energy Costs (1983$)	1-30
1-11	Economic Factors Used in Study	1-30
2-1	System Requirements and Analysis Assumptions	2-3
2-2	Baseline System Definition	2-5
2-3	Comparison of GSA Results to UTRC Report (15)	2-10
2-4	Sensitivity of Cycle Efficiency at Design Point to Component Efficiency Changes	2-25
2-5	Turbomachinery Survey Telephone Contacts	2-30
2-6	Work Scopes and Bid Price Range for 29 Installations of Gas Turbine Electricity Generation Systems	2-36
2-7	Component Unit Cost Data (1983 $)	2-45
2-8	Heliostat Field Capital Cost Results	2-47
2-9	Receiver Capital Cost Results	2-48
2-10	Receiver Efficiency Results	2-49
2-11	Heat Exchanger Cost Results	2-51
2-12	Piping Sizing Results	2-53
2-13	Piping Cost Results	2-55
2-14	System Capital Cost Summary - 25-MW_e	2-56
2-15	System Capital Cost Summary - 2-MW_e	2-57
2-16	Annual Power Production Data	2-61
2-17	Turbine Location Trade Results	2-65
3-1	Receiver Design Requirements	3-3
3-2	Receiver Concept Candidates	3-4

LIST OF TABLES

Table No.	Title	Page No.
3-3	Summary of Receiver Performance Data (9, 11)	3-22
3-4	Receiver Concepts Comparison	3-23
3-5	Selected Receiver Concepts for Further Evaluation	3-24
3-6	Assumed Receiver Radiative Properties	3-30
3-7	25-MW_e Receiver Energy Balance	3-35
3-8	2-MW_e Receiver Energy Balance	3-36
3-9	Falling Particle Receiver Design Data	3-40
3-10	Molten Salt Receiver Design Data	3-49
3-11	Window Mass Versus Spherical Arc Angle	3-57
3-12	Heat Exchanger Materials - Preliminary Design Requirements	3-63
3-13	Design-Critical Properties of Selected Heat Exchanger Materials	3-65
3-14	Normalized Properties of Selected Heat Exchanger Materials	3-67
3-15	Weighted Properties of Selected Heat Exchanger Materials	3-68
3-16	Selected Window and Transparent Tube Materials	3-72
3-17	Structural Grade Ceramics - Methods of Manufacture	3-78
3-18	Structural Grade Ceramics - Approximate Shape Limitations	3-79
3-19	Structural Grade Ceramics - Approximate Size Limitations	3-80
3-20	Structural Grade Ceramics - Subjective Assessment of Relative Fabrication Technology Maturity (Large Shapes Only)	3-81
3-21	Relative Levels of Materials Characterization	3-83
3-22	Approximate Relative Costs of Materials	3-84
3-23	Window and Transparent Tube Materials Fabrication Methods	3-86
3-24	Window and Transparent Tube Materials Approximate Shapes Available	3-87

LIST OF TABLES

Table No.	Title	Page No.
3-25	Window and Transparent Tube Materials Approximate Sizes Available	3-88
3-26	Window and Transparent Tube Materials Approximate Cost Information	3-89
3-27	Window and Transparent Tube Materials Subjective Assessment of Relative Fabrication Maturity (Large Shapes Only)	3-90
3-28	25-MW_e Steel Tower Design Summary	3-108
3-29	25-MW_e Receiver Design Summary	3-109
3-30	2-MW_e Receiver Design Summary	3-115
3-31	Receiver Concept Performance	3-116
3-32	25-MW_e Receiver Cost Estimate	3-117
3-33	2-MW_e Receiver Cost Estimate	3-117
3-34	Piping and Tower Cost Estimate	3-118
4-1	25-MW_e System Definition	4-2
4-2	2-MW_e System Definition	4-7
4-3	System Direct Capital Cost Estimates (1983 $)	4-10
4-4	Busbar Energy Costs (1983 $)	4-11
4-5	Alternative Economic Factors - Electric Utility Application (12)	4-12
5-1	Thomassen TF-10 Performance Data (17)	5-4

ACKNOWLEDGEMENTS

The constructive program guidance afforded by the personnel of Sandia National Laboratories - Livermore is gratefully acknowledged, especially Mr. Pascal DeLaquil III, Project Manager.

Sincere appreciation is expressed to the following Boeing personnel for their assistance on the Small Central Receiver Brayton Cycle Study:

Mr. Donald Bartlett	Program Manager
Mr. John Gintz	Solar Systems, Director
Mr. Robert Campbell	Executive Director, Energy Development
Mr. Russ Ashleman	Cycle Analysis
Mr. William Beverly	Technical Lead and Systems Analysis
Mr. Larry Brown	Turbomachinery Survey
Mr. Keith Halvorsen	Receiver Concept Identification and Assessment
Mr. Kenneth Hernley	Receiver Design Analysis
Ms. Gail Matson	Cycle Analysis
Mr. Antonio Rufin	Materials Survey and Assessment
Mr. Juris Verzemnieks	Materials Survey and Assessment
Mr. Art Able	Contracts
Mr. Bill Stewart	Finance
Ms. Sue Booth	Secretarial Assistance
Ms. Lorna Hale	Secretarial Assistance
Ms. Debbi Overlin	Secretarial Assistance
Mr. John Allen	Graphics Support

SMALL CENTRAL RECEIVER BRAYTON CYCLE STUDY

1.0 INTRODUCTION AND SUMMARY

Over a period of several years, the Solar Energy Systems group of the Boeing Engineering and Construction (BEC) Company has considered the design of gas-cooled solar cavity central receivers operating in open or closed Brayton power generation cycles (1-8). Each of these studies has been directed toward near-term, i.e., mid-1980's, technology. These solar Brayton design concepts were uncomplicated utilizing a minimum of system components. These simple designs provided the potential for high reliability and low maintenance power generating systems. The negligible water requirements of a solar Brayton system would allow siting central receivers in arid, high-insolation environments.

Several air-heating receiver concepts have been suggested by a number of different researchers (9). BEC studies determined that the metal gas-in-tube receiver concept was the only viable near-term (mid-1980's) air-heating receiver concept. Other concepts had unique and attractive design features, but would require additional design development not consistent with the mid-1980's projected application. Materials limitations constrained the metal gas-in-tube receiver to outlet gas temperatures in the 816-871°C (1500-1600°F) range. Conservative receiver design for first-of-a-kind items dictated that the metal, gas-cooled heat exchanger panels would be irradiated indirectly with re-reflected solar and re-emitted thermal fluxes. Large cavity receivers with the attendant increased thermal reradiation losses resulted. Using current-production gas turbomachinery derated to the 816-871°C (1500-1600°F) levels resulted in a reduced cycle efficiency. The reduced cycle efficiency and increased thermal losses resulted in metal, gas-in-tube central receiver systems that were less attractive from a levelized energy cost basis than other central receiver system approaches except possibly for small power plant sizes (10).

The Small Central Receiver Brayton Cycle Study was initiated as a scoping study to investigate the potential of small-scale, central receiver Brayton cycle systems to provide simple, highly reliable, low-maintenance electrical

generating systems. A mature commercial solar industry was assumed as would be available in the mid to late 1990's. Advances in manufacturing technologies and reasonably high receiver and heliostat production rates were postulated. These assumptions are consistent with a recently completed study of solar central receiver high-temperature process air systems (11).

This report documents the findings of the Small Central Receiver Brayton Cycle Study. This seven-month study was performed under Sandia Contract 81-7415 and began in December, 1982.

1.1 STUDY OBJECTIVES

The study objectives were to:

- Identify Brayton cycle configurations suited for high reliability central receiver systems generating electricity in the 2- and 25-MW_e power ranges.

- Evaluate and recommend high-temperature receiver designs most appropriate to the preferred cycle configurations.

1.2 STUDY GROUND RULES

The ground rules for the Small Central Receiver Brayton Cycle Study are summarized in Table 1-1. Electrical power was to be generated in a Brayton cycle, i.e., gas turbine, power system. The generating plant was to be located in an industrial setting as a remote, stand-alone system. Bottoming cycles and thermal energy storage were not considered in order to maintain system simplicity and to limit the study scope. Hybrid or fossil fuel firing was to be utilized for plant startup and to follow rapid transients such as loss of load events. A mature solar industry constructing four to five central receiver plants in the mid to late 1990's was assumed. Plant sizes of 2 and 25 MW_e were considered. The receiver working fluid temperature range considered was 816 to 1316°C (1500-2400°F).

Table 1-1. Small Central Receiver Brayton Cycle Study Ground Rules

1. Brayton cycle electrical power production

2. Stand-alone operation

3. Possibly remote site

4. No bottoming cycle

5. No thermal energy storage

6. Hybrid operation for:
   - Startup
   - Load-leveling

7. Mature solar industry

8. Size ranges: 2-MW_e and 25-MW_e

9. Receiver temperature range: 816° to $1316^{\circ}C$ (1500° to $2400^{\circ}F$)

1.3 PROGRAM WORK FLOW

The program work flow is illustrated in Figure 1-1. The study was accomplished in two technical tasks. The Brayton Cycle Configurations task determined a preferred cycle configuration for each of the two plant sizes: 2 and 25 MW_e. The High-Temperature Receiver Study identified a preferred receiver concept for each of the preferred cycle configurations.

1.4 SUMMARY OF RESULTS

1.4.1 System Level Requirements

A consistent set of requirements and assumptions was defined and held constant throughout the study. The assumed plant site is Barstow, California; the design point is solar noon, March 21st, 950 W/m^2 insolation, and 15°C (59°F) ambient temperature. A second generation glass heliostat was assumed. The heliostat cost was assumed at 113 $\$/m^2$ (1983 $). Economic factors were chosen to represent an industrial electric generation application. Cost estimates were based on 1983 $.

1.4.2 Baseline System Definition

A baseline system configuration was developed to which various cycle and receiver alternatives were compared. The baseline configuration was a cavity, ceramic tube receiver operating in a simple, open Brayton cycle. Preliminary receiver sizing was based on scaling previous BEC metal tube receiver designs (3). The gas turbine performance parameters were chosen to represent currently available turbomachinery.

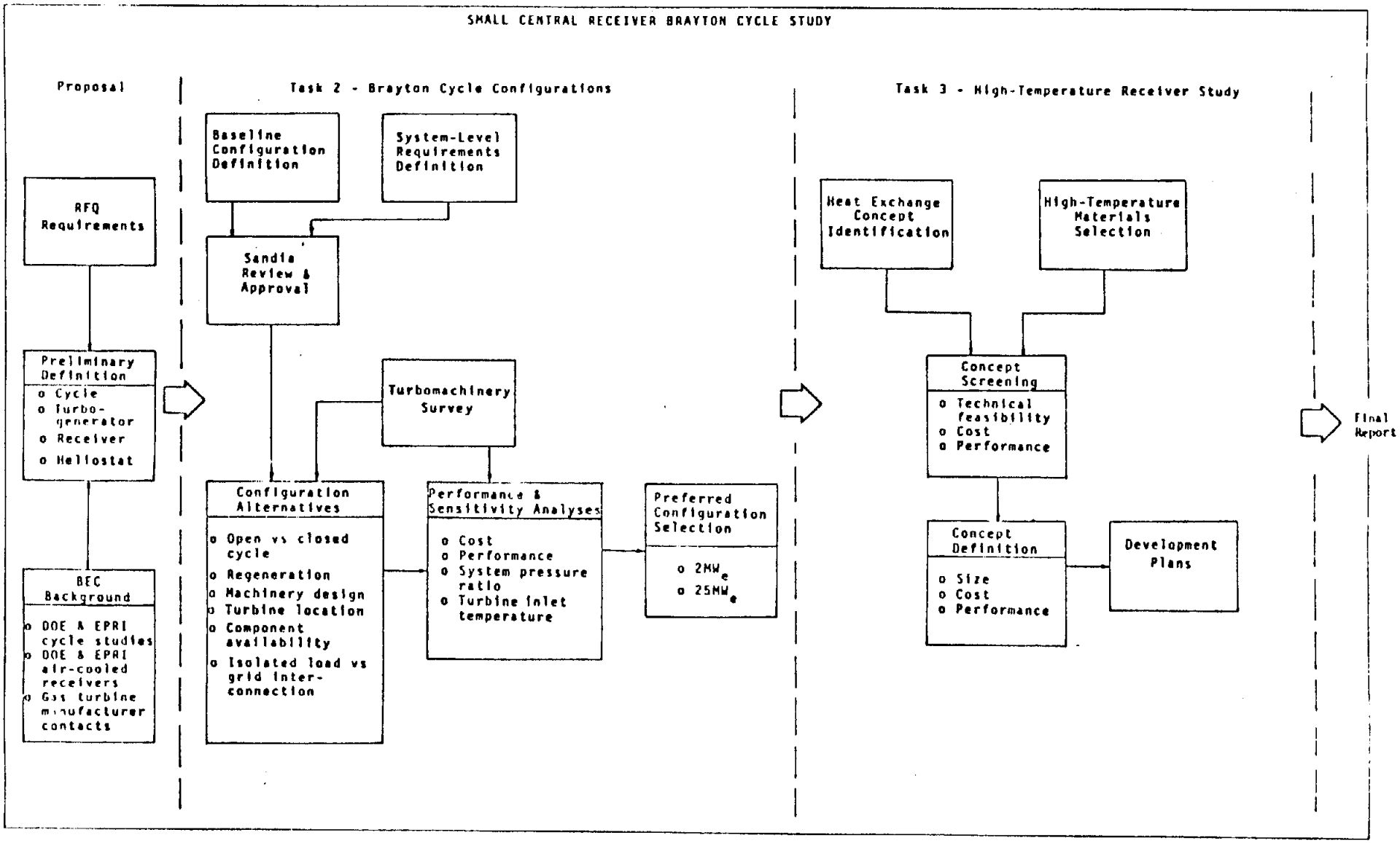

Figure 1-1. Work Flow Plan

1.4.3 Brayton Cycle Configurations Study

The Brayton Cycle Configuration Study identified preferred cycle configurations for each plant size range. The cycle configurations considered were:

- Open simple (OS)
- Closed simple (CS)
- Open regenerated (OR)
- Closed regenerated (CR)
- Open regenerated and intercooled (ORI)
- Closed regenerated and intercooled (CRI)

Cycle performance was calculated for each configuration and plant size range. The results are summarized in Figures 1-2 and 1-3. The open cycle regenerated and intercooled cycle configuration produced the highest cycle efficiency in each size range.

Cost estimates for each cycle configuration were generated. Levelized energy costs were calculated assuming an industrial plant application. The results are presented relative to a current technology baseline in Figure 1-4. For the 2-MWe plant, the open simple (OS) cycle produced the least direct capital costs. Although the ORI configuration has a higher cycle efficiency (see Figure 1-3), the cost of the recuperator and intercooler is larger than the reduction in heliostat field costs afforded by increased cycle efficiency. In this plant size range, the heliostat field is a smaller fraction of the total plant cost due to the increased field performance at smaller sizes, the larger turbomachinery unit costs ($/kWe) at small sizes, and relatively larger fixed costs (buildings, computers, controls, etc.). Reductions in heliostat field costs through increased cycle efficiency, therefore, have smaller leverage in the total system costs. When the effects of off-design performance are considered, the OS configuration also produces the lowest busbar costs.

For the 25-MWe plant, the cycle configuration rankings are slightly different. Three configurations, CRI, ORI, and OS, produce the least direct capital costs. In the larger plant size, the heliostat field performance is reduced

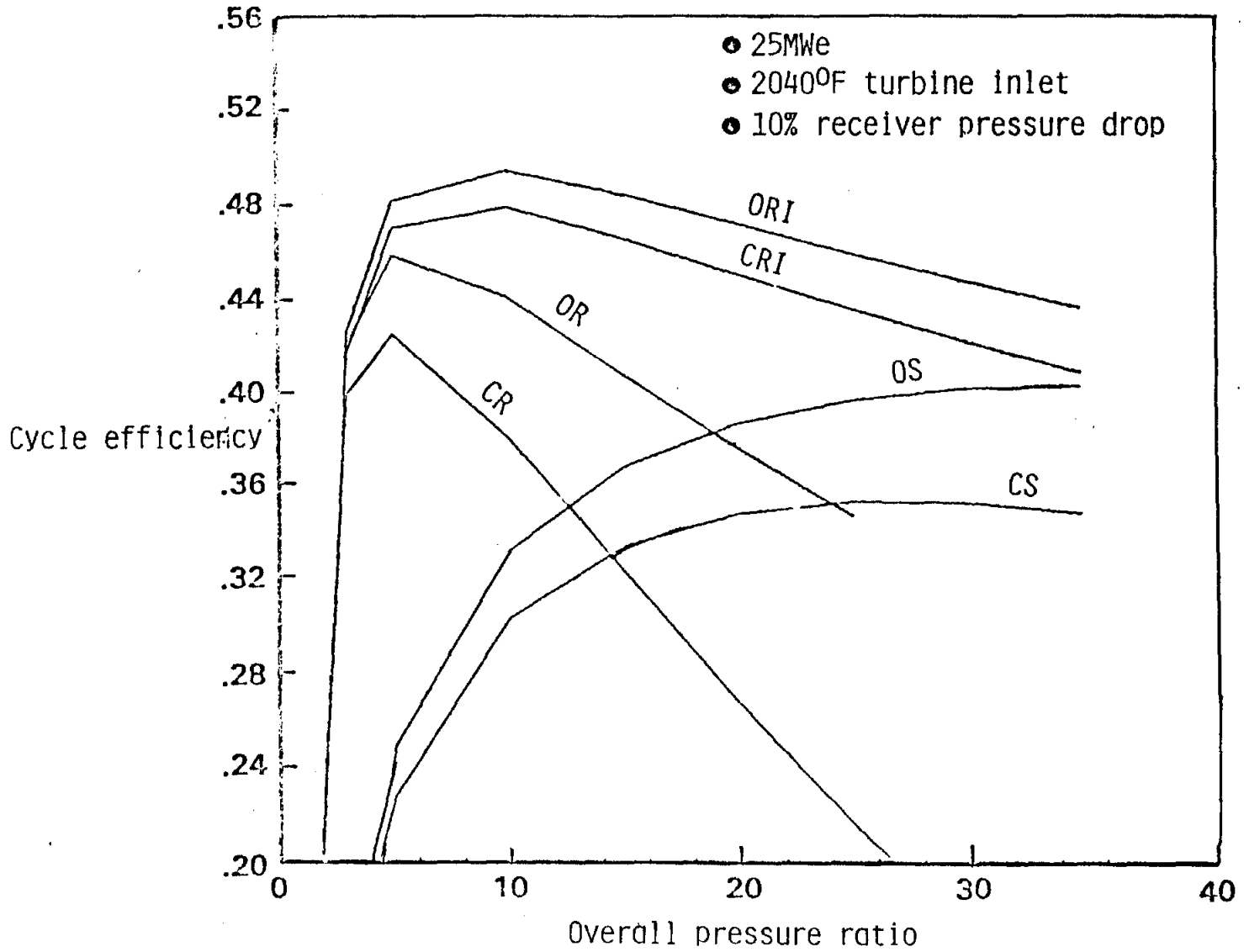

Figure 1-2. Cycle Efficiency Versus Pressure Ratio

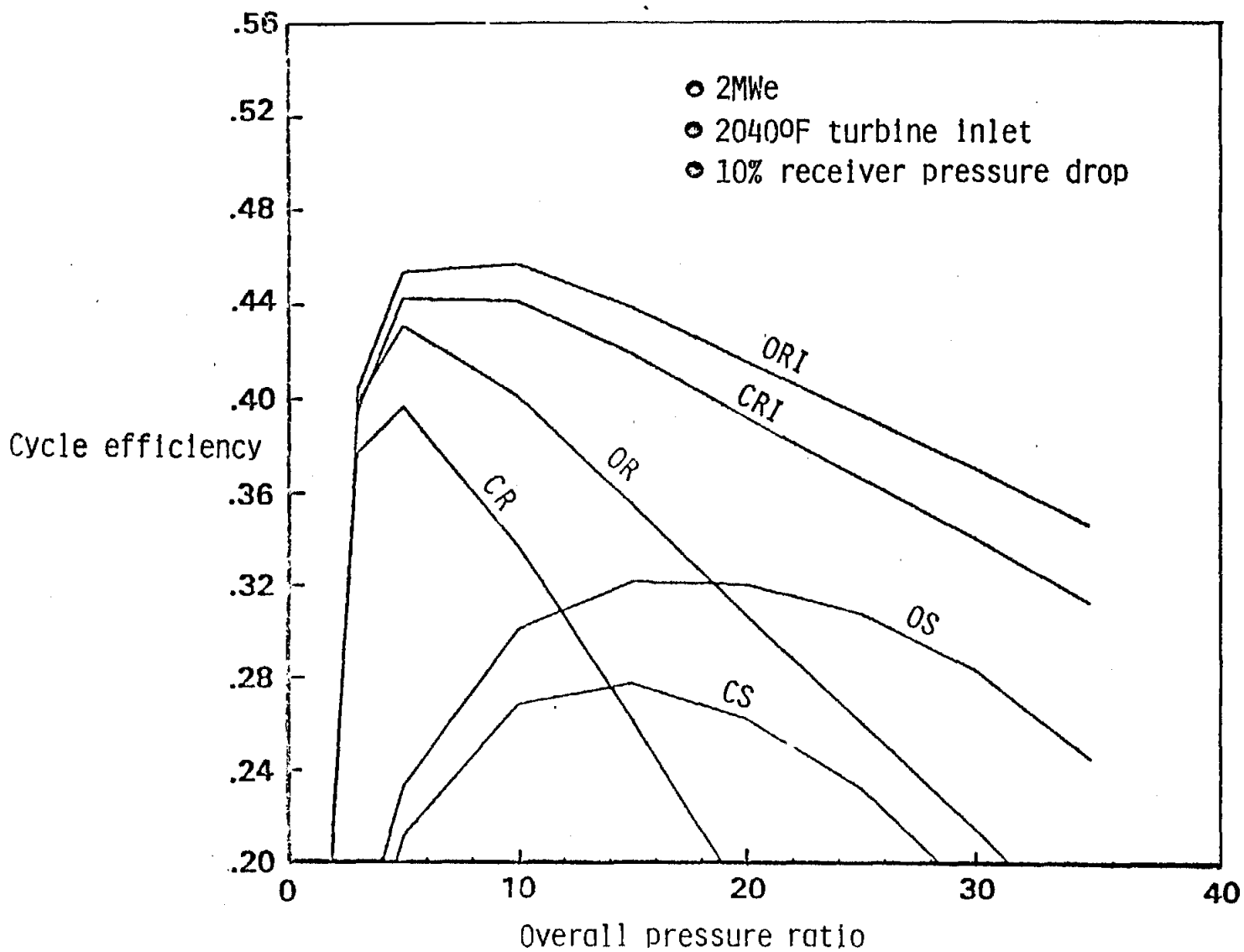

Figure 1-3. Cycle Efficiency Versus Pressure Ratio

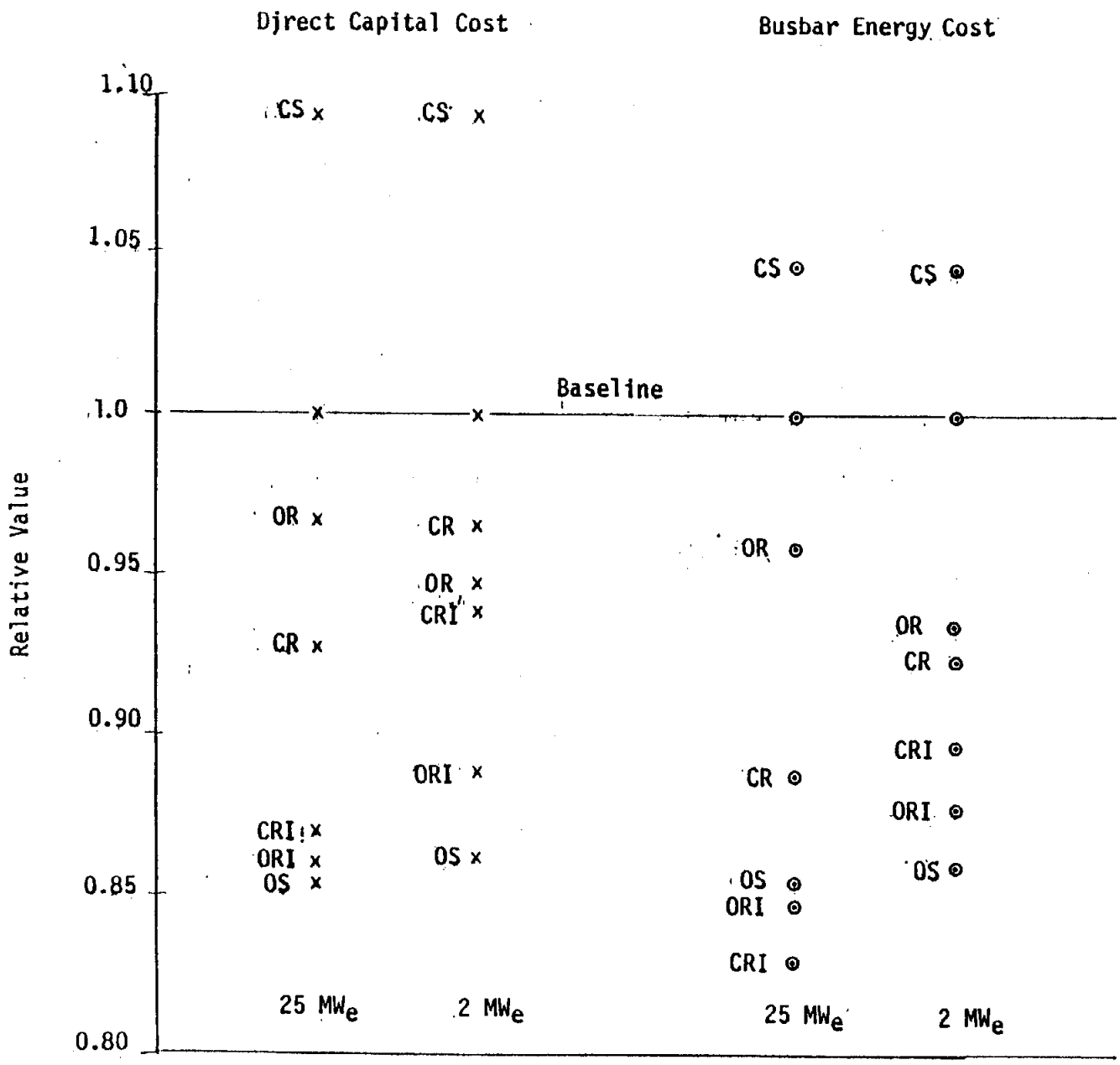

Figure 1-4. Relative Capital and Busbar Cost Results

as are the electric power generation unit costs. The heliostat field costs, therefore, are a larger fraction of the total plant costs. Increased cycle efficiency and the resulting reduced heliostat costs have a greater effect on the total plant costs. When off-design performance is considered, the more efficient CRI and ORI configurations produce the lowest busbar costs.

Preferred cycle configurations were selected based on cost, performance, availability, reliability, maintainability and operability. The open simple (OS) cycle configuration was chosen for the 2-MW_e plant size. The OS configuration is straight forward in design and readily available. It has proven itself as a reliable and easily maintained system. Open simple cycles are used as remotely located, unmanned peaking power plants. The OS configuration, tower-top location, also clearly produced the lowest capital costs and busbar energy costs for this size range. Figure 1-5 presents the preferred 2-MW_e cycle configuration flow schematic. Also presented are thermodynamic state point data around the flow circuit.

The open cycle regenerated and intercooled (ORI) configuration was chosen for the 25-MW_e plant size. The ORI configuration offers high cycle efficiency and reduced heliostat field and receiver sizes, while requiring low capital and busbar energy costs. Figure 1-6 presents the preferred 25-MW_e cycle configuration flow schematic. Thermodynamic state point data are also presented.

1.4.4 High-Temperature Receiver Study

The High-Temperature Receiver Study determined two preferred high-temperature receiver concepts for the two cycle configurations identified in the previous task. Receiver concepts identified as potentially applicable to the 1093°C (2000°F) air-heating requirements are listed in Table 1-2. An initial screening process was used to reduce the number of concepts. Screening criteria included materials availability, cost, thermal and optical efficiency. The concepts selected for further analysis for the 25-MW_e plant size were: ceramic tube, transparent tube, falling particles and molten salt. At the 2-MW_e plant size, the above four concepts plus the small particle receiver were selected for further analysis.

OPEN SIMPLE CYCLE

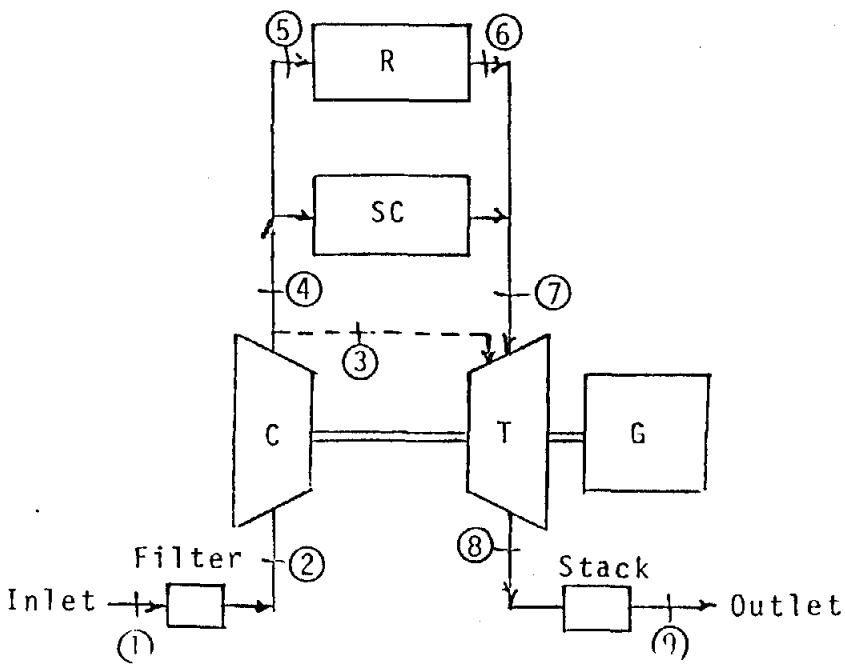

Station	$\dot{m}$ (lbm/s)	T (°F)	P (psia)
1	17.69	59	14.7
2	17.69	59	14.6
3	0.80	762.6	219.3
4	16.89	762.6	219.3
5	16.89	762.6	219.3
6	16.89	2040.0	197.4
7	16.89	2040.0	197.4
8	17.69	939.4	14.9
9	17.69	939.4	14.7

Cycle efficiency = 32.2%
Receiver efficiency = 85%
Solar input = 7.3MW_t

Figure 1-5. System Design Requirements - 2 MW_e Plant

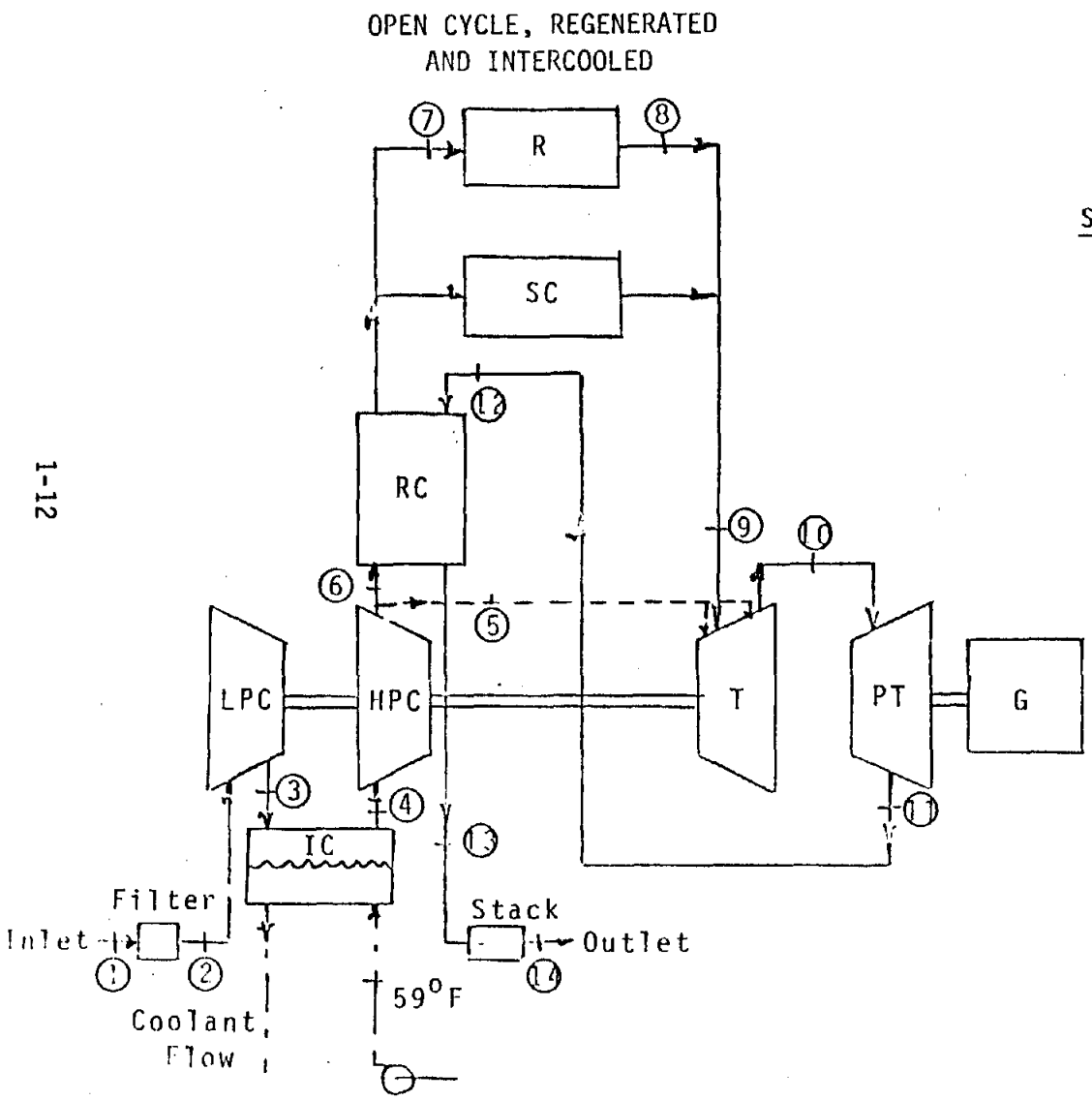

Station	$\dot{m}$ (lbm/s)	T (°F)	P (psia)
1	172.89	59	14.7
2	172.89	59	14.6
3	172.89	282.7	46.2
4	172.89	80	45.3
5	7.78	314.7	143.3
6	165.11	314.7	143.3
7	165.11	988.9	141.9
8	165.11	2040.0	127.7
9	165.11	2040.0	127.7
10	172.89	1575.2	55.6
11	172.89	1060.5	15.5
12	172.89	1060.5	15.5
13	172.89	423.5	14.9
14	172.89	423.5	14.7

Cycle efficiency = 49.5%

Receiver efficiency = 85%

Solar Input = 59.6 MW_t

Figure 1-6. System Design Requirements - 25 MW_e Plant

Table 1-2. RECEIVER CONCEPT CANDIDATES

Concept	Proponent
Intimate Contact Heat Exchange	
Atmospheric Pressure	
1. Ceramic Matrix	Sanders
2. Volumetric	PNL
Pressurized	
3. Ceramic Tube	Black & Veatch
4. Ceramic Dome	MIT
Direct Absorption Heat Exchange	
Transparent Tubes	
5. Small Particle	LBL
6. Fluidized Bed	Westinghouse
Windowed Receiver	
7. Small Particle	LBL
8. Absorbing Gas	
Intermediate Medium Heat Exchange	
Solid Medium	
9. Absorbing Particle	SNLL
10. Phase Change	U of W
Liquid Medium	
11. Molten Salt	SERI
12. Heat Pipe	Bechtel, Dynatherm
13. Molten Metal	
Gaseous Medium	

Thermal and mechanical analyses were completed on the above concepts. Thermal analyses included evaluation of reflection, reradiation, and working fluid heat transfer. Results for the 25-MW_e receiver are summarized in Table 1-3. There is not a strong difference from a receiver efficiency view among the candidate concepts; however, receiver size favors the higher peak flux capability receivers. Similar data for the 2-MW_e plant size are shown in Table 1-4. The small particle receiver is seen to be about 4 percentage points higher in thermal efficiency than the ceramic tube concept.

Mechanical design analyses were performed on each design concept to identify major technical issues. Consideration of a large number of potential design options with each receiver concept was not possible within the scope of this study. Configurations were chosen to represent the overall concept features.

The high temperatures used in the receivers necessitate the use of ceramic heat exchanger materials. A preliminary survey of high-temperature materials identified four promising structural ceramic materials: CVD silicon carbide, hot-pressed silicon nitride, siliconized silicon carbide, and sintered alpha-silicon carbide. The sintered and siliconized silicon carbides are most attractive from fabrication considerations. Some of the receiver concepts identified as being potentially applicable utilize transparent windows or tubes. The most promising high-temperature transparent ceramics were found to be: single crystal aluminum oxide (sapphire); fused silica; and Vycor® (96% silicia). Sapphire is desirable because of its strength and high-temperature capabilities but may not be feasible from size and cost considerations. Silica is fabricated in a wide variety of sizes and shapes but would probably require cooling to prevent slow crack growth and rapid devitrification.

After consideration of the thermal analyses results, the design analysis considerations, and the high-temperature materials assessment, a preferred receiver concept was developed for each plant size. The concept features were selected based on assessments of cost, performance, reliability, maintainability and operability.

Table 1-3. 25-MW_e Receiver Energy Balance

Parameter	RECEIVER CONCEPT				
	Ceramic Tube	Transparent Tube	Molten Salt	Falling Particle Solid	Falling Particle Phase Change
Peak Flux Level (kW/m^2)	450	600	600	1000	2000
Reflection (%)	1.6	1.6	1.8	3.9	6.3
Reradiation (%)	10.1	7.5	8.6	8.0	6.5
Convection + Conduction (%)	3.0	3.0	3.0	3.0	3.0
Receiver Efficiency (%)	85.3	87.9	86.6	85.1	84.2
Aperture area (m^2)	33.56	33.56	33.56	33.56	33.56
HX area (m^2)	458	331	331	206	103

Table 1-4. 2-MW_e Receiver Energy Balance

Parameter	Receiver Concept	
	Ceramic Tube	Small Particle
Peak Flux Level (kW/m^2)	450	2000
Reflection (%)	4.4	6.6*
Reradiation (%)	6.9	4.6*
Conduction and Convection (%)	3.0	
Receiver Efficiency (%)	85.7	88.9

*Assumed from Table 3-3, (9, 11)

25-MW_e Preferred Receiver Concept

The ceramic tube receiver concept was selected as the preferred concept for the 25-MW_e plant size. This concept has reasonable performance and cost through the use of a simple, straightforward design. Few high-temperature mechanical components are required. From a materials viewpoint, this concept is clearly the closest concept to technical feasibility. Ceramic components of the size, quantity and temperature capability are currently available. The ceramic tube concept is also in keeping with the desired simple, low-maintenance objectives of the overall study. This concept is the most likely to operate reliably in a remote, stand-alone electrical generation application. Figure 1-7 shows plan and elevation views of the ceramic tube conceptual design. Figure 1-8 shows a silicon carbide heat exchanger tube assembly.

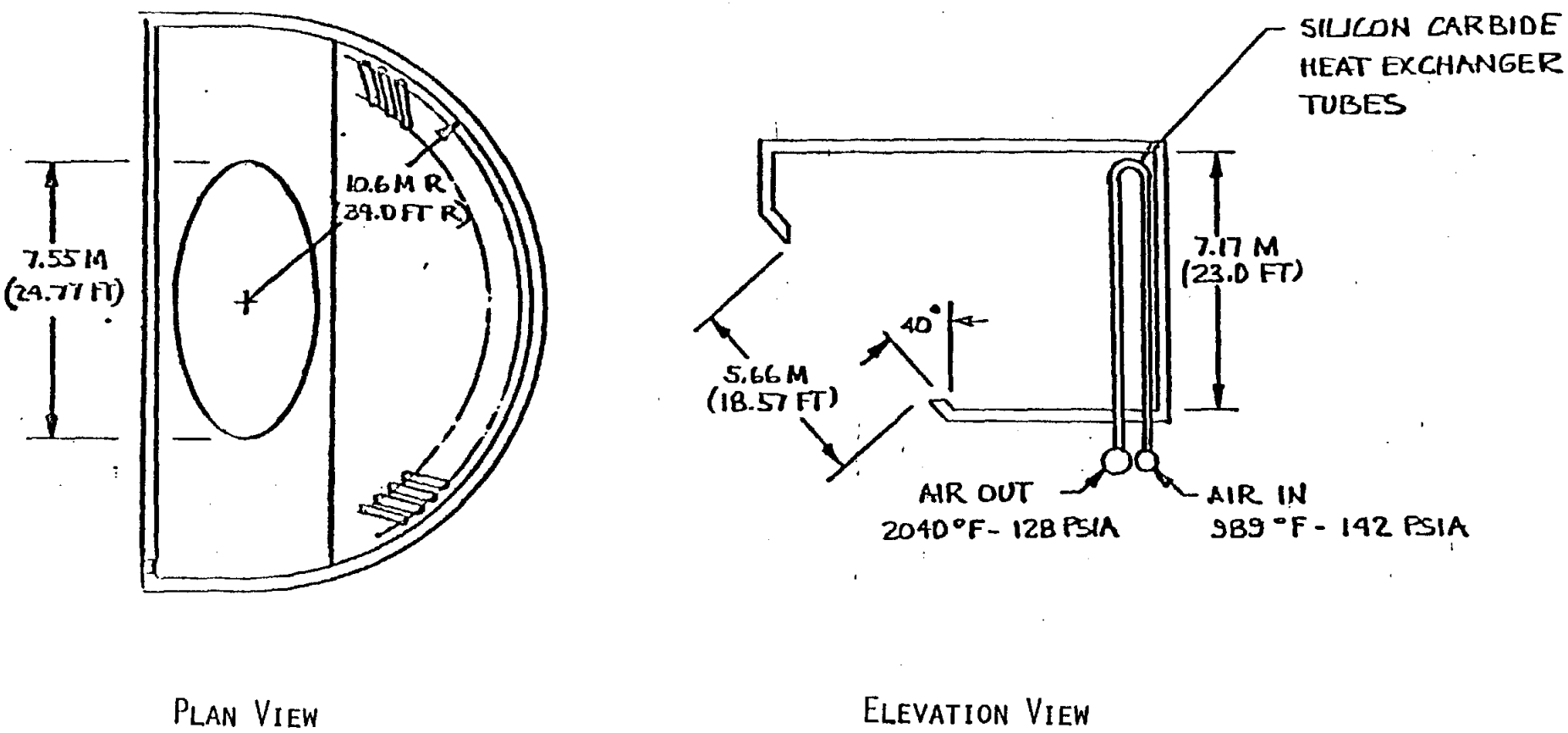

Figure 1-7. Plan and Elevation View of 25-MW_e Ceramic Tube Receiver

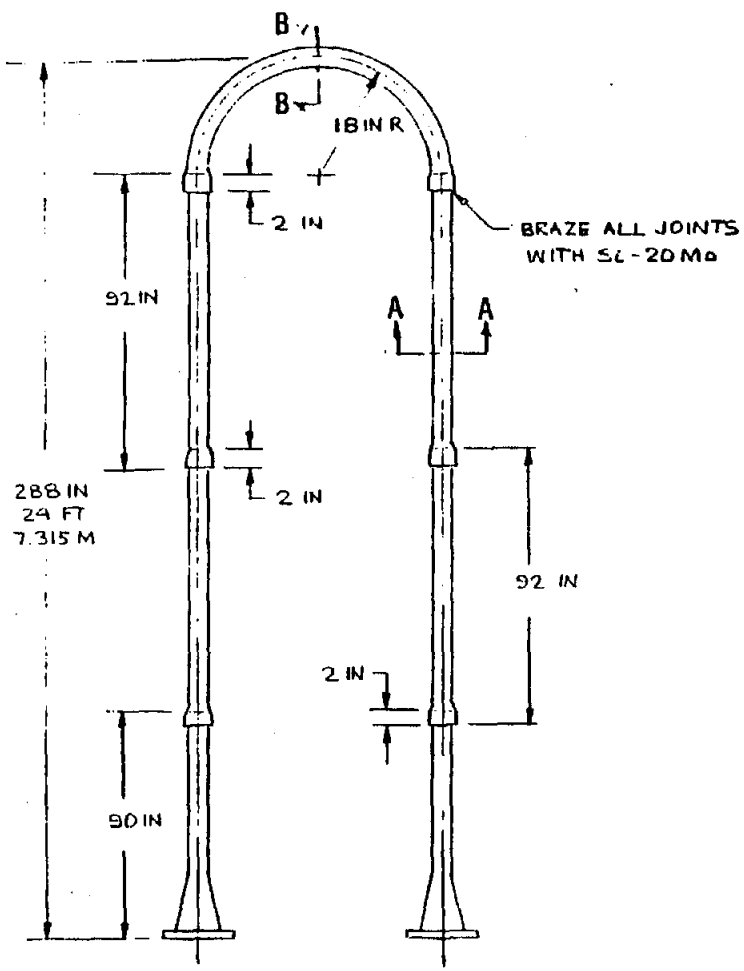

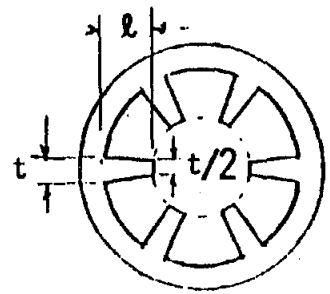

Section A-A

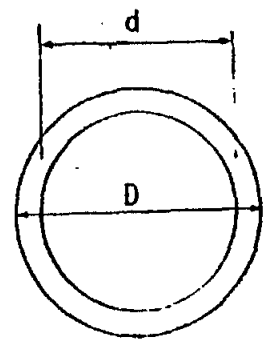

Section B-B

	Dimensions in.
d	2.50
D	3.00
t	0.25
ℓ	0.575

Figure 1-8. Heat Exchanger Tube Assembly

2-MW_e Preferred Receiver Concept

The small particle receiver concept was selected for the 2-MW_e plant size. This concept has superior performance and cost and reasonable reliability, maintainability and operability. From a materials viewpoint, the 3-m diameter quartz window presents a manufacturing challenge. Maintaining the window temperature below the devitrification point is also a requirement. Figure 1-9 illustrates the small particle receiver conceptual design. The fused quartz window design is presented in Figures 1-10 and 1-11.

Receiver Performance and Cost Estimates

Table 1-5 presents a summary of the receiver performance for both plant sizes. Table 1-6 presents the receiver concept cost estimates. The summary includes the material and labor required to fabricate and install each element of the system.

Preferred System Design

The preferred receiver designs were combined with the preferred cycle selection data of the previous section to produce a system level design. Figure 1-12 presents the tower arrangement for the 25-MW_e plant. The 2-MW_e arrangement is similar. Tables 1-7 and 1-8 present system design data for the 25-MW_e and 2-MW_e plants respectively. Figures 1-13 and 1-14 present design point system performance for each plant size. Annual average data are presented in Section 4.2. System direct capital cost estimates are presented in Table 1-9. Levelized busbar energy costs are calculated for the 25-and 2-MW_e plants. The results are presented in Table 1-10. The economic assumptions utilized are presented in Table 1-11. In order to assess the effect of economic assumptions on the busbar energy costs, the final system designs were re-evaluated based on the electric utility economic factors presented in Table 1-11. These economic factors were taken from the second generation heliostat comparison (12) except evaluated in 1983$. The results are also presented in Table 1-10. The levelized busbar costs for an electrical utility application are approximately 20 mil/kWh less than the industrial application. These data were derived using the DELSOL 2 computer code and are discussed in Section 4.3.

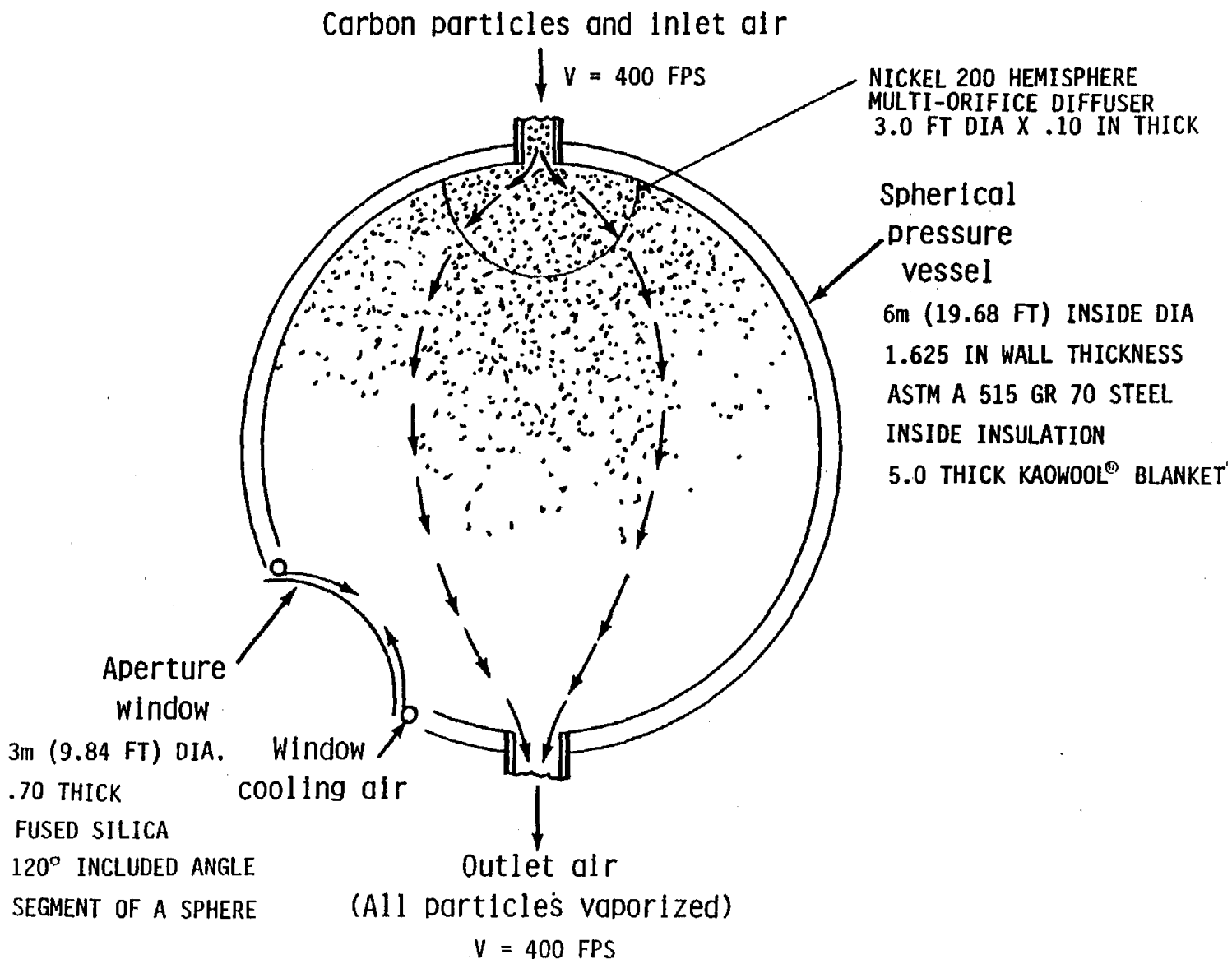

Figure 1- 9. 2-MW_e Small Particle Receiver

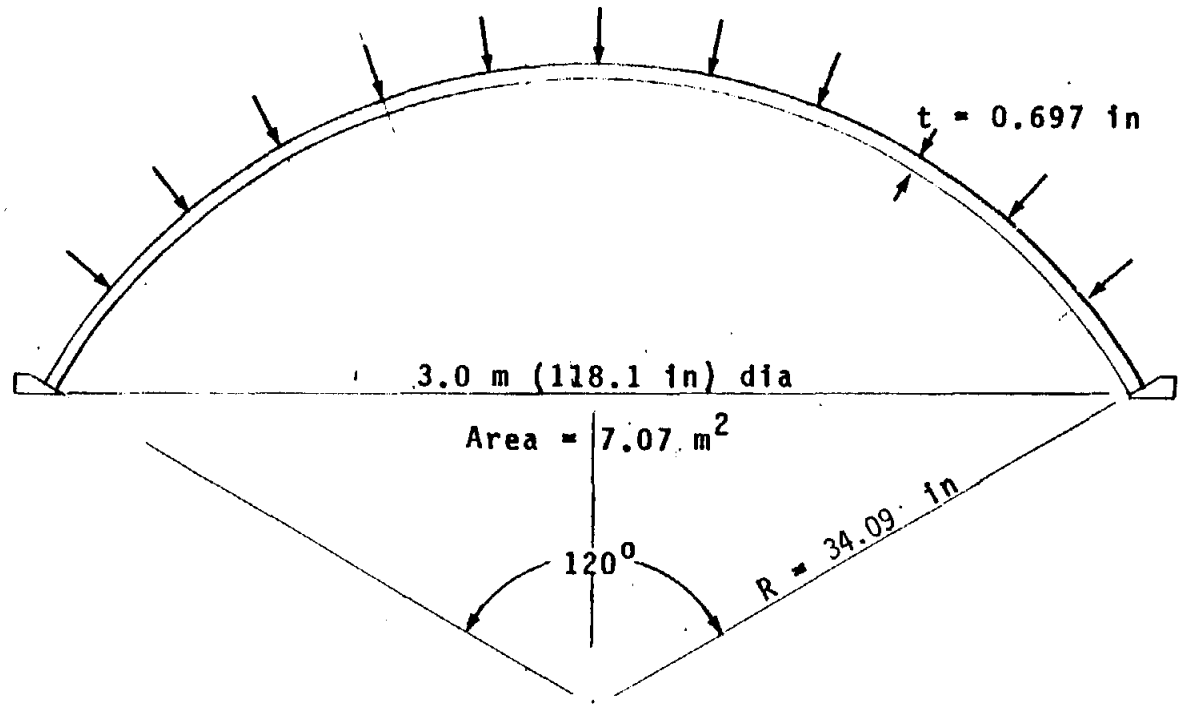

Figure 1-10. 3.0-m Diameter Fused Quartz Window Design

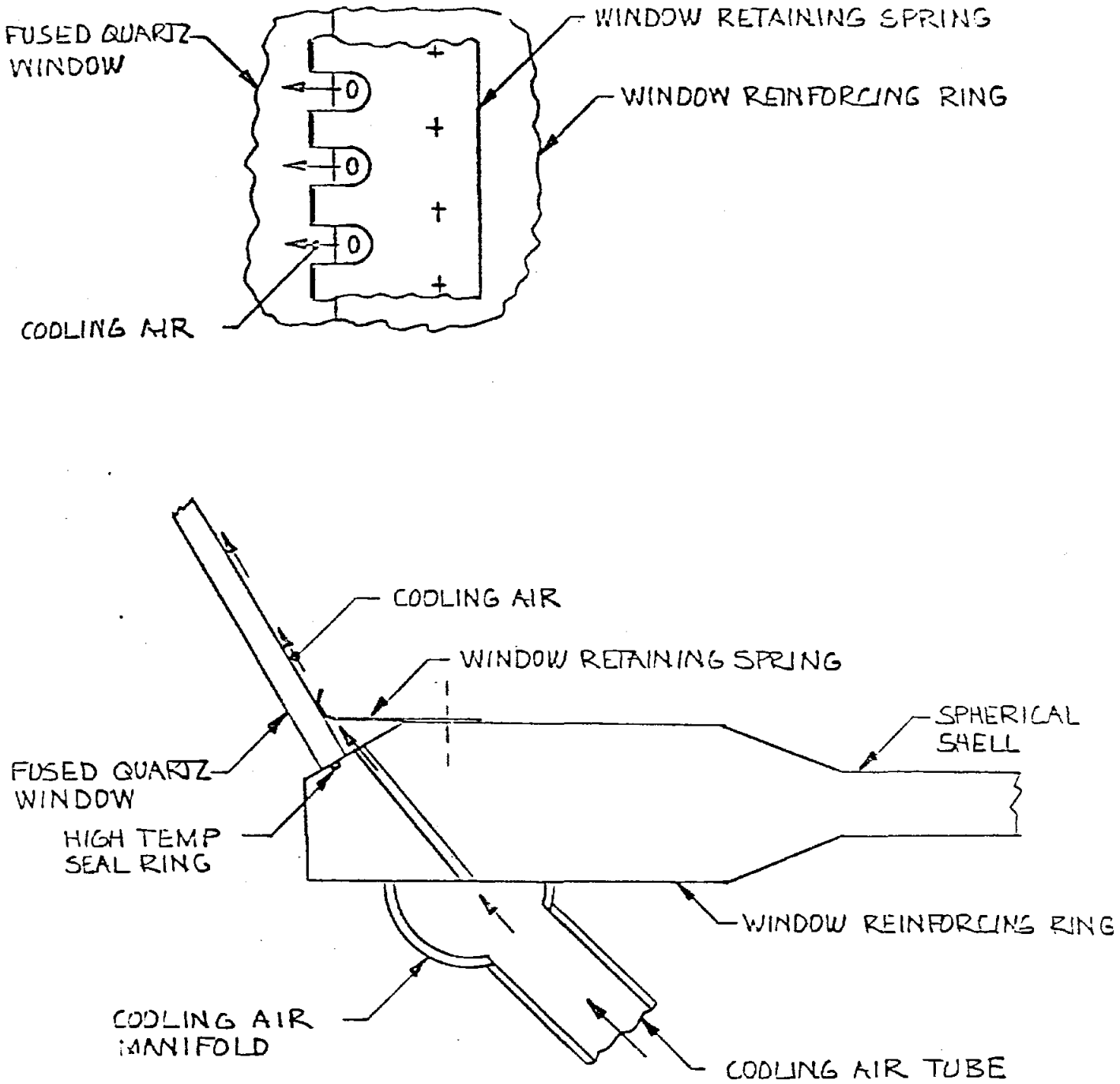

Figure 1-11. 3.0-m Diameter Window/Shell Interface Design

Table 1-5. Receiver Concept Performance

	25 MW_e Ceramic Tube		2 MW_e Small Particle	
	MW	%	MW	%
Reflection	2.62	4.4	0.462	6.6
Reradiation	4.11	6.9	0.322	4.6
Conduction & Convection	1.78	3.0		
Receiver	50.74	85.7	6.213	88.8
Solar Input	59.25	100.0	6.997	100.0
Pressure Loss	10%		5%	

Table 1-6. Receiver Cost Estimates

Component		Direct Capital Cost (10^3\$, 1983) 25 MW_e	2 MW_e
Steel work:	Material	40.5	42.0
	Labor	10.5	7.8
Insulation:	Material	384.0	21.0
	Labor	326.0	8.5
Heat Exchangers:	Material	512.4	--
	Labor	10.8	--
Manifolds:	Material	15.2	--
	Labor	22.0	
Window		--	120.0
Carbon Particle Generator		--	22.0
TOTAL		1,321.3	221.3

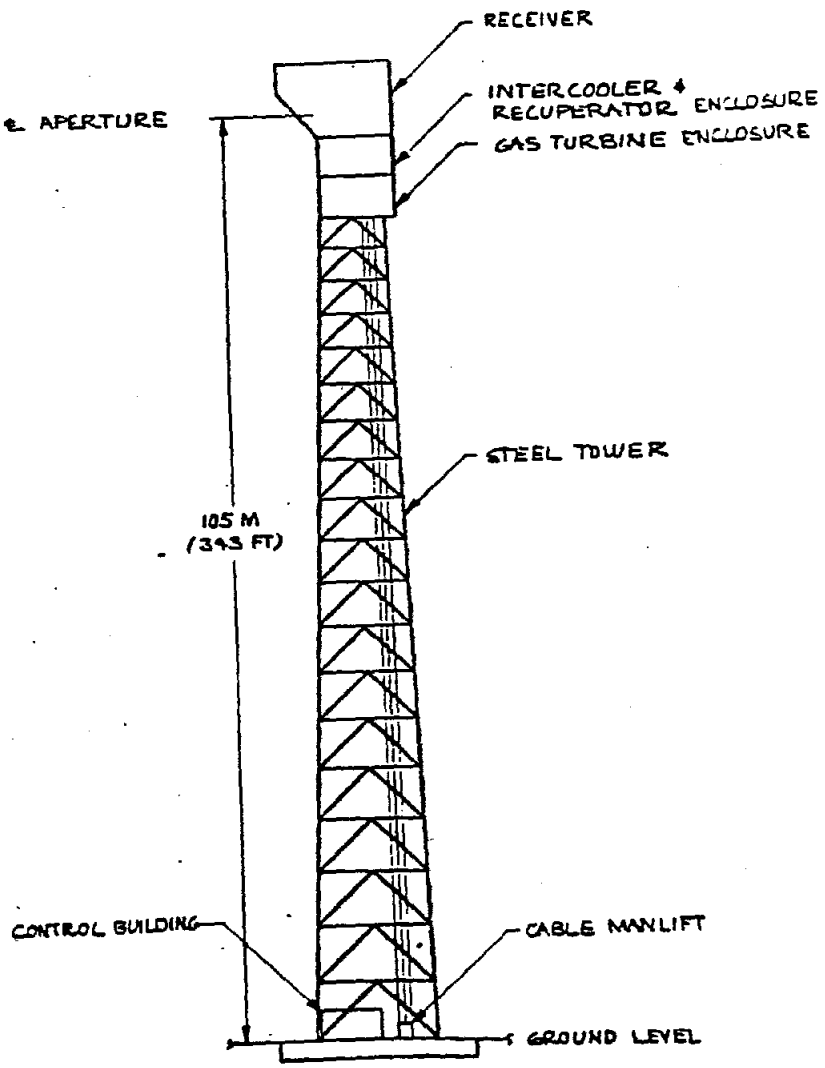

Figure 1-12. 25-MW_e Plant Tower Arrangement

Table 1-7. 25-MW_e System Definition

System:	
Power range, MW_e	25
Working fluid	air
Cycle configuration	open cycle, regenerated and intercooled
Collector Subsystem:	
Heliostat	MDC 2nd. Gen.
Field configuration	north
Field area, m^2	374,000
Mirror area, m^2	90,400
Number of heliostats	1,591
Receiver Subsystem:	
Receiver type	Cavity
Number of apertures	1
Aperture shape	Elliptical
Aperture width, m	7.55
Aperture height, m	5.66
Aperture area, m^2	33.56
Aperture inclination fm vert	40°
Cavity diameter, m	21.2
Cavity height, m	7.17
Total tube number	100
Tube outside diameter, cm	7.62
Tube length, m	14.02
Tube pitch	3.0 tube dia.
Inlet air temp, ^oC	531
Outlet air temp, ^oC	1116
Inlet pressure, MPa	0.98
Pressure loss, % of inlet	10
Tower height, m	97.8
Tower type	steel
Estimated receiver mass, kg	127,600
Electrical Power Generation Subsystem:	
Pressure ratio	10.0
Turbine inlet temp, ^oC	1116
Mass flow rate, kg/s	74.84
Cycle efficiency	49.5%
Turbomachinery location	Tower top

Table 1-7. 25-MW_e System Definition (Continued)

Turbine mass, kg	100,000
Recuperator diameter, m	3.5
Recuperator length, m	5.5
Recuperator pressure loss, %	4 (Hot side) 1 (Cold side)
Recuperator effectiveness, %	90
Recuperator mass, kg	53,000
Intercooler diameter, m	4.6
Intercooler pressure loss, %	2
Intercooler effectiveness, %	90
Intercooler mass, kg	46,000
Piping Subsystem:	
Riser flow diameter, m	0.46
Riser length, m	12.2
Riser insulation thickness, cm	7.62 (exterior)
Riser pressure loss, %	0.5
Riser heat loss (steady state), kW_{th}	34
Downcomer flow diameter, m	0.56
Downcomer length, m	12.2
Downcomer insulation thickness, cm	7.62 (interior)
Downcomer pressure loss, %	0.5
Downcomer heat loss (steady state), kW_{th}	174

Table 1-8. 2-MW_e System Definition

System:	
Power range, MW_e	2
Working fluid	air
Cycle configuration	open simple cycle
Collector Subsystem:	
Heliostat	MDC 2nd gen.
Field configuration	north
Field area, m^2	46,400
Mirror area, m^2	10,000
Number of heliostats	176
Receiver Subsystem:	
Receiver type	Cavity
Number of apertures	1
Aperture shape	Circular
Aperture diameter	3.0
Aperture area, m^2	7.07
Aperture inclination fm vert	40°
Cavity diameter, m	6
Inlet air temp, ^oC	405
Outlet air temp, ^oC	1116
Inlet pressure, MPa	1.52
Pressure loss, % of inlet	5
Tower height, m	35
Tower type	steel
Estimated receiver mass, kg	46,229
Electrical Power Generation Subsystem:	
Pressure ratio	15
Turbine inlet temp, ^oC	1116
Mass flowrate, kg/s	7.66
Cycle efficiency	33.6
Turbomachinery location	Tower top
Turbine mass, kg	18,150
Piping Subsystem:	
Riser outside diameter, m	0.102
Riser length,	9.1
Riser insulation thickness, cm	7.62 (exterior)
Riser pressure loss, %	0.5
Downcomer outside diameter, m	0.203
Downcomer length, m	6.1
Downcomer insulation thickness, cm	7.62 (interior)
Downcomer pressure loss, %	0.5

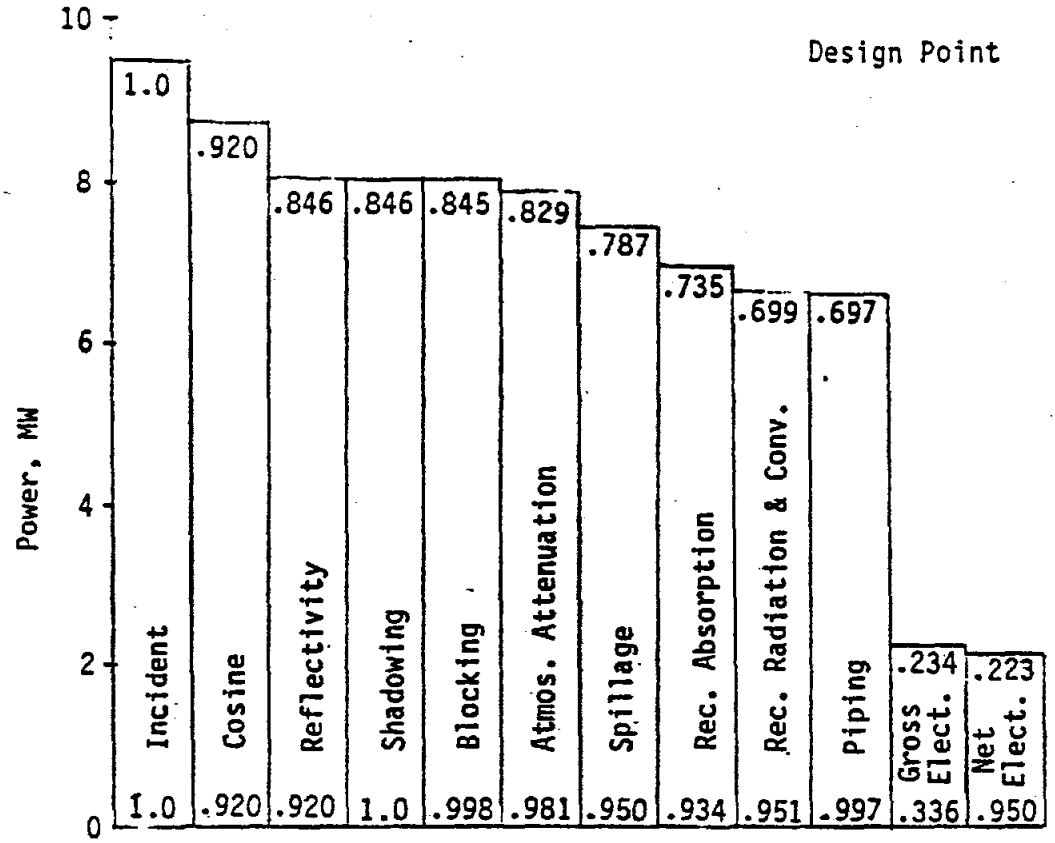

Figure 1-13. Design Point 2-MW_e System Performance

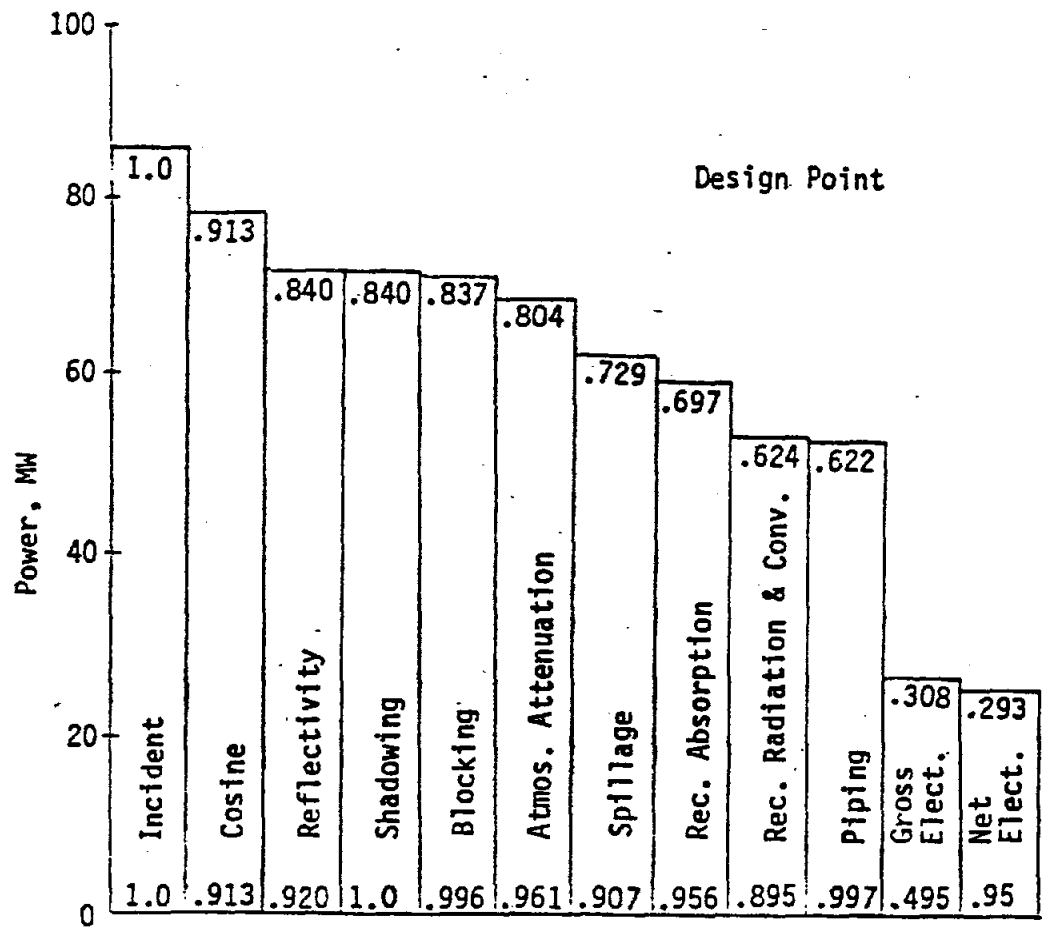

Figure 1-14. Design Point 25-MW_e System Performance

Table 1-9. System Direct Capital Cost Estimates (1983$)

Subsystem		Cost ($10^3$$) 25 MW_e	2 MW_e
Collector Field		10,235	1,132
Land		748	93
Piping		82	11
Receiver		1,321	221
Tower		565	76
Electric Power Generation:	Turbine	5,930	1,036
	Recuperator	1,000	--
	Intercooler	1,180	--
Fixed		540	285
TOTAL		21,601	2,854

Development Plans

After an assessment of the technology base and the critical technical issues, these areas were found to be most crucial to the development of the small Brayton receiver concept:

(1) High-Temperature Piping
(2) External Firing
(3) Ceramic Tube Heat Exchanger Elements
(4) Fused Quartz Window

The high-temperature piping is important because of the need to duct the hot 1093°C (2000°F) air from the receiver to the turbine inlet with low pressure losses. External firing of gas turbines requires reliable control systems and

Table 1-10: Busbar Energy Costs (1983$)

	mils/kWh	
	25-MW_e Plant	2-MW_e Plant
Industrial Plant Application	125	209
Electrical Utility Application	103	171

Table 1-11: Economic Factors Used in Study

	Industrial Application	Electric Utility Application
Cost Basis	1983 Dollars	1983 Dollars
Contingency	0%	0%
Spare Parts	0%	0%
Indirect Costs	15%	16%
Capital Escalation	8%	8%
General Inflation	8%	8%
Interest During Construction	5%	10%
Years to Construction Start	0	0
Plant Lifetime	20 Years	30 Years
Fixed Charge Rate	22.9%	15.9%
Discount Rate	18%	9.96%
Heliostat First Year O&M	1.7%	1.7%
Balance of Plant First Year	1.5%	1.5%

trim combustors which have not been demonstrated for solar-heated turbines. Ceramic tube fabrication of the sizes, shapes and applications envisioned herein have not been demonstrated, heretofore. Large fused quartz windows designed for high solar transmission, high temperature and pressure containment have never been attempted. A failure in any one of these areas would impair the technical feasibility of the preferred system concepts. The concepts were chosen to minimize the technical risks wherever possible, but since these systems are new, some risks remain.

A development plan was formulated to reduce the technical risks associated with these concepts. The first step would be a Preliminary Design Phase presented schematically in Figure 1-15. This phase would consist of system level studies to define design critical performance parameters. Assessments in each of the critical technology areas would be performed to define a consistent preliminary design of the entire system.

The preliminary design phase results would be input to an experimental phase. Subsystem Research Experiments (SRE) in each critical technology area would help resolve and define workable system designs. A system level experiment would allow a representation of the entire system in a scaled-down fashion. System level analysis updates will allow periodic revision of the cost and performance of the commercial-size plants. The experimental and system economics data will allow a definition of the final design.

Figure 1-16 presents a work flow plan for the preliminary design phase. System level performance would be calculated for time-of-day, day-of-year, and ambient temperature variations for actual expected conditions at the site location. Normal system mode transitions such as startup and shutdown will be considered. Control actions for emergency conditions such as loss-of-load events will be developed. Supporting these system level calculations would be detailed analyses of the receiver, the turbogenerator and the heat exchangers. These analyses will determine the design critical conditions for the piping, receiver heat exchanger, and window.

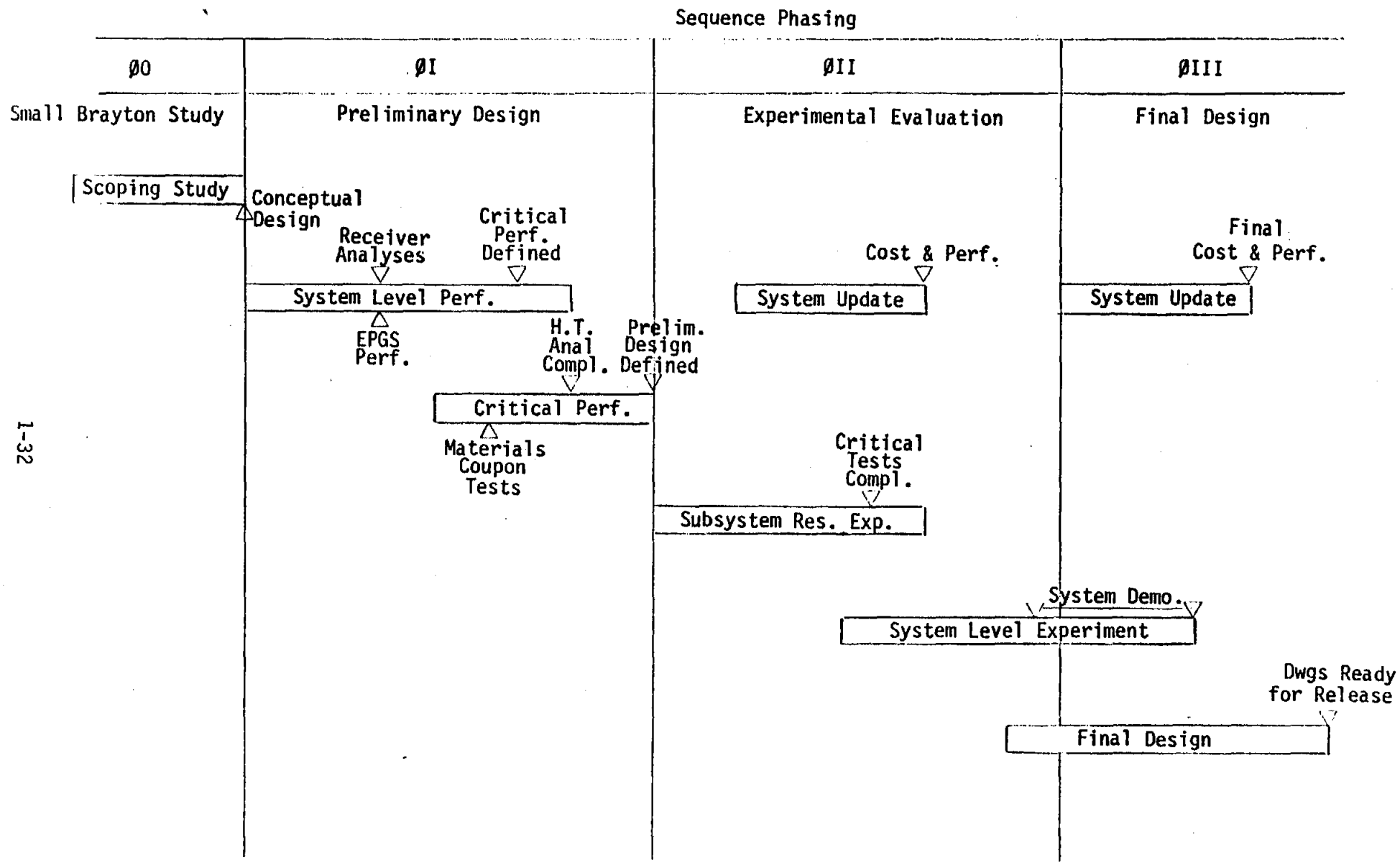

Figure 1-15. Program Development Plan

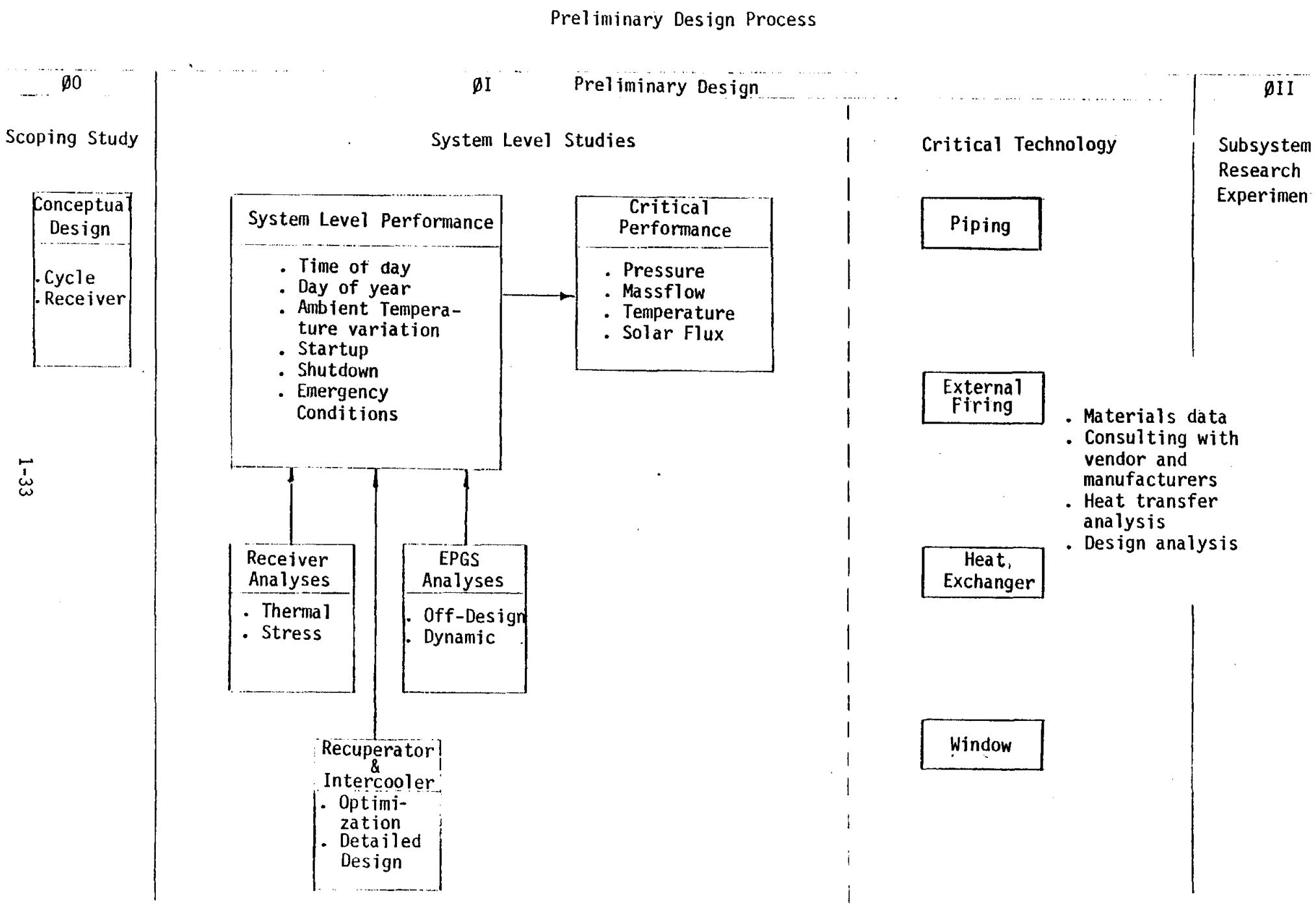

Figure 1-16. Preliminary Design Process

In the subsequent critical technology areas, material data bases will be developed on manufacturers' data and as determined from coupon tests. Close consultation with manufacturers will allow choice of the most appropriate materials and designs. Detailed heat transfer analyses of each technological area will support the stress analyses necessary to complete the design.

2.0 BRAYTON CYCLE CONFIGURATION STUDY

The Brayton Cycle Configuration Study plan is illustrated in Figure 2-1. The study began with a definition of the system-level requirements and baseline configuration. This allowed a common point of comparison for the remainder of the study. Cycle configuration alternatives were identified, and performance and sensitivity analyses were performed on the candidate configurations. In parallel, a survey of currently available turbomachinery and trends within the gas turbine industry was completed. The preferred cycle configuration was selected based on cost, performance, component availability, system complexity, and level of turbine modifications required. The following paragraphs describe the results from each of these subtasks.

2.1 SYSTEM REQUIREMENTS DEFINITION

The objective of this subtask was to define a consistent set of requirements and assumptions to be held constant during the remainder of the study. Table 2-1 presents the final set of these data. The assumed site, design point and insolation data were based on similar data used for evaluation of the second generation heliostat (12).

Since the heliostat was not the subject of this study, a glass/metal heliostat was baselined. The heliostat performance parameters assumed are shown in Table 2-1. The size of the study heliostat was an issue considered in this subtask. The current trend in glass/metal heliostat design is to outfit the second generation heliostat support structure with larger mirror panels to produce a heliostat of approximately 100-m^2 size. However, smaller size heliostats would be favored for the relatively small plant outputs (2 MWe and 25 MWe) of this study. For the purposes of this study, the heliostat size was held at the 57-m^2 second generation size. This 57-m^2 size represents the smallest heliostat expected to be available in commercial quantities in the future.

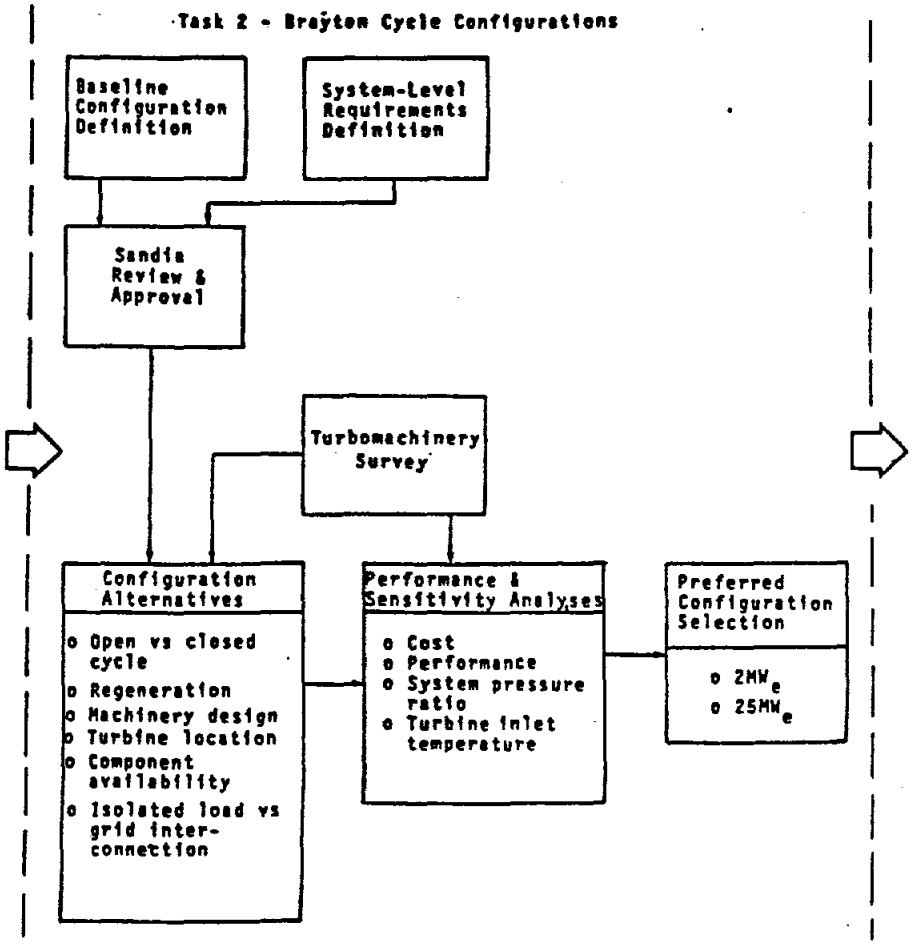

Figure 2-1. Brayton Cycle Configuration Study

Table 2-1. System Requirements and Analysis Assumptions

Site:	Location	Barstow, CA
	Longitude	116.83°W
	Latitude	34.87°N
	Altitude	593 m (1946 ft.)
	Topography	Flat, unrestricted boundaries
	Annual weather factor	0.83
Design Point:	Day	March 21, Day 81
	Hour	Solar noon
	Insolation	950 W/m^2
	Ambient temperature	15°C (59°F)
Insolation Profile:	Model	Meinel
	Precipitable water	20mm
	Relative pressure	93% of sea level
	Sunshape	Limb-darkened sun
	Visibility	25km
Collector field:	Max solar zenith	75°
	Layout pattern	Radial stagger
	Heliostat:	
	Width	8.66m
	Height	6.86m
	Reflective area	56.85m^2
	Azimuth error	4 mrad std. dev.
	Elevation error	4 mrad std. dev.
	Surface error	12 mrad std dev (horiz. and vert.)
	Canting	On axis
	Cant panels	14 (7 horiz., 2 vert.)
	Cant focal length	Slant range
	Panel focus	Two-dimensional
	Panel focal length	6.0 Tower Heights
Economic Factors:	Cost basis	1983$
	Contingency	0%
	Spare parts	0%
	Indirect costs	15%
	Capital escalation	8%
	General inflation	8%
	Interest during construction	5%
	Years to construction start	0
	Plant lifetime	20 years
	Fixed charge rate	22.9%
	Discount rate	18%
	Heliostat first year O & M	1.7%
	Balance of plant first year O&M	1.5%

The economic factors to be used in evaluating various configuration alternatives during the study are also presented in Table 2-1. These factors were obtained from Reference 11. These factors represent an industrial type of electrical generating plant application.

2.2 BASELINE SYSTEM DEFINITION

The objective of this subtask was to develop a baseline system configuration to which various cycle and receiver alternatives could be compared. Preliminary sizing and costing were employed subject to further refinement during the process of the study. Table 2-2 presents baseline system configuration data for each system size range.

The baseline system configuration in each size range was assumed as a cavity, ceramic tube receiver operating in a simple, open Brayton cycle. A single, north-facing aperture and a north collector field were chosen for both plant sizes. (Multiple apertures and a surround collector field were considered for the 25-MWe plant; however, both options were found to be less cost effective.) The collector field, tower height, and aperture size were optimized using the DELSOL 2 (13) computer code. Preliminary receiver sizing was based on scaling previous BEC metal-tube receiver designs (3). The gas turbine performance parameters were chosen to represent currently available turbomachinery. A steel tower was assumed for both plant sizes. The turbomachinery was assumed located at the tower base.

The baseline system performance is presented in Figures 2-2 and 2-3. Both design point and annual average data are presented.

2.3 CONFIGURATION ALTERNATIVE DEFINITION

The cycle configuration alternatives considered are illustrated in Figure 2-4. Six basic configurations were identified for each plant size range. The open simple cycle (OS) is the least complex and most readily available system. The closed regenerated and intercooled cycle (CRI) is the most complex and least readily available system. Open and closed systems with intercooling only showed no significant advantage over the simple cycles and were not considered

Table 2-2. Baseline System Definition

System:		
Power range, MW_e	2	25
Working fluid	air	air
Cycle configuration	Open cycle	Open cycle
Collector Subsystem:		
Heliostat	MDC 2nd Gen.	MDC 2nd Gen.
Field configuration	north	north
Field area, m^2	72,400	603,000
Mirror area, m^2	13,758	136,902
Number of heliostats	242	2408
Receiver Subsystem:		
Receiver type	Cavity	Cavity
Number of apertures	1	1
Aperture shape	Elliptical	Elliptical
Aperture width, m	4.80	9.70
Aperture height, m	3.12	7.28
Aperture area, m^2	11.76	55.46
Aperture inclination fm. vert.	40°	40°
Cavity diameter, m	8.93	17.98
Cavity height, m.	6.37	12.19
Heat exchanger tube	Ceramic tube	Ceramic tube
Number of HX panels	7	8
Total tube number	266	1128
Tube inside diameter, cm	1.65	1.65
Tube length, m	7.35	10.97
HX area, m^2	101.3	651.9
Tube pitch (minimum)	3.0 tube dia.	3.0 tube dia.
Inlet air temp, ^oC	315	417
Outlet air temp, ^oC	899	1204
Max tube temp, ^oC	982	1260
Inlet pressure, MPa	0.848	1.70
Pressure loss, % of inlet	10	10
Thermal efficiency	85%	85%
Solar input, kW_t	9013	78,000
Tower height, m	34	104
Tower type	steel	steel
Estimated receiver mass, kg	22,700	227,000
Electrical Power Generation Subsystem:		
Pressure ratio	9.0	18.0
Turbine inlet temp, ^oC	899	1204
Mass flowrate, kg/s	11.79	72.39
Cycle efficiency	24.1%	32.5%
Turbomachinery location	Tower base	Tower base

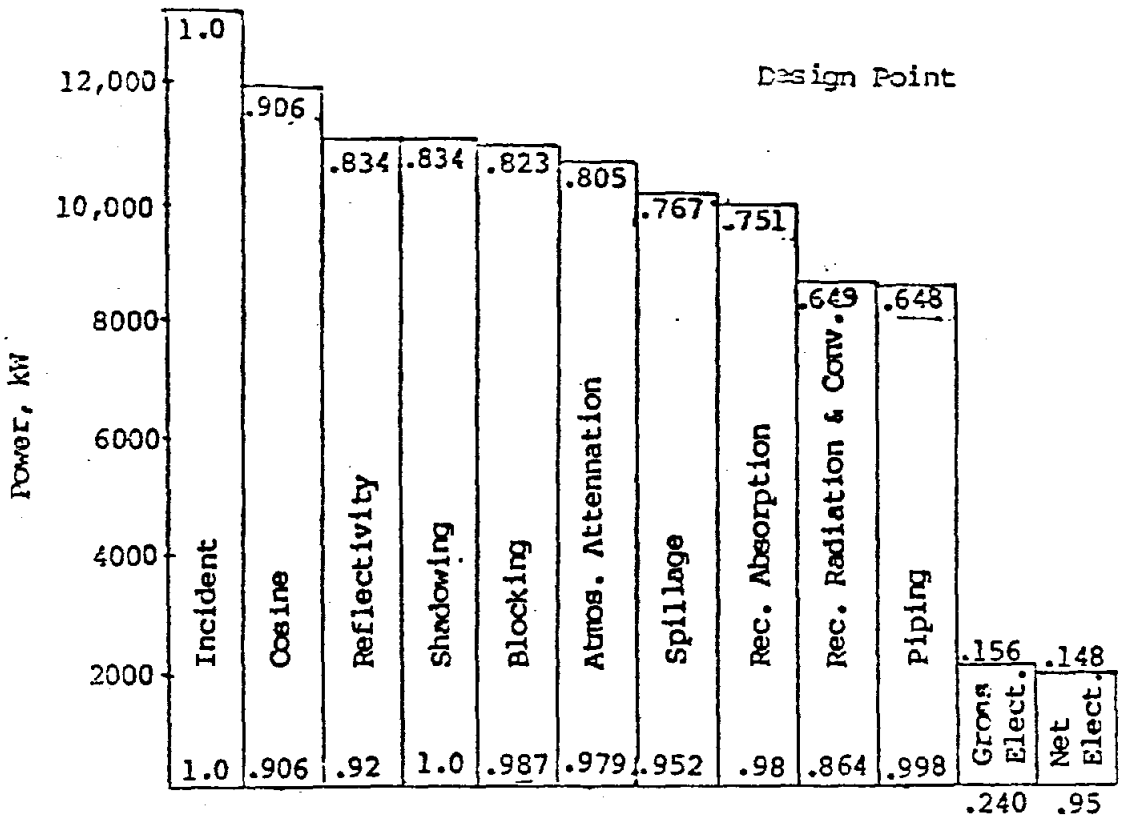

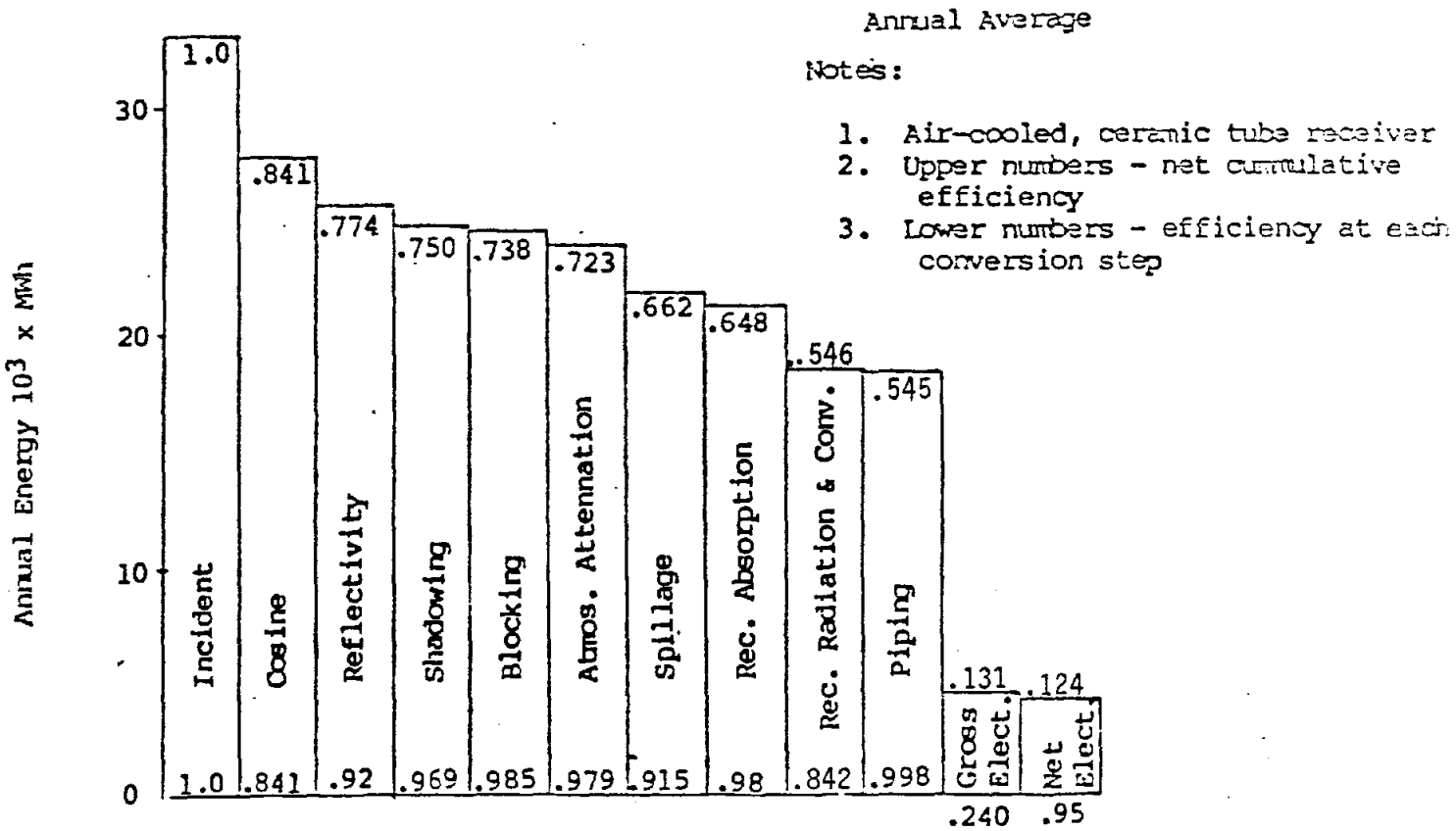

Figure 2-2. Baseline System Performance - 2MWe Plant

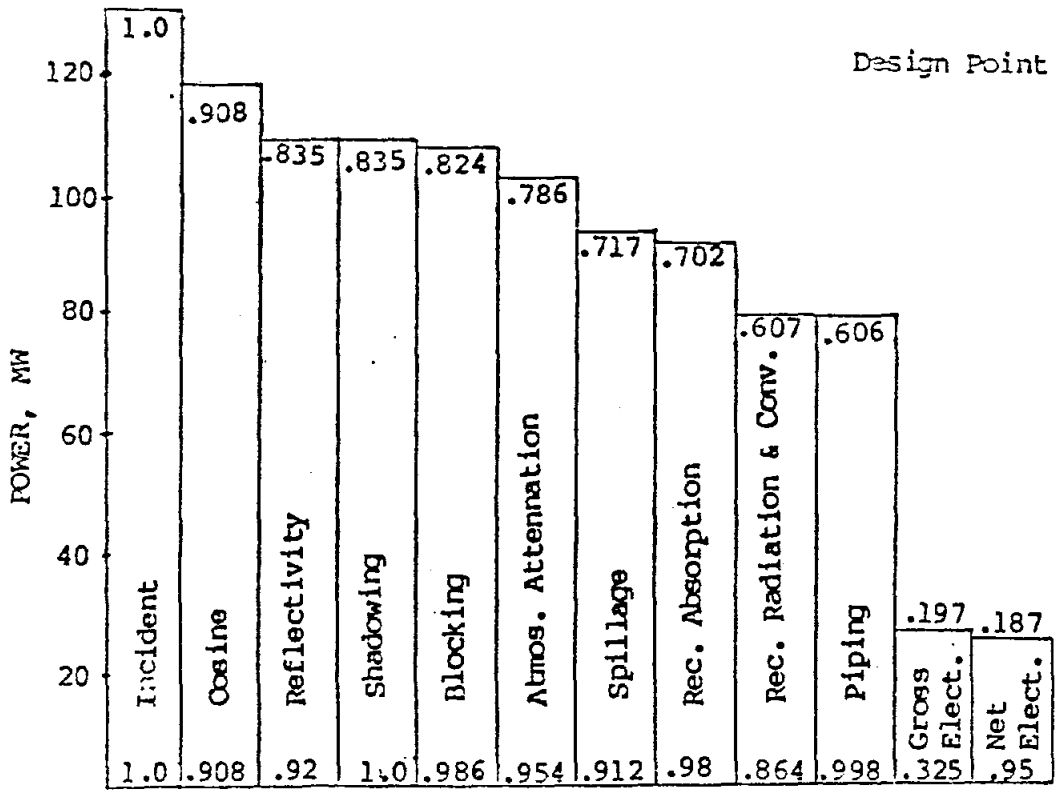

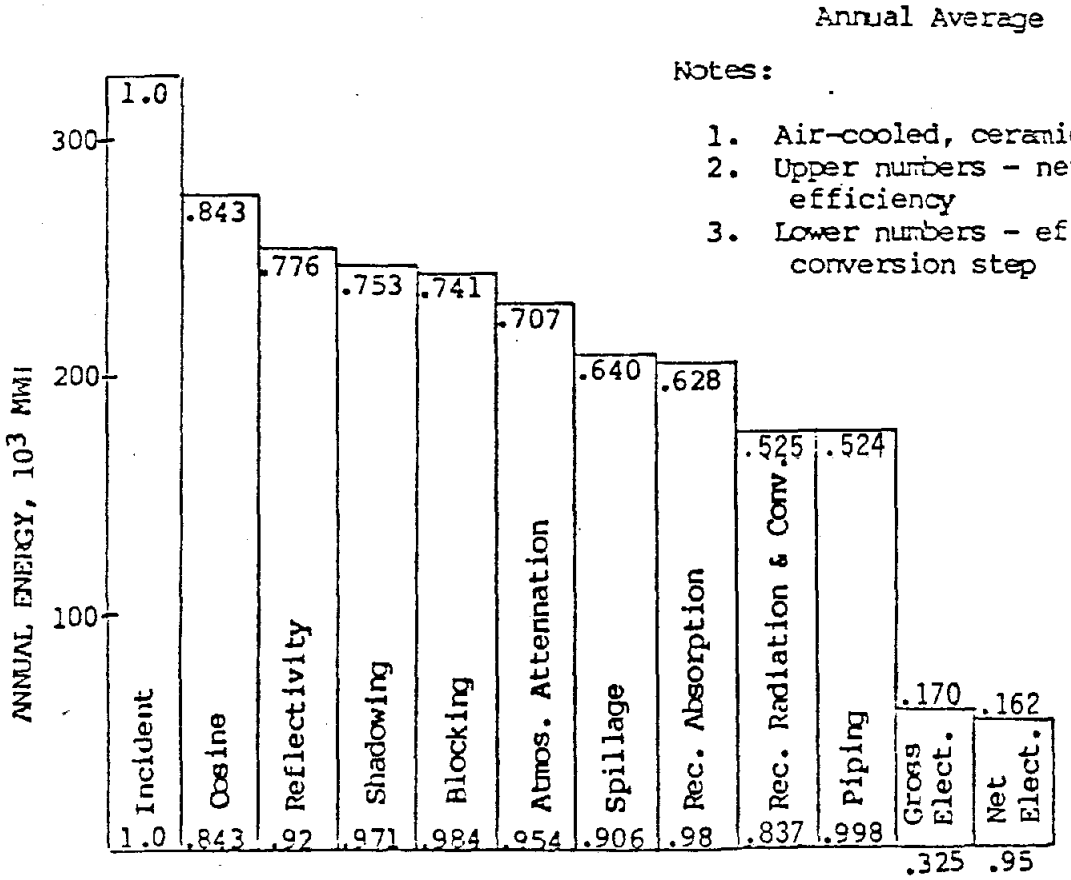

Notes:

1. Air-cooled, ceramic tube receiver
2. Upper numbers - net cumulative efficiency
3. Lower numbers - efficiency at each conversion step

Figure 2-3. Baseline System Performance - 25MWe Plant

further. The design point performance of each of these configuration alternatives was evaluated and compared. The methods and results are described in the following sections.

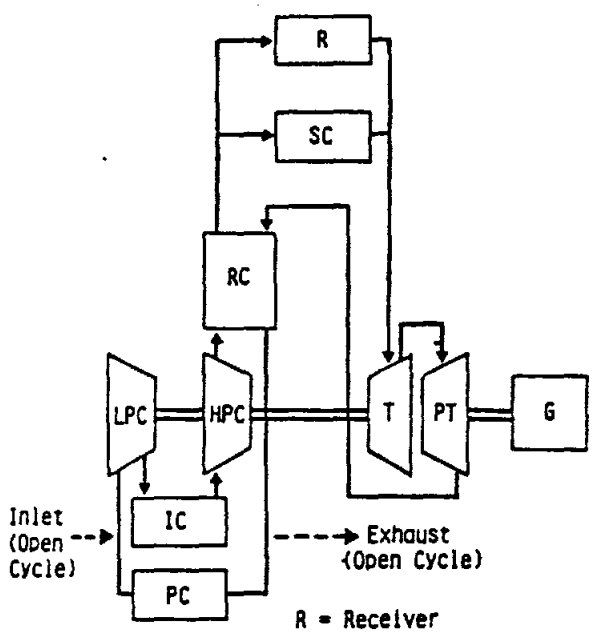

Configuration	Component: Turbomachine	Recuperator	Precooler	Intercooler	Designator
Closed, Simple	X		X		CS
Open, Simple	X				OS
Closed, Regenerated	X	X	X		CR
Open, Regenerated	X	X			OR
Closed, Regen. & Intercooled	X	X	X	X	CRI
Open, Regen. & Intercooled	X	X		X	ORI

R = Receiver
SC = Startup Combustor
C = Compressor
LPC = Low Pressure Compressor
HPC = High Pressure Compressor
PC = Precooler
IC = Intercooler
RC = Recuperator
T = Turbine
PT = Power Turbine
G = Generator

Figure 2-4. Cycle Configuration Alternatives

2.4 CYCLE PERFORMANCE ANALYSIS

The cycle efficiencies (ratio of electrical output to turbine thermal input) for the configurations of Figure 2-4 were evaluated over a range of pressure ratios and turbine inlet temperatures. Configurations were compared for both 2-MWe and 25-MWe power plants. In summary, the open cycle, regenerated and intercooled (ORI) cycle configurations produced the peak cycle efficiencies for both plant size ranges. Peak cycle efficiencies of up to 49.5% occurred at pressure ratios of 10 and turbine inlet temperatures of 1116°C (2040°F). The cycle model and detailed performance data are presented in the following sections.

2.4.1 Cycle Performance Model

The power plant design analysis used the Boeing proprietary computer program, GSA, which is a general purpose thermodynamic gas turbine simulation program (14). GSA is used by Boeing Commercial Airplane Company (BCAC) to model performance of engines proposed for current and future Boeing aircraft. The program calculations are based on dry air as a real gas with allowance for inclusion of hydrocarbon combustion products. Modular program inputs allow flexible arrangement of basic engine components such as inlets, nozzles, ducts, heat exchangers, transmissions, compressors, turbines, splitters, mixers and combustors.

GSA was used for design point and off-design analyses. In the design point analysis, the gas turbine was sized for each set of given parameters. In the off-design analysis, selected design cycles were considered with compressor and turbine performance maps representative of aircraft-derivative gas turbine power plants. Dynamic engine analysis would also be available with GSA with the addition of a control system, component inertias, volumes and thermal time constants to the base model. Dynamic analysis was beyond the scope of the present effort.

In 1978, BEC subcontracted to the United Technologies Research Center (UTRC) a study of closed cycle air turbines for the Advanced Central Receiver (7) program. The GSA closed cycle performance results were verified by matching data from the UTRC report (15) as shown in Table 2-3.

The design study used the following range of design variables:

Overall Pressure Ratio = 2-35

Turbine Inlet = 838-1394°C (1540-2540°F)

The values of pressure losses, heat exchanger effectivenesses, and component efficiencies used in this study are shown on Figure 2-5. The simulation diagram of Figure 2-5 shows the components modeled for an open cycle with recuperator and intercooler or a closed cycle with recuperator, intercooler and return duct precooler. Both the intercooler and precooler heat exchangers reject heat to an inexhaustible, constant 15°C (59°F) temperature reservoir.

Table 2-3. Comparison of GSA Results to UTRC Report (15)

- Efficiency 41.9%
- Output 75 MW_e

Cycle State Points	Temperature (°C)		Pressure (bar)		Mass Flow Rate (kg/sec)	
	UTRC	GSA*	UTRC	GSA*	UTRC	GSA*
1. Low Compressor Inlet	37.78	37.78	7.55	7.55	452.09	453.30
2. Low Compressor Outlet	127.56	127.32	16.82	16.83	452.09	453.30
3. Intercooler Inlet	127.56	127.32	16.77		452.09	453.30
4. Intercooler Outlet	37.78	37.80	16.60		452.09	453.30
5. High Compressor Inlet	37.78	37.80	16.56	16.57	452.09	453.30
6. High Compressor Outlet	125.99	125.96	36.08	36.10	449.83	451.03
7. Recuperator Cold Inlet	125.99	125.96	35.98		449.83	451.03
8. Recuperator Cold Outlet	466.63	468.62	35.72	35.74	449.83	451.03
9. High-Turbine Inlet	815.56	815.54	34.48	34.50	449.83	451.03
10. High Turbine Outlet	656.42	656.70	17.07	17.08	450.96	452.17
11. Power Turbine Inlet	656.42	656.70	17.07	17.08	450.96	452.17
12. Power Turbine Outlet	503.63	504.32	7.99	7.99	452.09	453.30
13. Recuperator Hot Inlet	503.63	504.32	7.95		452.09	453.30
14. Recuperator Hot Outlet	167.86	166.01	7.69	7.69	452.09	453.30
15. Precooler Inlet	167.86	166.01	7.67		452.09	453.30
16. Precooler Inlet	37.78	37.80	7.60	7.55	452.09	453.30

*Assumed values for GSA simulation

- Intercooler 100%
- Precooler 100%
- Gearbox 98.6%

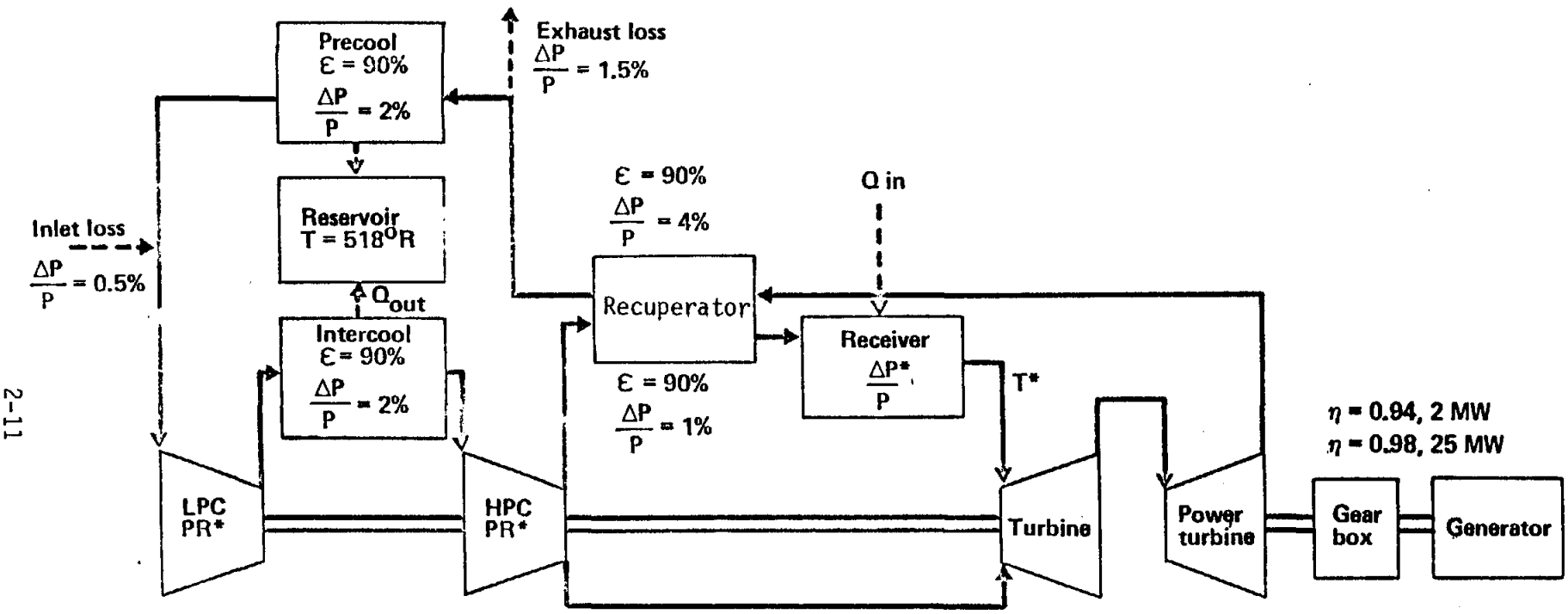

*denotes independent variables in study.

Figure 2-5. Cycle Model Configuration Diagram

The receiver pressure loss was selected as 10%. A two shaft gas turbine as shown in the figure was used for the design point analysis. A single shaft configuration would show similar characteristics in the design point study.

The model used polytropic compressor and turbine efficiencies consistent with projected 1985 component technology. The efficiencies used for the 25-MW_e power plant are shown on Figure 2-6. The compressor and turbine efficiencies for the smaller 2-MW_e power plant are also shown in Figure 2-6. These efficiencies were picked lower than those for the 25-MW_e power plant because of the decreased compressor and turbine size. The efficiencies worsen with rising design overall pressure ratio to simulate increased losses due to decreasing flow area of rear compressor and inlet turbine stages.

A portion of compressor discharge flow was used for turbine cooling in the model. No cooling is used for design turbine inlet temperatures less than 1010°C (1850°F). The cooling flow schedule was based on aircraft propulsion engines that have overall pressure ratios between 25 and 35 and have neither recuperators nor intercoolers. Because of this, the assumed cooling air flows are higher than would be required for regenerated and intercooled engines operating with pressure ratios between 5 and 10. These cycles would have cooler and more effective compressor discharge air available as cooling air delivered to the turbine.

The compressor-turbine power transmission efficiency was assumed to be 100%. There was no leakage modeled in the design studies.

2.4.2 Performance Analysis Results

<u>Design Point Cycle Performance</u>

Cycle efficiency was evaluated for a range of temperatures and overall pressure ratios as shown in Figures 2-7 to 2-10 for the following 25-MW_e cycle configurations: open simple (OS), open with recuperator (OR), closed with recuperator and intercooler (CRI) and open with recuperator and intercooler (ORI).

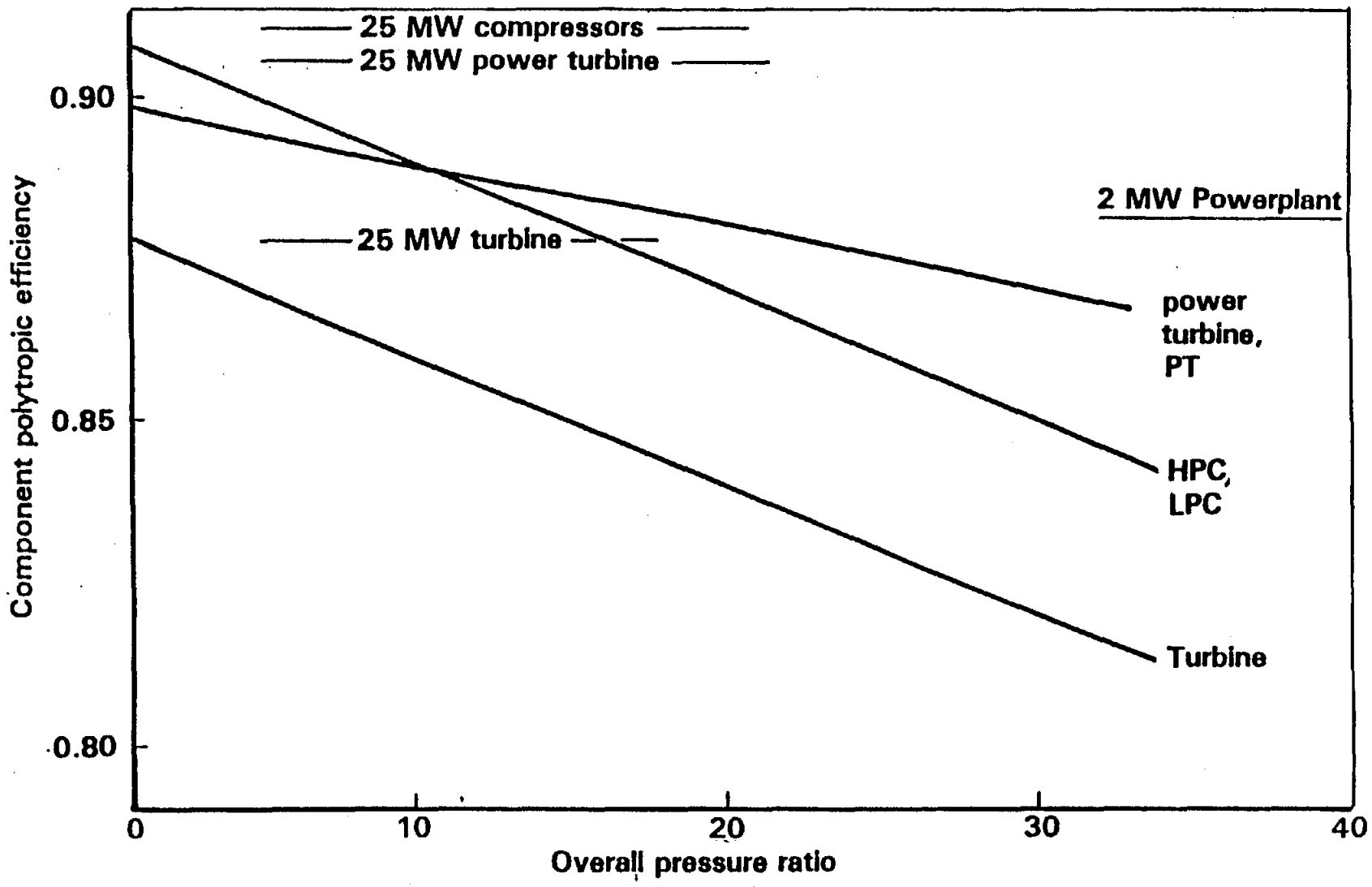

Figure 2-6. Component Polytropic Efficiencies Verses Pressure Ratio

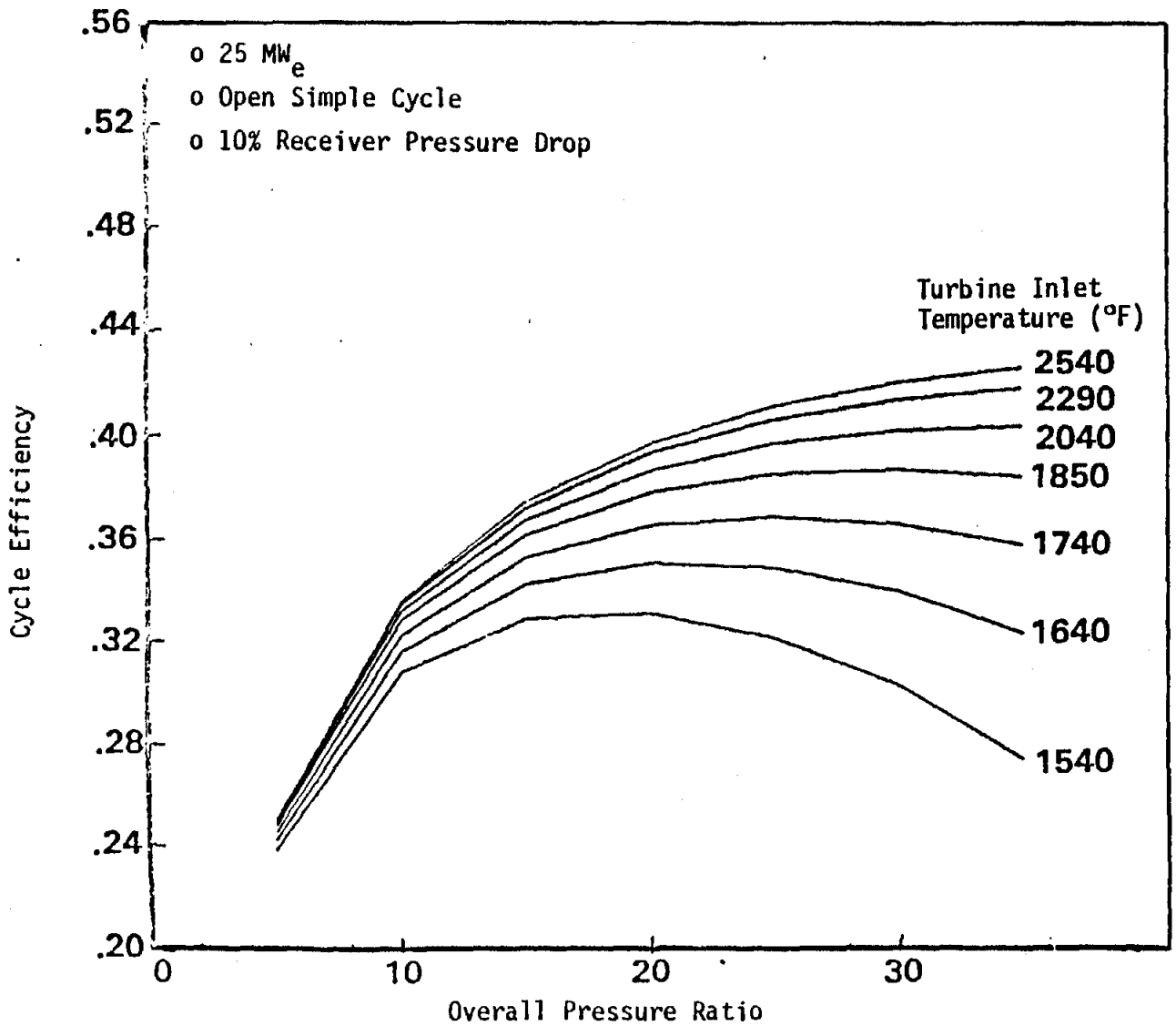

Figure 2-7. Cycle Efficiency Verses Pressure Ratio - 25-MW_e, Open Simple Cycle Configuration

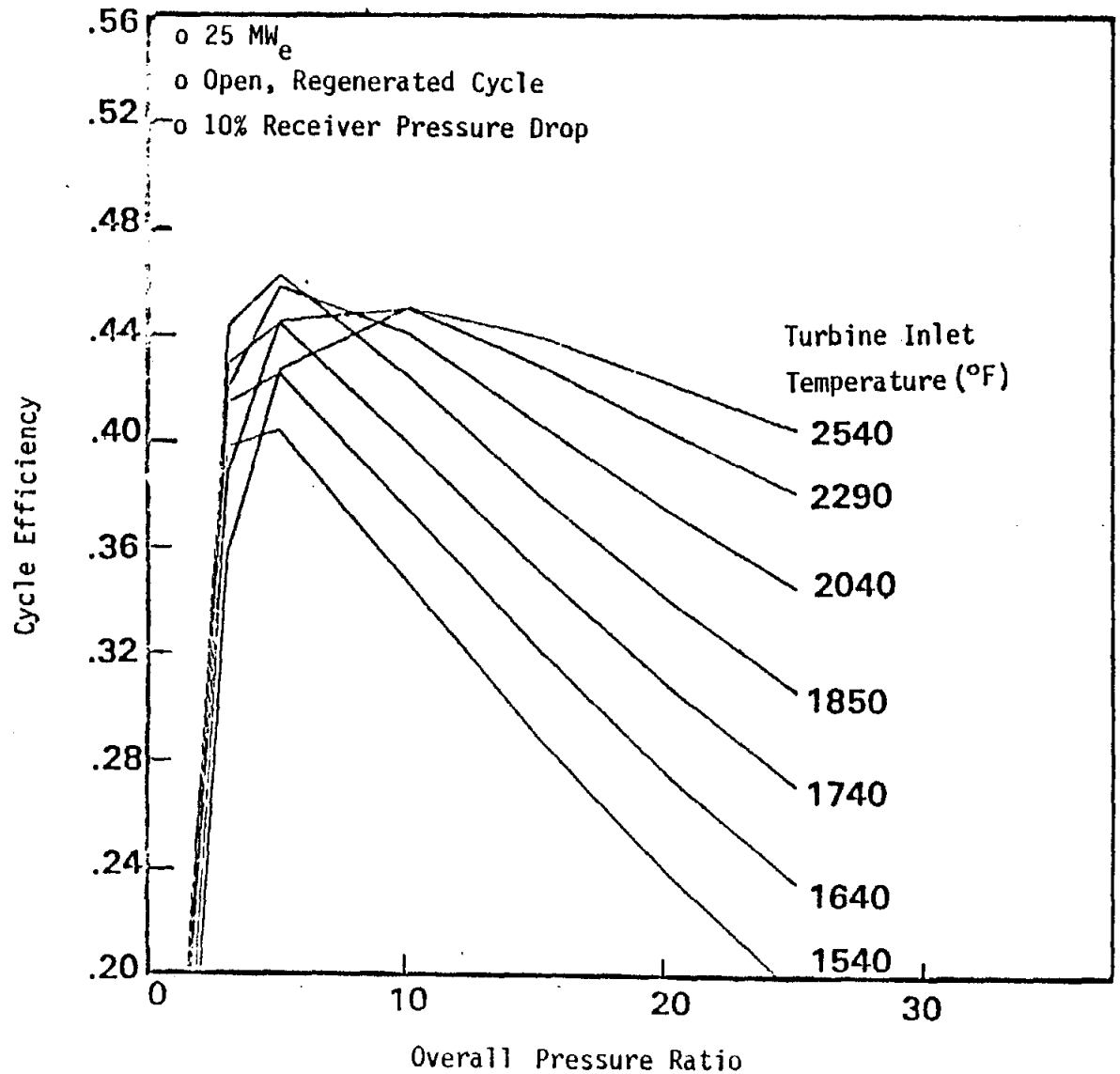

Figure 2-8. Cycle Efficiency Verses Pressure Ratio - 25-MW_e, Open Regenerated Configuration

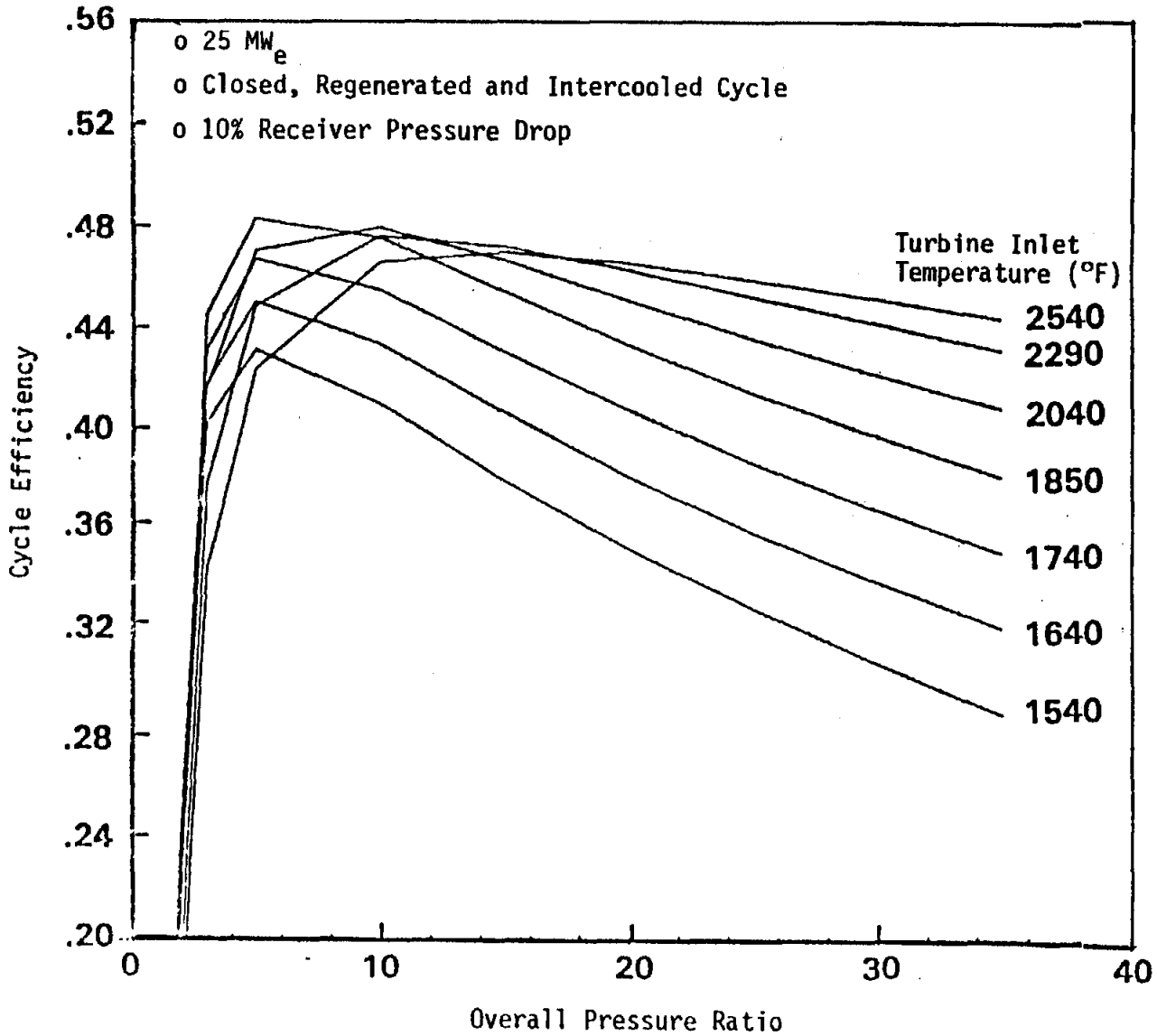

Figure 2-9. Cycle Efficiency Verses Pressure Ratio - 25-MW_e, Closed Regenerated and Intercooled Configuration

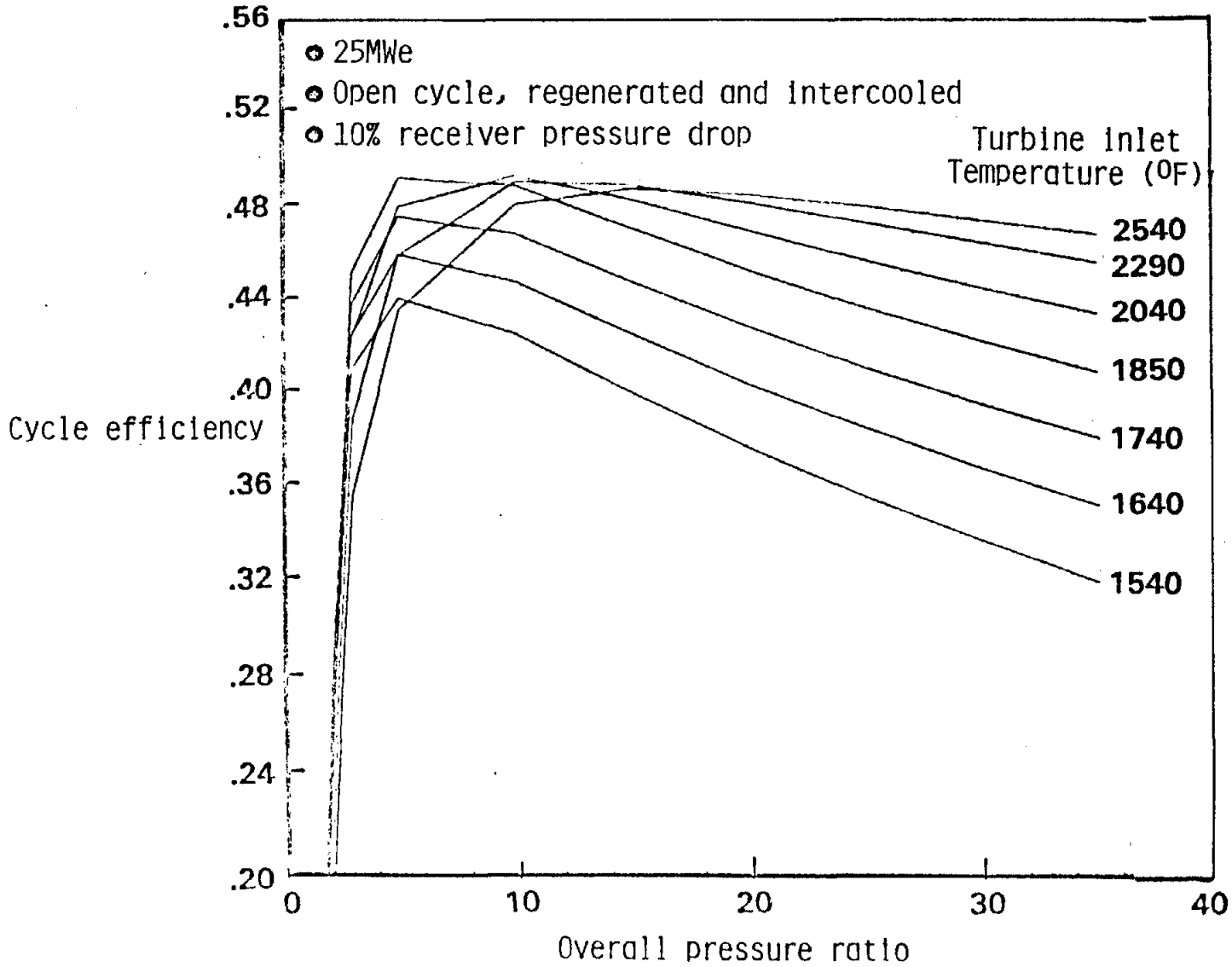

Figure 2-10. Cycle Efficiency Verses Pressure Ratio - 25-MW_e, Open Regenerated and Intercooled Configuration

The ORI configuration showed the highest thermal efficiency at 1116°C (2040°F) with an overall pressure ratio = 10. The 1116°C (2040°F) temperature was selected as the basis of comparison for all configurations.

The performance of the 25-MW_e cycle configurations studied are summarized in Figure 2-11 versus overall pressure ratio. The configurations are compared at 1116°C (2040°F) turbine inlet temperature. Cycle efficiencies for a 2-MW_e powerplant are compared in Figure 2-12 for selected configurations. Performance levels are lower than the 25-MW_e cycles due to decreased component efficiencies. The peak efficiency occurs at overall pressure ratio of 5 compared to 10 for the 25-MW_e plant. The following sections describe conclusions drawn from these figures.

Simple Cycle Configurations. The peak efficiency occurs at overall pressure ratios greater than 30 for the open simple (OS) cycle and at 25 for the closed simple cycle (CS). OS cycle performance was about 5 percentage points higher than the CS. The difference between open and closed cycle efficiencies occurs because the compressor inlet temperature was higher in the closed cycle. The cycles were compared at a standard temperature (15°C [59°F]) day. The open cycle delivers constant ambient temperature air to the compressor regardless of pressure ratio. The closed cycle delivers air to the compressor from a precooler which is rejecting heat to the atmosphere at an effectiveness of 90%. Therefore, the compressor inlet temperature for the closed cycle increased with pressure ratio. At higher pressure ratios, the compressor inlet temperature difference between open and closed cycles increases, causing the closed cycle performance to decrease. These open-closed cycle temperature differences were present in all the configurations compared.

Regenerated Cycle Configurations. The addition of a recuperator to the cycle transfers excess energy from the power turbine exit to the compressor exit. This increases the receiver inlet temperature, thus requiring less solar energy to be absorbed into the cycle for the same electrical output. The maximum cycle efficiency occurs at a lower pressure ratio than other configurations. Maximum open cycle efficiency is 6 percentage points greater with a recuperator.

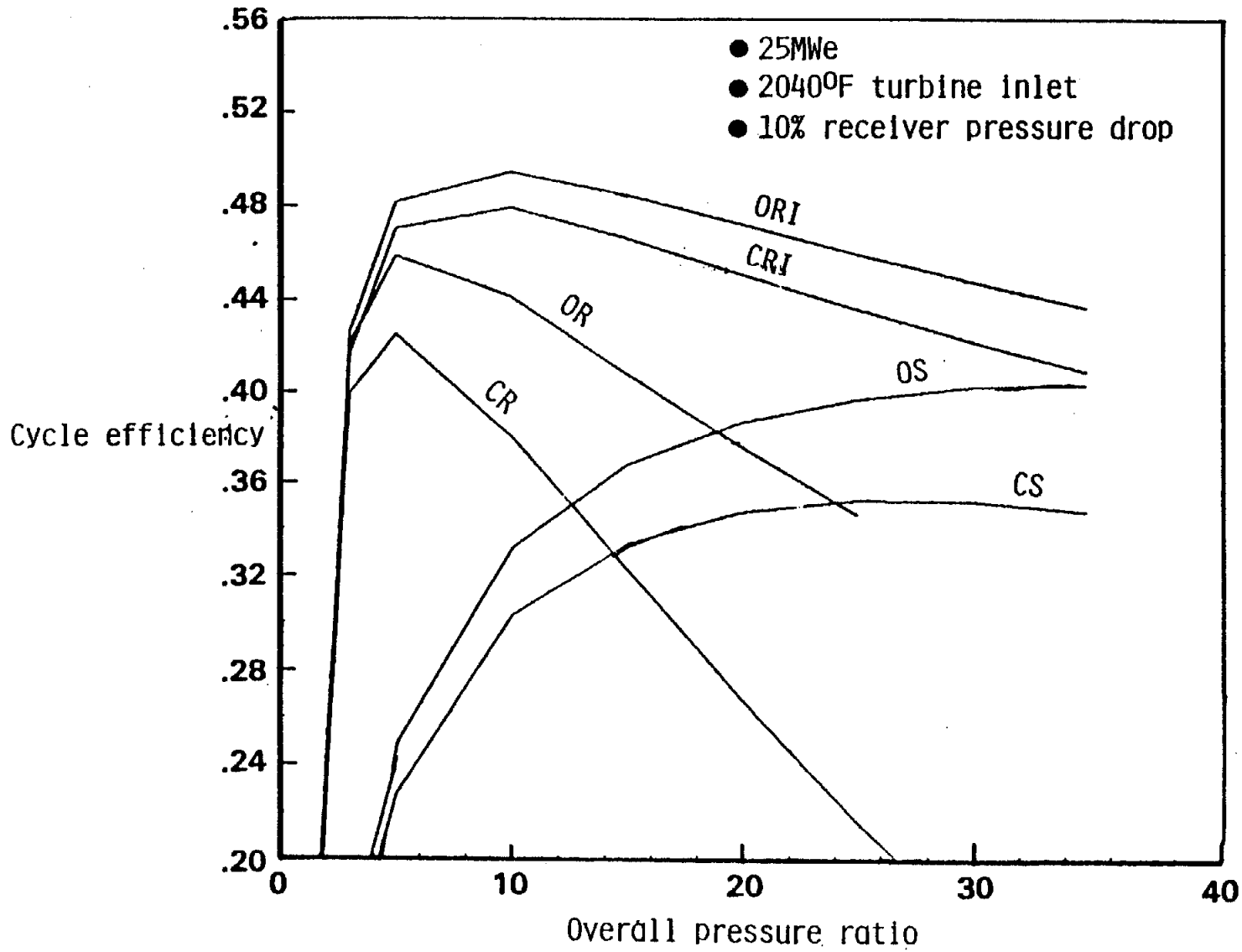

Figure 2-11. Cycle Efficiency Verses Pressure Ratio - 25-MW_e Cycle Configurations Comparison

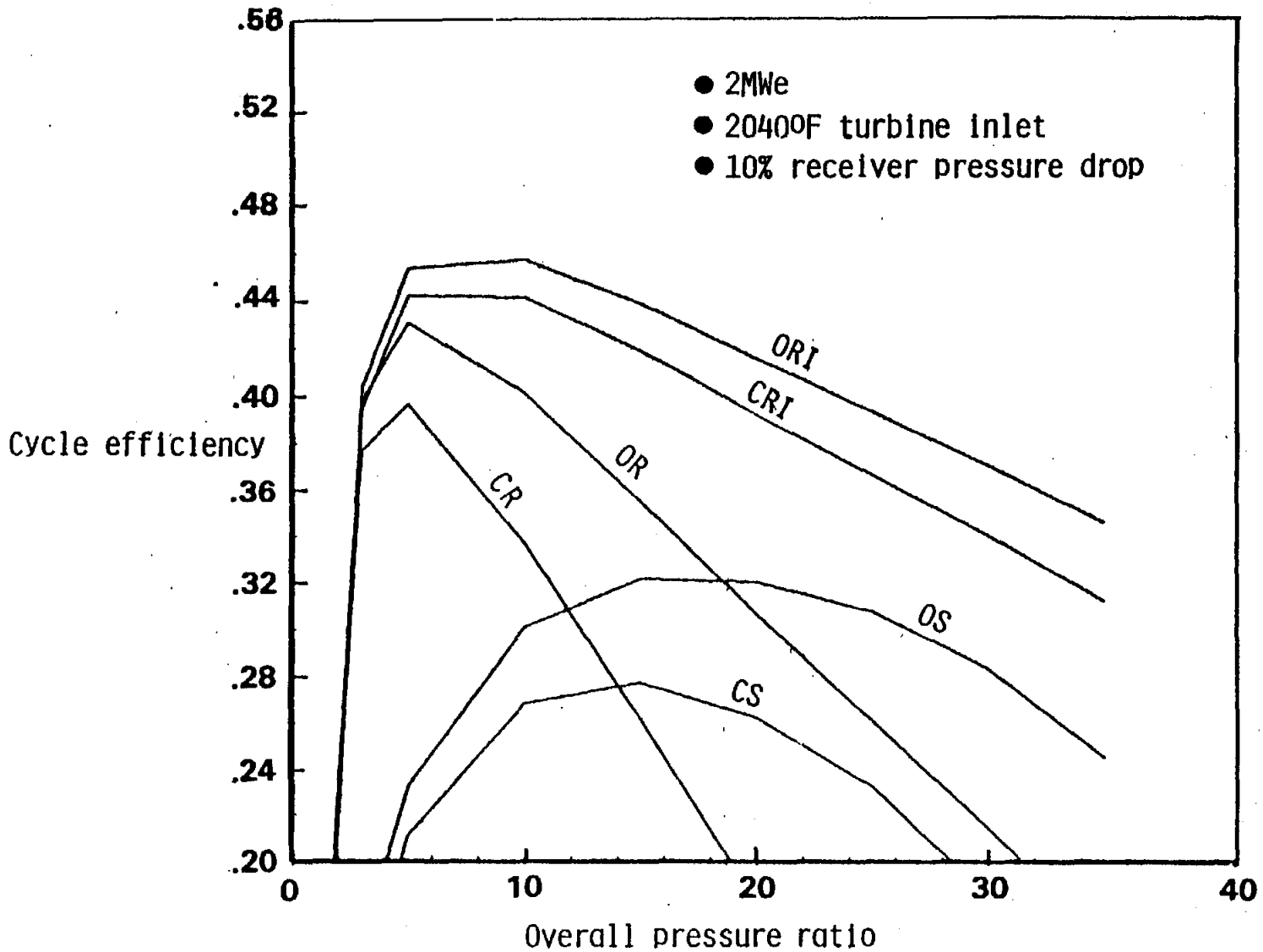

Figure 2-12. Cycle Efficiency Verses Pressure Ratio - 2-MW_e Cycle Configurations Comparison

Intercooled Cycle Configurations. Cooling during compression reduces the work required to increase the pressure to a given value. Use of intercooling alone, however, produces slight increases in cycle efficiency over the simple cycle configurations only at high pressure ratios (>20). Open or closed intercooled configurations without regeneration were not considered further.

Regenerated and Intercooled Cycle Configurations. Open and closed cycles with both recuperator and intercooler shows the best cycle performance. The addition of the intercooler reduced both the compressor work required and the high-pressure side recuperator inlet temperature. This allows more of the turbine exhaust energy to be transferred to the high pressure circuit. Peak efficiency for the ORI cycle occurs near a pressure ratio of 10 and is 10 percentage points better than the OS configuration. Efficiency falls off with increasing pressure ratio, but more slowly than with a recuperator alone.

Cycle Energy Transfer. A comparison of the energy transfer in the optimum ORI and optimum OS cycles is shown in Figures 2-13 and 2-14. Energy is input to the cycles from the receiver and is extracted from the power turbine to generate electrical power. Energy is lost to the surroundings by kinetic energy and heat rejected through the nozzle, intercooler, gearbox and generator.

Energy lost at the nozzle is primarily due to flow exiting with higher than ambient temperature. Losses may be reduced by the transfer of heat energy from the turbine exit to the compressor exit with the recuperator. Energy lost due to increased air velocity is small.

For an OS cycle, efficiency increases with increasing pressure ratio as shown in Figure 2-11. With the addition of a recuperator, the cycle efficiency is greatly improved at low pressure ratio, but the effect decreases with increasing pressure ratio. At lower pressure ratio, the cycle energy at the power turbine exit is higher than the compressor exit allowing a recuperator to transfer energy (Figure 2-13). As pressure ratio and the energy level at the compressor exit increase, the turbine requires more energy to drive the

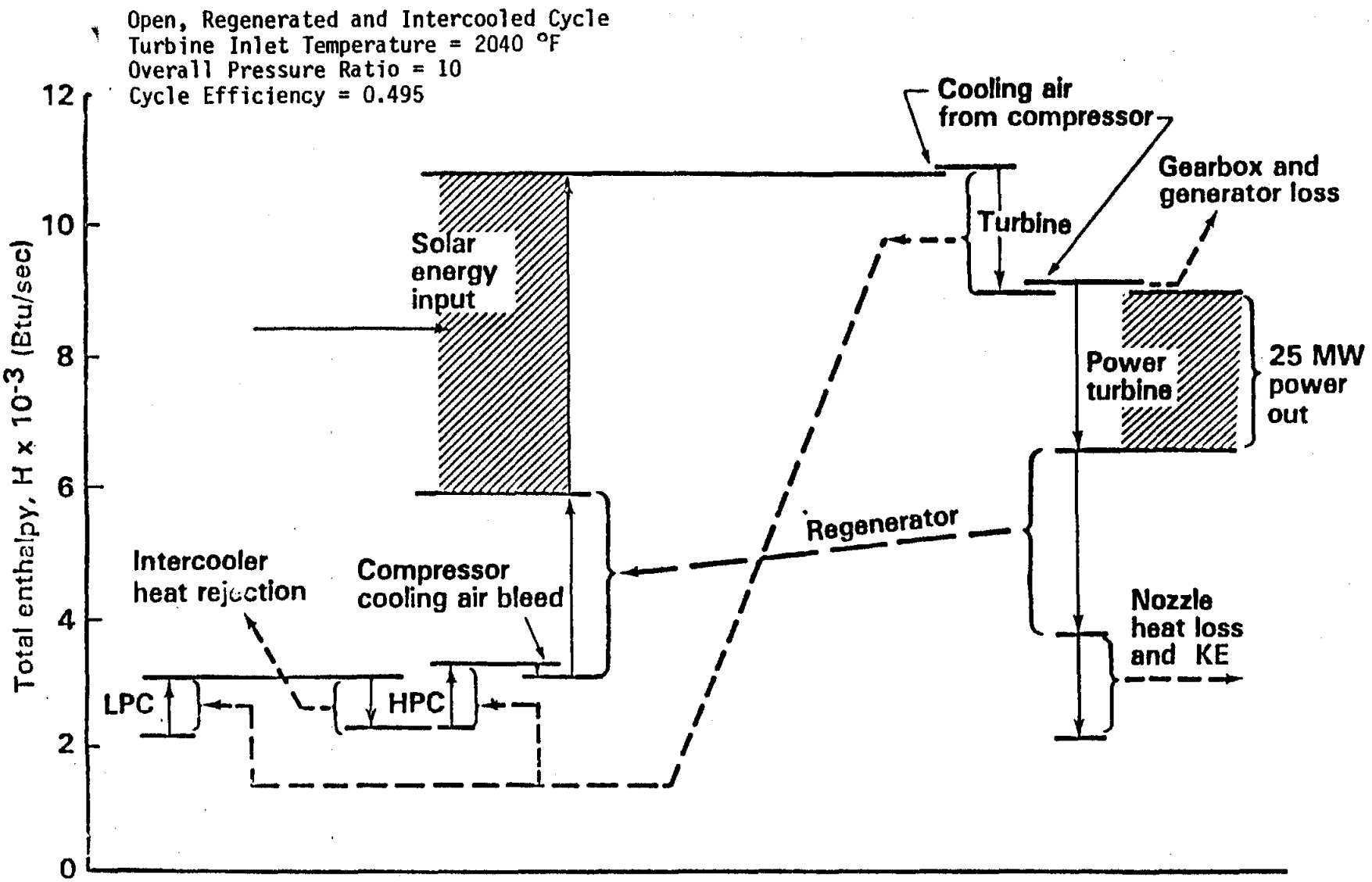

Figure 2-13. Energy Flow for an Intercooled and Regenerated Cycle

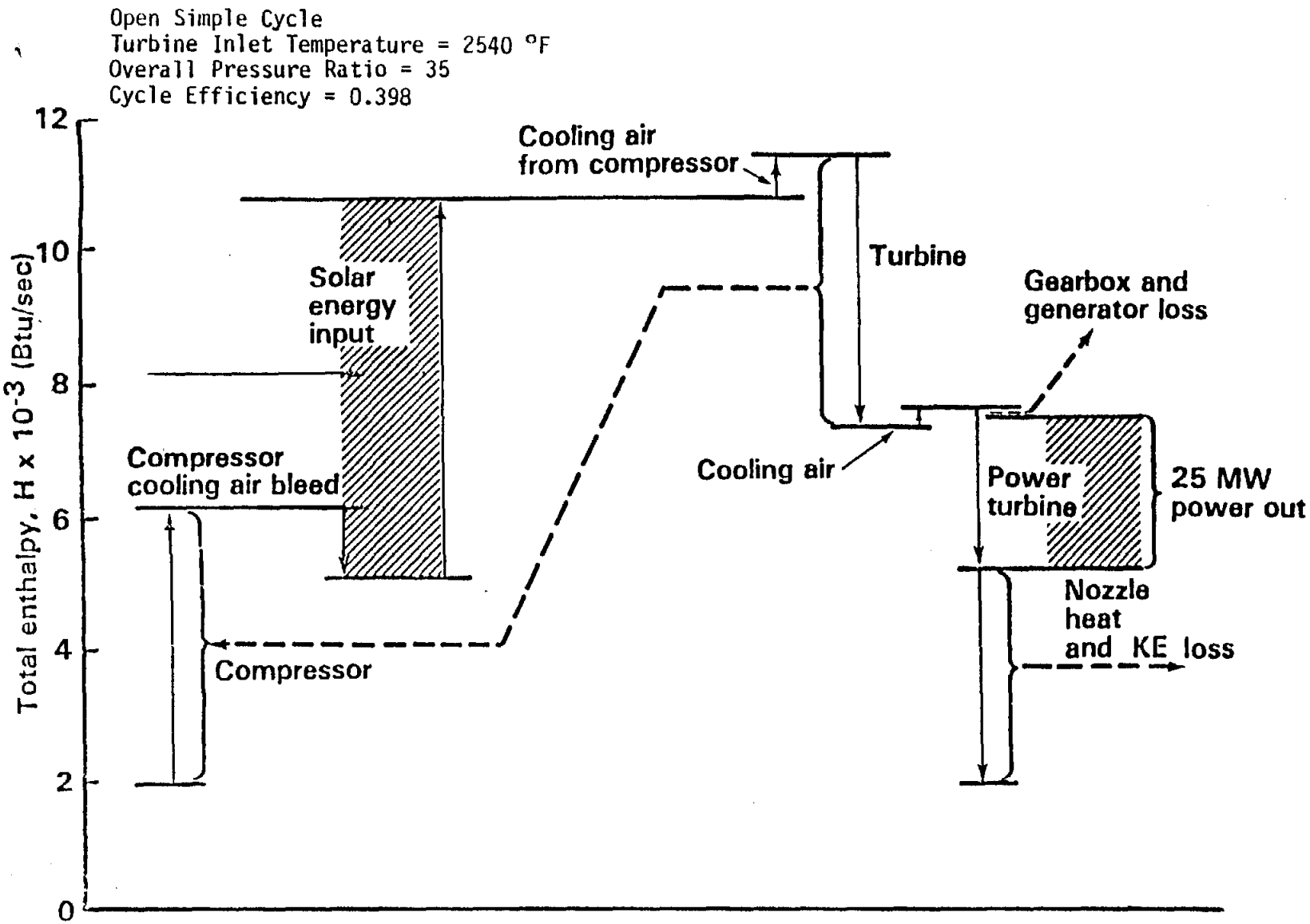

Figure 2-14. Energy Flow for a Simple Cycle

compressors, causing the power turbine exit energy level to decrease. This can be seen in Figure 2-14 which describes energy levels for a high pressure ratio machine.

The addition of an intercooler to the low pressure ratio regenerated cycle in Figure 2-13 lowers the energy level at the compressor exit, allowing more energy to be transferred by the recuperator. Because the compression occurs at a lower temperature, less energy is required to drive the compressor and therefore less must be provided by the turbine. This results in a higher power turbine exit energy level which also contributes to increased recuperator energy transfer.

Over 50% of the energy input to the simple cycle in Figure 2-14 is lost at the nozzle exhaust. This loss drops to about 30% for the regenerated and intercooled cycle in Figure 2-13.

The OS cycle has a higher optimum pressure ratio, and therefore a greater portion of cycle energy transfer occurs between the turbine and compressor. The higher optimum temperature (at the study limit of 1393°C [2540°F]) requires a greater cooling air flow.

Cycle Component Efficiency Influence Coefficients. Several component efficiency parameters were varied independently to determine their influence on performance for the ORI configuration. The results are shown in Table 2-4 for pressure ratio = 10, turbine inlet temperature = 1116°C (2040°F), and receiver pressure loss = 10%.

All pressure losses were varied separately and showed that generally a 1 percentage point change in any cycle pressure loss affects the cycle thermal efficiency by 0.2 percentage point. The receiver pressure loss was varied between 5% and 20%. The various configurations showed the same performance characteristics with varying turbine inlet temperature and pressure ratio.

Table 2-4. Sensitivity of Cycle Efficiency at Design Point to Component Efficiency Changes

Efficiency		49.5%	45.4%
		25 MW	2 MW
	Δ Variable	(%)	(%)
T inlet, precooler, intercooler	$-10^{o}F$	0.67	0.52
T intercooler reservoir (open cycle)	$-10^{o}F$	0.25	0.19
Gearbox-generator efficiency	1%	0.51	0.48
η_c, compressor efficiency	1%	0.52	0.40
Leakage, % compressor corrected flow	1%	0.43	0.36
ϵ, regenerator effectiveness	1%	0.32	0.55
	10%	3.03	4.96
η_{PT}, power turbine efficiency	1%	0.27	0.27
η_T, turbine efficiency	1%	0.18	0.17
ϵ_p, precooler effectiveness (closed cycle)	1%	0.16	0.13
ϵ_i, intercooler effectiveness	1%	0.06	0.03
$\Delta p/p$ cycle	1%	0.20	0.29
	2%	0.40	0.57
Additional power extraction for auxiliary equipment	100hp	0.14	3.23

The inlet temperature and reservoir temperature (temperature to which precooler and intercooler heat is rejected) were varied for both the ORI and CRI cycles. When the ORI cycle was assumed to have an intercooler reservoir temperature 5.6°C (10°F) less than ambient inlet air, the cycle efficiency improved 0.25 of a percentage point. The ORI cycle efficiency varied 0.67 of a percentage point when both the inlet and reservoir temperatures were varied by 5.6°C (10°F).

Off-Design Analysis. The open cycle 25-MW_e OS and ORI configurations were selected for an off-design analysis of the respective optimum efficiency design points. The off-design performance was compared as the cycles were varied between 20% and 115% of design point power output. In summary, the dual-shaft ORI cycle configuration produced the best performance over the power output range. Analysis details are presented in the following paragraphs.

The off-design performance of the OS and ORI configurations compared single and dual shaft gas turbines. The single shaft configuration has compressor, turbine and power output generator on a single shaft. The shaft speed must be held constant for electrical power frequency control. The dual shaft configuration has a separate constant speed power output shaft connecting a power turbine with the electric generator. A second independent shaft connecting the compressor and turbine is not speed controlled.

Since the single shaft configurations must run at constant speed, the compressor and turbines continue to operate near their design points as power output is varied. However, the compressor and turbine operating points in a dual shaft configuration vary with power output. Therefore, the nozzle expansion ratio decreases with turbine inlet temperature and power output in the dual shaft model and stays nearly constant in the single shaft model.

The power plants were assumed to produce power over a range from 20% to over 100% of the design output. Because of this, the design point nozzle area was set so that the nozzle expansion ratio at the 20% power output condition would be greater than 1.01 for engine stability. This caused nozzle expansion ratios at rated output power to be greater for the two shaft model than for the single shaft model. This results in a design point thermal efficiency 0.6 of a percentage point less for the dual shaft ORI model.

The off-design performance of the ORI and OS cycles are compared in Figure 2-15. The curves are normalized to the design point cycle thermal efficiencies and power output. Both single and dual shafts are compared for each cycle. The dual shaft ORI has a lower change of cycle efficiency with decreasing output power than the single shaft ORI cycle. There was no difference shown in cycle efficiency ratio versus power between the single and dual shaft OS cycles.

The shape of the off-design performance curves in Figure 2-15 is a function of the characteristics of the individual compressor and turbine components selected. Typical compressor and turbine maps were used in the off-design study. The off-design characteristics are also effected by the component map locations selected to correspond to the power plant design point. The desired off-design characteristics may be planned for during component design.

The data of this section are used in an evaluation of off-design performance effects on costs in Section 2.6.4.

The off-design performance for five real engines is shown in Figure 2-16. Line 1 represents a two-shaft regenerated engine with variable-area power-turbine nozzle. Line 2 represents a high-pressure ratio, two shaft, simple engine. Line 3 represents a small two-shaft simple turbine. Lines 4 and 5 are for industrial simple single-shaft and two-shaft engines. The predicted ORI, dual shaft off-design performance is better than some gas turbines but still below what is available with a variable-area, power-turbine nozzle.

2.5 TURBOMACHINERY SURVEY

The turbomachinery survey consisted of analysis of published turbomachinery performance and cost data (16) and of data from telephone interviews with engineers in the gas turbine industry. The purpose of the turbomachinery survey was to determine what machines are available commercially for the small central receiver Brayton cycle system size ranges and to identify and understand any obstacles in the way of improving the cycle efficiencies of these systems.

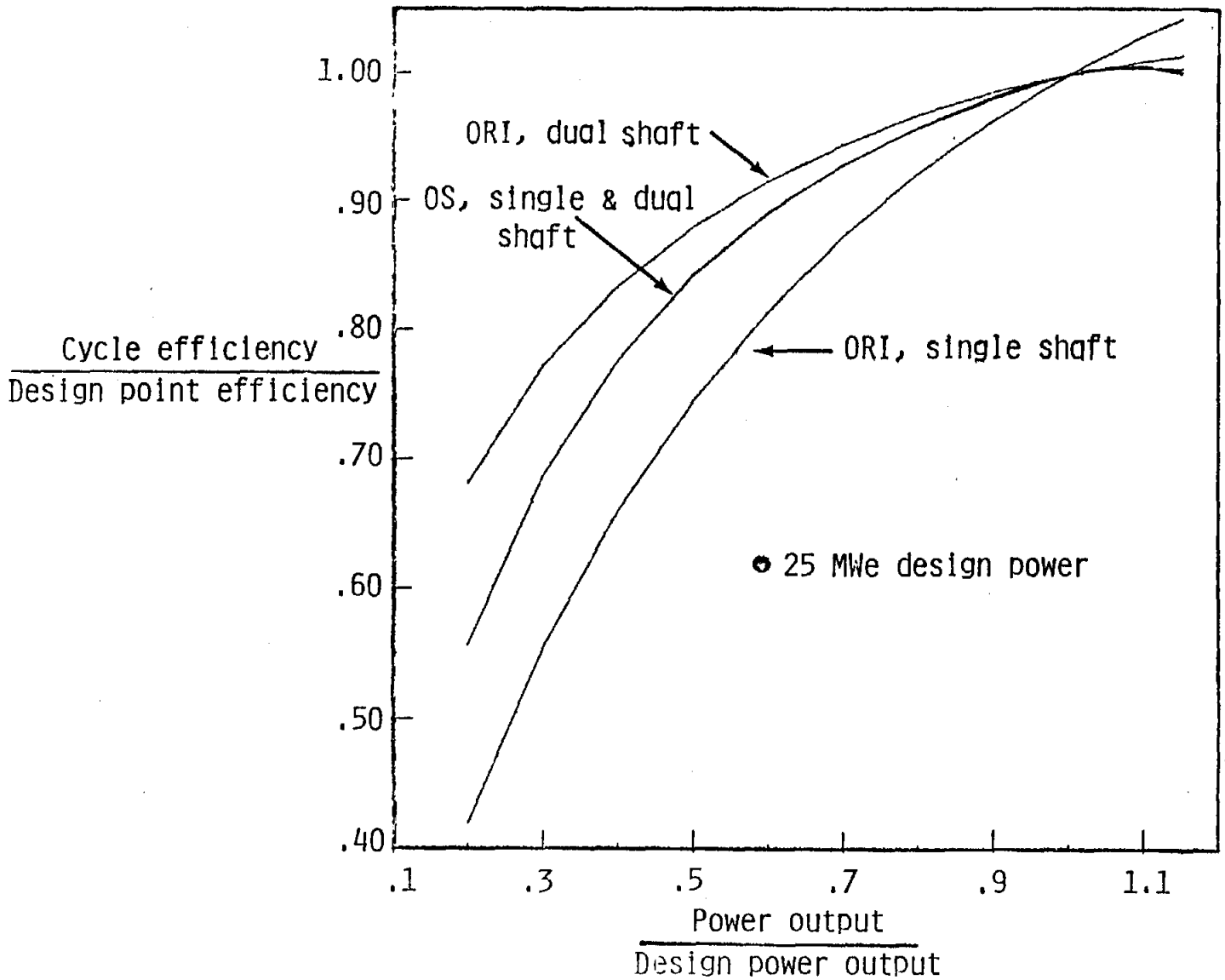

Figure 2-15. Off-Design Performance Effects

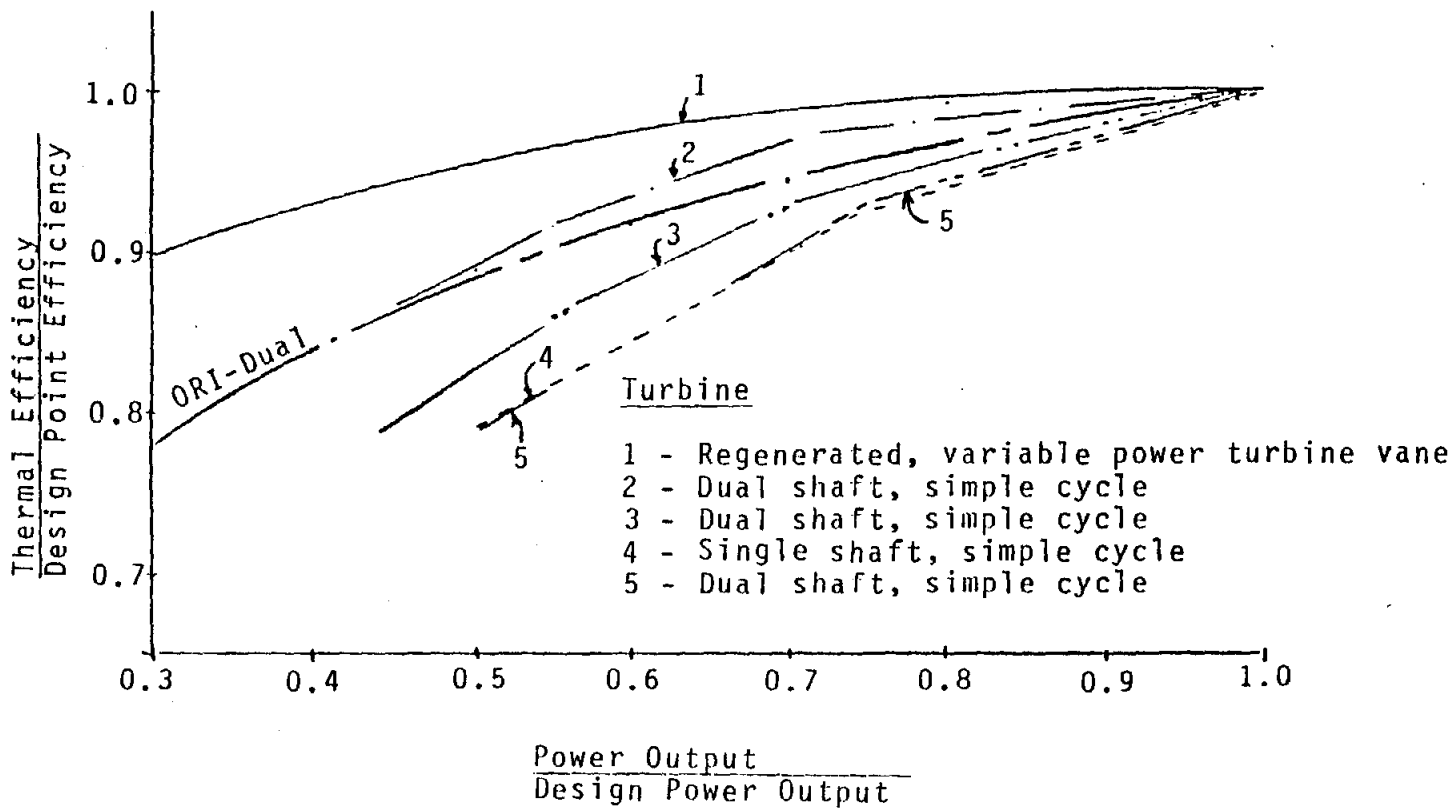

Figure 2-16. Comparison of Off-Design Performance Predictions with Five Real Engines

In summary, the turbomachinery survey identified 111 turbogenerators operating between 500 kWe and 40 MWe. The majority of the turbines are open single cycle configurations. Some regenerated cycles are also offered. Turbomachinery costs varied widely. For the 25 MWe plant, 169.6 $/kWe (1983 $) was chosen as the unit cost; 370 $/kWe was chosen for the 2-MWe plant. Ducting 1093°C+ (2000°F+) air in and out of the gas turbine was identified as a technical concern requiring additional development. Details in each of these areas are presented in the following paragraphs.

The telephone survey was conducted with representatives of companies listed in Table 2-5. Industry engineers were invited to discuss costs, recuperators, operating temperatures, the application of turbines to generate electricity in an isolated system, the effects of long pipes and thermal masses on control requirements, and the possiblity of modifying turbines to solar services. The survey was designed not as a statistical opinion poll but as an exploration of problems and solutions as viewed by these experienced and interested engineers.

Table 2-5. Turbomachinery Survey Telephone Contacts

AVCO LYCOMING, STRATFORD, CT
BROWN-BOVERI TURBOMACHINERY, INC., ST. CLOUD, MN
CURTISS-WRIGHT, WOODRIDGE, NJ
GENERAL ELECTRIC, TUKWILA, WA; SCHENECTADY, NY; CINCINNATI, OH
HAGUE INTERNATIONAL, PORTLAND, ME (RUSTON)
HISPANO-SUIZA, PARIS, FRANCE
KAWASAKI, TOKYO, JAPAN
KONGSBERG (NATCO), HOUSTON, TX
RUSTON GAS TURBINES, INC., HOUSTON, TX
SOLAR TURBINES, SAN DIEGO, CA
SULZER, ZURICH & WINTERTHUR, SWITZERLAND
THOMASSEN (FERN ENGRG, BOURNE, MA)
TURBOMECCA, PARIS, FRANCE
UTC POWER SYSTEMS, E. HARTFORD, CT
WESTINGHOUSE, TUKWILA, WA AND HAMILTON, ONTARIO, CANADA

The collection and analysis of data from reference 16 was performed as a background for the telephone interviews. In the course of this work the notion of the "unique turbine" was found helpful. A "unique turbine" is a turbine of a certain specification designed and produced by a certain manufacturer. That manufacturer may, and often does, license other manufacturers usually in other countries to produce that same turbine or to package it into electrical generating systems for sale under the same name or other names. These "cloned" turbines are considered to be the same as that unique turbine and are ignored in our listing of turbine types. Only unique turbines were considered except when the same turbine is offered with and without a recuperator.

A second distinction of gas turbine types is common in the gas turbine industry and stems from the origin of the turbine. Heavy-duty industrial turbines were designed originally to serve industry, usually by companies that also built steam turbines. These turbines are distinguished by their size and weight. Though smaller and lighter than steam turbines, they are still quite large and heavy. They need strong foundations; their shafts have high angular inertia to hold speed well; and they have thick wall casings and need to have a gradual startup and stop to avoid low-cycle fatigue failures due to thermal expansion. At the other end of the scale are aircraft engines adapted to industrial service. These turbine types are light weight and have thin walls of expensive material; therefore, they can be started more quickly, e.g., two minutes as compared to half an hour. Aircraft-derivative gas turbines are often mounted on comparatively light frames which are shipped with the turbine installed. Originally, aircraft-derivative gas turbines were used for electrical power generation peaking service, though many are used to continuously drive pumps or compressors on pipelines in remote locations. These aircraft derivatives are rarely fitted with recuperators. Size and weight distinction between industrial and aircraft-derivative units are strong at 25 MWe. In the small sizes, below 5 MWe, the size and weight differences lose significance, although the different origins still exist.

2.5.1 Turbomachinery Performance Data

The performance parameters for unique turbines are plotted in Figures 2-17 to 2-19. The abscissa is electrical power output in megawatts. The scale changes at 10 MWe, and several turbines up to 100 MW_e have been omitted from the plots. Simple cycles and regenerated cycles are noted. Pressure ratio is plotted against output power in Figure 2-17. Near 2-MWe, a pressure ratio of about 5 is common, although a few turbines are available with pressure ratios of about 10. Near 25 MW_e, a wide range of pressure ratios, from about 6 to 30, is available. The higher pressure ratios over the whole range are aircraft derivative turbines. Regenerated machines show pressure ratios of 10 or lower.

Turbine inlet temperature is plotted against power in Figure 2-18. The lowest temperature of about 760°C (1400°F) is found at both ends of the power output scale and indicates older technology. Temperatures above 980°C (1800°F) are found over the whole range of powers and indicate more modern technology. All but two of the regenerated engines have temperatures between 870 and 980°C (1600-1800°F). One regenerated engine has nearly 1090°C (2000°F) temperatures and will be discussed further later. Some of the aircraft-derivative engines approach 1200°C (2200°F). The shaded area of the figure indicates temperatures where air-cooled turbine blades are needed to ensure reasonable life in aircraft derivatives. Cooled blades are used in industrial turbines as low as 816°C (1500°F) to extend blade life.

Thermal or cycle efficiencies are plotted against power in Figure 2-19. There is a notable trend of efficiency with power. The data scatter about a parabola which comes to zero efficiency at zero power. Smaller turbomachinery is less efficient because Reynolds numbers are reduced and because of the inability to scale clearances and part accuracies. Regenerated engines have high efficiency in their groups, and two regenerated engines show outstanding efficiency. At the high power end, several aircraft-derivative engines show efficiencies near 0.35.

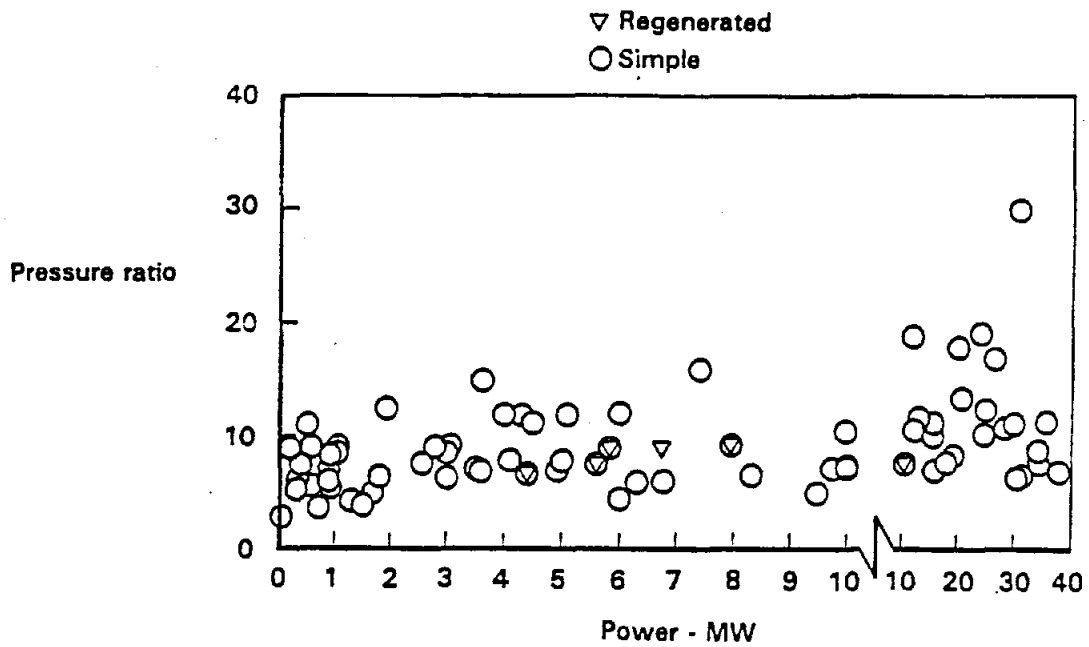

Source Gas Turbine World Handbook V.6

Figure 2-17. Pressure Ratio Verses Output Power

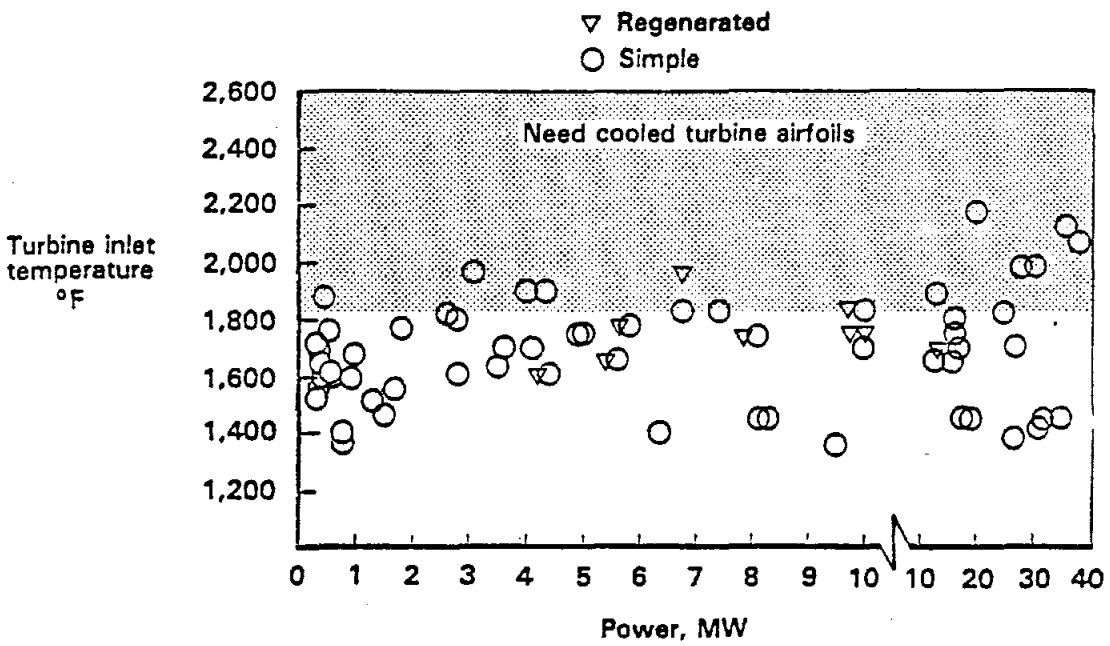

Source Gas Turbine World Handbook V.6

Figure 2-18. Turbine Inlet Temperature Verses Output Power

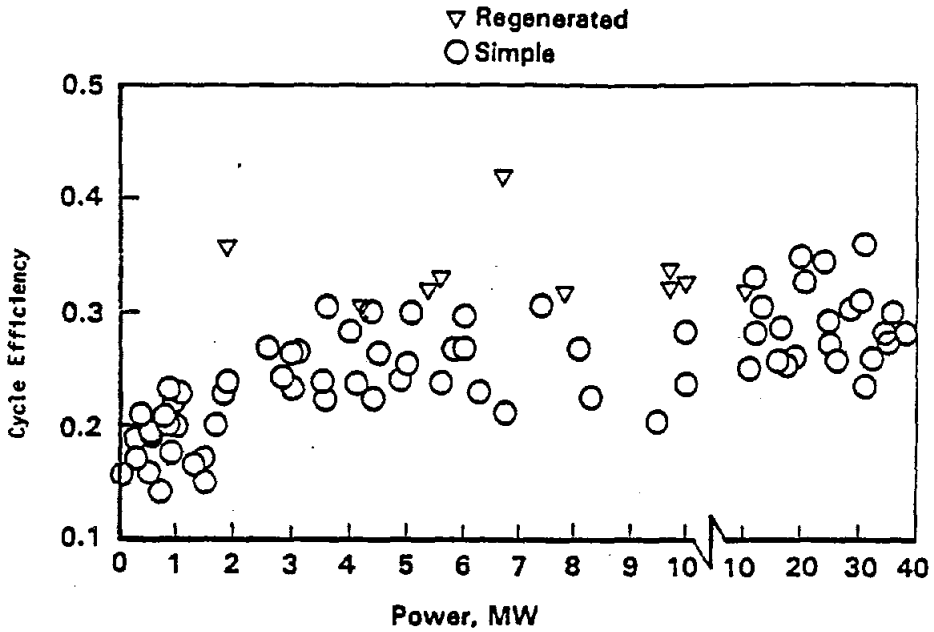

Source Gas Turbine World Handbook V.6

Figure 2-19. Cycle Efficiency Verses Output Power

The two regenerated engines at high efficiency warrant further discussion. The one at 2 MWe is a Solar-Caterpillar Model 565 reported in Gas Turbine World, Mar 1982. Its efficiency is above 0.36, and it has a relatively flat curve of efficiency verses power output. In part, this is achieved by a variable-setting vane for the single-stage, free power turbine. The compressor has two centrifugal stages driven by a single stage turbine.

The turbine at 7 MW_e is the Thomassen TF10 (17). This engine is intercooled and regenerated and has two centrifugal compressor stages driven by a single stage turbine at 1117°C (2042°F) turbine inlet temperature. The first compressor stage has two impellers back to back and the second has a single impeller. The power turbine has a single stage on a second shaft.

Both of these turbines can be modified for solar use as will be discussed in detail later. Neither one is at present available on the market. The 2-MW_e unit is undergoing field trials to evaluate and establish its reliability, and the 7-MW_e unit is in design stage. Both turbines are important because they show that Brayton cycle efficiency can be improved substantially above values obtainable from units that are presently offered for sale.

2.5.2 Turbomachinery Cost Data

Costs of a Brayton cycle set for generating 25-MW_e electricity was determined by analysis of bid data presented in References 16, 18 and 19. Data were reduced to 1982 dollars per kilowatt ISO and results are listed in Table 2-6 with details in Appendix A. ISO means power at 15°C (59°F) inlet air at sea level pressure without inlet or outlet pressure losses, and it represents standardized and idealized operating conditions.

Table 2-6 shows a range of work scopes and bid prices for 29 installations of Brayton-cycle electrical generation systems. The prices varied widely from above 800 to around 90$/kWe. The table demonstrates the bids were required to cover great variations of work scope at the sites. When this was understood, a single job was selected with bids shown in Figure 2-20. The bid price is plotted versus cycle efficiency, and shows no relationship. Furthermore, bids for the same turbine, having the same cycle efficiency, varied greatly depending on the supplier. These packages were complete, but unshipped and, of course, uninstalled. The value of 160 $/kW$_e$ (1982$) was chosen to represent the 25-MW_e size using additional data from aircraft engine prices and from the turbomachinery survey. Assuming 6% per year inflation, the unit cost in 1983$ would be 160 x 1.06 = 169.6 $/kWe. None of these gas turbines was regenerated.

Prices for the 2-MW_e size were not obtainable from pubished bid data. A value of 370$/kw$_e$ (1983$) was used after talking with several manufacturers.

Unit cost data for closed cycle systems for the 2-MW_e and the 25-MW_e plant sizes were not available. The closed cycle unit costs were assumed equal to the open cycle data except for the startup combustor. The open cycle startup combustor costs were assumed part of the basic unit costs. For the closed cycle machines, the startup combustor is a separate piece of equipment. The closed cycle combustor was assumed at 25% of the unit cost based on estimates for large scale closed cycle systems (20).

A factor of 1.4 was applied to the unit costs presented above to account for modifications for solar use; this price assumes a mature technology for the modification.

Table 2-6. Work Scopes and Bid Price Range for 29 Installations of Gas Turbine Electricity Generation Systems

Work Scopes	Bid Price Range and Work Occurrances		
Bid Prices 1982$/kW ISO	Above $275	$275 to $200	Below $200
Building and/or civil works	6	0	0
Fuel storage and handling	6	2	0
Dual fuel	4	1	0
Transformers	5	2	0
Switchgear	3	1	0
Combined cycle (or provide for)	2	0	1
Spares	0	5	1
Clutch	0	0	1
Used equipment	0	0	1

Source: Gas Turbine World Handbook V 5-7

- Unit size from under 17 MW to over 30 MW
- Range of bid prices 104 to 801 in 1982 dollars/kW-ISO
- Price variation from 10% to 20% standard deviation

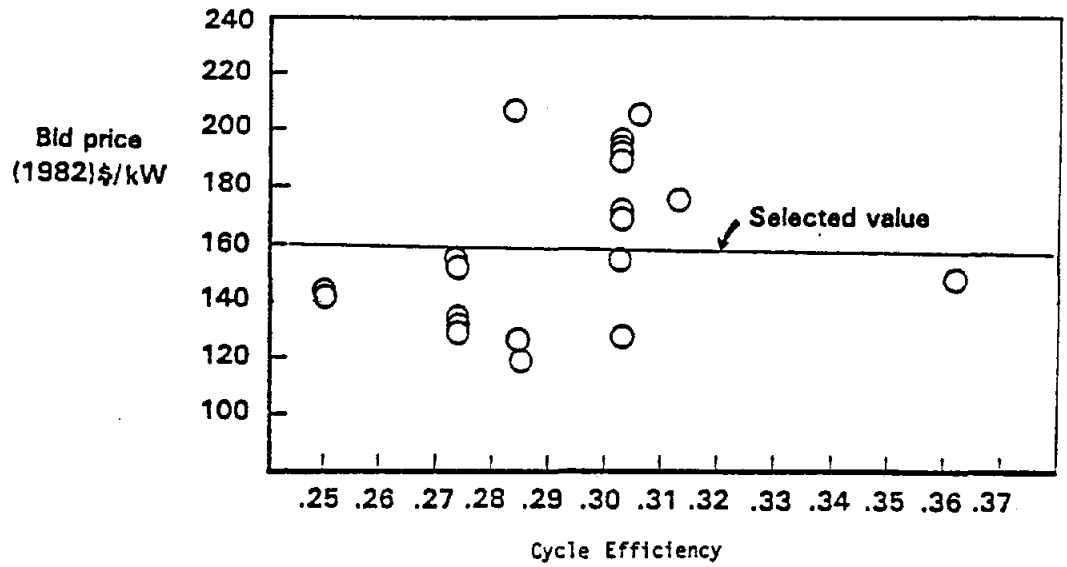

Source Gas Turbine World Handbook V.5

Figure 2-20. Gas Turbine Electricity Generator Bids for One Job

2.5.3 External Firing Assessment

Aircraft-derivative turbines operate at turbine inlet temperatures approaching 1200°C (2200°F) while industrial turbines tend to operate below 1000°C (1830°F). The higher temperature aircraft-type combustors are inline annular combustors. Industrial turbines favor can-type combustors that allow replacement of combustor parts without disassembly of the turbine. Regenerated turbines have combustors connected to pipes leading from recuperators. Both annular and can combustors are air-cooled to extend the combustor life.

External firing has two meanings. One meaning applies to closed cycle turbines in which clean gas flows through the turbomachinery and all heat is transferred across walls which contain the gas. In a gas-in-tube solar receiver, heat is added to the flow circuit in this same way. A trim burner for a closed cycle would also transmit heat through tube walls to the working gas. An open-cycle gas turbine ordinarily burns fuel in the working air and the combustion products pass through the turbine; this would be internal firing as opposed to external firing.

The second meaning of external firing has to do with the gas path that connects the compressor, the combustor, and the turbine. The compressor and turbine have axially symmetric annular flow paths, and an inline annular combustor connects them directly. With external firing in the second sense, compressor air is collected and ducted to a combustor located physically out of the annular flow path. After heating, the air and combustion products are returned, distributed around the turbine annulus and sent through the turbine. All regenerated turbines fit this description in part. In this latter sense, external firing is required for any gas turbine that works with a solar central receiver. The latter meaning for external firing is used in this study.

In the turbomachinery survey, six instances of external firing were discovered, but in each case the turbine inlet temperature was 850°C (1560°F) or lower. For a 1093°C (2000°F) turbine inlet application, a gap of 270°C (500°F) in turbine inlet temperature capability exists for regenerated engines and 350°C (630°F) for simple engines. When questioned about the possibility of closing the gap, turbine engineers all indicated that progress can be made with a suitable development program. Design studies have been made for a turbine at 980°C (1800°F).

The six instances of external firing discovered were as follows: three involved atmospheric fluidized beds, low-grade fuels, and cogeneration systems; two were closed cycle; and one uses a coal-fired pressurized fluidized bed combustor in place of the ordinary engine combustor. The need for higher turbine temperatures has been obscured by the difficulties in making pipe, valves, and instruments for temperatures above 871°C (1600°F). The turbine developments required for 1093°C (2000°F) operations are discussed in Section 2.5.5.

2.5.4 Maintenance and Durability

Maintenance of turbines is done normally "on condition", that is when the monitoring instruments give indications of need. In most cases, problems develop gradually, and repairs can be scheduled well before they are needed. Such repairs are performed by visiting specialists. In normal service an operator will be present at least for starting and stopping. The skills required may be electronic since much of the total system uses electrical and electronic sensors and measuring instruments. The training may have been obtained in the test shops of the engine manufacturer. The operator routinely checks that lubrication systems and performance monitoring systems are working. The operator inspects the system daily when running and weekly when not running. For industrial turbines the most common sources of trouble are the combustor and the fuel system.

Durability of aircraft turbines is indicated by statistical data from Reference 21 on performance in aircraft and marine service. An average engine in commercial transport service will range from 2000 to 5000 flight hours before removal for any repair. The mean time between overhauls is 10,000 to 20,000 hours, varying with engine types. In military service, 1200-3000 hours of service are obtained between overhauls.

Industrial engines tend to run longer hours and to have longer lives. 20,000 hours between overhauls is common. At 40,000 hours, the first-stage turbine blades would be replaced, and at 100,000 hours the remaining turbine blades would be replaced. A 20-year solar Brayton plant would be expected to operate about 50,000 hours. Cycles to failure data were not offered by any manufacturer, but the significance of the parameter was admitted.

2.5.5 Solar Application Modifications

Two items are discussed herein: the provision for external firing at increased temperature, and the adjustment of compressor and turbine matching to accommodate variation of receiver pressure loss. The latter is an engineering problem that involves the selection of a turbine and its operation. The former involves the system generally and will require advances in design, materials, and manufacture.

External Firing

The provision for external firing requires the replacement of the inline combuster of an aircraft or industrial turbine with a piping system to deliver hot air to the turbine at the same engine temperature, namely, 1070-1200°C (1960-2200°F). The aircraft engine combustor is annular and inherently distributes flow around the turbine inlet annulus. The industrial combustor is not necessarily annular, but it has a scroll system which distributes the air around the annulus at turbine inlet. The industrial combustor, especially if regenerated, should be easier to modify for external firing.

The combustor of a gas turbine has a casing which carries structural loads, and it also has a liner with a headplate. Between the casing and the liner flows a blanket of air which protects the casing from high temperature. That air blanket comes from the compressor or the recuperator; it is hot, but very much cooler than the gas inside the liner. The liner itself is convectively cooled by air passing through small holes and slots that create a film on the flame side, and it is also cooled by the outside air blanket. The fuel is injected in a fine spray or vapor through the headplate along with air in nearly stoichiometric proportions. The fuel burns in a primary combustion zone at temperatures near 1650°C (3000°F). As the hot gas moves down the combustor toward the turbine, it is quenched and diluted and mixed by strong jets that pass through large holes in the liner. At turbine entry the temperature has a radial gradient which peaks toward the middle of the annulus in a way that conveys the longest possible life to the turbine airfoils. The temperature at any one radius is ideally constant around the circumference of the turbine.

In an industrial machine, the combustor is often cylindrical or a "can" in its own casing. The gas path from the can to the turbine will be insulated to protect the casing. The combustor would be annular in an aircraft machine with an outer liner and a casing to carry structural loads and an inner liner and a casing to support bearings and lubrication systems. The aircraft annular combustor is much hotter than the industrial turbine and so presents a greater challenge in redesign to change this annulus to a pipe.

In a turbine modified to admit solar-heated air, the receiver exit flow would be directed into the region of the turbine normally occupied by the combustors described above. The entire receiver exit flow would be at the desired turbine inlet temperature. The blanket of cooler air that normally protects the turbine casing would not be available. Also, the radial air temperature gradient that extends the life of the airfoils would not be present. The turbine casing interior will require a high temperature insulation. The insulation must not separate or spall to avoid damage to the airfoils. Differential expansion is also a concern.

Although the modifications to admit solar-heated air will require careful consideration, the gas turbine industry engineers discussing these concerns consistently took a positive attitude. They had not had occasion to consider the design problem, but found it interesting.

Compressor and Turbine Matching

The pressure drop through the receiver affects the design and cost of the receiver; a high pressure drop helps the receiver heat transfer, but it hurts cycle efficiency. Another effect is the matching of the compressor and turbine flow capacity. A higher pressure drop requires a larger turbine or it moves the compressor closer to surge on its performance map. The effects are complicated and depend on the machine chosen for the job. In aircraft gas turbines, the location of the operating line is strongly affected by requirements for starting and for sudden and large power increments. Part-speed surge margin is very important and is affected by combustor pressure drops which are invariable in ordinary turbines. Solar applications offer possibilities of duct arrangements which may allow system pressure drop to vary. This may alleviate starting and accelerating problems. At the same time, a change of pressure drop may move the compressor to a region of higher or lower efficiency on the performance maps. The details would have to be worked out in the process of installation.

Generally, there are several sources of pressure drop in a gas turbine. The addition of fuel-free, solar-heated air will allow or even require a larger system pressure drop than the 2-5% usually experienced. The addition of fuel

to the turbine flow circuit is equivalent to a pressure drop. This could amount to 3% for a liquid fuel or 6% for a gaseous fuel. Since no fuel addition is required in the solar-heated case, that pressure loss could be transferred to the receiver with little effect on the turbine. Also, the high-speed surge margin in a gas turbine can be as great as 20%. If that margin can be reduced without causing part-speed surge problems, the receiver pressure drop can be increased. Finally, some manufacturers are able to vary the capacity of their turbines by selecting classes of fit or blade stagger which will adjust the turbine capacity in the desired direction. While most of these factors vary with particular installations, it is nevertheless concluded that the problem here is not a research problem but an engineering problem to be solved in the application of a machine to a job.

2.5.6 Turbomachinery Control

Two features of the control situation were explored in the survey: the service on an isolated grid, and the implications of thermal inertia on control.

Isolated Load vs Grid Interconnection

Operation on a large grid simplifies the control of output frequency because any load step is a small fraction of the total grid power and produces a negligible effect on speed and frequency. The same accuracy of frequency control cannot be obtained in an isolated system unless load steps can be kept small. A 25-MW_e, industrial, single-shaft turbine can hold frequency to 0.02% whereas a 2-MW_e, two-shaft turbine would hold frequency within 5%.

Thermal Inertia

In any system, an electrical fault may cause the shedding of all load from the turbine. This leads to interesting problems for the safety of systems with large thermal inertia.

Thermal inertia exists when the system contains components with large heat capacity. Passive storage devices, recuperators, pipes, receivers, and turbines themselves all have thermal inertia. The industry has experience

with recuperators and is alert to their effects on load shedding. The turbine must be unloaded rapidly before overspeed causes damage. If the heat input in a simple cycle turbine is turned off the turbine will slow and stop. If a recuperator is in the system, more than enough heat input can still be supplied to destroy the turbine and the electrical generator. Such problems also arise in fluidized bed externally-fired systems. The safety of the turbine and other elements of the system, particularly the receiver, must be considered. In normal operation when step load changes occur, either increasing or decreasing load, the thermal inertia of the system slows its response. For example, when a large increase of load occurs, an increase of turbine inlet temperature would be required which could be obtained by focusing more heliostats on the receiver or by burning more fuel. However, some of the added heat will go into the thermal capacitors such as the receiver, the pipes, and the recuperator. An excess of heat will be required momentarily to hold speed during a load change. The inverse situation exists for step off loads. One industry engineer called this a "stiff system" from a control viewpoint.

The requirements to solve the problem are a high trim burner capability to handle uploads and some sort of waste device to handle downloads. These devices must be chosen so that they will provide adequate control with safety for all system components even in emergency situations. Control strategies developed for a closed-cycle system and for a simple cycle are presented in references 15 and 1 respectively.

2.6 CYCLE CONFIGURATION COST ANALYSIS

This section describes the system cost analysis performed to support the preferred concept selection. The approach to this subtask was to use a common basis of unit costs for each cycle configuration and to compare capital and levelized energy costs to the baseline system configuration described in Section 2.2. A trade was also made as to the effect on costs of locating the turbomachinery at tower top or tower base. The results of these analyses are presented in the following paragraphs.

2.6.1 Component Unit Cost Assumptions

Table 2-7 presents the unit cost data developed for the various system components. The heliostat cost was assumed at 113.15\$/m^2. This value was assumed from a 95\$/m^2 (1980\$) value scaled to 1983\$ by assuming 6% per year inflation. The land and receiver costs were assumed from similar recent studies (9, 11). The receiver cost was based on cavity area. The electric power generator costs were derived from the turbomachinery cost data described in Section 2.5.2. Heat exchanger (precoolers, intercoolers, and recuperators) cost estimates were made based on the required heat exchange area and the temperature and pressure service expected. Fixed costs were based on an assumption of 500K\$ for computers and controls and 40K\$ for buildings. The riser and downcomer costs were estimated based on temperature and diameter and the data of reference 11.

2.6.2 Component Capital Cost Results

Heliostat Field

It was not feasible with the limited resources and scope of the present study to develop an optimized heliostat field for each cycle configuration and plant size (a total of 12 plants). Instead, the baseline heliostat field described in Section 2.5.2 was resized for the several receiver and cycle efficiencies. The resulting heliostat and land costs were nondimensionalized and displayed as shown in Figure 2-21. With these data, the field capital costs for each cycle configuration were estimated as shown in Table 2-8.

Receiver

Receivers for each cycle configuration alternative were scaled from the baseline receiver designs described in Section 2.5.2. The scaling relationships and methodology are described in Appendix B. The results are presented in Table 2-9.

The receiver efficiency also affects the size of the heliostat field. The baseline receiver was assumed to have a thermal efficiency of 85%. The assumed loss components are detailed in Table 2-10. These values were chosen

Table 2-7. Component Unit Cost Data
(1983$)

SYSTEM COMPONENT	UNIT COST	BASIS
Heliostat	$113.15\$/m^2$	$95\$/m^2 \times (1.06)^3$
Land	$2.00\$/m^2$	Current solar studies
Receiver*	$2529\$/m^2$	PNL (9), $2250\$/m^2 \times (1.06)^2$
Tower	$1.47 \times 10^6\$$ (25 MW_e) $0.66 \times 10^6\$$ (2 MW_e)	Liebenberg (22)
EPGS**	$237\$/kW_e$ (25 MW_e, open) $278\$/kW_e$ (25 MW_e, closed) $518\$/kW_e$ (2 MW_e, open) $607\$/kW_e$ (2 MW_e, closed)	Turbine survey
Heat Exchanger	$25\$/ft^2$ (high temp, high press) $25\$/ft^2$ (high temp, low press) $15\$/ft^2$ (low temp, low press)	BEC estimates
Fixed	$\$0.54 \times 10^6$	BEC estimates
Riser, downcomer	Varies with temp. and diameter	SNLL/Kaiser Engineers (11)

* Based on cavity area
** Includes 40% for modification for external firing

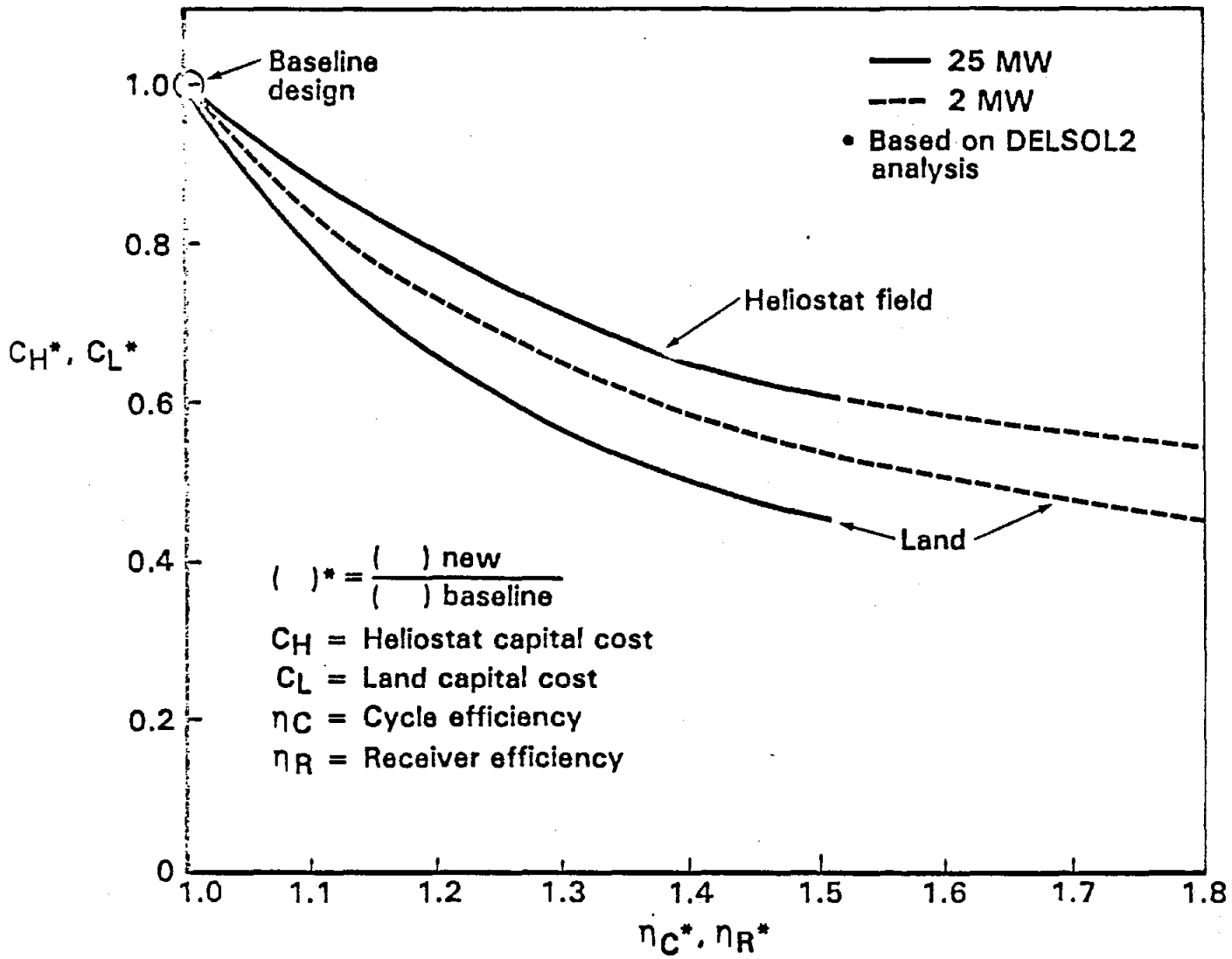

Figure 2-21. Relative Variation of Field Costs With Cycle and Receiver Efficiency

Table 2-8. Heliostat Field Capital Cost Results

	Cycle Designator	Cycle Efficiency	Heliostat Cost (10^6\$)	Land Cost (10^6\$)
25 MW	Baseline	.325	15.76	1.38
	CS	.350	14.03	1.09
	OS	.383	12.08	0.84
	CR	.425	10.81	0.72
	OR	.459	9.30	0.54
	CRI	.480	9.32	0.58
	ORI	.495	8.81	0.52
2 MW	Baseline	.240	1.56	0.145
	CS	.278	1.35	0.126
	OS	.322	1.05	0.089
	CR	.397	0.93	0.076
	OR	.431	0.79	0.059
	CRI	.445	0.83	0.066
	ORI	.458	0.77	0.056

Table 2-9. Receiver Capital Cost Results

	Cycle Designator	Inlet Pressure (psia)	Massflow (lbm/s)	Inlet Temperature (^oF)	Cavity Area (m^2)	Cost (10^6\$)
25 MW	Baseline	247	159.7	781	677	1.71
	CS	500	242.9	1023	482	1.22
	OS	294	186.3	838	546	1.38
	CR	495	249.9	1240	366	0.93
	OR	72	228.2	1228	1112	2.81
	CRI	485	170.7	990	325	0.82
	ORI	142	165.1	989	636	1.61
2 MW	Baseline	123	26.0	599	124	0.314
	CS	500	23.0	964	72	0.183
	OS	221	16.9	763	96	0.243
	CR	495	21.6	1245	49	0.125
	OR	72	19.6	1233	169	0.428
	CRI	485	15.0	1004	45	0.115
	ORI	142	14.5	1002	94	0.239

- T_{out} = 2040^oF
- T_{Tube} = 2140^oF (max)
- $\Delta p/p$ = 10%

Table 2-10. Receiver Efficiency Results

	Cycle Designator	Relative Pressure	Relative Cycle Efficiency	Relative Aperture Area	Relative Cavity Area	Receiver Efficiency	Relative Receiver Efficiency	
25 MW	Baseline	1.0	1.0	1.0	1.0	0.850	1.0	
	CS	2.028	1.077	0.904	0.712	0.861	1.012	
	OS	1.192	1.178	0.800	0.806	0.878	1.033	. $(T_{ef})^* = 0.942$
	CR	2.007	1.298	0.708	0.541	0.870	1.024	
	OR	0.291	1.412	0.644	1.643	0.911	1.072	
	CRI	1.967	1.474	0.616	0.480	0.877	1.031	
	ORI	0.575	1.520	0.608	0.940	0.903	1.062	
2 MW	Baseline	1.0	1.0	1.0	1.0	0.850	1.0	
	CS	4.055	1.158	0.808	0.583	0.804	0.946	
	OS	1.788	1.338	0.668	0.773	0.843	0.992	. $(T_{ef})^* = 1.15$
	CR	4.013	1.638	0.580	0.397	0.830	0.977	
	OR	0.587	1.792	0.532	1.364	0.880	1.035	
	CRI	3.933	1.838	0.523	0.366	0.837	0.985	
	ORI	1.151	1.900	0.508	0.760	0.872	1.025	

based on previous BEC receiver design experience. The receiver efficiency for each cycle configuration was adjusted for changes in aperture and cavity as shown in the loss models below:

- Reflection (%): 4.0 (A_{ap}*/A_c*)

  A_{ap}* - Aperture area scales as the number of heliostats, i.e., field cost.

  A_c* - Cavity area from receiver sizing.

- Reradiation (%): 7.4% A_{ap}* (T_{ef}*)^4

  Tef* - Scales as the maximum tube temperature.

- Conduction and convection (%): 3.6 constant

The receiver efficiency adjustment results are shown in Table 2-10. The field costs presented earlier in Table 2-8 already reflect the adjustments required by changing receiver efficiency.

Heat Exchanger Costs

Detailed sizing and cost estimating of each recuperator, precooler and intercooler was beyond the scope of the present effort. However, a detailed recuperator design from the BEC/DOE Advanced Central Receiver program was available. This recuperator design was scaled to the desired operating environments for each cycle configuration alternative. The scaling relationships and methodology are described in Appendix B. Each heat exchanger was assumed to be a counterflow, air-to-air, shell-and-tube design. The heat exchanger effectiveness was assumed at 90%. The pressure losses were 1% (cold side) and 4% (hot side) for the recuperators and 2% (cold side) for the precooler and intercoolers. The results are displayed in Table 2-11.

Table 2-11. Heat Exchanger Cost Results

	Cycle Designator	Component	U (Btu/h-ft^2 ^{o}F)	NTU	A (ft^2)	Unit Cost ($/ft^2)	Cost ($10^6$$)
25 MW	CS	Precooler	8.58	7.3	191,700	15	2.88
	CR	Recuperator	55.5	7.3	30,532	25	0.763
		Precooler	24.0	7.3	69,555	15	1.04
	OR	Recuperator	13.9	7.2	108,823	20	2.18
	CRI	Recuperator	56.2	7.4	20,410	20	0.408
		Precooler	15.0	7.3	75,010	15	0.490
		Intercooler	34.2	7.3	32,696	15	1.13
	ORI	Recuperator	22.8	7.4	50,147	20	1.00
		Intercooler	13.7	7.3	78,600	15	1.18
2 MW	CS	Precooler	9.3	7.3	16,882	15	0.253
	CR	Recuperator	52.9	7.3	2,765	25	0.069
		Precooler	22.6	7.3	6,397	15	0.096
	OR	Recuperator	13.3	7.2	9,797	20	0.196
	CRI	Recuperator	53.4	7.3	1,860	20	0.037
		Precooler	14.2	7.3	6,962	15	0.045
		Intercooler	32.5	7.3	3,027	15	0.104
	ORI	Recuperator	21.7	7.3	4,413	20	0.083
		Intercooler	13.3	7.3	7,090	15	0.106

Piping Costs

In the baseline configuration, the turbomachinery was located at the tower base, thus necessitating a riser and downcomer to duct air to and from the receiver. The riser and downcomer flow diameters were sized to the following requirements and assumptions:

Pressure loss = 0.5% of inlet pressure

Temperature = 1116°C (2040°F) for downcomer, variable for riser

Length = Tower height + 10%

The piping sizing results are presented in Table 2-12.

Piping costs were estimated based on interior insulated piping data generated in Reference 11. Figure 2-22 presents the downcomer design concept and the component costs. Similar data were available for the riser. The resulting piping cost data for the piping sizes presented in Table 2-12 are shown in Table 2-13.

Tower Costs

Tower costs were estimated for the baseline concept using the steel tower cost algorithims suggested by Liebenberg (22).

The tower cost was maintained constant for each cycle configuration. For the 25-MW_e plants, the tower cost assumed was 1.47×10^6\$. For the 2-MW_e, the value was 0.66×10^6\$. Since relatively small variations in tower height were expected between cycle alternatives and since the steel tower is usually a smaller cost component, the assumption of a constant tower cost was justified.

2.6.3 System Capital Cost Comparison

The capital cost data from the various system components were assembled as shown in Table 2-14 for the 25-MW_e plant and in Table 2-15 for the 2-MW_e plant. The capital costs are also displayed graphically in Figures 2-23 and

Table 2-12. Piping Sizing Results

	Cycle Designator	Massflow (lbm/s)	Pressure (psia)	DOWNCOMER Inlet Temperature (°F)	DOWNCOMER Inside Diameter (in)	RISER Inlet Temperature (°F)	RISER Inside Diameter (in)
25 MW	Baseline	159.7	222	2200	26.5	781	22.1
	CS	183.3	450	2040	20.5	1023	18.0
	OS	242.9	265	2040	28.4	838	24.2
	CR	228.2	446	2040	22.3	1240	20.3
	OR	249.9	72	2040	51.7	1228	47.8
	CRI	165.1	437	2040	19.9	990	17.4
	ORI	170.7	142	2040	33.8	989	30.1
2 MW	Baseline	26	111	1650	13.7	599	11.5
	CS	16.9	450	2040	6.7	963	5.8
	OS	23.0	198	2040	10.7	763	8.9
	CR	19.6	445	2040	7.2	1245	6.6
	OR	21.6	65	2040	16.6	1233	15.1
	CRI	14.5	437	2040	6.5	1003	5.7
	ORI	15.0	128	2040	10.9	1002	9.6

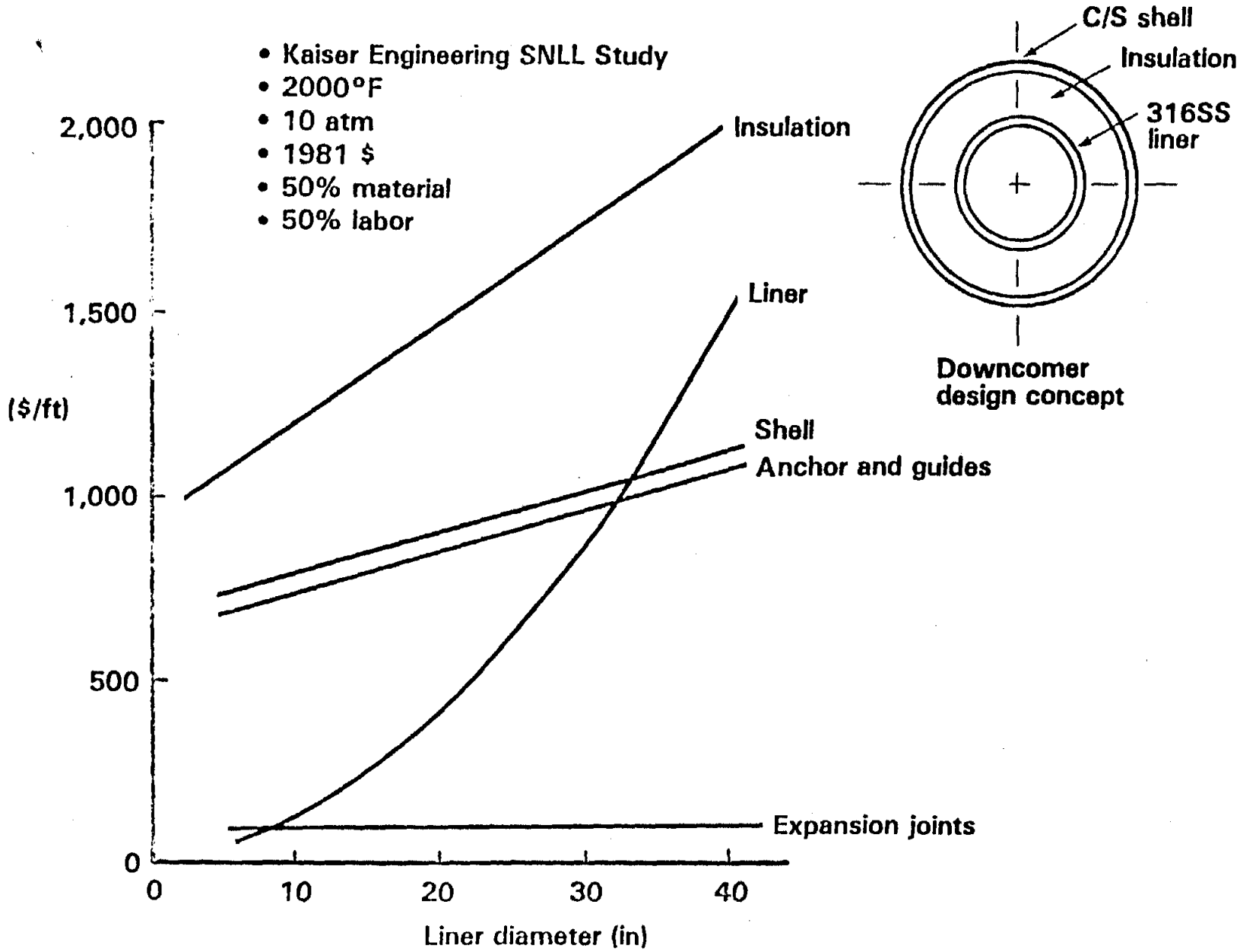

Figure 2-22. Downcomer Cost Data (11)

Table 2-13. Piping Cost Results

	Cycle Designator	Downcomer Cost (10^6\$)	Riser Cost (10^6\$)	Total Cost (10^6\$)
25 MW	Baseline	1.904	0.381	2.285
	CS	1.949	1.637	3.586
	OS	2.065	0.467	2.532
	CR	2.045	1.703	3.748
	OR	2.954	2.402	5.355
	CRI	1.933	1.621	3.554
	ORI	2.134	1.826	3.960
2 MW	Baseline	0.437	0.067	0.504
	CS	0.486	0.385	0.871
	OS	0.427	0.052	0.479
	CR	0.503	0.382	0.885
	OR	0.434	0.363	0.797
	CRI	0.482	0.379	0.861
	ORI	0.402	0.328	0.730

Table 2-14. System Capital Cost Summary

-25 MW_e-

10^6\$

Cycle Designator	Heliostat	Land	Piping	Receiver	Electric Power Generation	Total Cost	Relative Cost	Rank
Baseline	15.76	1.38	2.29	1.71	5.93	29.08	1.0	3
CS	14.03	1.09	3.59	1.22	9.83	31.77	1.093	4
OS	12.08	0.84	2.53	1.38	5.93	24.77	0.852	1
CR	10.81	0.72	3.75	0.93	8.75	26.97	0.927	2
OR	9.30	0.54	5.36	2.81	8.11	28.13	0.967	3
CRI	9.32	0.58	3.55	0.82	8.98	25.26	0.869	1
ORI	8.81	0.52	3.96	1.61	8.11	25.02	0.860	1

- Tower cost = 1.47 x 10^6\$
- Fixed cost = 0.54 x 10^6\$

Table 2-15. System Capital Cost Summary

-2 MW_e-

10^6\$

Cycle Designator	Heliostat	Land	Piping	Receiver	Electric Power Generation	Total Cost	Relative Cost	Rank
Baseline	1.56	0.145	0.504	0.314	1.04	4.76	1.0	4
CS	1.35	0.126	0.871	0.183	1.47	5.20	1.092	5
OS	1.05	0.089	0.479	0.243	1.04	4.10	0.861	1
CR	0.93	0.076	0.885	0.125	1.38	4.60	0.966	3
OR	0.79	0.059	0.797	0.428	1.24	4.51	0.947	3
CRI	0.83	0.066	0.861	0.115	1.40	4.47	0.939	3
ORI	0.77	0.056	0.730	0.239	1.23	4.23	0.889	2

- Tower cost = 0.66 x 10^6\$
- Fixed cost = 0.540 x 10^6\$

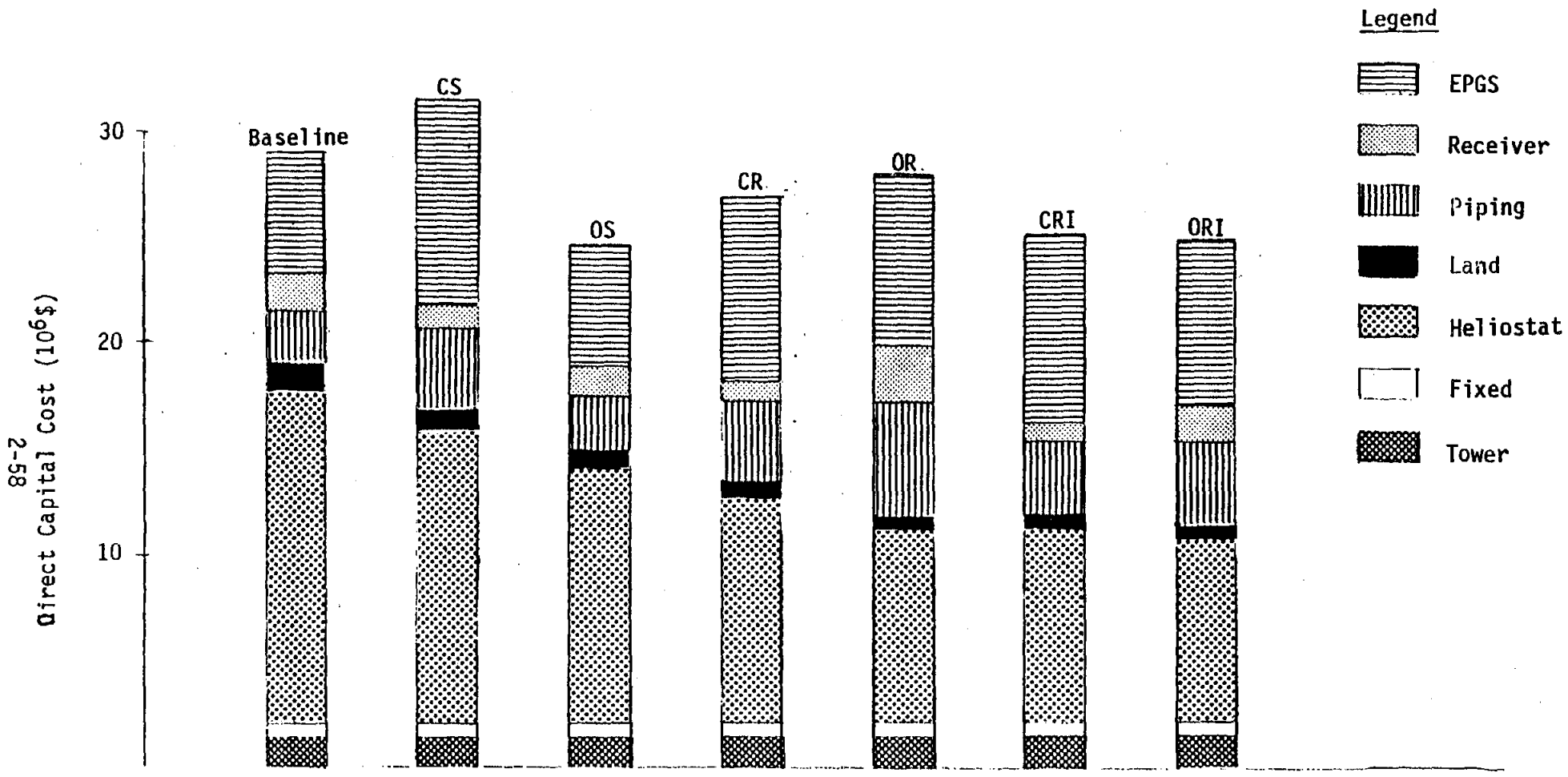

Figure 2-23. Direct Capital Cost Comparison--25 MW_e

2-24. For the 25 MW_e plant, the OS, CRI and ORI configurations have very nearly the same capital costs. In the 2-MWe size range, the OS configuration has the lowest capital costs.

2.6.4 Off-Design Performance Assessment

As indicated in the turbomachinery survey discussion, the closed cycle configurations by the use of inventory control offer better off-design performance than their open cycle counterparts, whereas the open cycle configurations produce performance advantages at design point conditions. This section presents the results of a limited assessment of these effects.

The approach chosen for this limited assessment was to use the GSA cycle performance computer model (see Section 2.4.1) to consider the 25-MWe plant turbomachinery. Typical compressor and turbine maps were used. The preferred open cycle, regenerated and intercooled (ORI) configuraton and an open simple cycle (OS) were considered. Also two shaft and single shaft turbomachinery design options were evaluated. The relative change in cycle efficiency from design point conditions was calculated for each option over a range of power outputs of 20 to 115% of design value.

The DELSOL2 computer program (13) was used to predict the constant-cycle-efficiency (closed cycle) annual power production. Tower height, aperture size, and field size were optimized for a design point cycle efficiency of 49.5%. The DELSOL2 program calculated hour-by-hour performance data for five days of the year (days 355, 35, 81, 126 and 172). These hour-by-hour performance data were adjusted for the off-design effects found from the GSA program output. The total estimated power production was summed and compared to the constant-cycle-efficiency case.

The results from the GSA program were presented earlier in Figure 2-15. The open simple cycle (OS) configuration, dual and single shaft data showed no differences at off-design. The ORI, dual shaft option produced the flattest response showing 67% of design point efficiency at 20% power. The OS configuration, dual or single shaft showed the next best performance followed by the ORI, single shaft.

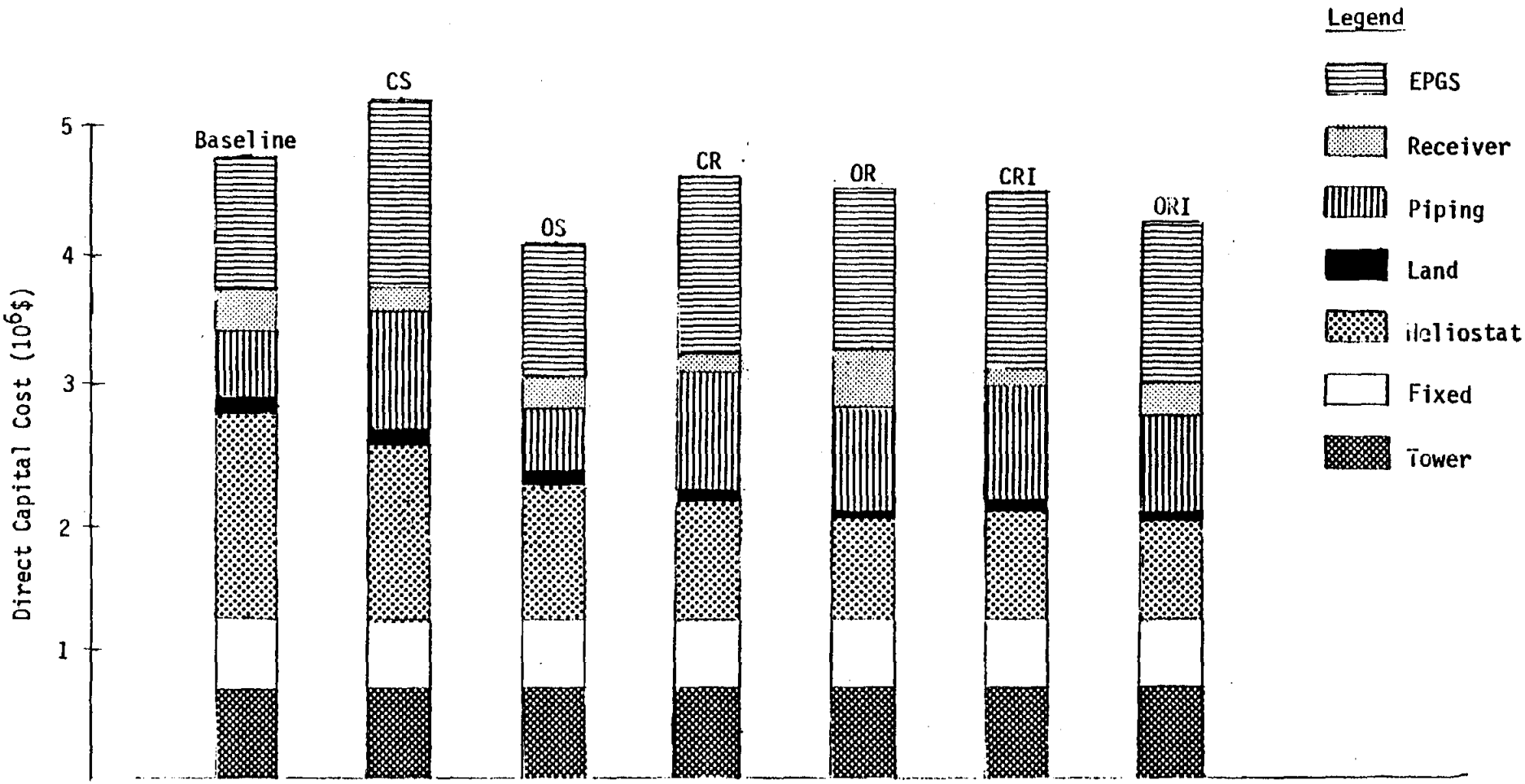

Figure 2-24. Direct Capital Cost Comparison--2-MW_e

The ORI, dual shaft daily power production is compared to the closed cycle configuration in Figure 2-25. The effect on daily and annual power production is shown in Table 2-16. As can be seen, the ORI annual power production is only 3.4% below the closed cycle configuration.

Table 2-16. Annual Power Production Data

Cycle	Relative Annual Power Production
Closed cycle	1.0
Open cycle, regenerated and intercooled, dual shaft	0.966
Open simple cycle	0.956

The conclusions that can be drawn from this study of off-design performance are as follows:

1. The open cycle (OS) configuration off-design performance is not influenced by a choice of dual or single shaft turbomachinery.

2. The open cycle, regenerated and intercooled (ORI) off-design performance significantly favors the dual shaft approach over the single shaft version.

3. The annual power production for the ORI configuration is reduced by about 3.4% when off-design performance effects are estimated.

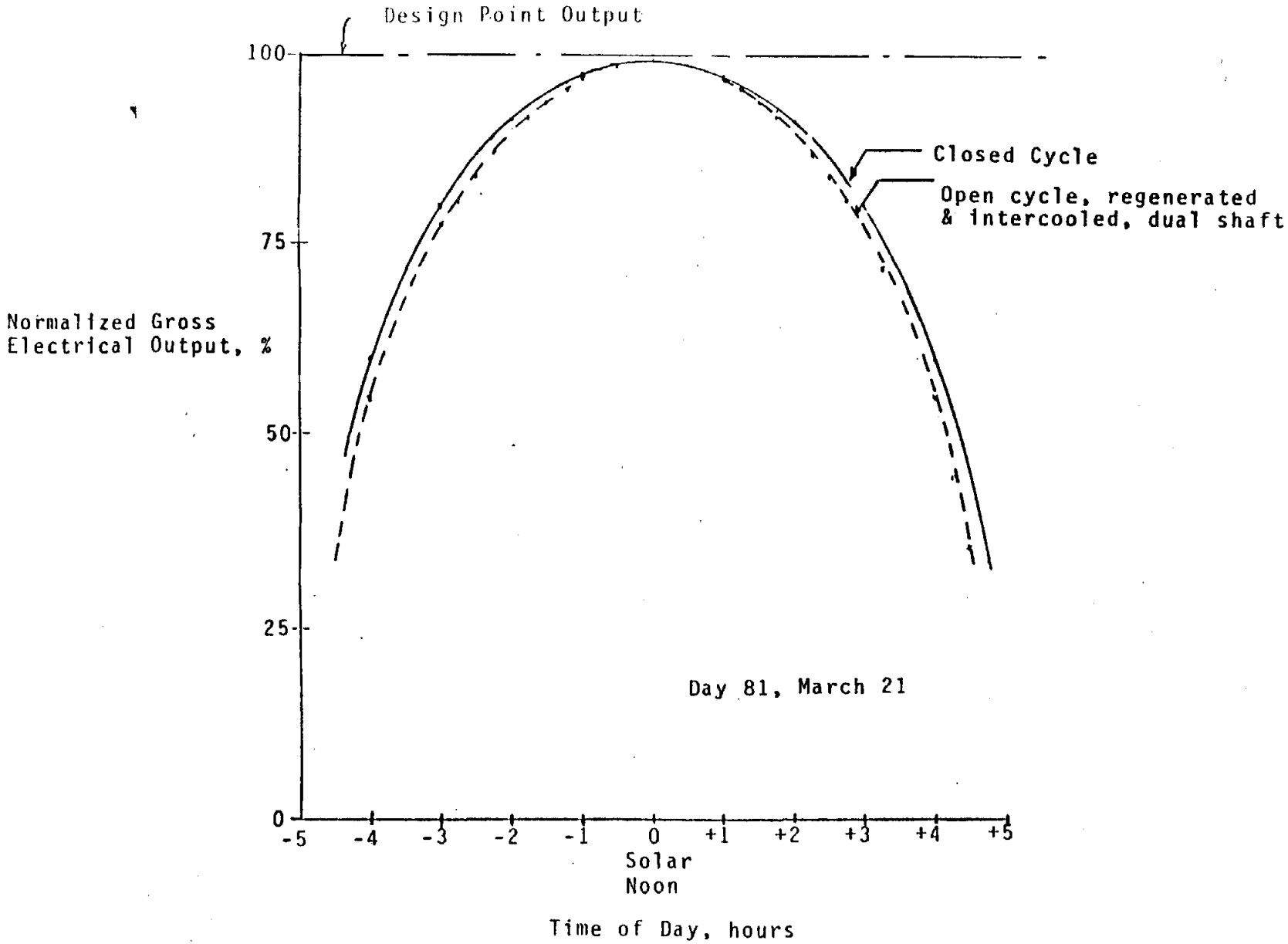

Figure 2-25. Off-Design Daily Electric Generation Comparison

2.6.5 Busbar Energy Cost Comparison

Busbar energy costs were estimated for each cycle configuration. The results are presented relative to the baseline reference case in Figure 2-26. The OS configuration showed the lowest energy costs for the 2-MW_e plant size. The open simple turbomachinery is also relatively easy to modify and readily available. In the 25-MW_e size range the CRI configuration produces the lowest costs. However, consideration of turbomachinery availability greatly favors the open cycle configurations while producing only slightly higher busbar costs.

2.6.6 Turbine Location Trade Results

A trade was performed to determine the most cost-effective location of the turbomachinery. The baseline reference system located the turbomachinery at the tower base. This location facilitates ease of installation and maintenance, while producing lesser tower costs. However, the tower top location reduces the need for an expensive downcomer. Also, pressure and thermal losses can be reduced. Thermal inertia and flow volume concerns are also lessened.

The approach taken in the turbine location trade was to use the baseline reference case and estimate the costs for relocating the turbine to the tower top. Tower costs were estimated from the data of Reference 22. Piping cost data were based on the data given in Section 2.6.2. For locating the turbine at the tower top, the receiver mass and receiver height were increased by 100%. The piping costs in both plant sizes were reduced by 91% for the tower top location. Benefits for reduced pressure and thermal losses at the tower top location were not considered.

The trade results are shown in Table 2-17. The tower top location allows a reduction of 6% in capital costs for the 25-MW_e plant and 9% for the 2-MW_e plant.

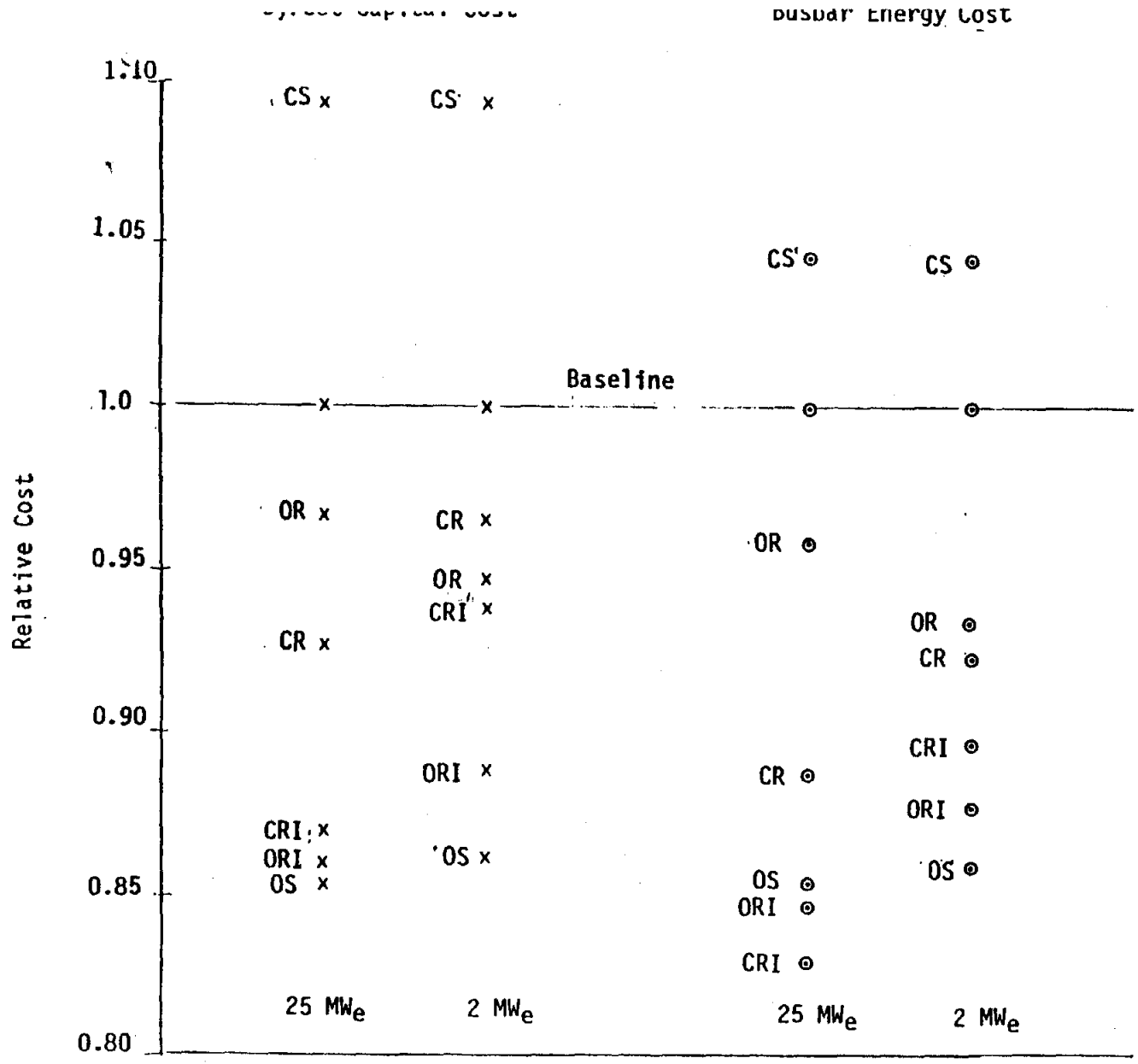

Figure 2-26. Relative Capital and Busbar Cost Results

Table 2-17. Turbine Location Trade Results

	Tower Base Location			Tower Top Location			
Power Level (MW_e)	Total System Cost (10^6\$)	Piping Cost (10^6\$)	Tower Cost (10^6\$)	Piping Cost 10^6\$	Tower Cost 10^6\$	Total System Cost 10^6\$	$\frac{\text{(Total) TT}}{\text{(Total) TB}}$
25	29.08	2.29	1.47	0.208	1.77	27.30	0.939
2	4.76	0.504	0.66	0.046	0.67	4.31	0.906

2.7 PREFERRED CYCLE CONFIGURATION SELECTION

The preferred cycle configuration for each plant size was selected not only on cost and performance, but also on component availability, reliability, maintainability and operability. This section presents the results of that selection.

2-MWe Plant Size

The open simple (OS) cycle configuration was chosen for the 2-MW_e plant size. The OS configuration is straight forward in design, and readily available. It has proven itself as a reliable and easily maintained system. Open simple cycles are used as remotely located, unmanned peaking power plants. The OS configuration, tower top location, also clearly produced the lowest capital costs and busbar energy costs for this size range.

Figure 2-27 presents the preferred 2-MW_e cycle configuration flow schematic. Also presented are thermodynamic state point data around the flow circuit.

25MW_e Plant Size

The open cycle regenerated and intercooled (ORI) configuration was chosen for the 25-MW_e plant size. The ORI configuration offers high cycle efficiency, reduced heliostat field and receiver sizes, while requiring low capital and busbar energy costs. This configuration is currently being developed as a highly efficient state-of-the-art power system (17).

Figure 2-28 presents the preferred 25-MW_e cycle configuration flow schematic. Thermodynamic state point data are also presented.

OPEN SIMPLE CYCLE

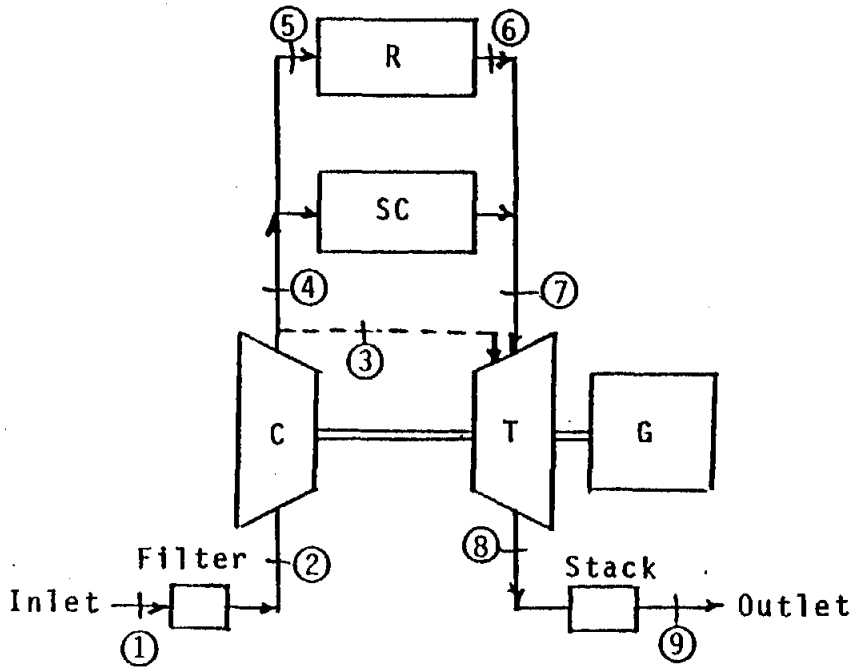

Station	$\dot{m}$ (lbm/s)	T (°F)	P (psia)
1	17.69	59	14.7
2	17.69	59	14.6
3	0.80	762.6	219.3
4	16.89	762.6	219.3
5	16.89	762.6	219.3
6	16.89	2040.0	197.4
7	16.89	2040.0	197.4
8	17.69	939.4	14.9
9	17.69	939.4	14.7

Cycle efficiency = 32.2%
Receiver efficiency = 85%
Solar input = 7.3MW_t

Figure 2-27. 2-MW_e Preferred Cycle Configuration Flow Schematic

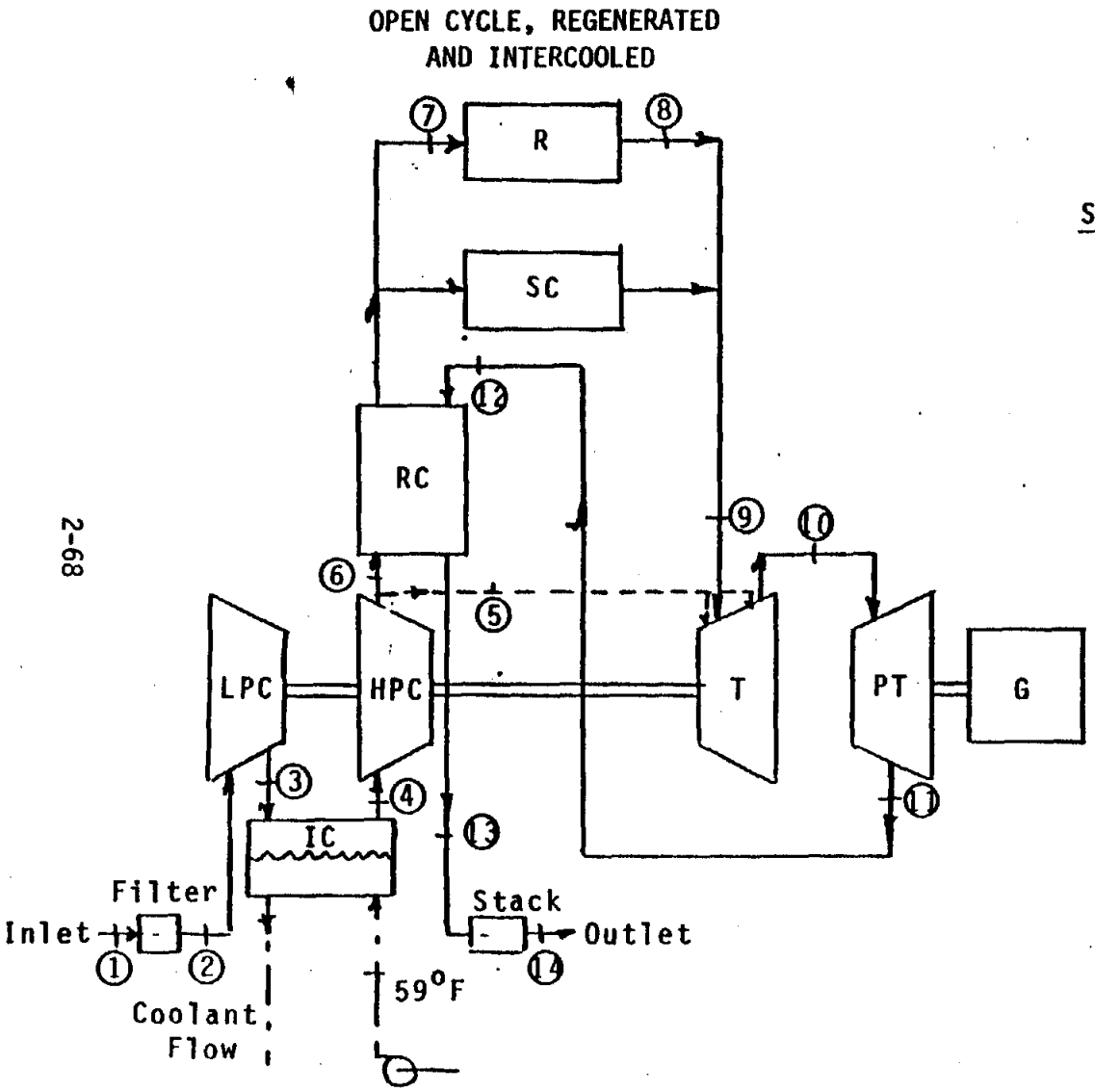

Station	$\dot{m}$ (lbm/s)	T (°F)	P (psia)
1	172.89	59	14.7
2	172.89	59	14.6
3	172.89	282.7	46.2
4	172.89	80	45.3
5	7.78	314.7	143.3
6	165.11	314.7	143.3
7	165.11	988.9	141.9
8	165.11	2040.0	127.7
9	165.11	2040.0	127.7
10	172.89	1575.2	55.6
11	172.89	1060.5	15.5
12	172.89	1060.5	15.5
13	172.89	423.5	14.9
14	172.89	423.5	14.7

Cycle efficiency = 49.5%
Receiver efficiency = 85%
Solar input = 59.6MW_t

Figure 2-28. 25-MW_e Preferred Cycle Configuration Flow Schematic

2.8 ALTERNATIVE CLOSED CYCLE WORKING FLUID ASSESSMENT

In the evaluation of closed cycle systems for this study, only closed cycle air systems were considered. This decision was made largely on the results of previous BEC studies which compared closed cycle helium and air systems (5, 6). Those comparisons showed the capital and busbar energy costs for the closed cycle air system lower than for the closed cycle helium system.

Recently, researchers have explored the possibilities of mixing helium with carbon dioxide, argon or xenon (23, 24). By mixing high molecular weight gases with helium, early calculations showed the high heat transfer available with helium could be maintained with reduced turbomachinery sizes and costs plus increased cycle efficiency. A limited assessment of the use of helium mixtures as potentially affecting the preferred cycle selection was included in this study.

Helium mixtures appear to have some potential heat transfer and thermodynamic performance benefits for closed cycles. However, the cost effectiveness of helium mixtures has not been established. This is especially true for mixtures with rare and expensive gases such as xenon. The most attractive mixture to date appears to be helium and carbon dioxide. At the 1093°C (2000°F) working fluid temperatures considered in this study, carburization caused by the CO_2 would be a concern. Recent experimental studies (25, 26) of gas mixtures are showing the mixture heat transfer properties not as high as first estimated. If this trend continues, some of the original impetus to use of helium mixtures will disappear.

The conclusion of this limited assessment is that there is no strong incentive to consider alternatives to closed cycle air in this study. It is not clear from the data available presently that helium mixture working fluids offer enough cost and performance benefits to justify the increased system complexity. The availability of turbomachinery operating with these gas mixtures is also an issue.

3.0 HIGH-TEMPERATURE RECEIVER STUDY

As a result of the Brayton Cycle Configurations Study described in the previous section, a preferred cycle configuration was selected for each plant size range. The objective of the High-Temperature Receiver Study was to determine preferred air-heating receiver concepts for each of the preferred cycle configurations.

The High-Temperature Receiver Study plan is illustrated in Figure 3-1. A high-temperature materials study was initiated to determine which materials would be appropriate for the high-temperature receiver application. Receiver heat exchange concepts were identified as potentially being applicable to the chosen preferred cycles. A screening process identified those receiver concepts to receive further assessment. A preferred receiver concept was selected for each size range. Additional design analyses were performed to allow an estimate of the system cost and performance. Plans to reduce the technical risk were developed. The following paragraphs describe the results from each of these subtasks.

3.1 HIGH-TEMPERATURE HEAT EXCHANGE CONCEPT IDENTIFICATION

3.1.1 Receiver Design Requirements

The performance requirements for the receiver subsystem at design point conditions (950 W/m^2, 15°C [59°F], March 21, solar noon) are presented in Table 3-1 for the 2-MW_e and 25-MW_e plants.

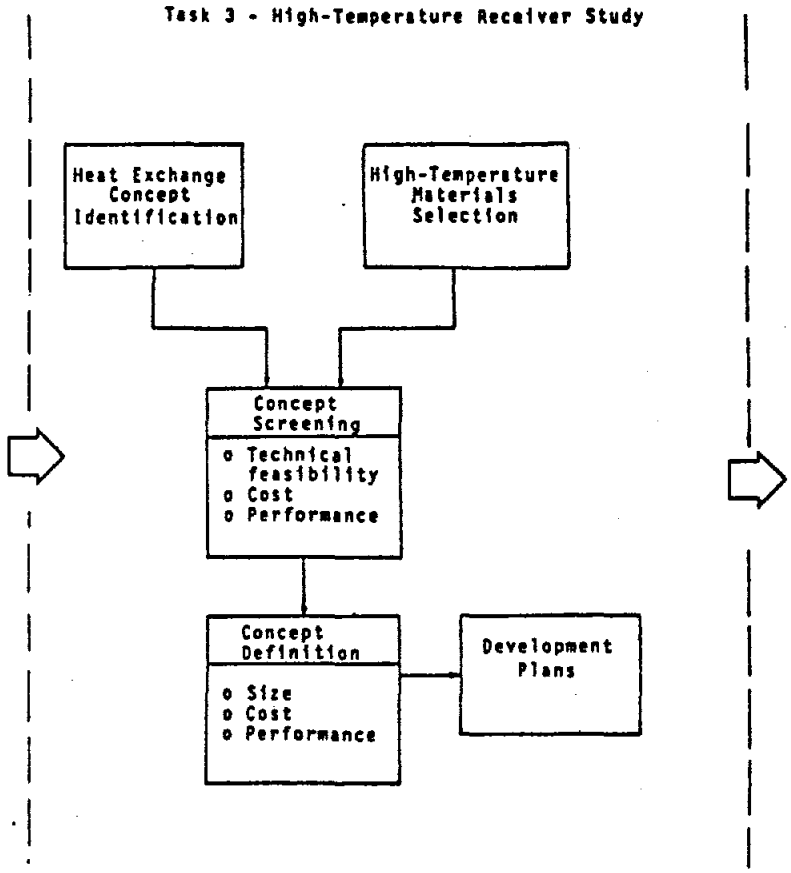

Figure 3-1. High-Temperature Receiver Study

Table 3-1. Receiver Design Requirements

	25-MW_e Plant	2-MW_e Plant
Mass Flowrate, lbm/s	165.1	16.89
Inlet temperature, ^oF	989	763
Outlet temperature, ^oF	2040	2040
Inlet pressure, psia	142	219
Outlet pressure, psia	128	197
Receiver efficiency, %	85	85
Solar input, MW_e	59.6	7.3

3.1.2 Classification of Receiver Concepts

Table 3-2 presents a list of the identified receiver concepts applicable for operation at 1093°C (2000°F). Concept proponents and references are noted where available. The concepts are classified by heat exchange type. The intimate contact heat exchange classification includes concepts wherein the solar absorption and air-heating occur simultaneously, i.e., air is the receiver working fluid. Also the solar absorption process occurs at a surface which becomes hot and is cooled by the circulating air. A temperature difference then exists between solar absorber and the circulating air. In the direct absorption concepts, solar absorption and air heating also occur simultaneously and air is the receiver working fluid. However, solar absorption occurs on a volume basis by the presence of suspended particles or packed beds. The solar absorber and circulating air are at essentially the same temperature. Reradiation from the inner particles is hindered by the presence of the outer particles. In the intermediate medium heat exchange concepts, the solar-absorption and air-heating processes are separated. Media with high heat transfer capability absorb the solar energy in a compact receiver and in a secondary heat exchange process produce the heated air.

Table 3-2. Receiver Concept Candidates

- o Intimate Contact Heat Exchange
  - Atmospheric Pressure
    - Ceramic matrix (Sanders, Ref. 9)
    - Volumetric (PNL, Ref. 9)
  - Pressurized
    - Ceramic tube (B&V, Ref. 9 & 27)
    - Ceramic dome (MIT, Ref. 9)
- o Direct Absorption Heat Exchange
  - Transparent tubes
    - Suspended particles (LBL, Ref. 9 & 28)
    - Fluidized bed (Westinghouse, Ref. 29)
  - Windowed Receiver
    - Small particle (LBL, Ref. 9 & 28)
    - Absorbing gas
- o Intermediate Medium Heat Exchange
  - Solid medium
    - Absorbing particle (SNLL, Ref. 30)
    - Phase change (U of W, Ref. 31)
  - Liquid medium
    - Molten salt (SERI, Ref. 32)
    - Heat Pipe (Bechtel, Dynatherm, Ref. 9)
    - Molten metal
  - Gaseous medium

The intimate contact heat exchange concepts are broken into atmospheric pressure and pressurized categories. Flow schematics for the atmospheric pressure receivers are shown in Figures 3-2, -3 and -4. Since the receiver operates at atmospheric pressure and the gas turbine at 10-20 atm, a secondary heat exchange is required. Three options are shown: a secondary heat exchanger, two checker stoves, and three checker stoves. All three options require the receiver outlet air temperature to be higher than the required 1116°C (2040°F) turbine inlet temperature from Table 3-1. An induced draft fan provides the motive force to draw atmospheric pressure air into the receiver and through the secondary heat exchange system.

In the secondary heat exchange option, an effectiveness of 90% was assumed. The lowest receiver outlet temperature for 1116°C (2040°F) turbine inlet temperature occurs when the mass flow-heat capacity product, i.e., $\dot{m}\ C_p$, is equal for both the hot and cold side of the heat exchanger. This results in a requirement of 1181°C (2157°F) from the receiver. The receiver air stream is cooled to 596°C (1106°F), however, the air must still flow through the induced draft fan. Fans with a 593°C (1100°F) temperature capability can be identified (33) for small pressure ratios across the fan. Drawing a vacuum of 18.675 Pa (75 in H_2O) at STP conditions (1 atm, 15°C = 59°F) is approximately maximum for such a fan. At 596°C (1106°F), this maximum vacuum translates into 6200 Pa (0.9 psi) or a pressure ratio of 1.065. Use of such a fan would require designing the receiver and secondary heat exchanger to a 6.5% pressure drop which would be very difficult to accomplish. As an alternative, a precooler is utilized in Figures 3-2, -4, and -4 to cool the fan inlet air temperature to a level where higher presure ratio fans can be used. The checker work options shown in Figures 3-3 and -4 require a lesser receiver outlet temperature, but still require a fan precooler. The three checker stove option would allow elimination of the recuperator in the 25-MW_e plant case. The ceramic receiver matrix and volumetric receiver concepts are illustrated in Figures 3-5 and 3-6 and are described in more detail in References 9 and 11.

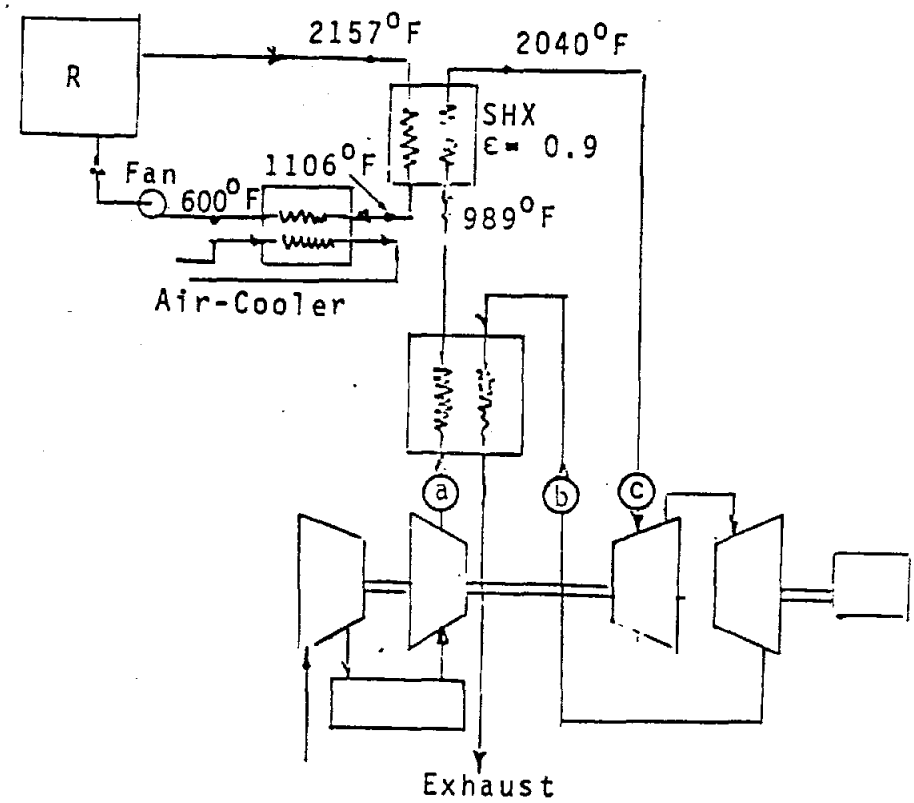

Figure 3-2. Atmospheric Pressure Receiver Flow Schematic - Option 1

TWO CHECKER STOVES

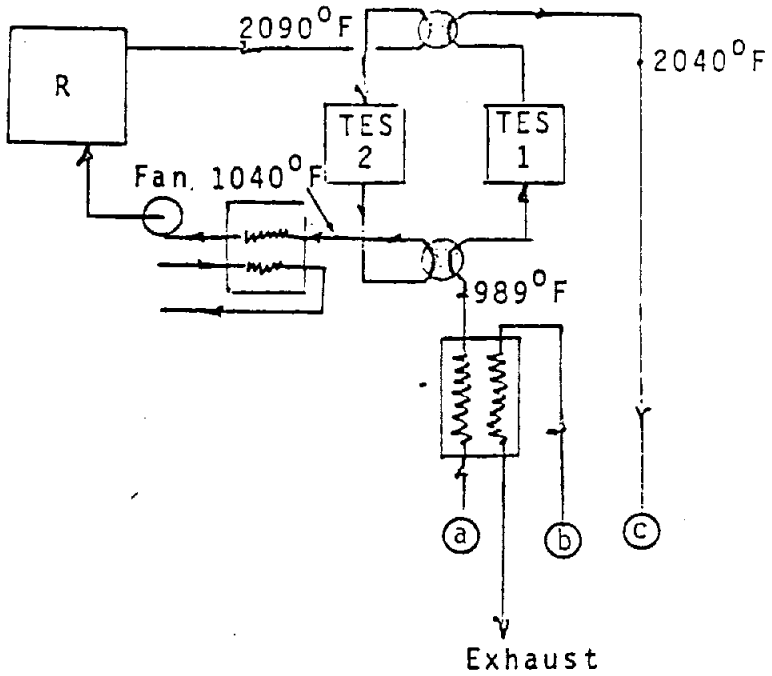

Figure 3-3. Atmospheric Pressure Receiver Flow Schematic - Option 2

THREE CHECKER STOVES

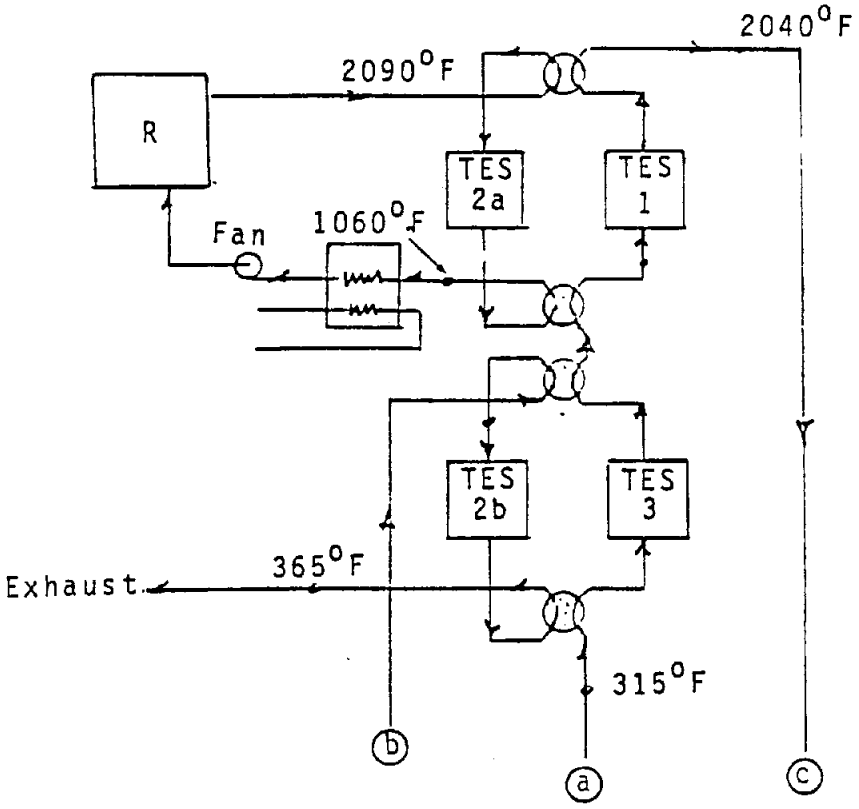

TES 3 AND 2B REPLACE RECUPERATOR

Figure 3-4. Atmospheric Pressure Receiver Flow Schematic - Option 3

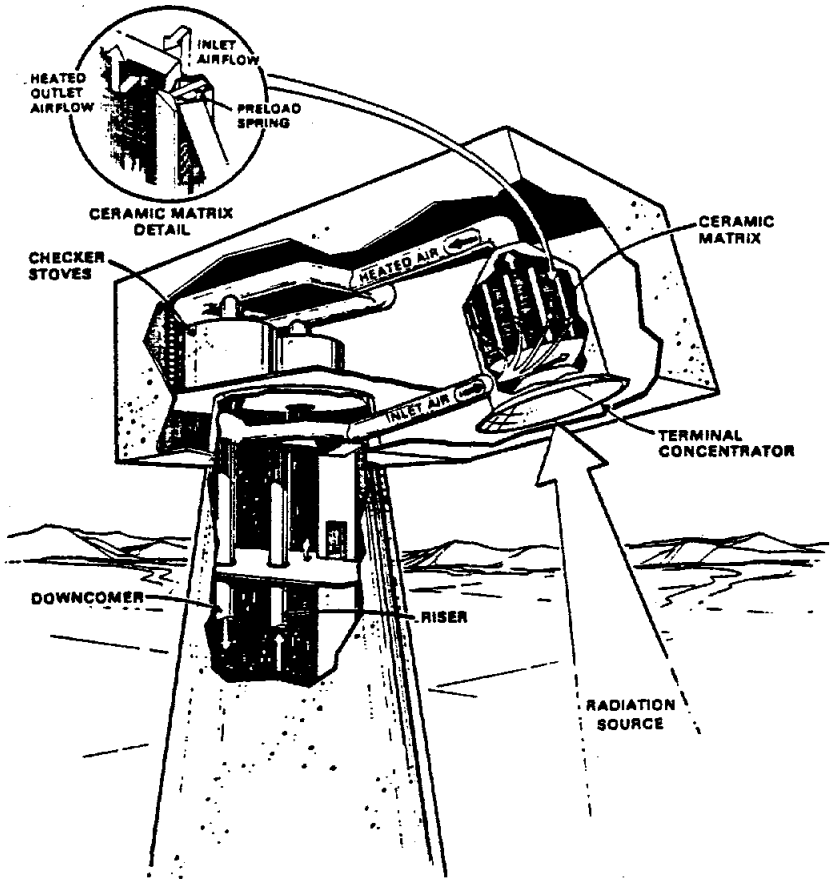

Figure 3-5. Ceramic Matrix Receiver Concept

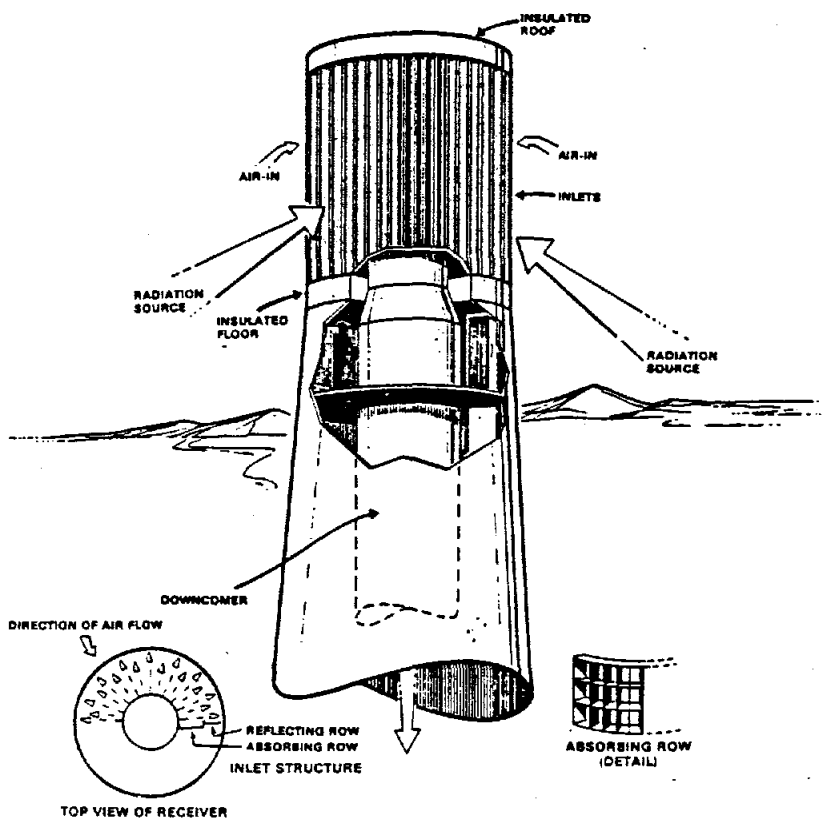

Figure 3-6. Volumetric Receiver

A flow schematic for the pressurized receiver concepts is shown in Figure 3-7. The air-cooled heat exchanger is irradiated in a solar cavity. Ceramic tube approaches are illustrated in Figure 3-8. The ceramic dome approach is illustrated in Figure 3-9.

Direct absorption heat exchange concepts use the flow schematic shown in Figure 3-7. This concept type is divided into two categories: transparent tubes and windowed receiver. Transparent tube concepts are illustrated in Figure 3-10. Windowed receivers are illustrated in Figure 3-11.

The intermediate heat exchange concept flow schematic is shown in Figure 3-12. This schematic is similar to that of Figure 3-2 except that a pump or conveyor is used to return the heat transfer medium to the receiver. These concepts also require a higher receiver outlet temperature than the gas turbine inlet temperature. The intermediate medium can be solid, liquid or gaseous. The solid medium category concepts are illustrated in Figures 3-13 and 3-14. The absorbing particle concept absorbs the solar energy in the sensible heat of the particle whereas the phase change particles become molten.

In the liquid intermediate medium, a molten salt or a liquid metal is used as the receiver fluid. The molten salt can be contained in tubes as is done in the current lower temperature molten salt receivers. An alternative is to use a blackened molten salt and to absorb the solar energy directly into the salt as illustrated in Figure 3-15. A direct contact heat exchanger could be used to heat the air for the gas turbine.

Several options are also available for the liquid metal approach. A liquid metal heat pipe could be used as illustrated in Figure 3-16. Also a molten metal could be used in tubes as in the lower temperature central receiver concepts. An alternative would use a closed container of a boiling metal which is cooled by air flowing through ceramic tubes as illustrated in Figure 3-17. Another option would be to use a liquid metal bath as also illustrated in Figure 3-18.

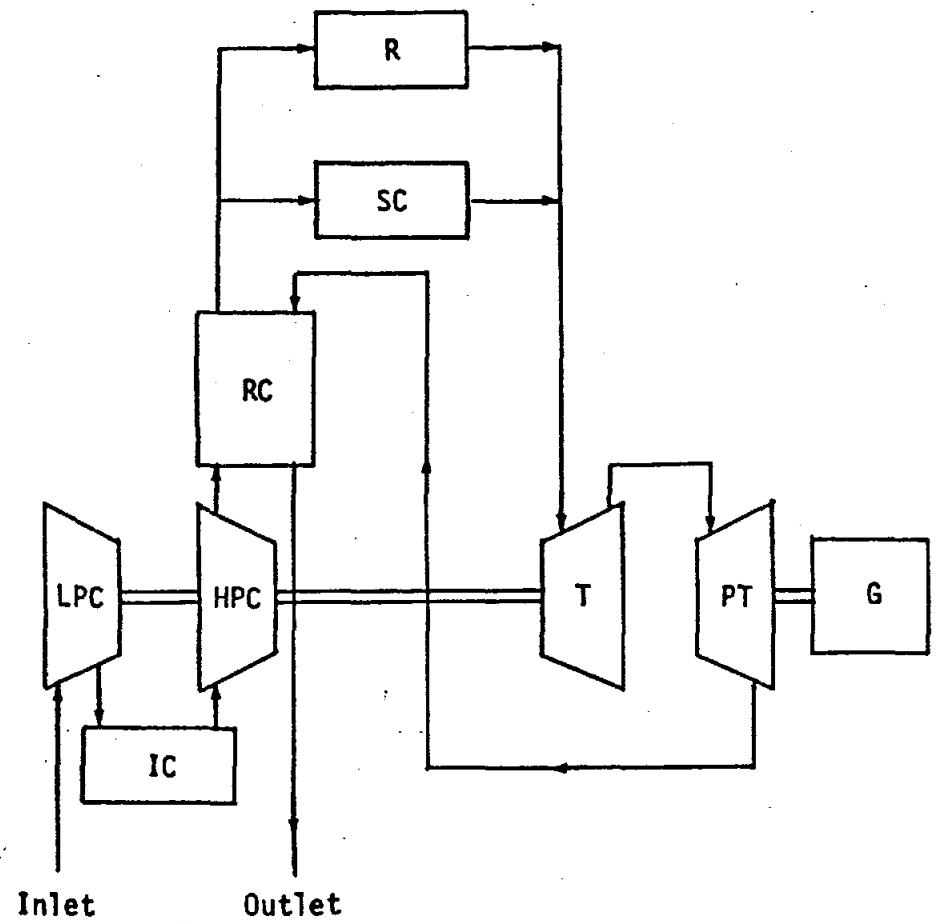

R = RECEIVER
SC = STARTUP COMBUSTOR
C = COMPRESSOR
LPC = LOW PRESSURE COMPR.
HPC = HIGH PRESSURE COMPR.
IC = INTERCOOLER
RC = RECUPERATOR
T = TURBINE
PT = POWER TURBINE
G = GENERATOR

Figure 3-7. Pressurized Receiver Flow Schematic

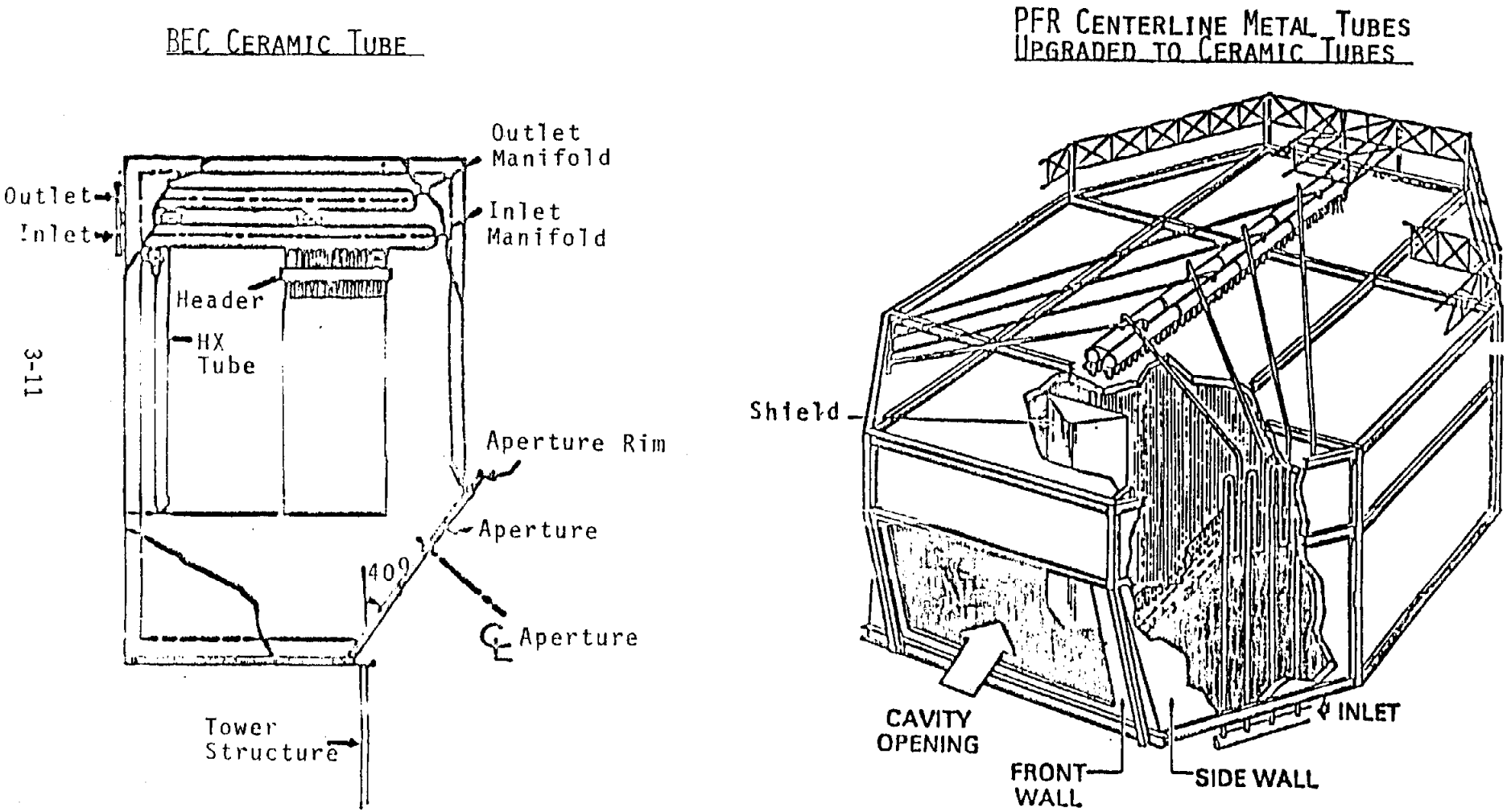

Figure 3-8. Ceramic Tube Receiver Concepts

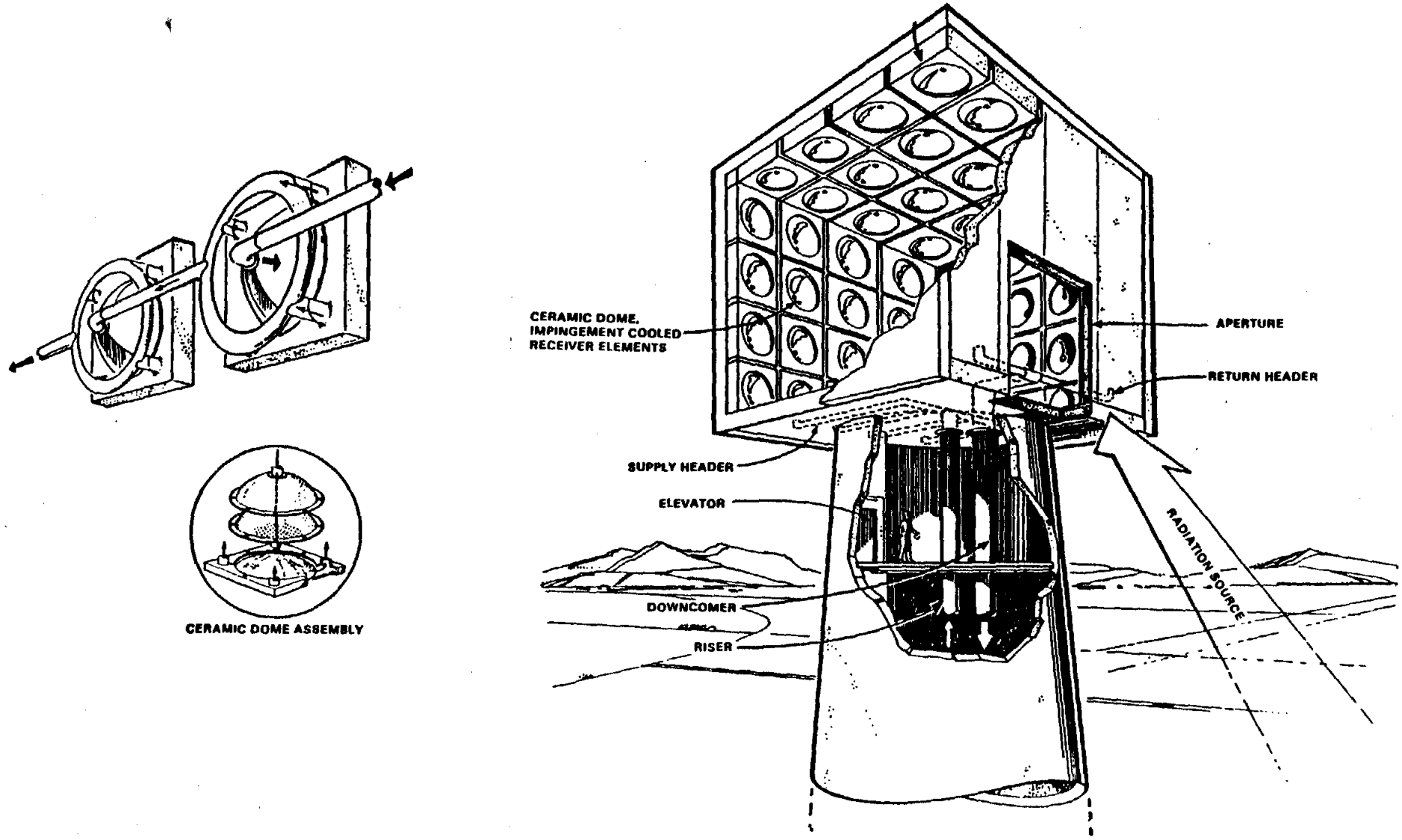

Figure 3-9. Ceramic Dome Receiver Concept

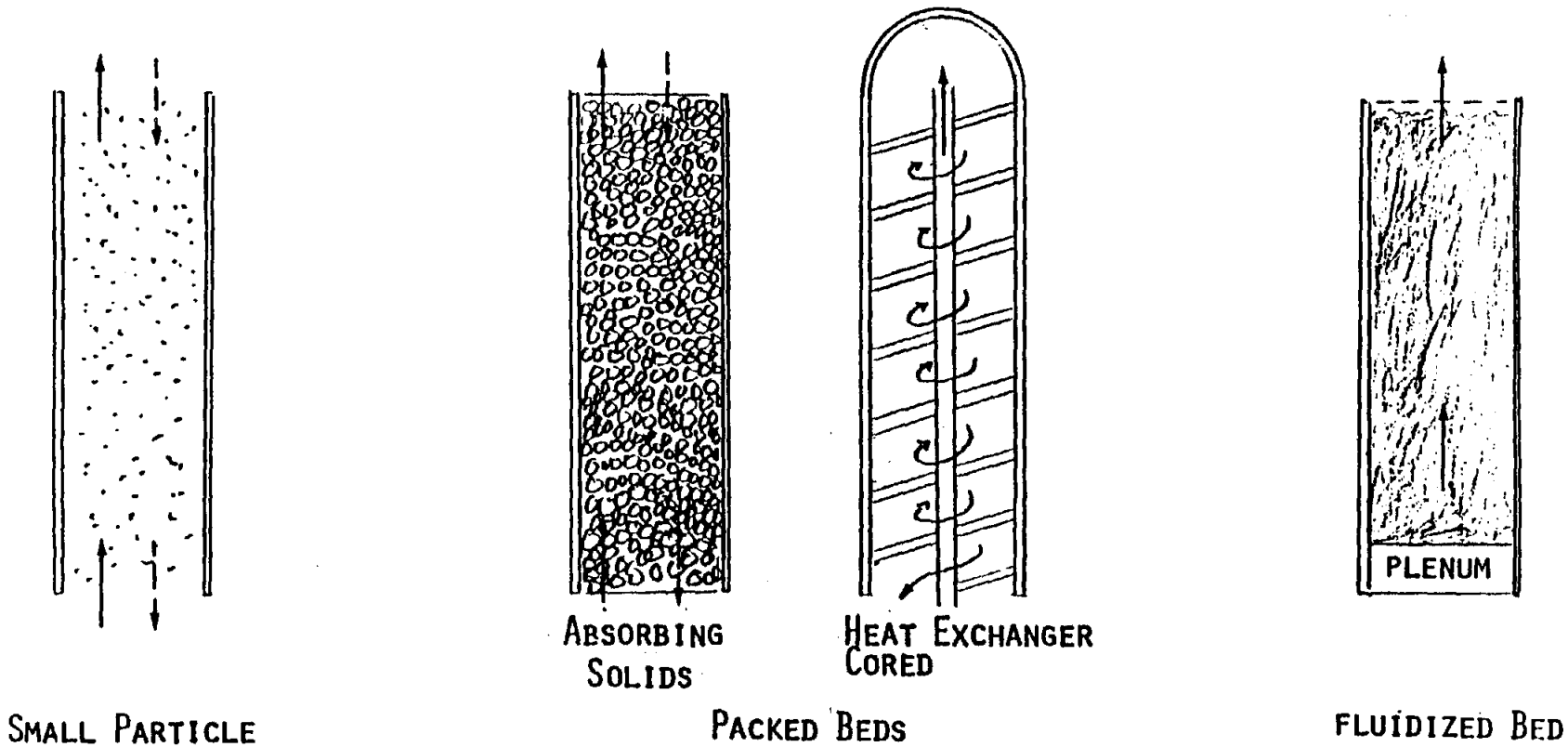

Figure 3-10. Transparent Tube Receiver Concepts

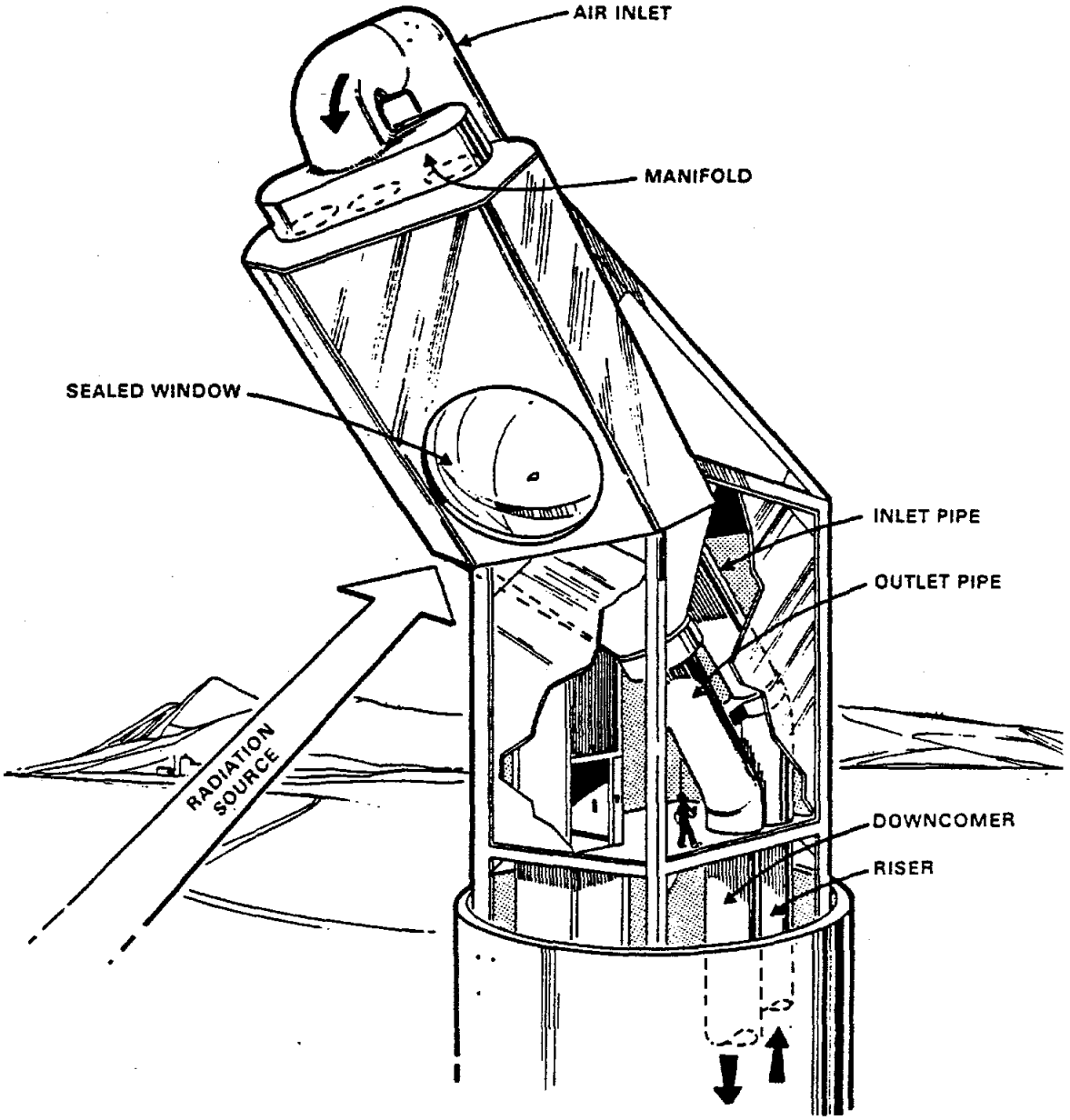

Figure 3-11. Small Particle Receiver Concept

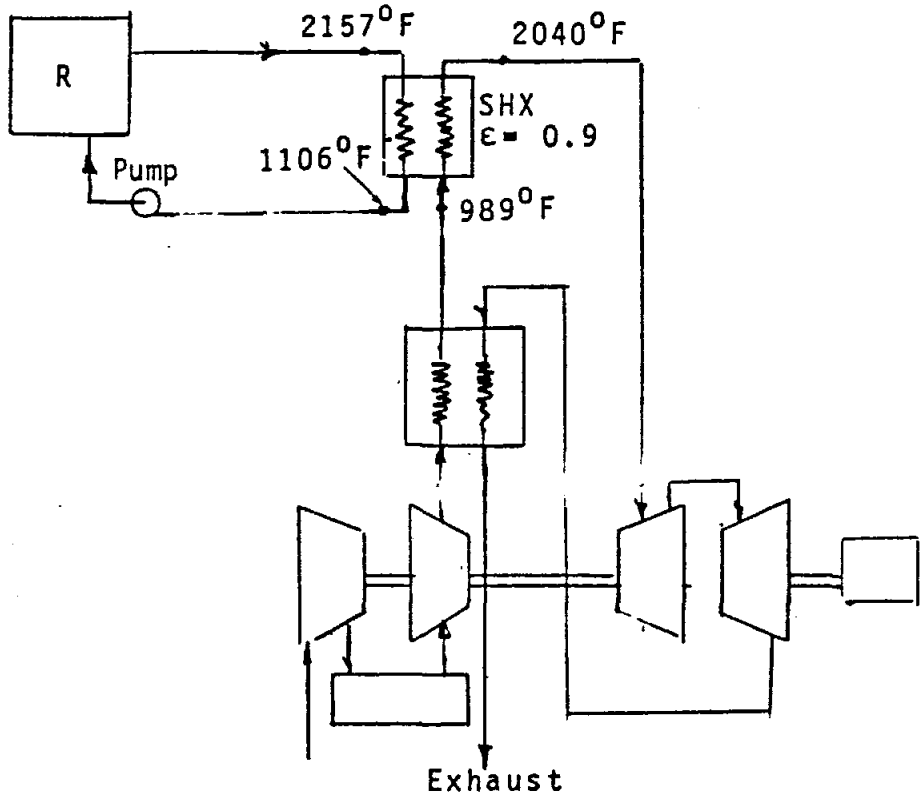

Figure 3-12. Intermediate Fluid Heat Exchange Flow Schematic

ALTERNATIVE CONCEPT

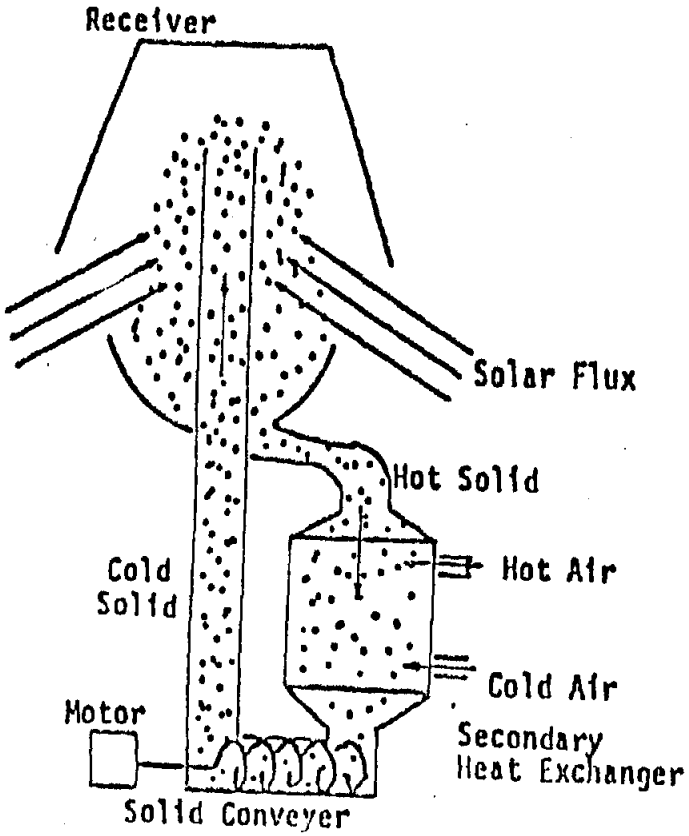

ASCUAS RECEIVER

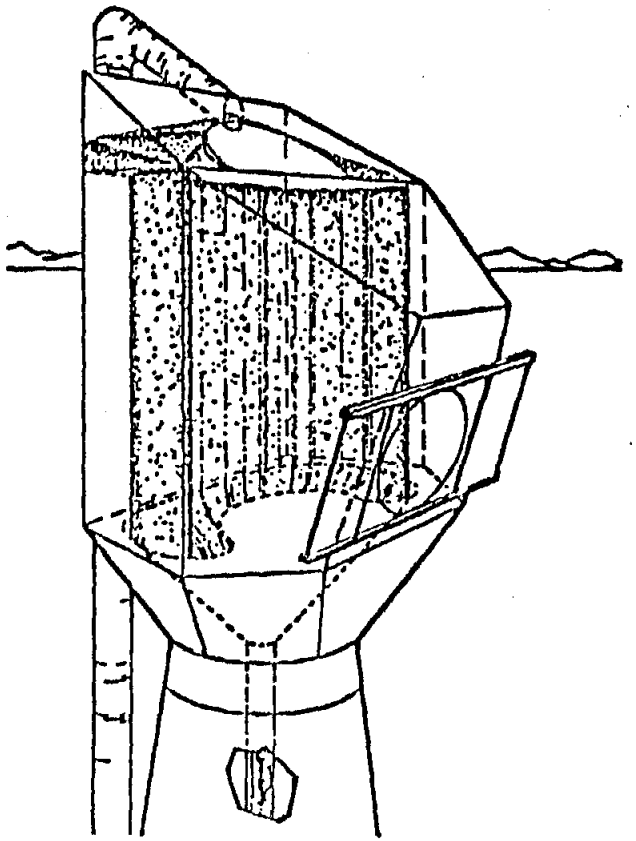

Figure 3-13. Falling Particle Receiver Concepts

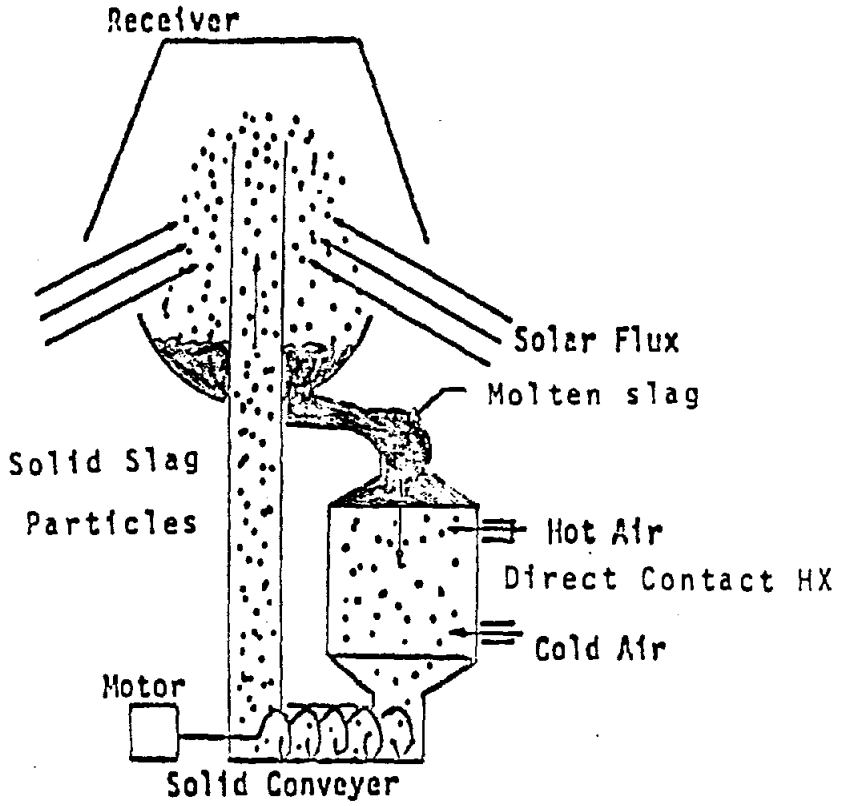

Figure 3-14. Phase Change Falling Particle Receiver Concept

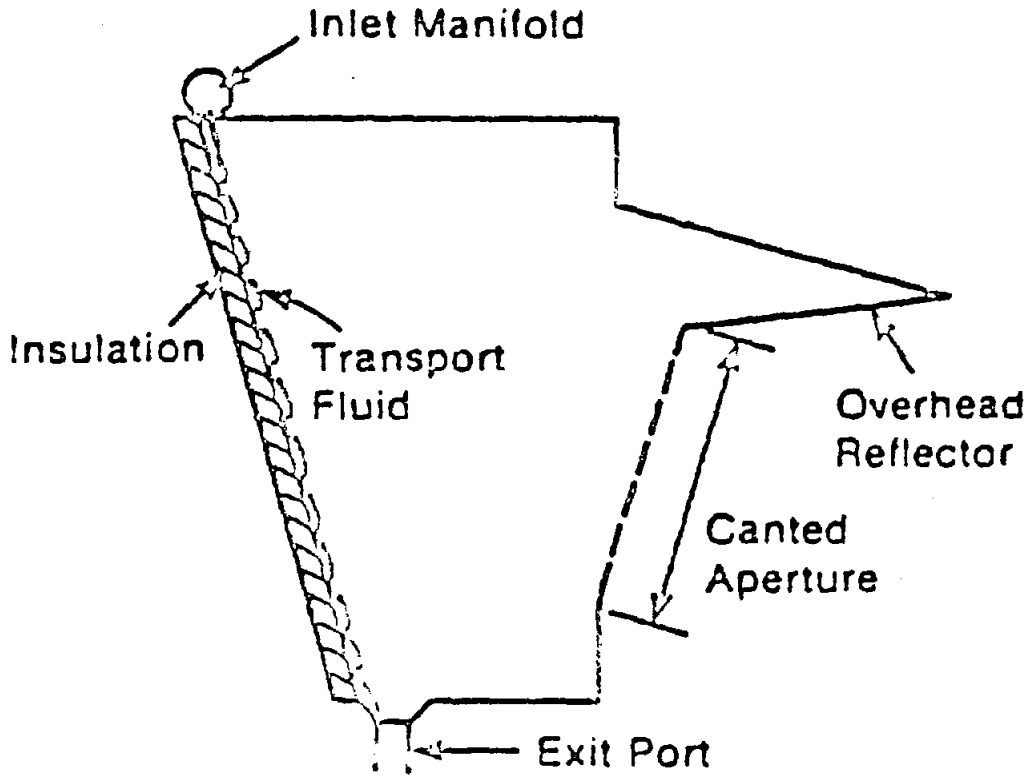

Figure 3-15. High-Temperature Molten Salt Receiver Concept

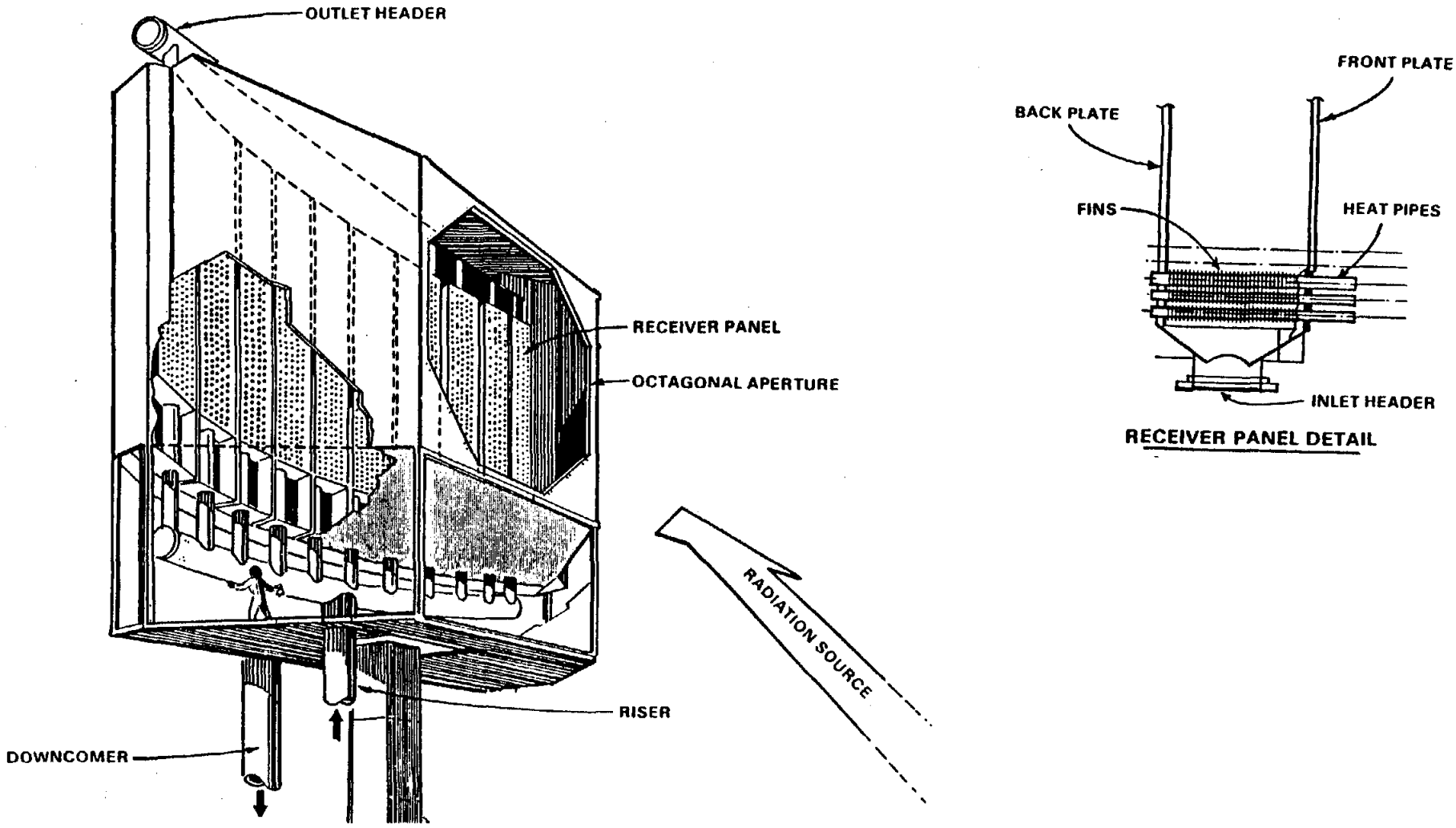

Figure 3-16. Liquid Metal Heat Pipe Receiver Concept

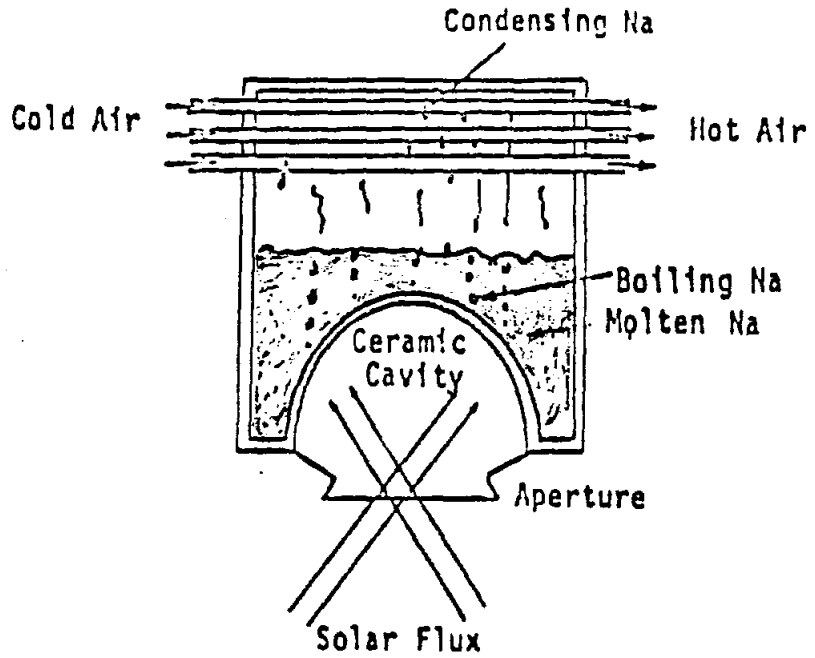

Figure 3-17. Boiling Metal Receiver Concept

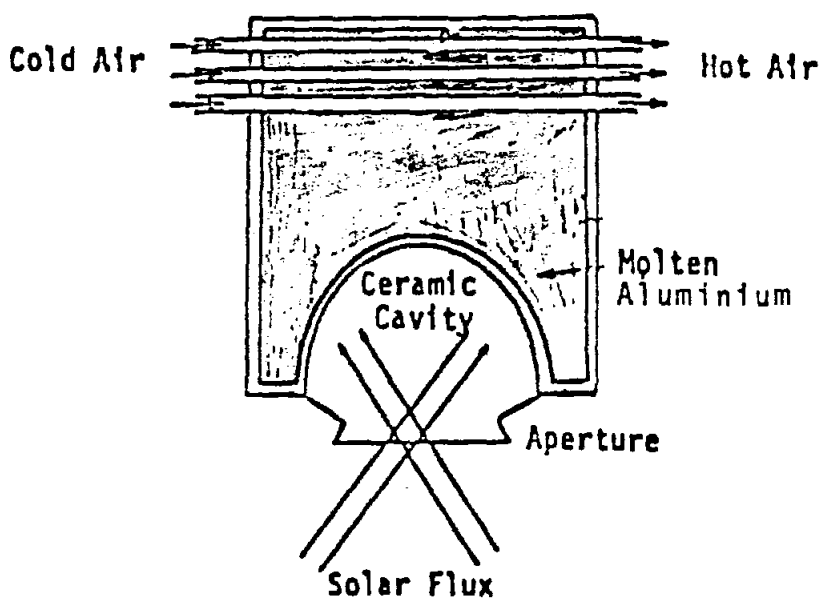

Figure 3-18. Liquid Metal Bath Receiver Concept

The heat pipe and molten metal concepts require a heat transfer medium capable of temperatures of at least 1093°C (2000°F). To use sodium, the heat pipe and boiling metal concepts would have to be pressurized to about 0.55 MPa (80 psia). These requirements were felt to be beyond foreseeable power plant technology. Molten aluminum is also a possible liquid heat exchange medium at these temperatures. However, contact with knowledgeable aluminum experts (34) showed little experience with molten aluminum as a heat transfer fluid owing to its corrosive effect on most materials. For these reasons, the molten metal concepts were dropped from further consideration.

Conceptually, a gaseous intermediate medium could also be used. However, high pressure gas would have to be used to approach the heat transfer capabilities of molten salt or liquid metal. Also, power would be required to run the compressor and a precooler would be required to reduce the compressor inlet temperature. Because of these considerations, the gaseous intermediate concept was dropped from further consideration.

3.2 RECEIVER CONCEPT INITIAL SCREENING

3.2.1 Preliminary Screening

The objective of the preliminary screening subtask was to reduce the 15 concepts of Table 3-2 to a smaller number for further evaluation. References 9 and 11 considered air-heating receivers for process heat applications. In those studies, several of the same receiver concepts presented in Table 3-2 were evaluated over a matrix of thermal output, receiver pressure, and receiver outlet temperature. One such combination was 50 MW_t (into fluid), 10 atm, and 1093°C (2000°F). Comparison with the requirements for the 25-MWe plant, open cycle, regenerated and intercooled configuration reveals a need for 50.7 MW_t (into fluid), 10 atm, and 1116°C (2040°F) or nearly the same as the previous study. Therefore, many of the data from those references were directly applicable to this study.

Table 3-3 presents a summary of data for five receiver concepts from References 9 and 11. A small particle version at 10 atm, 1092°C (2000°F) and 50 MW_t was not considered in the reference 9 and 11 studies although a 10 atm, 816°C (1500°F), 50-MW_t version was considered. Comparison of 5-atm, 50-MW_t 816°C (1500°F) and 1093°C (2000°F) receivers showed differences only in the carbon particle loading rate. Therefore, the 10-atm, 816°C (1500°F), 50-MW_t receiver data are displayed in Table 3-3 assuming the carbon particle loading rate is adjusted to produce 1093°C (2000°F).

Table 3-4 shows the same five receiver concepts adjusted for the ORI, 25-MW_e configuration. The atmospheric pressure receivers show the increased receiver outlet temperature and mass flow rate required to transfer 50.7 MW_t into the gas turbine fluid circuit. The exhaust from the fan (fan efficiency = 90%, pressure ratio = 1.5, inlet temperature = 316°C [600°F]) at 371°C (700°F) is ducted to the ceramic matrix inlet. For the volumetric receiver, ambient temperature air is assumed at the receiver inlet. Because of the requirement for cooling the receiver air after the secondary heat exchanger and before the circulating fan, the amount of energy transferred to the receiver fluid circuit to yield a 50.7MW_t transfer in the gas turbine circuit is substantially higher for the two atmospheric pressure concepts. To calculate the relative solar input to the receiver subsystem, the field efficiency for the various receiver concepts was assumed equal. Intercept, receiver absorption, and thermal efficiencies were assumed from Table 3-3. Their product was used to yield an effective receiver efficiency (also includes spillage). The required solar inputs are as shown.

Table 3-4 shows that the atmospheric pressure receivers require substantially more solar input than the ceramic tube concept. Even if the secondary heat exchanger, air precooler and fan were free, it is very doubtful that the atmospheric pressure receivers could compete with the other concepts. For that reason the atmospheric pressure concepts were dropped from further study. If a steam bottoming cycle or an industrial process were included instead of the fan precooler, these concepts would be much more attractive. However, steam bottoming and industrial process heat were beyond the current study scope.

Table 3-3. Summary of Receiver Performance Data (9, 11)
50 MWt, 2000°F Air-Heating Receiver Concepts

	PARAMETER	UNITS	RECEIVER CONCEPT				
			CERAMIC TUBE	CERAMIC DOME	SMALL PARTICLE	CERAMIC MATRIX	VOLUMETRIC
Design	Pressure	atm	10	10	10	1	1
	Inlet temp	°F	663	663	663	59	59
	Mass flow	lbm/s	133.3	133.3	133.3	93.3	93.3
	Tower ht.	m	85	90	90	90	55
	Aperture size	m	7 x 7	6.5 x 6.6	6.0 dia.	11.5 dia.	--
	Absorber area	m^2	859.6	243.8	28.3	177	78.5
Performance	Field eff.	--	.775	.771	.774	.778	.712
	Intercept eff.	--	.809	.737	.659	.896	.881
	Receiver abs.	--	.989	.968	.934	.902	.988
	Thermal eff.	--	.818	.769	.954	.881	.987
	Total recr. eff.*	--	.654	.549	.587	.712	.859
	Power into fluid	MWt	50.9	50.9	50.9	50.2	50.2
	Solar input to RCR**	MWt	77.8	92.7	86.7	70.5	58.4

*Total receiver eff = intercept x receiver abs. x thermal eff.
**Solar input up to receiver (includes spillage)

Table 3-4. Receiver Concepts Comparison

	PARAMETER	UNITS	CERAMIC TUBE	CERAMIC DOME	SMALL PARTICLE	CERAMIC MATRIX	VOLUMETRIC
Design	Receiver Inlet	^{o}F	989	989	989	700	59
	Receiver outlet	^{o}F	2040	2040	2040	2157	2157
	Mass flow	lbs/s	165.1	165.1	165.1	166.7	172.7
	Pressure	atm	10	10	10	1	1
Performance	Intercept eff.	--	.809	.737	.659	.896	.881
	Receiver absorpt.	--	.989	.968	.934	.902	.988
	Thermal eff.	--	.818	.769	.954	.881	.987
	Total rec. eff.	--	.654	.549	.587	.712	.859
	Power into RCR fluid	MW_{th}	50.7	50.7	50.7	70.3	101.2
	Solar input to RCR	MW_{th}	77.5	92.3	86.4	98.7	117.8
	Relative solar input	--	1.0	1.19	1.11	1.27	1.52

The ceramic dome concept suffers from spillage and high thermal losses. It also is less attractive than the ceramic tube concept based on the amount of solar input required.

The small particle receiver aperture window diameter was assumed at 6.0 m for this evaluation. This diameter is consistent with manufacturing limits on available window materials (9). Table 3-4 shows the intercept efficiency to be small relative to the other concepts because of the 6.0-m window diameter constraint. The small particle receiver absorption and thermal efficiency are relatively higher. However, the required solar input to the small particle receiver is about 10% higher than that for the ceramic receiver concept thus making the small particle concept less attractive.

Out of the five concepts shown in Table 3-4, the ceramic tube concept is preferred. However, several other receiver concepts from Table 3-2 have not been considered. Table 3-5 shows the remaining generic receiver concepts suggested for further evaluation. Each of the 25-MW_e receiver concepts absorb the solar input in a cavity and reradiate to an aperture. Because of this, the cavity heat transfer is similar for each concept.

Table 3-5. Selected Receiver Concepts for Further Evaluation

- 25-MW_e Plant
  - Ceramic tube
  - Transparent tubes
  - Falling solid
  - Molten salt
- 2-MW_e Plant
  - Ceramic tube
  - Transparent tube
  - Small particle
  - Falling solid
  - Molten salt

At the 2-MW_e plant size, the small particle receiver was also included in the list of concepts for further evaluation. At the smaller plant size, the small particle receiver window diameter would not be a limiting factor. The small particle's high absorption and thermal efficiency make it an attractive alternative.

The approach for the further evaluation of the concepts of Table 3-5 was to analyze the cavity heat transfer and the design-related issues of each concept. These areas are discussed in the following subsections.

3.2.2 Cavity Thermal Analysis

A steady-state thermal model of a generalized 25-MW_e cavity receiver was developed to facilitate comparison of the receiver concepts listed in Table 3-5. The model was developed with the objectives of determining gross physical sizing and overall receiver thermal performance. Average fluxes and temperatures were utilized. Peak cavity temperatures would not be available from such a model. Detailed receiver thermal analyses under varying worst case plant operation scenarios would be required to ensure that excessive temperatures could be avoided. Such detailed analyses would be required for a successful final design but were beyond the scope of this study. The level of thermal analysis used in this study is appropriate for determining gross absolute performance and accurate relative performance between alternative designs.

Another objective in this thermal analysis subtask was to assess each receiver concept to the same level of detail. A generalized receiver cavity model was used with similar assumptions for each receiver concept. In this way, relative performance between the concepts would be discernable with no one concept penalized or favored because of additional modeling detail.

The cavity thermal analysis began with the generalized receiver cavity described in Figure 3-19. This 25-MW_e plant receiver cavity was sized with DELSOL2 (13) assuming a 600-kW/m^2 peak flux, receiver thermal efficiency = 85%

GENERALIZED RECEIVER

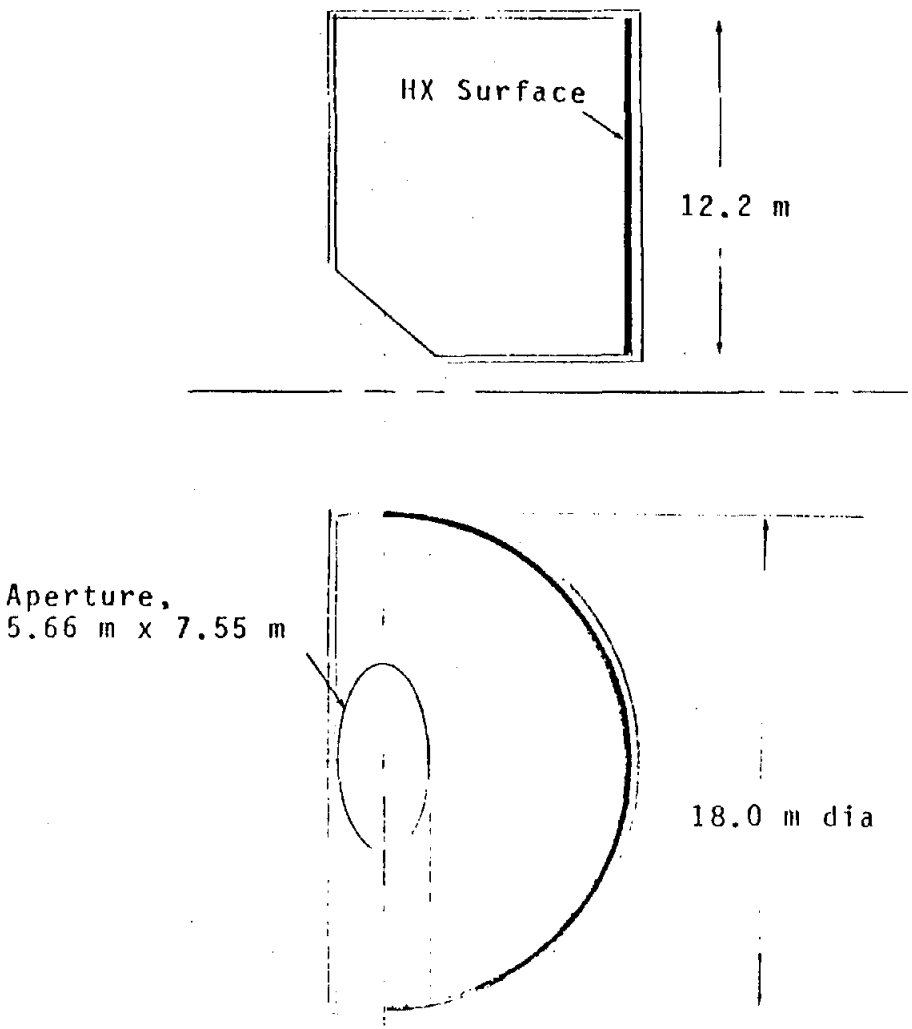

- 25-MWe PLANT RECEIVERS
- USED DELSOL2 TO SIZE RECEIVER
  - 600 kW/m^2 PEAK FLUX
  - RECEIVER EFF. = 85%
  - CYCLE EFF. = 49.5%
- FLUX MAPS PRODUCED BY DELSOL2

Figure 3-19. Generalized 25-MW$_e$ Receiver Cavity Configuration

and a cycle efficiency of 49.5%. The first incident solar flux on the cavity wall is illustrated in Figure 3-20. The peak value occurs on the south wall directly opposite the aperture about 25% up the cavity wall.

The receiver concepts of Table 3-5 each have their own peak flux capabilities. Redesigning a receiver and field for each concept was beyond the resources of this study. However, by keeping the aperture size constant and scaling the distance from the aperture centerline, the approximate cavity size for varying receiver peak fluxes can be obtained as shown in Figure 3-21. Keeping the receiver height to diameter ratios constant will keep the flux distribution approximately constant.

Each cavity was broken into one aperture zone and four heat exchange surface zones as depicted in Figure 3-22. The remaining surfaces were considered adiabatic. Radiative exchange factors, $\mathcal{F}_{ij}$, were calculated using a generalized radiactive interchange computer code (35). The assumed radiative properties are given in Table 3-6.

The solar flux from Figure 3-20 was averaged azimuthally around the cavity wall. Integration of the flux profile produced the distribution of the first incident solar energy. These calculations showed about 13% of the total solar energy entering the aperture was first incident on non-heat exchange surfaces, principally the cavity ceiling. The first incident solar energy was redistributed within the cavity by the following relation:

$$\mathcal{A}_i = \overbrace{\alpha_s S_i}^{\text{Absorbed First Incident}} + \overbrace{(1 - \alpha_s) \sum_{j=1}^{5} S_j \mathcal{F}_{ji}}^{\text{Reflected and Absorbed From HX Surfaces}} + \overbrace{S_i'}^{\text{Reflected From Remaining Cavity Walls}} , \quad i = 1, 2, \ldots 5$$

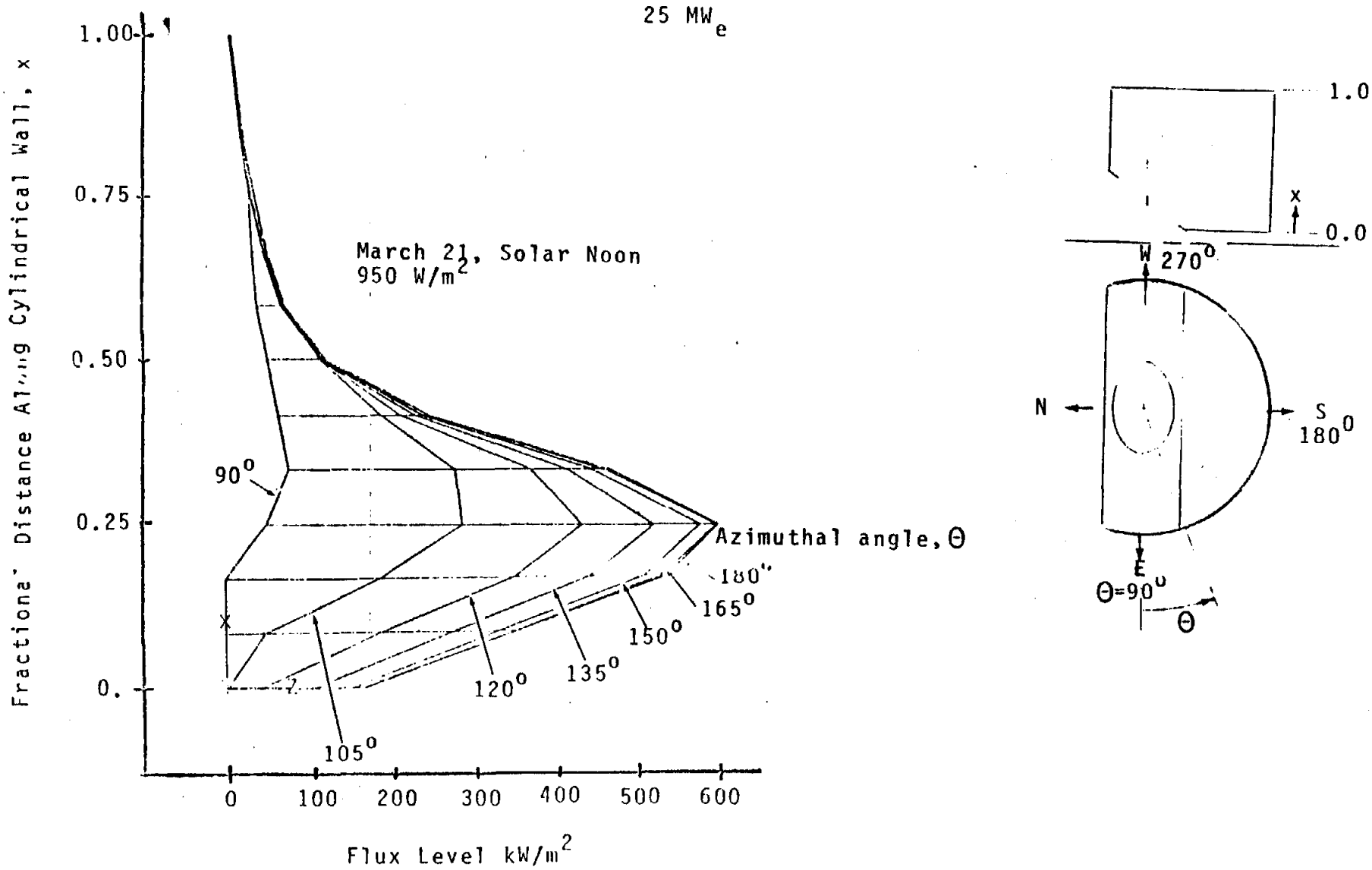

Figure 3-20. First Incident Solar Flux Map

- 450 kW/m^2 = CERAMIC TUBE
- 600 kW/m^2 = MOLTEN SALT, TRANSPARENT TUBE
- 1000 kW/m^2 = FALLING PARTICLE/SOLID
- 2000 kW/m^2 = FALLING PARTICLE/PHASE CHANGE

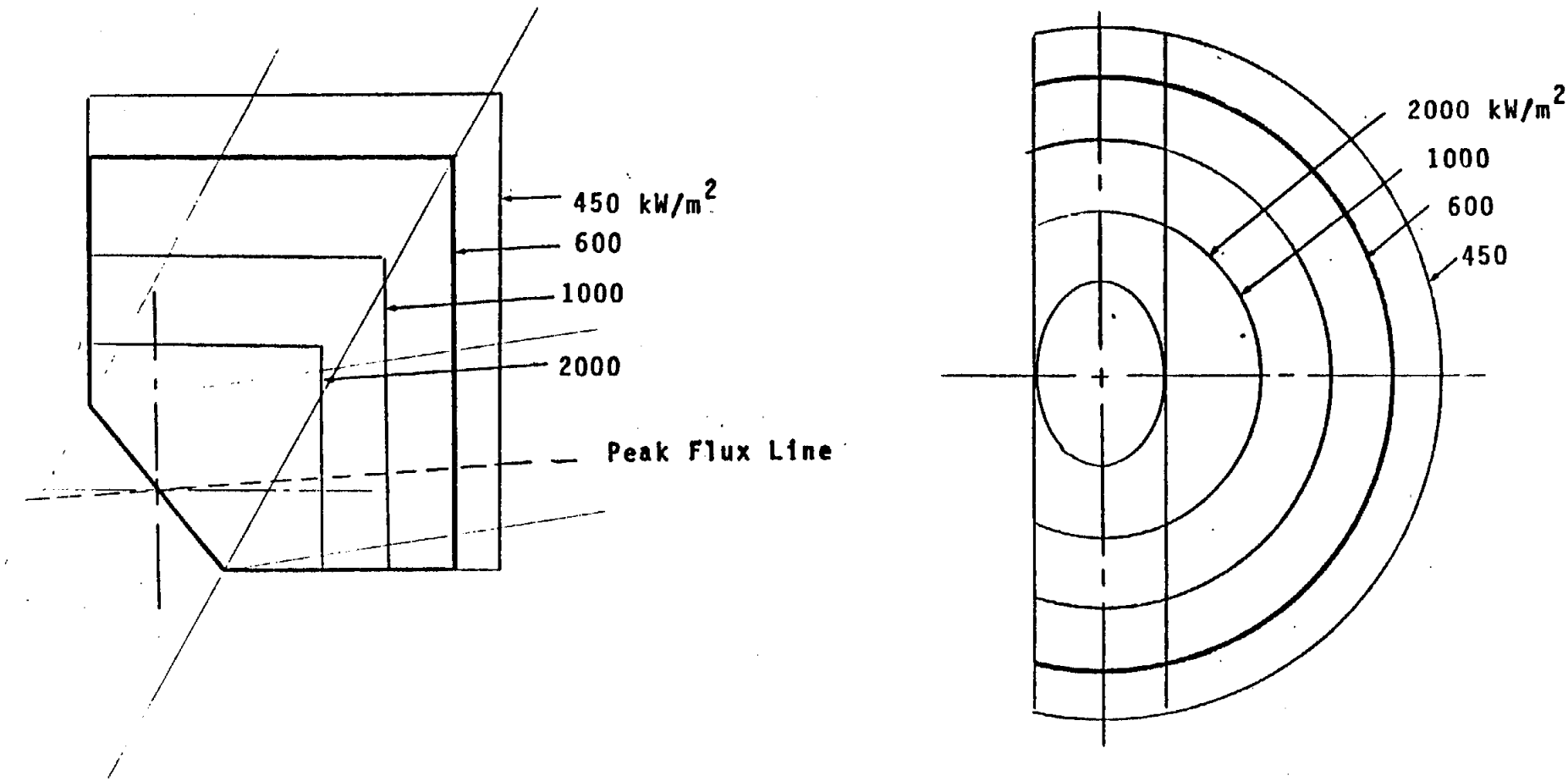

Figure 3-21. Adjustment of Cavity Size for Peak Flux

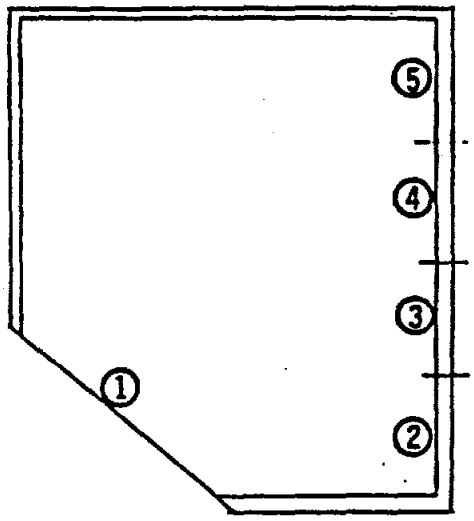

- CAVITY BROKEN INTO ZONES
  - 1 APERTURE ZONE
  - 4 HX SURFACE ZONE
  - REMAINING WALLS TREATED AS ADIABATIC
- EXCHANGE FACTORS, $\mathcal{F}_{ij}$, DETERMINED FOR EACH CAVITY SIZE

Figure 3-22. Radiative Interchange Model

Table 3-6. Assumed Receiver Radiative Properties

Concept	Flux Level kW/m^2	HX Surface Emissivity	Remaining Cavity Wall Emissivity
Ceramic Tube	450	0.90	0.37
Transparent Tube	600	0.95	0.37
Molten Salt	600	0.90	0.37
Falling Particle-Solid	1000	0.85	0.37
Falling Particle-Phase Change	2000	0.85	0.37

Similarly, for the thermal reradiation,

$$\mathcal{A}_i^T = \sum_{j=1}^{5} \sigma A_j \mathcal{F}_{ji} (T_j^4 - T_i^4) \quad , \qquad i = 1, 2, \ldots 5$$

The intermediate heat exchange concepts (molten salt and falling particles) are assumed to require a secondary heat exchange. The intermediate working fluids enter the receiver at 596°C (1106°F) and exit at 1181°C (2157°F). For the transparent and ceramic tube receivers, air enters at 531°C (989°F) and exits at 1116°C (2040°F).

The maximum available heat exchange area for each concept was assumed as the cylindrical cavity wall area depicted in Figure 3-19. The net solar and thermal reradiative inputs as calculated from the above equations were assumed deposited on the heat exchange zones illustrated in Figure 3-22. For the molten salt, falling particle and transparent tube receivers, the energy input was assumed deposited uniformly across the molten salt, falling particle, or carbon particle curtain thickness. The temperature rise for each heat exchange zone was calculated from the net energy input, the medium mass flow rate and heat capacity. The heat exchange zone average fluid temperature was used to calculate the zone reradiated energy. Since the energy input to a given zone depends on a reradiated energy from all the other zones, an iterative process was utilized to determine the final fluid temperature distribution. The total solar input through the aperture was iterated to obtain the desired receiver fluid exit temperature. Figure 3-23 presents the resulting receiver fluid temperature distributions from these analyses.

The ceramic tube receiver was modeled similarly except the energy input was assumed deposited on a ceramic tube wall. The wall was cooled by forced convection and reradiated at the local average wall temperature. An average forced convective coefficient of 300 W/m^2-°C was assumed. This value represents a minimal convective coefficient at these pressures and temperatures based on previous BEC analyses. Figure 3-24 presents the tube wall and gas temperature distribution from these analyses.

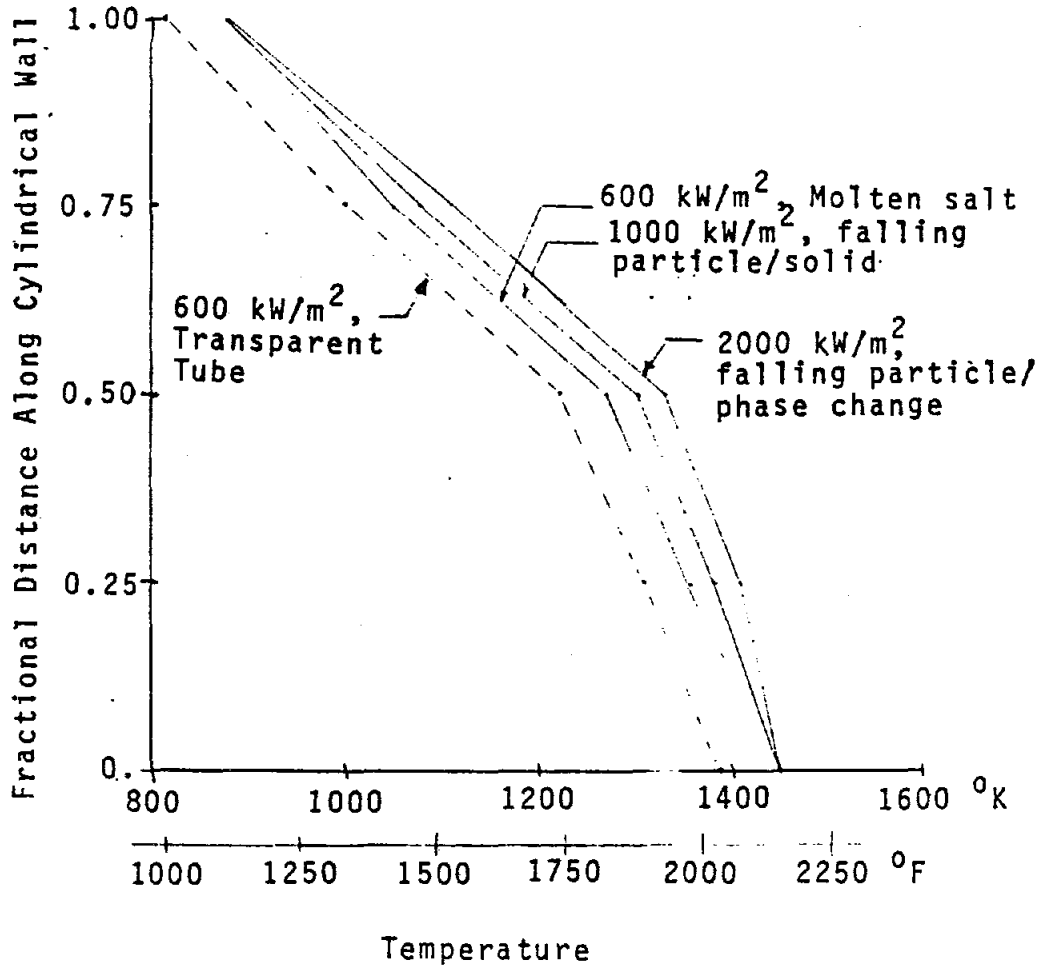

Figure 3-23. Receiver Temperature Distribution

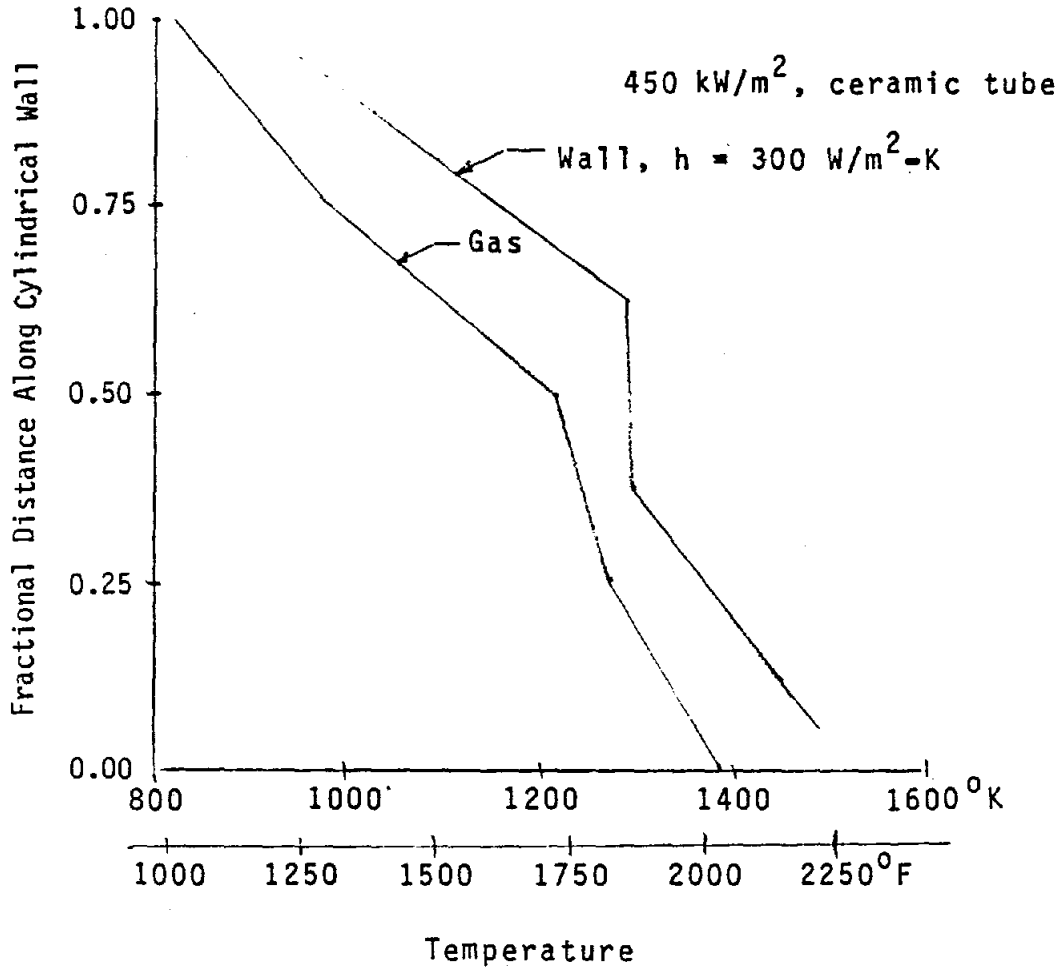

Figure 3-24. Ceramic Tube Receiver Temperature Distribution

The resulting energy balance for each 25-MWe receiver concept is shown in Table 3-7. The resulting receiver efficiency, i.e., fraction of energy transferred to fluid, varies from a low of 84% to a high of 88%. These data show the larger ceramic tube cavity with a larger thermal radiative loss. However, since the ratio of cavity area to aperture area increases for the larger cavity, the reflection losses decrease. The net result is that the receiver efficiency, to the level of this simplified analysis, is relatively constant from concept to concept.

Similar analyses were performed for the 2-MW_e receiver. A comparison between the ceramic tube and the small particle receiver is shown in Table 3-8. The thermal model of the small particle receiver developed in Reference 9 was adapted. The values from Table 3-3 for the small particle receiver reflection and reradiation were assumed as applicable to the 2-MWe size. DELSOL2 analyses of the 2-MW_e plant showed an optimized receiver aperture of 3-m diameter was required. A 3-m diameter window was determined to be within fabrication capabilities. The small particle receiver efficiency is seen to be approximately 4% greater than the ceramic tube receiver.

3.2.3 Design Analyses

The four 25-MW_e receiver concepts of Table 3-5 were sized, and their mechanical design was considered in more detail. Also the design of a 3-m diameter window was also considered. The purpose of the design analysis was to define designs sufficiently to identify the major technical problems associated with each concept. Consideration of a number of potential design configurations for each concept was not possible within the scope of this study. Configurations were chosen to represent the overall concept features. The results are described in the following paragraphs.

Falling Particle Receiver Concept

As described in Section 3.1.2, the falling solid receiver concept uses an intermediate solid medium to absorb solar energy and heat compressed air in a secondary heat exchange. For this design study, silicon carbide particles were assumed based on the results of the ASCUAS program (30). The particle diameter was assumed at 0.7mm with a particle spacing of 10 particle

Table 3-7. 25-MW_e Receiver Energy Balance

Parameter	RECEIVER CONCEPT				
	Ceramic Tube	Transparent Tube	Molten Salt	Falling Particle Solid	Falling Particle Phase Change
Peak Flux Level (kW/m^2)	450	600	600	1000	2000
Reflection (%)	1.6	1.6	1.8	3.9	6.3
Reradiation (%)	10.1	7.5	8.6	8.0	6.5
Convection + Conduction (%)	3.0	3.0	3.0	3.0	3.0
Receiver Efficiency (%)	85.3	87.9	86.6	85.1	84.2
Aperture area (m^2)	33.56	33.56	33.56	33.56	33.56
HX area (m^2)	458	331	331	206	103

diameters. The receiver cavity diameter was sized for a peak first incident flux of 1,000 kW/m^2. The cavity height was chosen to allow heating of the falling particles to the desired temperature level. The particle flowrate was chosen based on equal massflow-heat capacity products, i.e., $\dot{m}c_p$, across the direct contact heat exchanger.

Figure 3-25 shows a plan and a section view of the receiver. Figure 3-26 shows a flow diagram of the falling particle receiver and heat exchanger systems.

The particles pass down from the upper hopper through tubes and spreader nozzles into ten vibratory feeders. The feeders spread the particles out into thin curtains which fall down adjacent to the back wall of the receiver. Solar insolation heats the particles from 596°C (1106°F) to 1181°C (2157°F) as they fall a distance of 9.45m (31 feet). At the bottom of the receiver, the particles are collected in a row of refractory faced hoppers and pass through a series of collecting tubes into a single downcomer. The particles pass through the downcomer from the 97.5-m (320-ft) level down to the 27.4-m (90-ft) level and into a hopper.

Table 3-8. 2-MW_e Receiver Energy Balance

Parameter	Receiver Concept	
	Ceramic Tube	Small Particle
Peak Flux Level (kW/m^2)	450	2000
Reflection (%)	4.4	6.6*
Reradiation (%)	6.9	4.6*
Conduction and Convection (%)	3.0	
Receiver Efficiency (%)	85.7	88.9

*Assumed from Table 3-3, (9, 11)

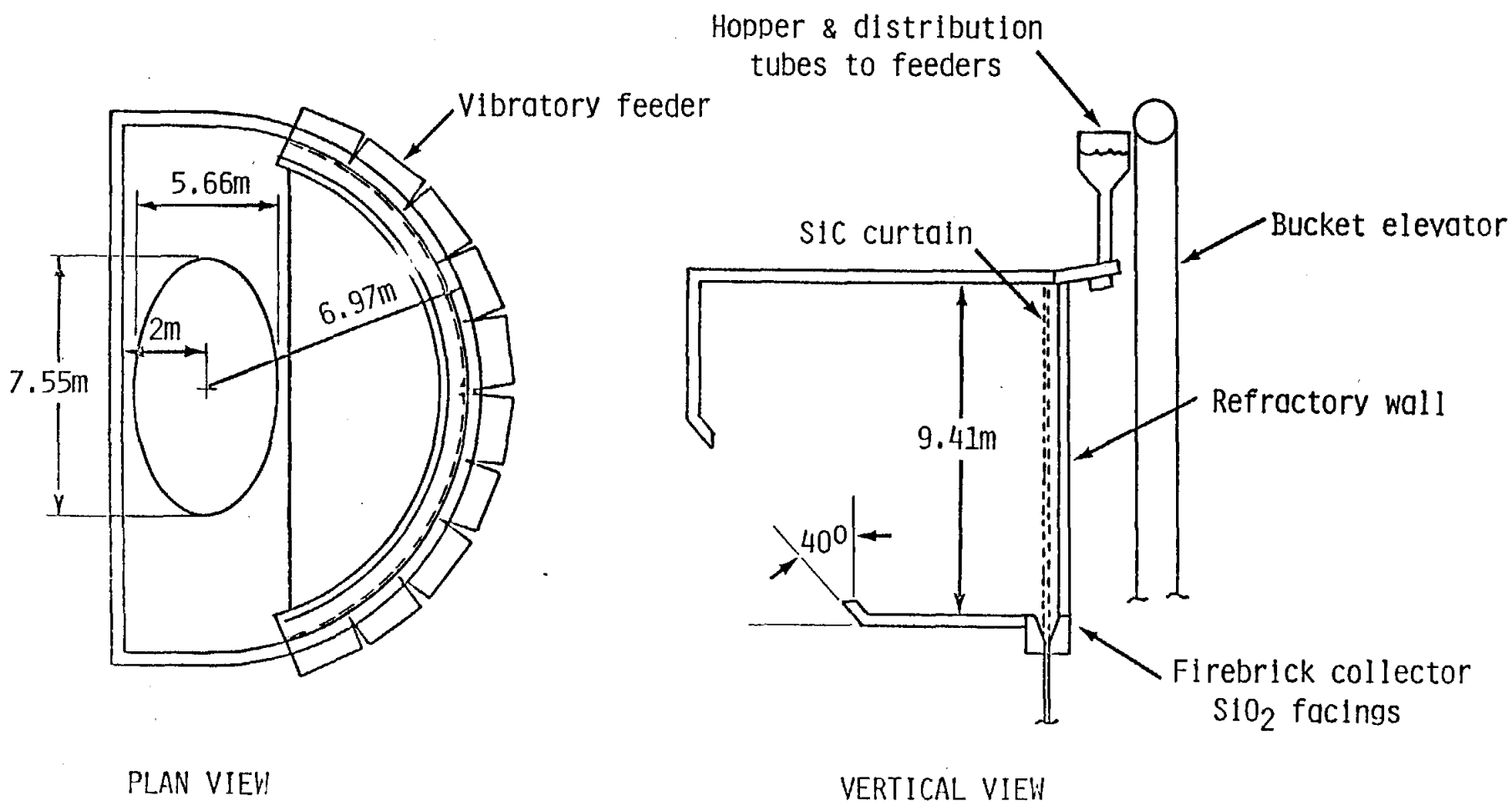

Figure 3-25. Plan and Section Views of Falling Particle Receiver Concept

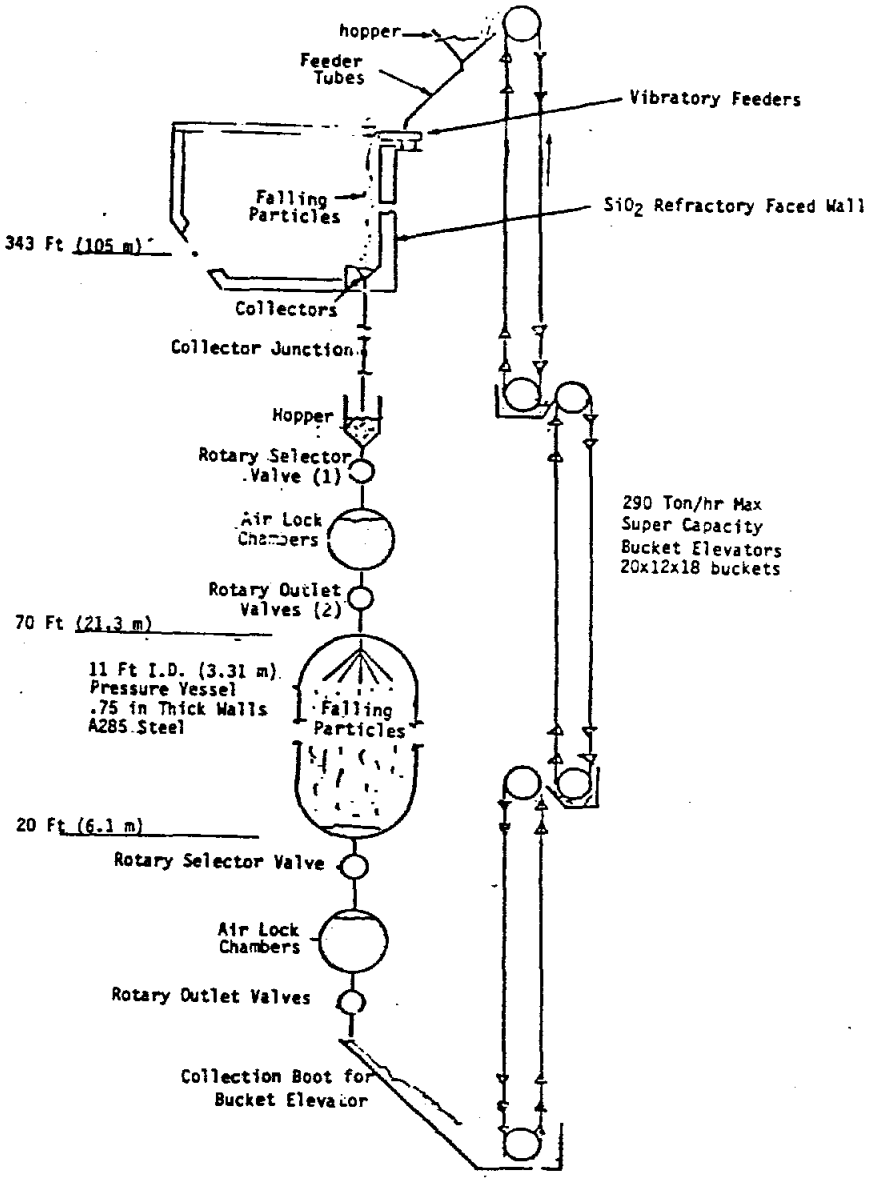

Figure 3-26. Falling Particle Receiver Flow Diagram

An air lock system is required to pass the particles from ambient pressure to 0.88MPa (128 psia) and into the heat exchanger. The air lock system consists of two chambers each with an inlet and an exit valve. The inlet valve to the first chamber is opened. After the chamber is filled, the inlet valve is closed, and the exit valve is opened. After the air pressure equalizes, the particles flow down into the heat exchanger. The inlet to the second chamber has opened, filling the second chamber, while the first chamber is emptying. When the first chamber is empty, the exit valve is closed and the inlet is opened to refill. The valve to the second chamber is closed and the exit valve is opened. The particles from the second chamber flow into the heat exchanger. The valve openings and closings of the two chambers are synchronized to establish a near constant flow into the heat exchanger.

Distribution tubes within the upper end of the direct contact heat exchanger spread the falling particles into an upward flow of air. At the top of the heat exchanger, the air velocity is 2.92m/s (9.57 ft/sec). The particle terminal velocity is 3.67m/s (12.03 ft/sec) so that the particles will fall at a reduced rate. The velocity differential across the diameter of the heat exchanger drum helps disperse the particles. The particles fall 11.6m (38 ft) down the heat exchanger to where the air temperature is 531°C (989°F) and the pressure is 0.98MPa (142 psia). The air flow rate is 1.87 m/s (6.14 ft/sec) and the terminal velocity of the particles is 2.67m/s (8.76 ft/sec). The particles enter the heat exchanger at 1181°C (2157°F) and exit at 596°C (1106°F). The air enters the heat exchanger at 531°C (989°F) and exits at 1116°C (2040°F).

Below the heat exchanger the particles exit to ambient pressure through another pair of airlock chambers identical to the upper chambers. A three stage bucket elevator picks up the particles at ground level and lifts them 117m (385 ft) to the upper hopper where the cycle is repeated.

Design data are tabulated in Table 3-9.

Pro Features. The falling particle curtain permits ambient operation of a receiver without pressurization or a window. The falling curtain will permit a very high first incident solar flux level, as well as placement of the

Table 3-9. Falling Particle Receiver Design Data

Receiver cavity radius (characteristic)	6.97m (22.86 ft)
Receiver height	9.41m (30.86 ft)
Peak solar flux	1000 kW/m^2
Aperture shape	Elliptical
Aperture inclination from vertical	40°
Aperture height	5.66m (18.56 ft)
Aperture width	7.55m (24.76 ft)
Aperture area	33.56m^2 (361.2 ft^2)
Particle material	Silicon carbide
Particle diameter	0.77mm
Particle spacing	10 particle diameters
Particle specific heat	0.29 (at 2000^oF)
Particle flowrate	68 kg/s (150 lb/s)
Particle inlet temperature	596^oC (1106°)
Particle exit temperature	1181^oC (2157^oF)
Heat exchange surface area	206m^2 (2217 ft^2)
Direct contact heat exchanger:	
Inside diameter	3.35m (11 ft)
Height	15.2m (50 ft)
Wall thickness	1.9cm (0.75 in)
Wall material	A285 steel
Vibratory feeders:	
Quantity	10
Size	1.7x0.76m (5.6x2.5 ft)
Power consumption	7.5 kW_e
Bucket elevators:	
Quantity	3
Rating	290 tons/hr
Bucket volume	0.071m^3 (2.5 ft^3)
Power consumption	157 kW_e

turbine and secondary heat exchange systems at ground level or at lower positions in the tower. It may be possible to replace the falling particle heat exchanger with a smaller fluidized bed heat exchanger that will reduce material costs and reduce the length of the piping to and from the turbine.

Con Features. Introduction of an intermediate particle heat exchange material results in a complicated system. With repeated cycling the SiC particles may fracture into smaller sizes where their terminal velocity is reduced below the heat exchanger upflow rate and they will be carried out of the system. A cyclone separator will have to be provided to prevent these fine particles from damaging the turbine blades. The falling particle heat exchanger is a large and costly structure requiring refractory lining to reduce shell temperatures and reduce heat loss. The interior surfaces will have to be sheathed with SiC to prevent abrasion of soft fibrous insulation. A bucket elevator system is required to lift 269 tons of particles per hour to a height of 177m (385 ft). A vibratory feeder system is required to spread the particles into a 17.4m (57 ft) wide curtain within the receiver. All piping will require abrasion resistant facing on the inside diameter to protect the internal insulation against particle abrasion. The air lock system will require development of large rotary valves that will pass the abrasive particles yet effectively seal against 0.98 MPa (142 psia) air with valve internal surfaces exposed to 1181°C (2157°F).

High-Temperature Molten Salt Receiver Concept

The high-temperature molten salt concept is similar to the falling particle concept except that a blackened molten salt is used in place of a falling solid curtain. Several high temperature molten salts have been suggested for this application (32). Molten sodium hydroxide (NaOH) was chosen for this preliminary evaluation. NaOH was chosen because of its wide melt-boil temperature range (186-1000°C), its relatively high heat capacity (2050 J/kg-°C, 0.49 Btu/lb-°F), and its low cost. BEC has also considered this salt for high-temperature thermal energy storage (36). Other high-temperature salts such as carbonates, chlorides, or fluorides could also be considered.

The receiver diameter was sized for a peak flux of 600 kW/m^2. The salt massflow was chosen to match the air massflow-heat capacity product in the secondary heat exchanger. Direct contact air-to-salt heat exchangers are possibilities for such a design. However, carryover of small quantities of molten salt or impurities into the turbine was a serious concern. Also, solidification of the salt on the cooler recuperator tubing is a potential problem. Because of these concerns a secondary heat exchanger was included in the molten salt receiver design.

Figure 3-27 shows a flow diagram for the 25-MW_e molten salt receiver. Figure 3-28 shows plan and elevation views of the receiver. Solar insolation from the heliostat field enters through the aperture and heats a semicircular wall of refractory covered with a film of falling darkened molten NaOH. The refractory wall is formed of arch bricks and is spring loaded at both ends to accommodate thermal expansion and to form a rigid arch that will resist lateral earthquake loads.

Molten NaOH at 596°C (1106°F) is uniformly distributed along a ceramic feeder. The NaOH is metered through a slot to form a 0.25cm (0.1 inch) thick film which wets the refractory receiver wall and falls as a viscous boundary layer. The NaOH temperature is raised to about 1181°C (2157°F) by the time it has descended to the lower collection trough.

The heated salt enters a downcomer, as shown in Figures 3-29 and 3-30 which consists of an inner nickel liner and an outer steel pipe fabricated in 6.1 m (20 ft) long sections with flanges at both ends. The cavity between the pipes is filled with a porous refractory fiber material such as Kaowool®. Each section of the downcomer is air pressurized to match the internal pressure of the molten NaOH at that elevation. The NaOH liner is then free of stresses that would result from differential pressures. The downcomer transports the molten NaOH about 34.1m (112 ft) to where the head is equivalent to about 0.88 MPa (128 psia) to match the pressure of the hot air leaving the heat exchanger. This maintains the pressure-stress-free condition of the inner heat exchanger tube.

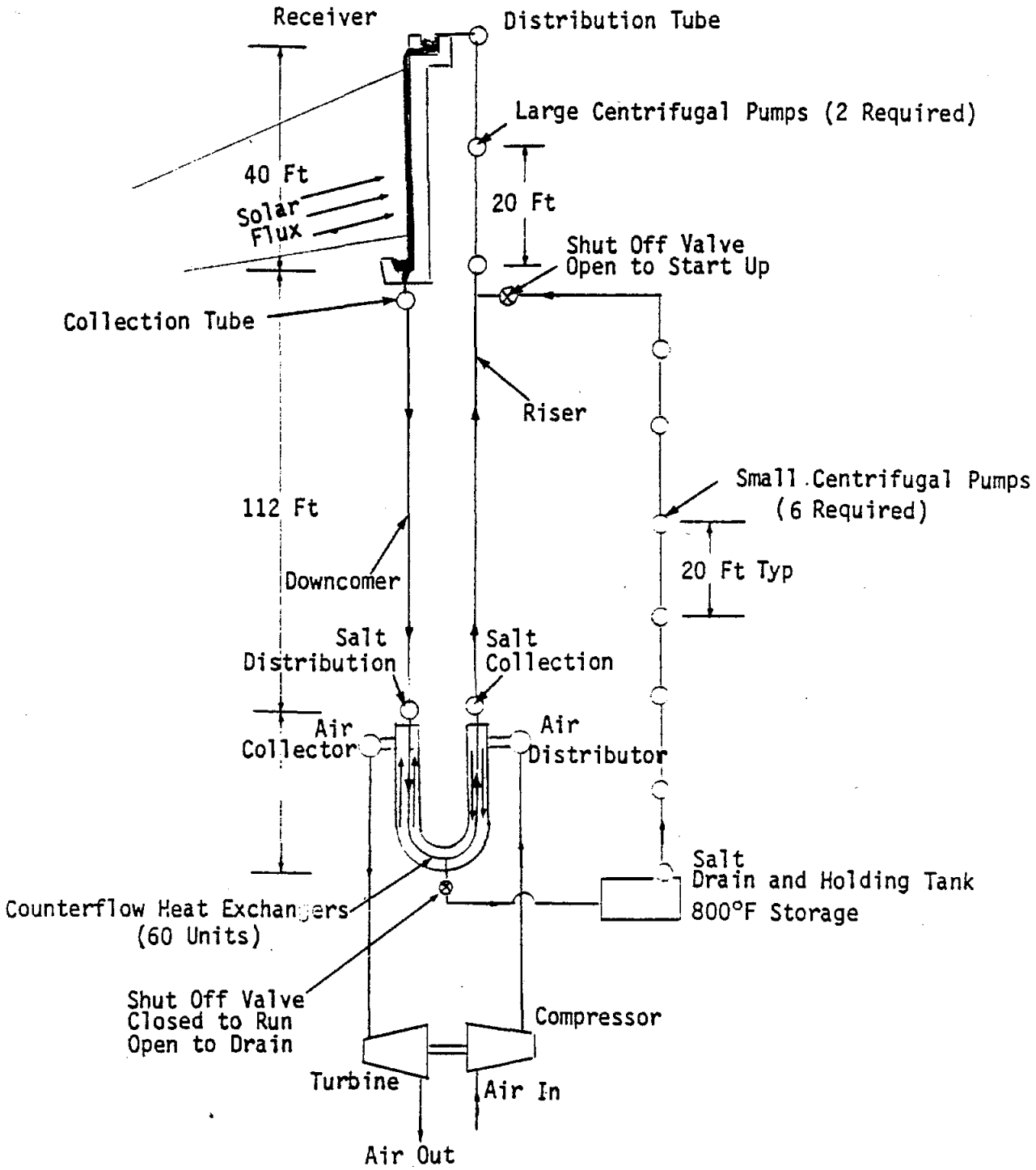

Figure 3-27. High-Temperature Molten Salt Receiver Flow Diagram

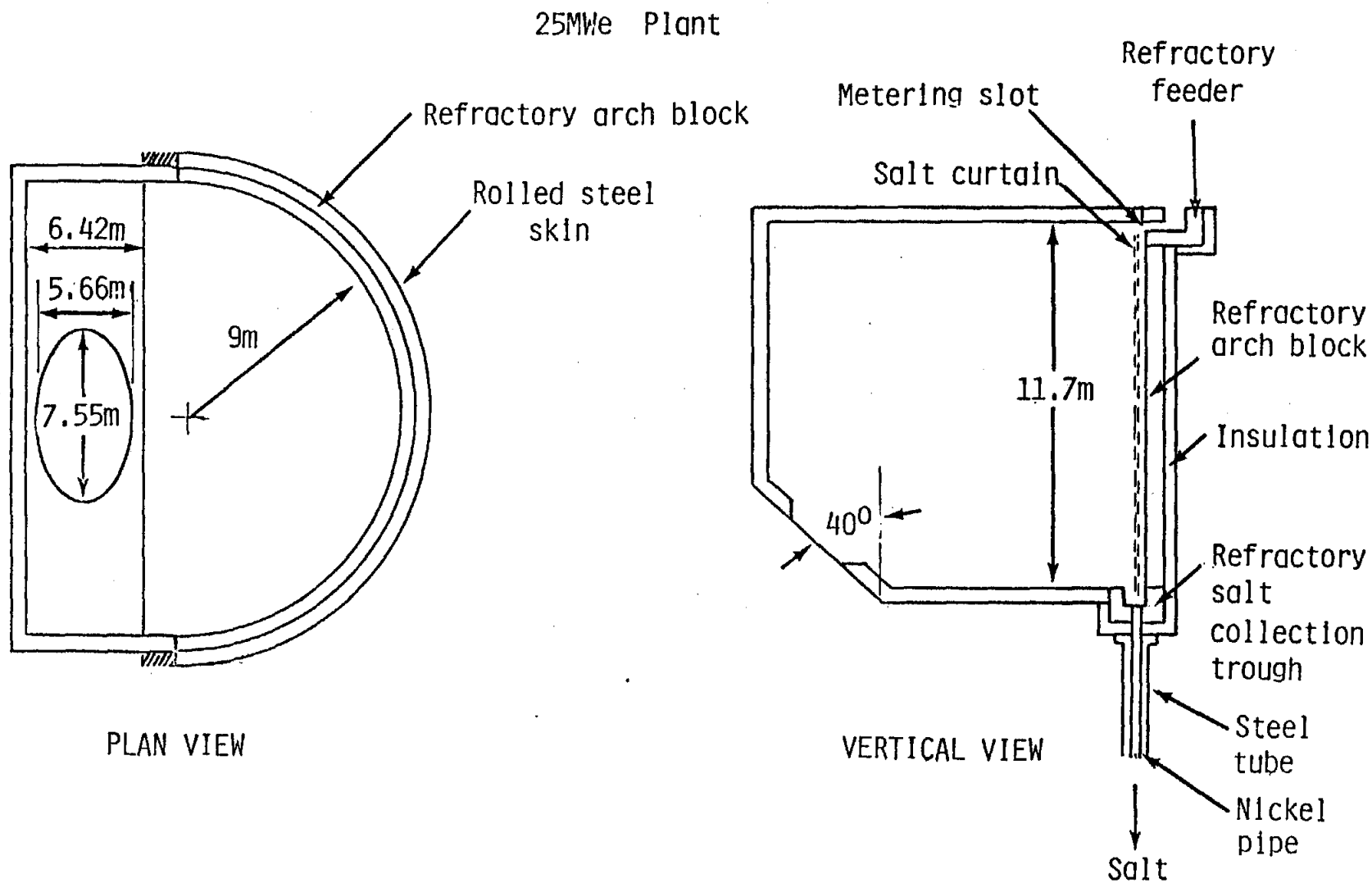

Figure 3-28. Plan and Elevation Views of Molten Salt Receiver Concept

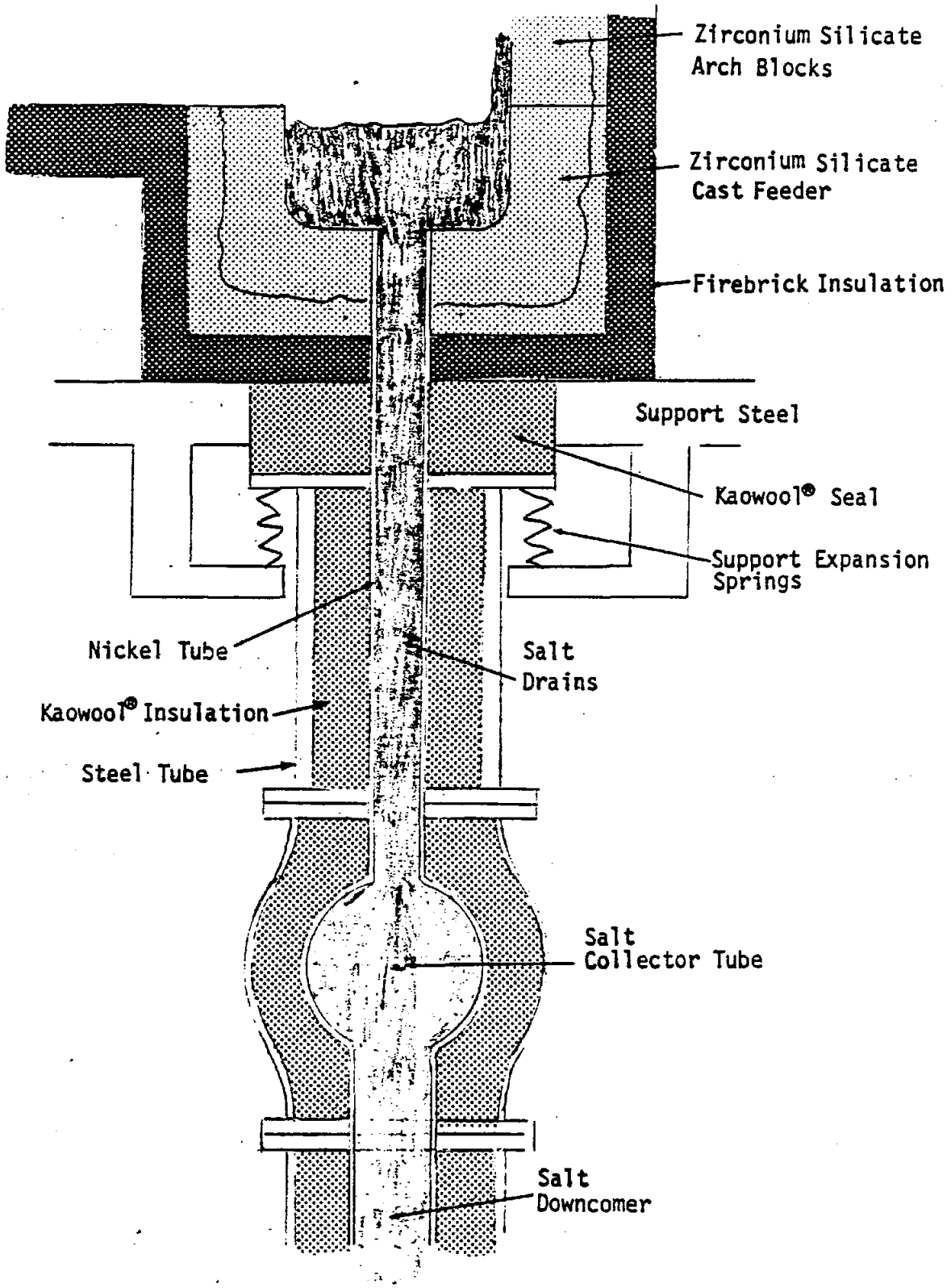

Figure 3-29. Molten Salt Receiver Collector and Downcomer Piping Concept

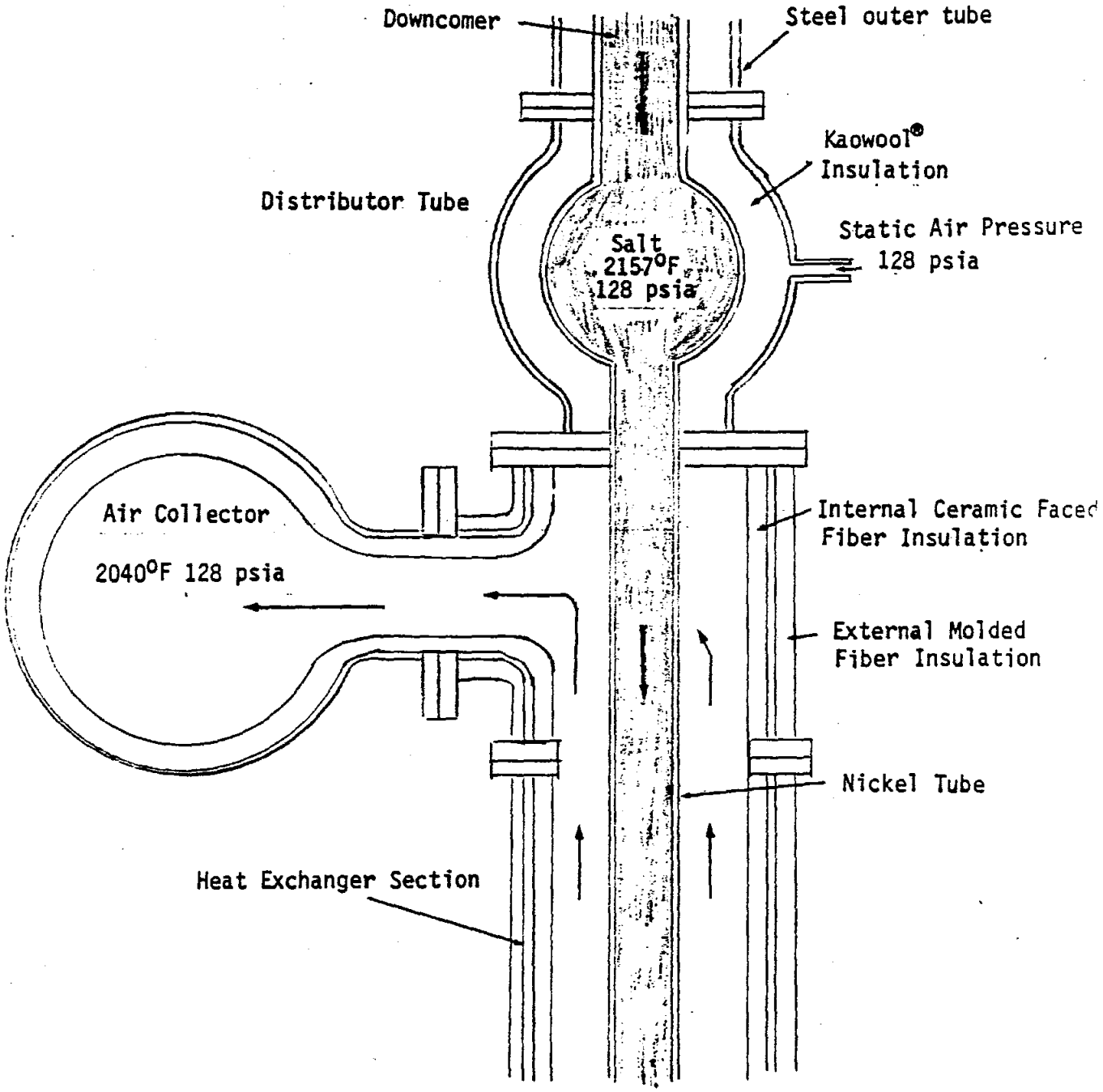

Figure 3-30. Molten Salt Heat Exchange Concept

The heat exchanger consists of 60 "U" tube assemblies, each with an inner tube for molten NaOH and an outer tube to contain the high pressure air. The 60 NaOH tubes are connected by a distribution tube to the NaOH downcomer. The 0.88 MPa (128 psia), 1116°C (2040°F) air exits into a collector pipe. Inlet air at 0.98 MPa (142 psia) and 531°C (989°F) is fed through a distribution pipe. NaOH at 0.88 MPa (128 psia) and 596°C (1106°F) exits from the exchange tubes into a collector tube and is returned to the receiver through a riser of similar construction to the downcomer.

The molten NaOH returns to the level of the lower collector trough without external assistance. The salt is lifted 6.1m (20 ft) by the first stage centrifigual pump then an additional 6.1m (20 ft) by the second stage centrifugal pump, see Figure 3-31. As shown in Figure 3-27, the first stage centrifugal pump is located near the bottom of the receiver. This pump location was chosen to maintain the pump impeller immersed in the molten salt (see Figure 3-31). Similarly the second stage pump location was chosen to immerse its impeller (see Figure 3-31). By maintaining the impeller imersed in the salt, sealing concerns should be lessened. After the salt is pumped to the receiver top, it is fed at several locations into the distribution trough. In normal shutdown the entire system of molten NaOH drains by gravity to a lower sump, see Figure 3-27. In start-up the molten NaOH is lifted to the receiver by 6 stages of small centrifugal pumps. The heat exchanger is then filled and the larger upper pumps are started to initiate receiver wall flow. The lower drain valve and small pumps are then shut off. Design data are tabulated in Table 3-10.

Pro Features. The molten NaOH falling film concept permits high-temperature working temperatures of 1181°C (2157°F) in a receiver operating at atmospheric pressure. By setting the heat exchanger at the correct elevation, the hydrostatic head of the molten NaOH can match the air pressure and relieve the exchanger tubes of having to withstand high differential pressures. The reduced tube stresses will permit higher temperature operation of the nickel tubes than would normally be attempted.

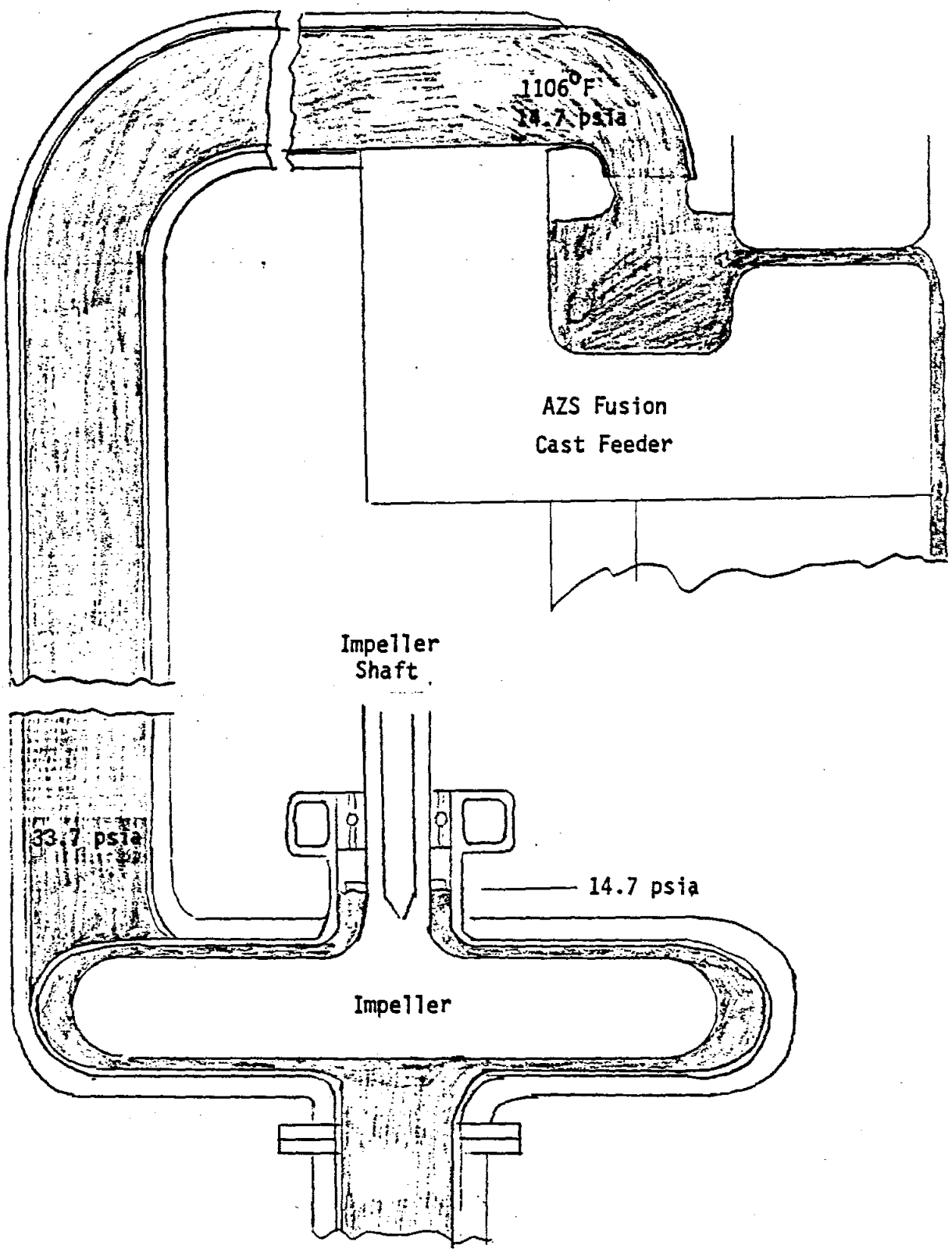

Figure 3-31. Molten Salt Second Stage Centrifugal Pump and Distibutor Concept

Table 3-10. Molten Salt Receiver Design Data

Receiver cavity radius (characteristic)	9.0m (29.5 ft)
Receiver height	11.7m (38.4 ft)
Peak solar flux	600 kW/m^2
Aperture shape	Elliptical
Aperture inclination from vertical	40°
Aperture height	5.66m (18.56 ft)
Aperture width	7.55m (24.76 ft)
Aperture area	33.56m^2 (361.2 ft^2)
Molten salt type	NaOH
Salt specific heat	0.49
Salt flowrate	42.4 kg/s (93.4 lb/s)
Salt inlet temperature	596^oC (1106^oF)
Salt outlet temperature	1181^oC (2157^oF)
Salt inventory	13460kg (29670 lbm)
Heat exchange surface area	331/m^2 (3563 ft^2)

The boiling point of NaOH is 1390°C (2534°F) which gives a margin of safety should the temperature inside the receiver attempt to rise above 1181°C (2157°F). The NaOH would boil until the insolation is reduced or the flow rate of NaOH is increased.

Having 60 sets of "U" tubes in the heat exchanger permits maintainability against unexpected premature failure of exchanger tubes. If one "U" tube fails it can be readily replaced. The "U" tubes are made up of standard replacement sections. It is very likely that only the hottest end of the tube will need replacement at more frequent intervals.

Con Features. There is no available data that shows the rate of corrosion of nickel against molten NaOH at 1181°C (2157°F). There may be a crystaline phase change in nickel at some temperature within the operational range that will give short life in a frequently cycled temperature range.

The heat exchange tubes will have very small stresses due to pressure differentials, but they will not be free of longitudinal stresses due to the temperature differential with the outer tubes. This will require careful analysis and design to operate the outer tubes at as high a temperature as possible.

The receiver wall refractories will be subjected to thermal shocks far in excess of those conditions in operating glass tanks. The shock of going from ambient temperature to 1186°C (2157°F) many thousands of times will probably cause progressive spalling of the heated face. This will be minimized by keeping the wall in a low level of compression as a spring loaded arch.

The NaOH will react with the refractory to form a surface layer of glass. On cool down this layer of glass will fracture and induce fine cracks in the refactory face. This may increase the rate of spalling.

In glass tank usage, sidewall refractories undergo errosion to a depth of six or more inches in 3 to 4 years of continuous operation. The scrubbing velocity in a glass tank is much lower than will be encountered in the

receiver falling boundary layer. This increased exposure to the active, glass-forming NaOH may result in much higher errosion rates than encountered in the glass industry.

Transparent Tube Receiver Concept

Figure 3-32 presents a plan and elevation view of a transparent tube receiver. The working fluid is air seeded with fine carbon particles. Solar insolation enters the aperture, passes through the transparent tubes, and is absorbed by the carbon particles. The carbon particles vaporize, form CO_2 and heat the air working fluid.

Figure 3-33 presents two potential methods of distributing the flow. In the first, a U-tube arrangement is used to duct the air and carbon particles into and out of the receiver cavity. In the second arrangement, a ceramic insert in the center of the transparent tube inputs the air and carbon particles which then flow down the annular region between the ceramic insert and the transparent tube.

Pro Features. The transparent tube concept is capable of high heat fluxes since the solar absorption is accomplished by fine carbon particles. The pressure containment function is accomplished by the transparent tubes. A large portion of the solar energy reflected by the transparent tubes is re-reflected back to the tubes by the cavity interior.

The transparent tube concept allows the use of small compact receivers as available with other high flux concepts, but does not require the secondary heat exchange equipment required by the intermediate medium concepts.

Con Features. The concept is dependent on a high-temperature transparent tube material. Repeated cycling between ambient and 1093°C (2000°F) temperatures may cause significant devitrification of potential materials. These issues are discussed in more detail in Section 3.3.

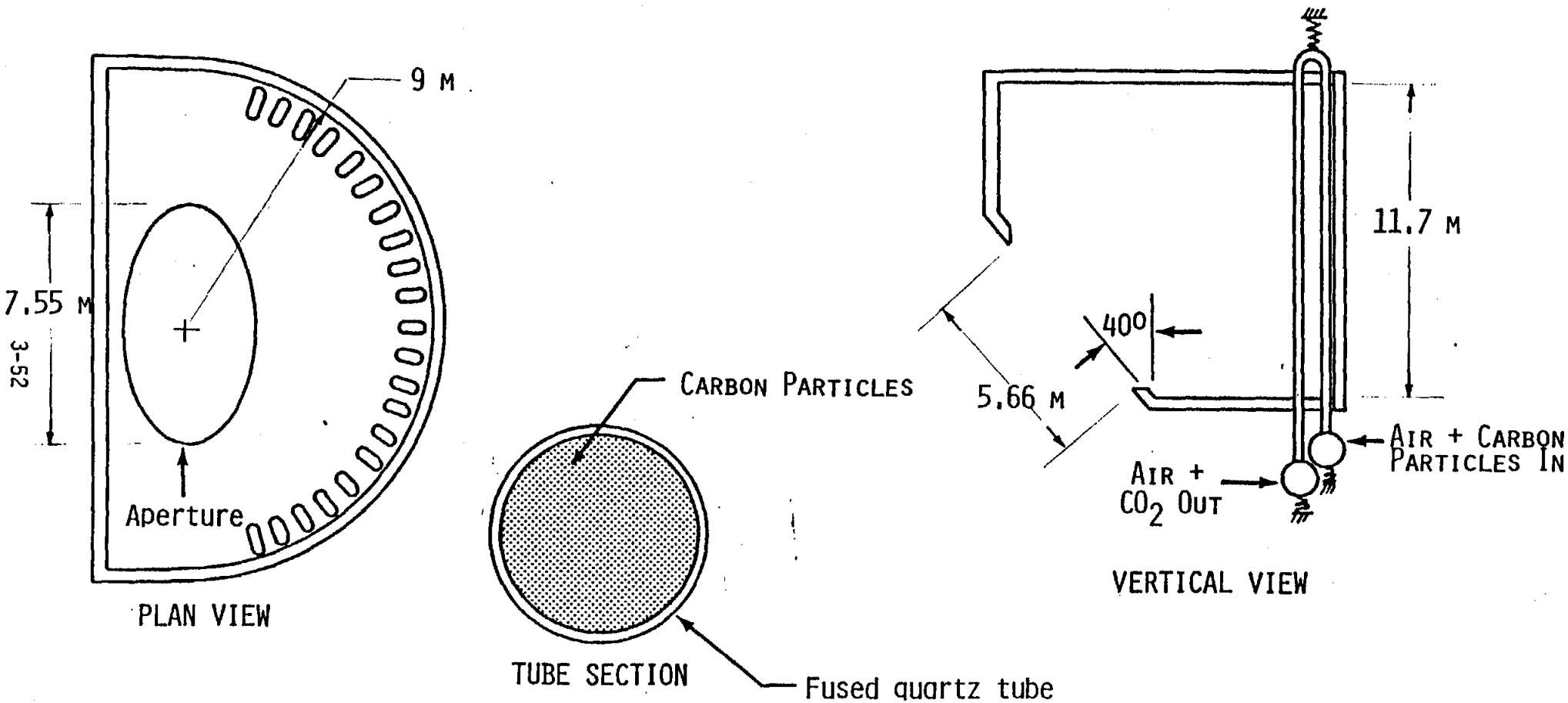

Figure 3-32. Plan and Elevation Views of Transparent Tube Receiver Concept

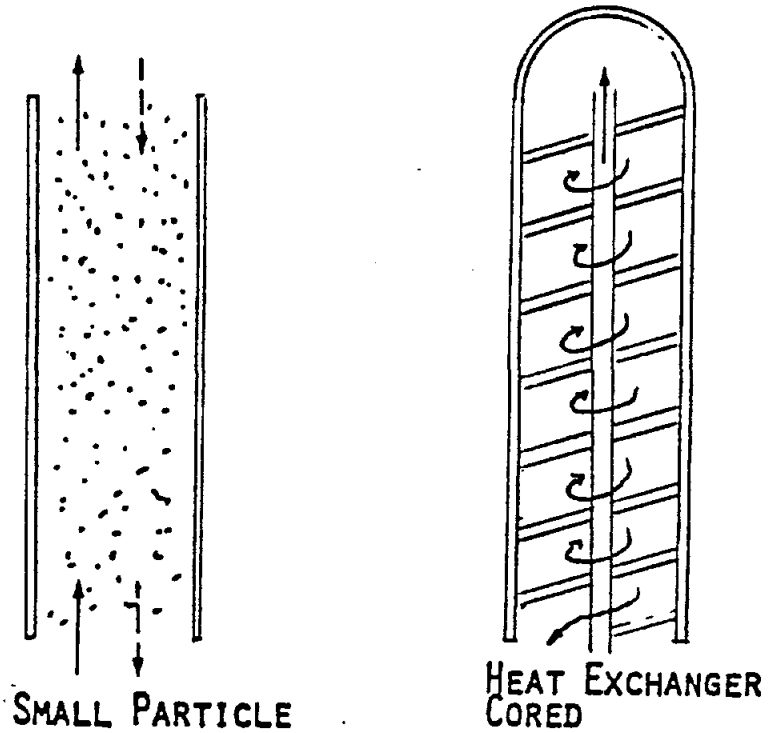

Figure 3-33. Transparent Tube Receiver Alternative Flow Concepts

The concept also depends on the development of a system to insert carbon particles into a high pressure air flow. Recent tests (37) of the SPHER receiver program at ACTF are encouraging.

Ceramic Tube Receiver Concept

Figure 3-34 presents a plan and elevation view of a ceramic tube receiver. Solar insolation enters the aperture and is absorbed by the ceramic tubes. The tube walls are cooled by the air working fluid.

Figure 3-35 shows a conceptual ceramic tube heat exchanger assembly. The individual tube elements are formed, sintered, and assembled with a brazing compound then furnace brazed. These tube assemblies operate with the highest solar flux on the discharge side of the loop. The tube inlet is nearest the receiver wall. The upper end of the heat exchanger loop is unsupported allowing the assembly to elastically distort under thermal expansion.

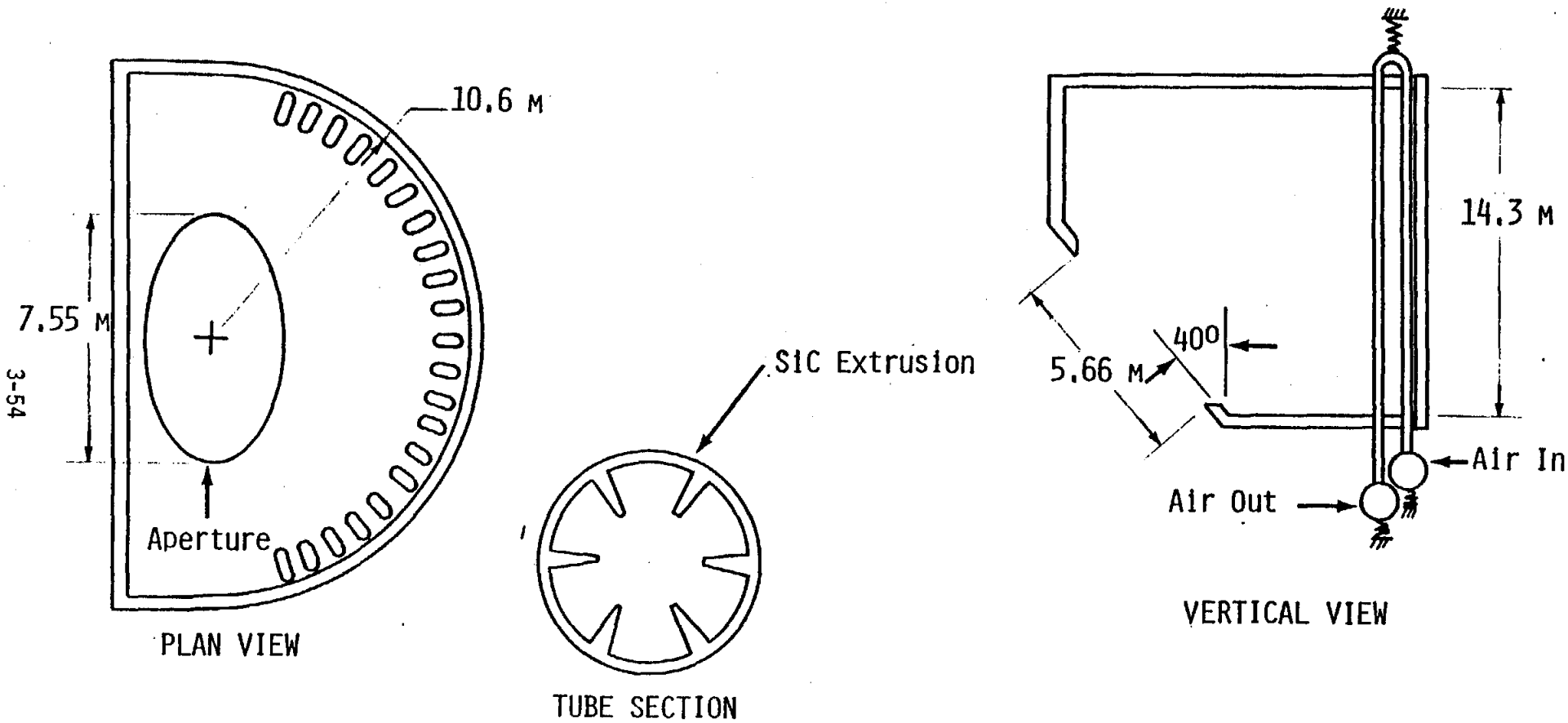

Figure 3-34. Plan and Elevation View of Ceramic Tube Receiver Concept

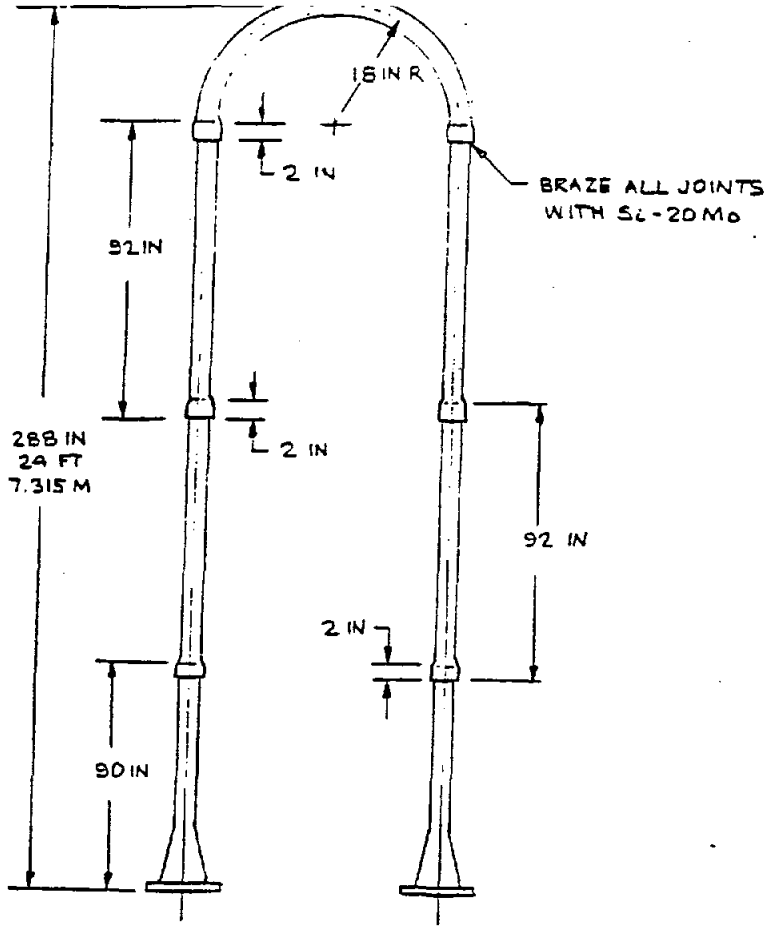

Figure 3-35. Ceramic Tube Heat Exchanger

Pro Features. The ceramic tube concept requires the least technological advances of any high-temperature receiver concept. Its passive design is uncomplicated. No secondary heat exchange is required.

Con Features. In order to limit the thermal stresses in the heat exchanger assembly, the peak solar flux is limited. This flux limit produces larger cavities than available with the higher flux concepts. Also, sealing the heat exchanger assemblies is a significant concern.

Small Particle Receiver Concept

Figure 3-36 illustrates the small particle receiver concept. Solar insolation enters the windowed cavity and is absorbed by carbon particles seeded into the gas flow. A spherical pressure vessel provides the receiver cavity.

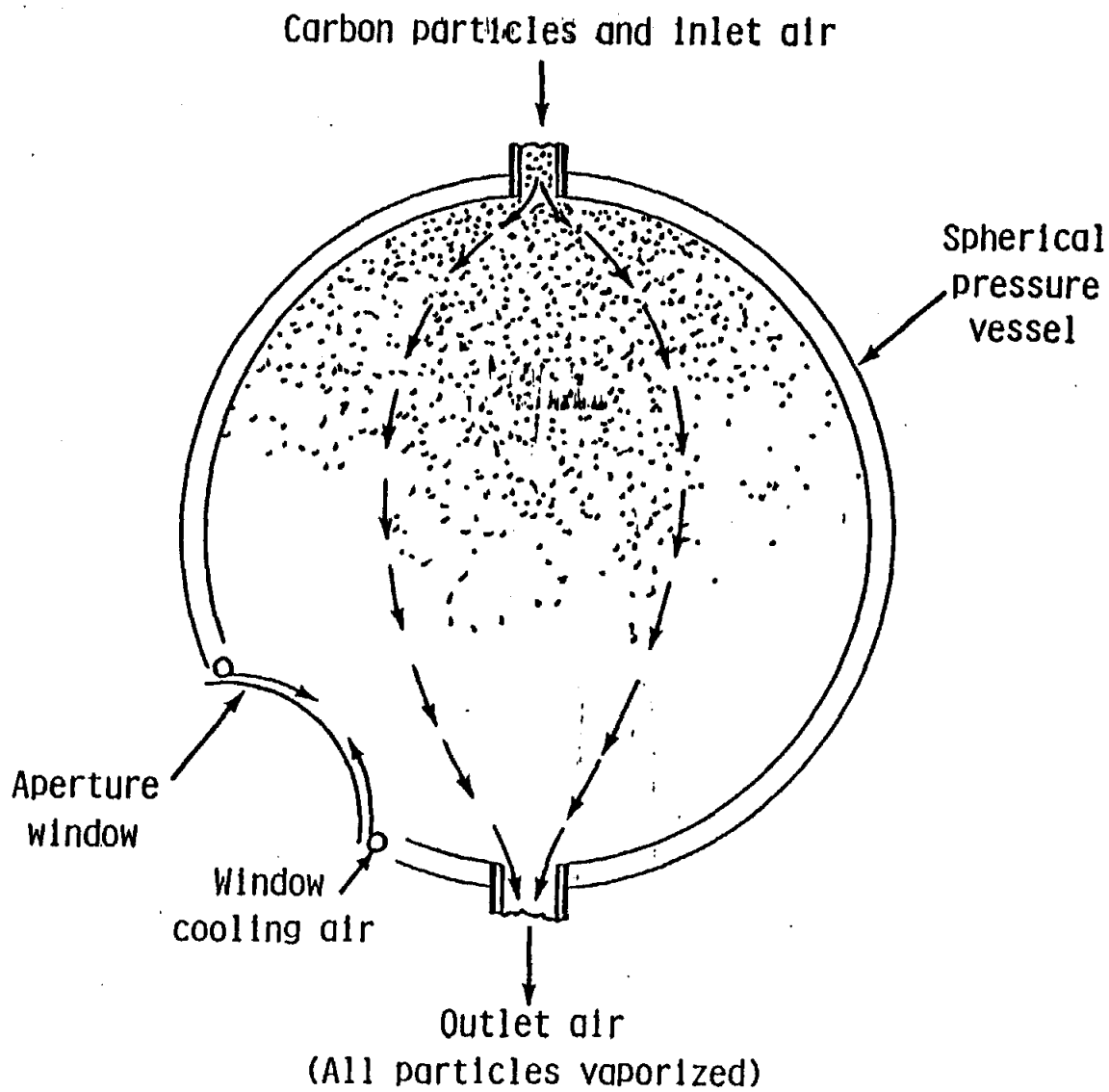

Figure 3-36. Small Particle Receiver Concept

In Reference 9, a 6-m diameter window was determined as the largest window that could be reasonably fabricated. However, even at 6-m diameter, Section 3.2.1 shows the spillage to be unacceptably high for the 25-MW_e size plant. For the 2-MW_e plant, a 3-m diameter window was found to have acceptable spillage values.

Figures 3-37 and 3-38 present a conceptual design of a 3-m diameter quartz window. The window is maintained in compressive loading by arching inwardly. Cooling air from the turbine compressor is fed around the periphery of the window. A metal seal design is used to maintain receiver pressure while also allowing for thermal expansion and contraction.

The 120° spherical arc window shown in Figure 3-37 was chosen based on an assessment of window mass verses arc angle. An allowable stress of 69 MPa (10,000 psi) was assumed. The results are shown in Table 3-11. The 120° arc window design is the minimum mass design.

Table 3-11. Window Mass Verses Spherical Arc Angle

3-m Dia. Aperture

Arc Angle (°)	Sphere Radius (in)	Window Thickness (in)	Window Mass (lbs)
180	59.05	.603	1052
150	45.30	.624	864
120	34.09	.697	810
90	24.46	.853	871
60	15.82	1.206	1127

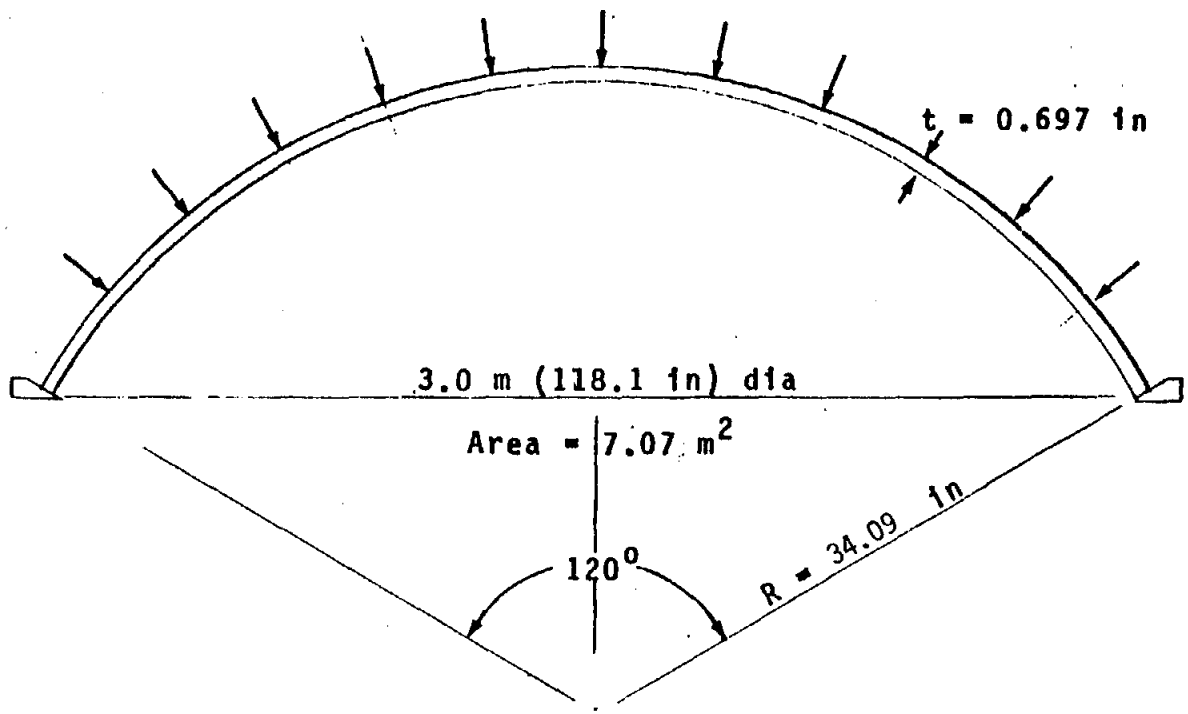

Figure 3-37. 3.0-m Fused Quartz Window Design

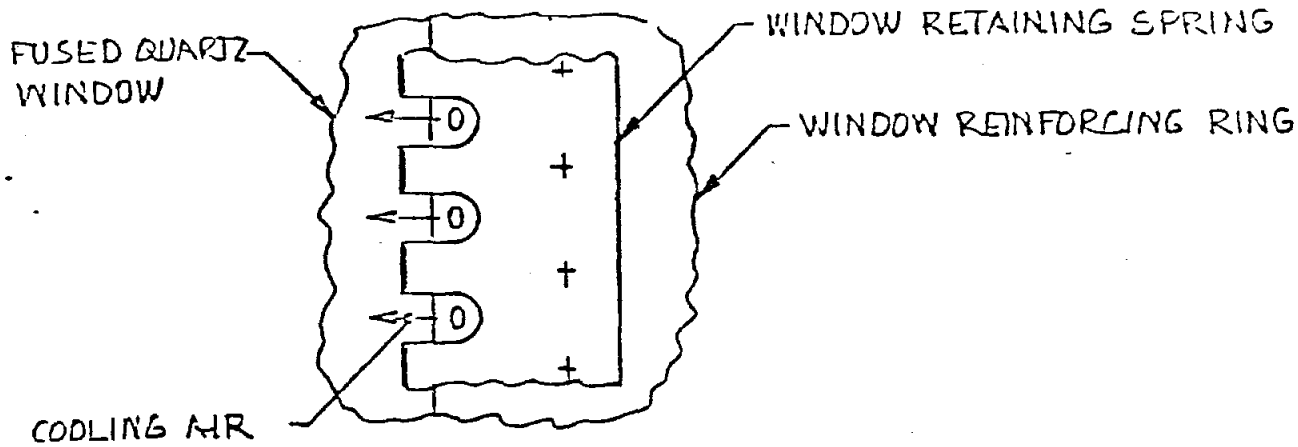

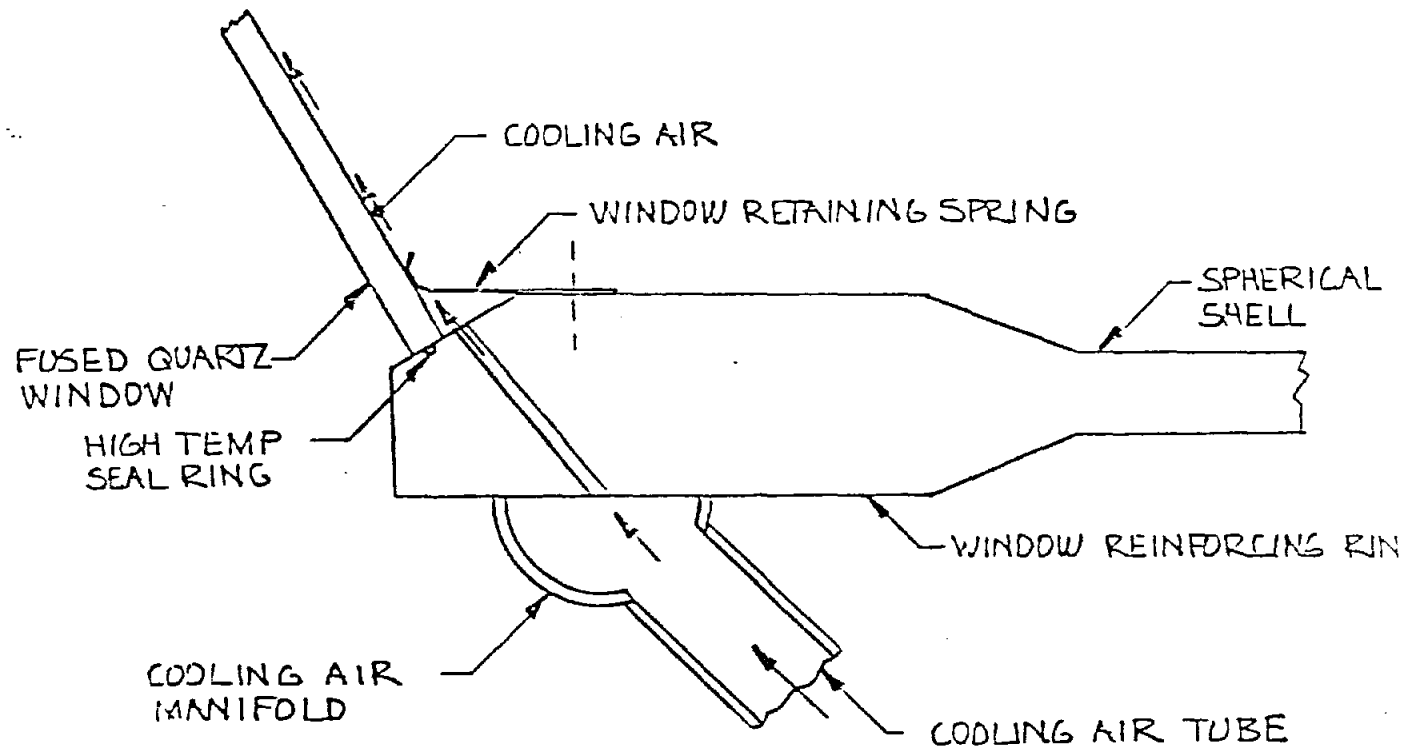

Figure 3-38. 3.0-m Diameter Window/Shell Interface Design

An alternative approach to the single window design would be to use several smaller windows. Arrays of such windows could be used to produce the desired aperture area as shown in Figure 3-39. The 1.5-m diameter is within current fabrication capabilities. The regions between the windows would be in high flux zones and would have to be actively cooled.

3.3 HIGH-TEMPERATURE MATERIALS CANDIDATE SELECTION

Ceramic materials have historically been used in refractory applications where their high temperature capability and oxidation resistance have been most important but structural requirements have not been demanding. However, recent programs to develop ceramics for high-temperature, load-bearing applications such as heat exchangers and engine components have focused on structural requirements at elevated temperatures. Progress in these programs has been very encouraging even though the full potential of ceramics in critical designs is far from being realized. The progress that has been achieved has made available design methodologies and materials for consideration in solar receiver applications.

Although ceramics have unique high temperature capabilities, the toughness of ceramic materials is an order of magnitude lower than for structural steels. Mechanical failures usually occur by brittle fracture. Since ceramics are not ductile and do not deform plasticly, the design of ceramic structures is much more demanding than that of similar metallic structures. These characteristics require that the selection of a particular material be a product of close cooperation between designer, materials engineers and fabricators.

Structural ceramics are those which have capabilities beyond simply suporting compressive loads. This study examined the availability of structural ceramics for solar receiver/heat exchanger application to temperatures of 1205° C (2200°F) and pressurization to 15 atmospheres. Structural ceramics fall into four material classes: (1) silicon carbides; (2) silicon nitrides, (3) alumino-silicates (glass-ceramics); and (4) oxides. The temperature and

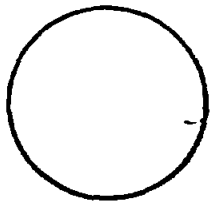

1 Window Array, Area = 1.77 m^2

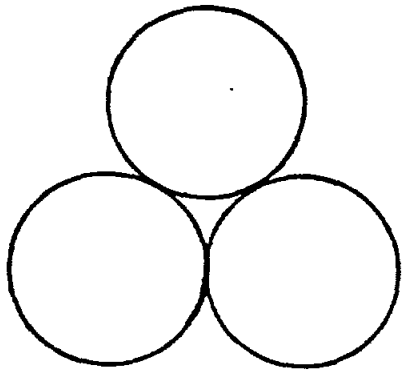

3 Window Array, Area = 5.31 m^2

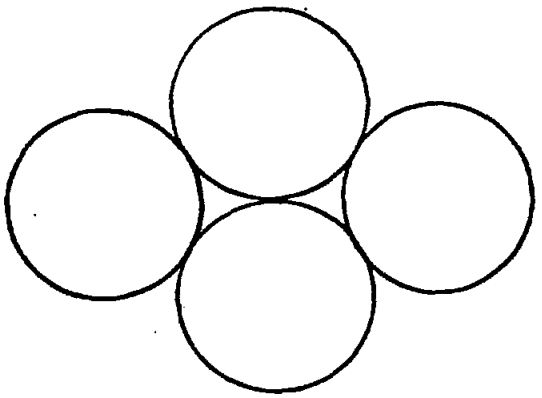

4 Window Array, Area = 7.08 m^2

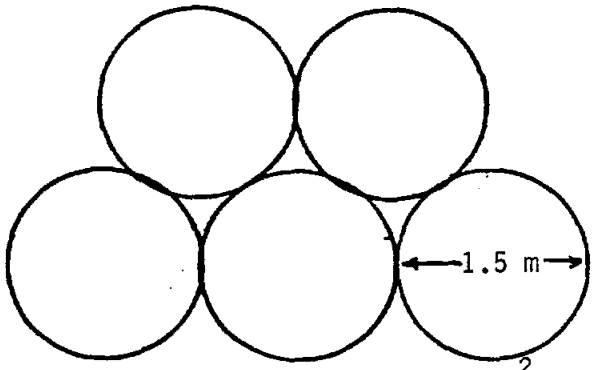

5 Window Array, Area = 8.85 m^2

Figure 3-39. Multiple Facet Windowed Aperture Concept

pressurization requirements of this study eliminated all but the non-porous (or those with no open porosity) silicon carbides, nitrides and the purer aluminum oxides from consideration. Lack of sufficient thermal shock resistance eliminated other materials from general consideration.

General fabrication constraints were considered and compared to possible receiver concept requirements for structural (pressure containing heat exchanger) and also for window (transparent or transluscent) uses.

3.3.1 Materials Survey and Initial Screening

Heat Exchanger Materials: Survey

At the beginning of the study, the materials selection process was necessarily broad. An initial survey was made of ceramic materials with structural capabilities at temperatures above 983°C (1800°F). Included were the silicon carbide and silicon nitride families of materials, oxides, glass-ceramics, ceramic composites and transparent or transluscent ceramics. The various receiver/heat exchanger concepts being evaluated included many ceramic applications with varying structural pressure containment and chemical compatibility requirements. Selection of the turbomachinery and operating cycle parameters for generation of electrical power defined the temperature and operating pressure requirements of the high temperature heat exchanger given in Table 3-12.

These basic requirements result in the elimination of the glass-ceramic family of materials, glasses and all but the very pure oxides. In addition, system pressurization requires materials with little or no open porosity. A porosity of less than 1% (closed and nonconnected pores only) may be considered acceptable for this kind of an application. The following commercially available materials meet both temperature and porosity requirements:

1. Hot-pressed silicon nitride (Norton NC-132)
2. Sintered silicon nitride (Asahi Ceraroi-N, GE-128, Kyocera SN-201)

Table 3-12. HEAT EXCHANGER MATERIALS - PRELIMINARY DESIGN REQUIREMENTS

o TEMPERATURE:	2200°F MAX.
o PRESSURE:	15 ATM. MAX.
o HEATING RATES:	UP TO 60°F/MIN.
o THERMAL CYCLES:	18000 MAX/MIN TEMP. CYCLES
o LIFETIME:	20 YEARS (MAX.)
o LEAKAGE:	< 3%

3. Siliconized silicon carbide (Carborundum Super KT, Norton NC-430, Norton Crystar HD, Purebide/Refel SiC, Coor's reaction bonded SiC)
4. Sintered alpha-silicon carbide (Carborundum SASC, Asahi Ceraroi-C, Kyocera SC-201)
5. CVD silicon carbide (MTC CVD SiC, DCI CVD SiC)
6. Alumina (Kyocera Alumina, Duramic Alumina, Coors Alumina, etc., various grades)

(The manufacturers are listed for information only and are not meant to limit consideration of one manufacturer's material over another of the same generic type.)

If the porosity requirement is relaxed, then the following materials, 7 through 13, can also be included and could be used as candidates for heat storage devices or erosion resistant insulation, where porosity is not a critical factor.

7. Mullite (Kyocera K-690)
8. Reaction-bonded/recrystallized SiC (Norton Crystar, Coors SiC)
9. Silicon nitride-bonded silicon carbide (Carborundum Refrax 20)
10. Reaction-bonded silicon nitride (Norton NC-350)
11. Beryllia (National Beryllia Berlox K-150)
12. Other oxides (Asahi LOTEC-T and LOTEC-Z)

Heat Exchanger Materials: Preliminary Selection

A preliminary materials selection for the heat exchanger was begun by selecting fundamental material properties for consideration, then normalizing the values for each material, and finally weighting each according to importance in order to rank the material candidates. Some of the design critical properties of materials 1 through 6 are listed in Table 3-13. The selection of these particular properties is based on the conclusions of previous studies (38), as well as engineering judgement. Selection of the thermal shock factor R' (39) in Table 3-13 is justified by the expected

Table 3-13. DESIGN-CRITICAL PROPERTIES OF SELECTED HEAT EXCHANGER MATERIALS

PROPERTY \ MATERIAL	HOT-PRESSED Si_3N_4	SINTERED Si_3N_4	SILICONIZED SiC	SINTERED α-SiC	CVD SiC	ALUMINA
Thermal Shock Factor, $R' \approx \frac{0.7k\sigma_f}{\alpha E}$ (10^3Btu/hr ft) ~2000°F:	7.5	4.0	7.8	6.0	11.0	0.5
Flex. Strength, ground bars, σ_f (ksi) RT:	100	90	40	44	80	80
~2000°F:	90	50	40	50	75	60
Young's Modulus, E (10^6 psi) RT:	45	40	55	60	60	60
~2000°F:	40	35	45	60	50	55
Thermal Conductivity, k (Btu/hr°F ft) ~2000°F:	9	7	30	24	25	2.5
Thermal Expansion Coefficient, α (10^{-6}in/in°F) RT- ~2000°F:	1.9	1.8	2.4	2.4	2.4	3.8

characteristics of the "through-the-thickness" thermal gradients in the heat exchanger components and the inclusion of the thermal conductivity in its definition. The values shown in Table 3-13 are conservative averages of data previously obtained in similar programs in the technical literature and data obtained from material manufacturers (40-58).

Table 3-14 contains normalized property values. These were obtained by calculating the ratios of the individual material properties to the highest value in the appropriate row in Table 3-13 except for the thermal expansion coefficients. The magnitudes of the normalized thermal expansion coefficients were determined by dividing the lowest thermal expansion coefficient by the individual values for each material.

Table 3-15 lists the weighted material properties. Weight factors were individually assigned to each property on the basis of estimated relative importance, in accordance with some of the recommendations of previous work (38).

The results of Table 3-15 indicate that CVD silicon carbide, hot-pressed silicon nitride and siliconized silicon carbide would be the best heat exchanger material candidates, followed (in that order) by sintered alpha-silicon carbide, sintered silicon nitride and finally, alumina. This classification is purposely very strongly influenced by resistance to thermal shock, strength, thermal conductivity and thermal expansion coefficient at temperature. In this ranking questions of fabricability and consistency of properties were not addressed; those will be discussed in Section 3.3.3. However, it should be noted here that reference 54 mentions that CVD SiC strenghs can vary considerably and values as low as 50 to 60 ksi might be expected. CVD silicon carbide may not be a viable candidate and its elimination would reorder the relative rankings, but the important conclusion to be made from this ranking would not change: The SiC family of materials and hot-pressed silicon nitride were the prime material candidates prior to assessments of fabricability. It would have been premature to consider fabricability before the ceramic shapes or even the preferred concepts had been selected.

Table 3-14. NORMALIZED PROPERTIES OF SELECTED HEAT EXCHANGER MATERIALS

PROPERTY \ MATERIAL	HOT-PRESSED Si_3N_4	SINTERED Si_3N_4	SILICONIZED SiC	SINTERED α-SiC	CVD SiC	ALUMINA
Thermal Shock Factor	0.70	0.35	0.70	0.55	1.00	0.05
Flex. Strength	1.00	0.90	0.40	0.45	0.80	0.80
	1.00	0.55	0.45	0.55	0.85	0.65
Young's Modulus	0.75	0.65	0.90	1.00	1.0	1.00
	0.65	0.60	0.75	1.00	0.85	0.90
Thermal Conductivity	0.30	0.25	1.00	0.80	0.85	0.10
Thermal Expansion Coefficient	0.95	1.00	0.75	0.75	0.75	0.45

Table 3-15. WEIGHTED PROPERTIES OF SELECTED HEAT EXCHANGER MATERIAL

PROPERTY	WEIGHTING FACTOR	MATERIALS:	HP Si_3N_4	SINT. Si_3N_4	SILIC. SiC	SINTERED α-SiC	CVD SiC	ALUMINA
Thermal Shock Factor								
	4		2.80	1.40	2.80	2.20	4.00	0.20
Flex. Strength,								
	2		2.00	1.80	0.80	0.90	1.60	1.60
	3		3.0	1.65	1.35	1.65	2.55	1.95
Young's modulus								
	1		0.75	0.65	0.90	1.00	1.00	1.00
	1		0.65	0.60	0.75	1.00	0.85	0.90
Thermal conductivity								
	3		0.90	0.75	3.00	2.40	2.55	0.30
Thermal Expansion Coefficient								
	3		2.85	3.00	2.25	2.25	2.25	1.35
		TOTALS:	12.95	9.85	11.85	11.40	14.80	7.30

Chemical compatibility also is a very important consideration in the design of a high temperature heat exchanger but a ranking for this was not included in Tables 3-13 through 3-15. These materials are among the most resistant to air or combustion gas environments at the anticipated temperatures. But the relevance of chemical compatibility questions is a direct function of the selected receiver concept. Generalized comparisons are not possible because of a lack of comparable test results on all the materials at a variety of test conditions such as environment, time and temperature. Slow crack growth and creep data, while important, have also not been included as a consequence of their strong dependence upon environment and test conditions.

Flow Containment Materials

The requirements for flow containment materials are nearly the same as those for heat exchanger materials and therefore all of the ceramics listed in the survey section above could satisfactorily be used for flow containment purposes. No additional monolithic materials meeting the requirements for flow-containment exclusively have been found.

Other concepts for flow containment not necessarily involving monolithic ceramics, such as internally insulated metal components, may be more efficient; that question was left to be addressed in the design portion of the study.

Insulation Materials

Bartlett, et al (59) designed and tested many fiberous insulation materials and design concepts to temperatures approaching 1649°C (3000°F) . Their studies resulted in a tested design which is considered the candidate for cavity insulation at the design temperature of 1316°C (2400°F). Temperature excursions above 1316°C (2400°F) are well tolerated with this design. It incorporates the rigid board products in two layers; the surface layer of 1649°C (3000°F) rated material backed with a 1427°C (2600°F) board and the two separated with an alumina fiber (Saffil®) mat. This facing concept for the hot surface was backed by layers of less expensive fiberous blanket rated for continuous use at 1260°C (2300°F). This design is shown in Figure 3-40.

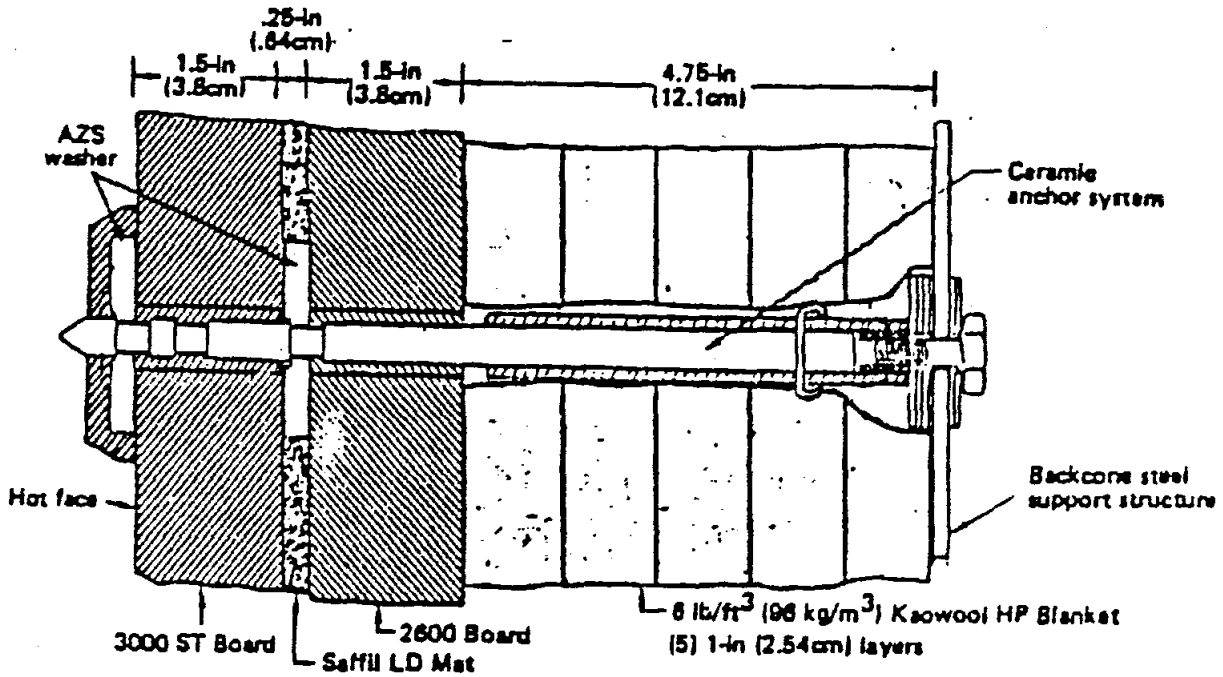

Figure 3-40. Cavity Insulation Material Design

Members of the fiberous insulation family are also candidates for lining the hot gas ductwork as mentioned in the previous section. Metal ductwork, protected by insulation from excessive temperatures, would contain the pressurized gas. Vacuum formed products are available in a variety of grades and densities and have been fabricated in the approximate 2-ft. diameters foreseen. Densification of surfaces with colloidal silica techniques, or application of surface coatings are possibilities for eliminating or minimizing erosion if erosion is a concern with these fiberous products. A more cost effective method of applying the insulation may be spraying, which is under development at Babcock and Wilcox (B&W). A significant amount of data on erosion (and its prevention) exists for the B&W materials. B&W feel that for flow velocities of 200 to 500 feet/sec and temperatures of 1116°C (2040°F) the design and engineering of insulation systems are not a major technical concern. Colloidal silica can be used for densification at temperatures of 1116°C (2040°F). Higher density insulation sleeves can be

incorporated on the inner surface if higher air velocities are anticipated. The design choices are many and can only be properly made on a specific design requirement which defines temperatures, flow velocities, type of flow, and geometry of the piping.

Window Materials

Ewing and Zwissler (38) list the following important window material properties:

- High transmission in solar spectrum
- Low absorptance
- Defined absorptance change with temperature
- Resistance to degradation at operating temperatures
- Chemical stability at operating temperatures
- Withstand thermal and mechanical loads
- Slow crack growth and creep resistance
- Thermal shock (not critical unless absorptance is high)

A preliminary material selection based primarily upon availability for general use is given in Table 3-16. Although service temperatures of around 1093°C (2000°F) have been considered, a maximum-use temperature is not frequently listed in the literature or manufacturer's data. Static fatigue, slow crack growth and creep (especially in the case of the glasses) are extremely important and dependent upon the specific temperatures and stresses of the design configurations. Relatively simple analyses (60) have resulted in estimates of window temperatures approximately 222°C (400°F) lower than the average receiver cavity temperature. Experiments at Georgia Institute of Technology (61) have found severe thermal gradients and higher-than-expected temperatures on the cavity-side surface of the window (1000°C [1830°F] on cavity-side surface, 222°C [400°F] on the exterior surface), with cavity temperatures ranging from 1093 to 1205°C (2000 to 2200°F).

Material Candidates Preliminary Selection: Summary

An extensive survey of heat exchanger, flow containment, insulation and window materials has been conducted in the present study in order to select potential

Table 3-16. SELECTED WINDOW AND TRANSPARENT TUBE MATERIALS

	MATERIALS					
	Vycor, 96% silica (Code 7913)	Fused silica (Code 7940)	AlON spinel	$MgAL_2O_4$ spinel	Poly-Crystal Al_2O_3	Single Crystal Al_2O_3
Supplier	Corning	Corning	Raytheon	Coors	Coors GE	Kyocera
Suplier-suggested maximum operating temperature (°F) (1)	<2000	2000	2200 (air)	>2500	>2500	>2500
Flexural strength (ksi)						
RT:	--	7.2 (2b)	44.0	16.0	40	100
~2000°F:	--	10.8 (2a)	30.0	20.0 (3)	~35	---
Thermal Conductivity, ~2000°F (Btu/hr°F ft)	--	--	--	~3	~3	~2.4
Thermal Expansion Coefficient, RT-~2000°F (10^{-6} in/in)	0.42	0.31	3.9	4.4	4.4	~3.0
Transmittance	~0.9	~0.9	--	0.9	0.8 Trans lucent	0.85 Trans parent
Fabrication Process:	Glass	Glass	Sintered	Hot-pressed	Sintered	Grown From Melt

(1) Maximum use temperature will be very much design dependent. Static fatigue, slow crack growth, creep, de-vitrification and oxidation (in one case) are concerns

(2a) 1650°F, (2b) abraded

(3) 1830°F

material candidates for specific applications in a solar receiver system. Preliminary results for the heat exchanger materials portion of the study indicate that CVD silicon carbide, hot-pressed silicon nitride, siliconized silicon carbide, and sintered alpha silicon carbide would be the best currently available materials for consideration for this particular application. The same materials could also be used for flow containment purposes, but the utilization of other flow containment concepts (such as metals with internal ceramic liners) could make this choice considerably less restrictive.

Insulation materials technology based on low density fiberous structures is well advanced and material systems for cavity insulation have been designed and tested for the environment anticipated in this study. Lining materials for flow containment are also commercially available.

There are relatively few available window materials that will meet the stringent operating temperature requirements of a solar receiver system. Of these materials, sapphire (single crystal alumina) would be the most desirable from a review of properties although size would be a severe restriction. Thus 96% fused silica (Vycor®) and 100% fused silica appear to be the most attractive candidates, based on their availability, cost and optical and thermal/mechanical properties. Other window materials, such as the $MgAl_2O_4$ spinel (62) spinel offer better temperature capability, but their usefulness is constrained at this time by processing limitations, which prevent fabrication of large, e.g., diameters above 12.7 cm (5 in.), components.

Finally, it should be pointed out that several additional materials have been produced experimentally but are not adequately characterized nor commercially available at the present time. These do show promise and may be of importance in the near future. These materials include: (1) CVD SiC-densified fiber preforms of Nextel® or silicon carbide which offer improved toughness characteristics; (2) Organosilicon-infiltrated and/or HIP densified reaction bonded silicon nitride (RBSN) materials; (3) Sintered RBSN, and (4) Ceramic fiber/matrix composites based on developing organosilicon technologies.

3.3.2 Fabrication and Design Considerations

The previous section discussed the initial screening of ceramic materials for the High Temperature Receiver Study based on suitability for a pressurized system with the requirements of Table 3-12. This section addresses the fabrication issues which may affect the choice of material and limit the design based on fabrication feasibility.

Before the fabrication issues can be properly presented several considerations must be noted, including: (1) design with ceramics (brittle materials) advancement over the past decade, and (2) the state of maturity of high performance ceramics technology.

To be used efficiently ceramic structures should be designed with probabilistic techniques. This important factor is addressed below in the section entitled, Designing for Mechanical Reliability.

The maturity level of ceramics processing technology is more difficult to address, much less to attempt to quantify. Ceramic technology has been progressing dramatically over the past decade led by the design methodologies and mechanical models. Recognition of flaws, their definition and relating them to process deficiencies is well underway even though many of the materials are fairly recent developments. However, industry standards are still a few years away as a recent ASTM committee on high technology ceramics determined (63). One of the stumbling blocks, for example, is the lack of even a standard mechanical property test method. The difficulties are directly related to the characteristics listed below in the section entitled Designing for Mechanical Reliability.

Ceramic materials may not have a mature technology as yet in the style of metals, but the emerging successes of heat engine and also heat exchanger programs show that successful design with ceramics in demanding applications is possible with newly developed tools; much work, however, remains. An assessment of relative maturities is made in the section entitled Fabrication Considerations below.

Designing for Mechanical Reliability

One of the greatest difficulties encountered when designing with structural ceramics is the prediction of mechanical reliability. Generally, structural ceramics exhibit the following characteristics:

(i) Linear elastic behavior up to fracture (except possibly at high temperatures), with virtually no crack arrest capability under tensile loads.

(ii) Macroscopically identical components under the same loads may have considerably different strengths.

(iii) Size effect: Strengths decrease significantly as the structure volume under stress increases (see Figure 3-41).

(iv) Sensitivity to multiaxial stress states: different failure stress levels are observed when components of equal size are subjected to different degrees of stress multi-axiality.

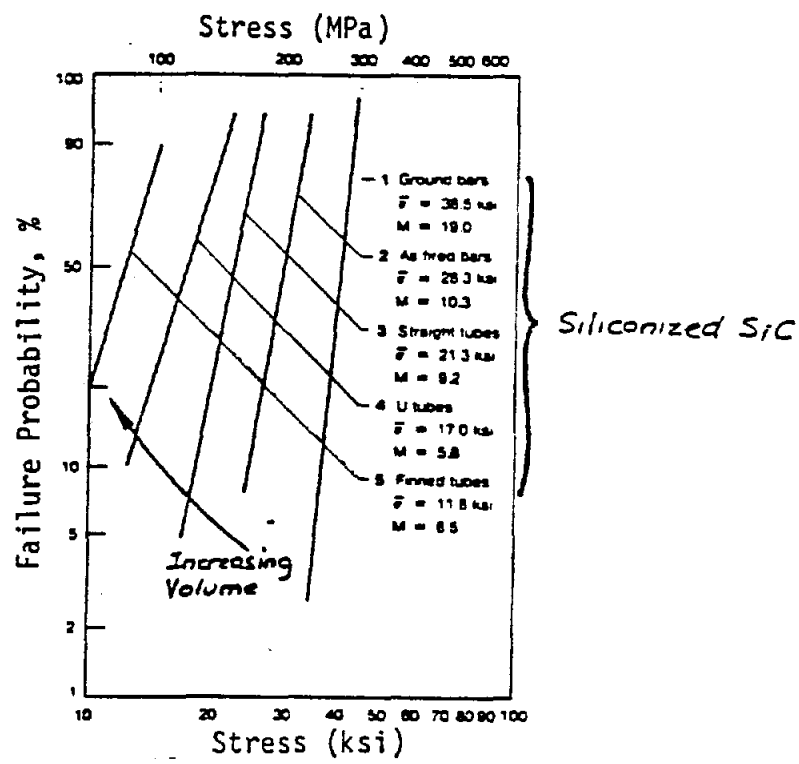

Figure 3-41. Effect of Component Size and Complexity on Fracture Strength and Variability (64)

These effects cause structural ceramics to be extremely unforgiving of stress concentrations and large structures under significant tensile loads. Improved processing techniques can alleviate some of these effects by, for example, reducing typical flaw sizes or introducing convenient compressive residual stresses fields in the finished components (for most structural ceramics, the average strengths in compression are approximately an order of magnitude higher than the average tensile strengths).

Because of the considerations mentioned above, the use of design allowables alone is not generally recommended for design purposes; this technique introduces an element of arbitrariness (the magnitudes of the allowable stresses). The use of a single design allowable does not account for scatter in strengths, size effects and multiaxial stress state effects.

In recent years a different approach involving failure statistics has been used with success (see reference 65). This method allows the prediction of the probability of failure of a given structure subjected to a given set of loads once the failure statistics for the same material in the same environment under a simple stress state (such as flexure of small rectangular bars) are known. Most statistical models usually allow for all of the brittle material effects listed above. A description of the basic theory is available in the literature (66-68).

For the purposes of the present study, the statistical approach can be used in two ways:

1. At a preliminary design stage, for simple component geometries, such as tubes or hemispherical shells, a pre-established probability of failure level can be used for initial sizing.

2. A second technique, discussed in reference 64 is to determine the component geometry using a deterministic approach, e.g., stress "allowables", and then carry out a probability of failure analysis of the component under the design loads. If the resulting values were found to be unacceptable, one would then proceed to a second design iteration where

critical stresses would be reduced in magnitude, or component sizes or thicknesses would be reduced. This simpler approach was used in the structural analysis of the 25-MW_e receiver heat exchanger tubes (Appendix C).

Fabrication Considerations, Structural Heat Exchanger Materials

The four structural grade ceramic materials selected in the previous section have restrictions on shape and size which are in large part dependent upon their method of manufacture. Tables 3-17 through 3-20 list the four materials, their fabrication methods, approximate shape and size limitations and an assessment of the relative maturity level of the technology. On the scale used here, 3 would denote a mature ceramic technology. In these terms, alumina (Al_2O_3) technology would be a high 3; metals technology would be over 10. It should be stressed strongly that these maturity assessments are highly subjective and apply only to generally large shapes. In fact, for smaller shapes the maturity level and especially quality of many of these high performance ceramics is every bit a match for metals or plastics materials technologies. It should also be kept in mind that these comparisons are in the style of the "apples and oranges" argument. Metals and ceramics are materials with different behaviors with their own specific advantages. Structural ceramics have obvious advantages for high temperature applications but the technology for their routine application in very demanding systems is not completely developed yet. Their use in demanding applications requires a design and fabrication sophistication and level of skill that is not thoroughly developed at this time although rapid progress is being made.

The limitations on component size are usually geared to production equipment size, so that in some cases the fabricators can make adjustments based on the customers' needs and level of demand. It should be noted that consultation of the user with the fabricator in the design stage is necessary.

Table 3-17. STRUCTURAL GRADE CERAMICS

METHODS OF MANUFACTURE

FREE-STANDING CVD SiC	HOT PRESSED Si_3N_4	SILICONIZED SiC	SINTERED SiC
DEPOSITION FROM VAPOR REACTION ONTO SUB-STRATE; REMOVE SUB-STRATE	PRESSING UNDER TEMP-ERATURE IN CARBON DIES	FIRST . FORM BY MANY COMMON CERAMIC METHODS; PRESS, SLIP CAST, PRE-CISION CAST EXTRUDE THEN . REACTION SINTER WITH LITTLE OR NO DIMENSIONAL CHANGE	FIRST . FORM BY MANY COMMON CERAMIC METHODS THEN . SINTER WITH ACCOMPANYING SHRINKAGE

Table 3-18. STRUCTURAL GRADE CERAMICS

APPROXIMATE SHAPE LIMITATIONS

FREE-STANDING CVD SiC	HOT PRESSED Si_3N_4	SILICONIZED SiC	SINTERED SiC
TUBES, COMPLEX SHAPES LIMITED BY SUBSTRATE REMOVAL AND GRAPHITE/ CARBON SUBSTRATE SIZES	FLAT TO SIMPLE CONTOUR. CONICAL SHAPES HAVE BEEN EXPERIMENTALLY MADE	SMALL INTRICATE SHAPES, TO TUBES, TO COMPLEX SLIP-CAST SHAPES	GENERALLY SAME AS FOR SILICON-IZED SiC

Table 3-19. STRUCTURAL GRADE CERAMIC

APPROXIMATE SIZE LIMITATIONS

FREE-STANDING CVD SiC	HOT PRESSED Si_3N_4	SILICONIZED SiC	SINTERED SiC
TUBES: 1 IN DIA. BY 2 FT LENGTHS DOMES: UNDER 2 FT DIA. THIN FILMS ON CARBON SUBSTRATES TO 24 IN DIAMETER	6 TO 12 IN DIA. AND 1 IN THICK	TUBES 1 TO 9 IN DIA BY 8 FT LENGTH COMPLEX SHAPES OF THIN WALL 18 IN DIA BY 2-1/2 FT 2 BY 6 FT IS A CURRENT FURNACE LIMITATION	SIMILAR TO THOSE FOR SILICONIZED SiC

Table 3-20. Structural Grade Ceramic: Subjective Assessment of Relative Fabrication Tech. Maturity (Large Shapes Only)

Free-Standing CVD SiC	Hot Pressed Si_3N_4	Siliconized SiC	Sintered SiC
0-1	2	2	2

Polycrystalline Al_2O_3 Technology Would Rank 3+

Table 3-21 is an attempt to assess the relative degree of material characterization for the preliminary candidates. The table reflects the recent development and emerging nature of these materials. What data exists, is generally of a very specific nature and dependent upon the design for which it was generated.

Cost estimates for hardware made from these high performance ceramics are difficult at best and highly dependent upon the specific design. There are no per pound figures available on costs because of (1) the design dependence, (2) lack of high volume production history (in most cases), (3) the development nature of some of these materials, and (4) dependence on specific tolerances required for the components.

The fabricators will be the best and perhaps only source of price information based on extrapolation of their knowledge of costs.

Table 3-22 lists an approximate relationship between costs for the preliminary materials. As can be seen, there can be a substantial cost difference between materials. Examples of future projections based on anticipated process improvement are:

- Coors is projecting a cost of $15/ft for extruded SiC tubes in several years (69)
- A projecton for NC-430 tubes (in 5 to 10 years) made in 1978 was $4 to $6/pound
- M.T.C. of Dallas estimated costs of 3-ft diameter CVD SiC domes at approximately $2000 each although they can only make less than 2-foot diameter currently at a much higher cost (70)

Silicon carbide tubes are now the fabricated form with the greatest maturity in heat exchanger concepts and most experience currently is with slip-cast SiC tubes. Extruded tubes are predicted to have much better uniformity and hence development is underway on extrusion for SiC tubes. The Gas Research Institute (GRI) is sponsoring a manufacturing technology program and hopes to have tube costs eventually down to $15/ft, around $10 per pound (71). GRI is currently working with Norton, Carborundum, and Coors.

Table 3-21. Relative Levels of Materials Characterization

	CVD SiC	HP Si_3N_4	Siliconized SiC	SASC
Failure Statistics				
- at RT	0	2	2	1-2
- at 2000°F	0	2	2	1-2
Chem. Compatibility at Temperature *	1	1	1	1
Chem. Corrosion Effects on Properties at Temperature	0	0-1	0-1	0-1
Stable Crack Growth and Fatigue at Temperature	0	2**	1-2	1-2
Creep and Plasticity at Temperature	0	1-2	1	1
Processing Effects on Mat. Properties	0	3	1-2	2-3

* A few studies have been reported, but range of T's and especially long times are not available.

** Stress Rupture Only

(Sources: Manufacturers, technical literature, Contractual Studies)

0 = None to minimal
1 = Fair
2 = Good
3 = Excellent

Table 3-22. APPROXIMATE RELATIVE COSTS OF MATERIALS

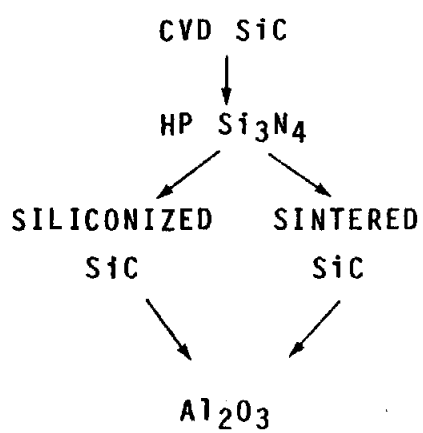

GENERIC MATERIAL	REL. COST ESTIMATE
CVD SiC	10 to 100
HP Si_3N_4	
SILICONIZED SiC	2 to 5
SINTERED SiC	
Al_2O_3	< 1

Fabrication Effects on Materials Selection: Structural Heat Exchanger Materials

Hot-pressed silicon nitride and CVD silicon carbide were eliminated from consideration because of fabrication limitations. Large items of free standing CVD SiC do not appear to promise high levels of reproducibility nor the potential of low costs. Hot-pressed silicon nitride does offer excellent properties but the fabrication method severely limits the types of items that are feasible.

The siliconized silicon carbides and, perhaps, sintered alpha-silicon carbide are the materials selections for structural heat exchanger elements. Their properties are excellent at temperature and their potential costs are very attractive because of expected high demand for high temperature heat recuperators. These high volume industrial uses are expected to lower the costs dramatically for other applications, such as solar receivers, that can use the same tubular types of components.

Fabrication Considerations: Window Materials

A survey of candidate window material manufacturers and their literature was made similar to that for the structural heat exchanger materials in the above section. The results for fabrication methods, approximate shape and size limitations with a subjective assessment of the relative maturity of their technologies are summarized in Tables 3-23 through 3-27.

Fabrication Effects on Materials Selection: Windows

Based on properties alone, single crystal alumina (sapphire) would be the most attractive window material candidate. Current size limitations, however, weigh heavily against single crystal alumina.

Fused silica can conceivably be made in the 3-m diameter sizes contemplated for a window. However, the use of fused silica (even in a state of compression) would require design provision for cooling the inner surface to

Table 3-23. WINDOW AND TRANSPARENT TUBE MATERIALS FABRICATION METHODS

TRANSLUCENT POLYCRYSTALLINE Al_2O_3	TRANSPARENT SAPPHIRE SINGLE CRYSTAL Al_2O_3	$MgAl_2O_4$	VYCOR® 96% SiO_2	FUSED SILICA 100% SiO_2
PRESS AND THEN SINTER IN H_2	EDGE FORMED FILM FED GROWTH FROM MELT	HOT PRESS	FORM AS A GLASS, HEAT TREAT, LEACH, AND SINTER	FUSED POWDER OR CRYSTALS OF SILICA (QUARTZ)

Table 3-24. WINDOW AND TRANSPARENT TUBE MATERIALS APPROXIMATE SHAPES AVAILABLE

TRANSLUCENT POLYCRYSTALLINE Al_2O_3	TRANSPARENT SAPPHIRE SINGLE CRYSTAL Al_2O_3	$MgAl_2O_4$	VYCOR® 96% SiO_2	FUSED SILICA 100% SiO_2
SMALL TUBES AND PLATES	SMALL TUBES AND PLATES	FLAT PLATE TO SIMPLE DOMES	PLATE, ROD, TUBE, BLOWN AND PRESSED WARE	DOMES, PLATES, WINDOWS, TUBES

Table 3-25. WINDOW AND TRANSPARENT TUBE MATERIALS APPROXIMATE SIZES AVAILABLE

TRANSLUCENT POLYCRYSTALLINE Al_2O_3	TRANSPARENT SAPPHIRE SINGLE CRYSTAL Al_2O_3	$MgAl_2O_4$	VYCOR® 96% SiO_2	FUSED SILICA 100% SiO_2
TUBES: UP TO 1/2 IN DIA, 10 IN LONG, 0.030 IN WALL PLATES: SEVERAL INCHES DIAMETER, <1/8 IN THICK	TUBES: UP TO 1 IN DIA, 40 IN LENGTH, 0.060 IN WALL PLATES: UP TO 5 IN DIA	TO 7 IN DIA., EXPECT LARGER WITHIN 2 YRS	2 FT BY 2 FT PLATE TUBING: 4 IN DIA, 3 FT LENGTH, 0.15 IN WALL	DOMES TO 5 FT DIA, LARGER BY FUSION JOINING TUBING: 7 IN DIA, 1.0 IN WALL, 8 FT LENGTH--CAN JOIN LONGER

Table 3-26. WINDOW AND TRANSPARENT TUBE MATERIALS APPROXIMATE COST INFORMATION

TRANSLUCENT POLYCRYSTALLINE Al_2O_3	TRANSPARENT SAPPHIRE SINGLE CRYSTAL Al_2O_3	$MgAl_2O_4$	VYCOR® 96% SiO_2	FUSED SILICA 100% SiO_2
BECAUSE OF HIGH VOLUME, SMALL TUBES <$10	4 IN WINDOW IN HIGH QUANTITY <$100 MUCH MORE EXPENSIVE THAN POLYCRYSTALLINE Al_2O_3	3 IN DOME FOR QTY >2000 APPROX. $500 EACH	COST CAN BE APPROX 1/10 OF FUSED SiO_2 MAX SIZE TUBES ARE APPROX. $200 TO $1000 DEPENDING ON QTY	LARGE TUBING IS $100 TO 200/FT. QUOTED 1.7 METER DIA DOME AT $40K SEVERAL YRS AGO

Table 3-27. Window and Transparent Tube Materials: Subjective Assessment of Relative Fabrication Maturity (Large Shapes Only)

Translucent Polycrystalline Al_2O_3	Transparent Sapphire Single Crystal Al_2O_3	$MgAl_2O_4$	Vycor® 96% SiO_2	Fused Silica 100% SiO_2
3	2-3	1	1	2-3

Polycrystalline Structural Grade Al_2O_3 Technology Would Rank 3+

below 982°C (1800°F) to prevent rapid devitrification. In compression, surface devitrification may not be considered a gross fault; however, possible complex stress states in such a large window and their effects on failure probabilities need to be examined in detail. In addition, design concepts incorporating small window sections in a "mosaic" fashion may bypass the size of fabrication constraint.

3.4 PREFERRED RECEIVER CONCEPT SELECTION

After consideration of the thermal analyses results, the design analysis considerations, and high-temperature materials assessment, a preferred receiver concept was selected for each plant size. The concept selection was made based on assessments of cost, performance, reliability, maintainability and operability. The following subsections discuss the receiver concepts in each of these areas.

3.4.1 25-MW_e Plant Receiver

As indicated in Section 3.2.1, four receiver concepts were selected for additional consideration at the 25-MW_e plant size: (1) falling particle receiver, (2) high-temperature molten salt, (3) transparent tube receiver, and (4) ceramic tube receiver. Thermal analyses results of these concepts were presented in Section 3.2.2. Design analyses results were presented in Section 3.2.3, and materials considerations were presented in Section 3.3. An assessment of these receiver concepts in the areas of performance, cost, reliability, maintainability and operability are presented in the following paragraphs.

Performance

The results of the thermal analysis show no clear advantage of one receiver concept over the others. Each concept had a receiver efficiency of about 85%, with any preference going to the transparent tube concept. The results of this study show no performance advantage for the more complex, high flux intermediate medium concepts based on the limited thermal analysis performed.

Cost

Detailed cost estimates on each receiver concept were beyond the scope of this study. However, the design analysis results allowed projection of the relative costs of the concepts. The falling particle and high-temperature molten salt receiver concepts are considerably more complex than the ceramic tube and transparent tube concepts. The intermediate medium cavities, although smaller than the tubed concepts, require considerable amounts of high-temperature refractories, which will probably have to be replaced periodically over the life of the receiver. It is not clear that the smaller, high flux receivers will be less expensive than the ceramic tube and transparent tube receivers. Intermediate medium receivers also require considerable support equipment to accomplish the secondary heat exchange. The 1093°C+ (2000°F+) temperatures required in handling the hot solids or hot molten salt requires the use of relatively expensive materials. Preliminary calculations showed the piping cost alone for the molten salt concept to account for 60-70% of the total cost of the ceramic tube concept.

Reliability

Because of the additional equipment (piping, valves, heat exchangers, etc.) for the intermediate medium concepts, the passive design of the ceramic and transparent tube concepts is preferred from a reliability viewpoint. The transparent tube concept suffers from the devitrification problem described in Section 3.3. At 1093°C (2000°C), a quartz tube will experience significant devitrification. Cyclical cooling to ambient temperatures will cause cracking and spalling of the tube, making the transparent tube unreliable as a pressure containment device.

Maintainability and Operability

The more complex the system, the more the requirements for maintenance and operating personnel. The ceramic tube concept has few moving parts and requires only routine inspection. Both the falling particle and molten salt concepts have more equipment to inspect and substantial amounts of

high-temperature moving or mechanical equipment. Careful consideration of potential abrasive and corrosive attacks on equipment must be constantly surveyed.

Concept Selection

The ceramic tube receiver was selected as the preferred concept for the 25-MW_e plant size. This concept has reasonable performance and cost through the use of a simple, straightforward design. Few high-temperature mechanical components are required. From a materials viewpoint, this choice is clearly the closest to technical feasibility. Ceramic components of the size, quantity and temperature capability are currently available. The ceramic design is also in keeping with the desired simple, low maintenance objectives of the overall study. This concept is the most likely to operate reliably in a remote, stand-alone electrical generation application.

Further Discussion

Although the ceramic tube concept is preferred for the application under study, a change of study ground rules could easily influence the final decision. For example, the inclusion of thermal energy storage would significantly favor the intermediate medium concepts. Thermal energy storage for an air-cooled receiver is difficult to accomplish cost effectively. However, storage of a hot solid or molten salt is more straightforward and, based on previous studies, has shown to lower busbar costs at high capacity factors. Also, for larger plant sizes where the investment in secondary heat exchange equipment is a less significant portion of the plant, the intermediate medium systems may be more attractive.

The transparent tube concept has several very attractive features: high flux capability, compact size, no secondary heat exchange. If the turbine inlet temperature were reduced 100°C (180°F), the devitrification of the quartz tubing would be significantly reduced. The performance analyses of Section 2.4.2 show a relatively small cycle efficiency penalty for the 25-MW_e open

cycle regenerated and intercooled concept at the reduced turbine inlet temperatures. This reduced temperature/transparent tube combination may produce a cost- effective receiver/cycle system configuration.

Inclusion of a steam bottoming cycle with the volumetric receiver concept described in Section 3.1.2 would allow the removal of the induced draft fan precooler heat exchanger while increasing the overall efficiency of the central receiver system. The results of Reference 9 indicate attractive receiver absorption and reradiation properties for the volumetric receiver. The inclusion of the steam bottoming cycle may make this receiver more attractive as an electrical generating system.

3.4.2 2-MW_e Plant Receiver

As indicated in Section 3.2.1, the four receiver concepts discussed in the previous section plus the small particle receiver were to be considered for the 2-MW_e plant size. The discussion of the receiver concept features presented in the previous section applies as well to the 2-MW_e size range. The ceramic tube and small particle receivers will be compared in the following paragraphs.

Performance

Based on the thermal analyses results of Section 3.2.2, the small particle receiver concept has a slight advantage in terms of receiver efficiency over the ceramic tube concept (89% versus 85%). Also, the open cavity of the small particle receiver allows a reduction in receiver pressure loss. This translates into higher cycle efficiencies for the 2-MW_e, small particle receiver system. For example, a reduction of receiver pressure loss from 10% to 5% would allow an increase of cycle efficiency from 32.2% to 33.6%.

Cost

The major cost item for the small particle receiver is the 3-m diameter quartz window. The remainder of the cavity is an interior insulated spherical pressure vessel. The small particle receiver also would not require a manifolding system as required for the ceramic tube concept. Preliminary calculations showed that the small particle receiver would cost 60% less than the ceramic tube receiver.

Reliability

The major reliability concern for the small particle receiver is the window design. By using cooling air to maintain the window below the devitrification zone, the reliability can be significantly increased.

Maintainability and Operability

Both the small particle and the ceramic tube concepts are simple and passive in design. Both should be easily maintained and operated.

Concept Selection

The small particle receiver was selected as the preferred concept for the 2-MW_e plant size. This receiver has superior performance and cost and reasonable reliability, maintainability and operability. From a materials viewpoint, the 3-m diameter quartz window presents a manufacturing challenge. Maintaining the window temperature below the devitrification point is also a requirement.

3.5 PREFERRED RECEIVER CONCEPT DEFINITION

The preferred receiver concepts described in the previous sections were considered in more detail. The objective was to define a receiver design sufficient to determine an estimate of the capital cost. The design definition was concentrated on the 25-MW_e receiver subsystem. The 2-MW_e receiver values were scaled from the 25-MW_e results where appropriate.

3.5.1 Materials Assessment

The selected receiver design concepts were the ceramic tube receiver for the 25-MW_e plant and the small particle receiver (requiring a window) for the 2-MW_e generating system.

The materials selected for the ceramic tube concept are the silicon carbides which can be divided into two general classes: sintered alpha silicon carbide and the siliconized reaction bonded silicon carbides. As described in Section 3.3, these silicon carbides are preferred based on considerations of strength, temperature capability, component availability and fabricability. Of these two silicon carbides, the siliconized reaction bonded silicon carbide was chosen as the preferred heat exchanger tube material. This choice was made after a preliminary structural analysis of the chosen heat exchanger configuration (see Appendix C). The siliconized silicon carbide was chosen because of its lower projected expense and state of technology development. The sintered alpha silicon carbide, however, offers the potential of lower probability of failure with more development.

The candidate material for the pressurized small particle receiver window is fused silica. This material was chosen because of its cost and fabrication experience. Nevertheless, a 3-m diameter fused quartz window will be a manufacturing challenge. The window will also require cooling of the cavity-side window surface. Such a cooling scheme was presented earlier in Section 3.2.3.

3.5.2 Concept Design Definition

<u>25-MW_e Receiver</u>

Figure 3-42 shows an elevation view of the 25-MW_e ceramic tube receiver, turbine room and tower. Figure 3-43 shows interior views of the receiver, and general arrangement of the heat exchanger tubes. Figure 3-44 is a detail view showing the receiver interior insulation and the method of attachment to the receiver wall. This insulation concept would be used where the highest first incident solar flux occurs. For the remainder of the cavity, layers of Kaowool® blanket would be used.

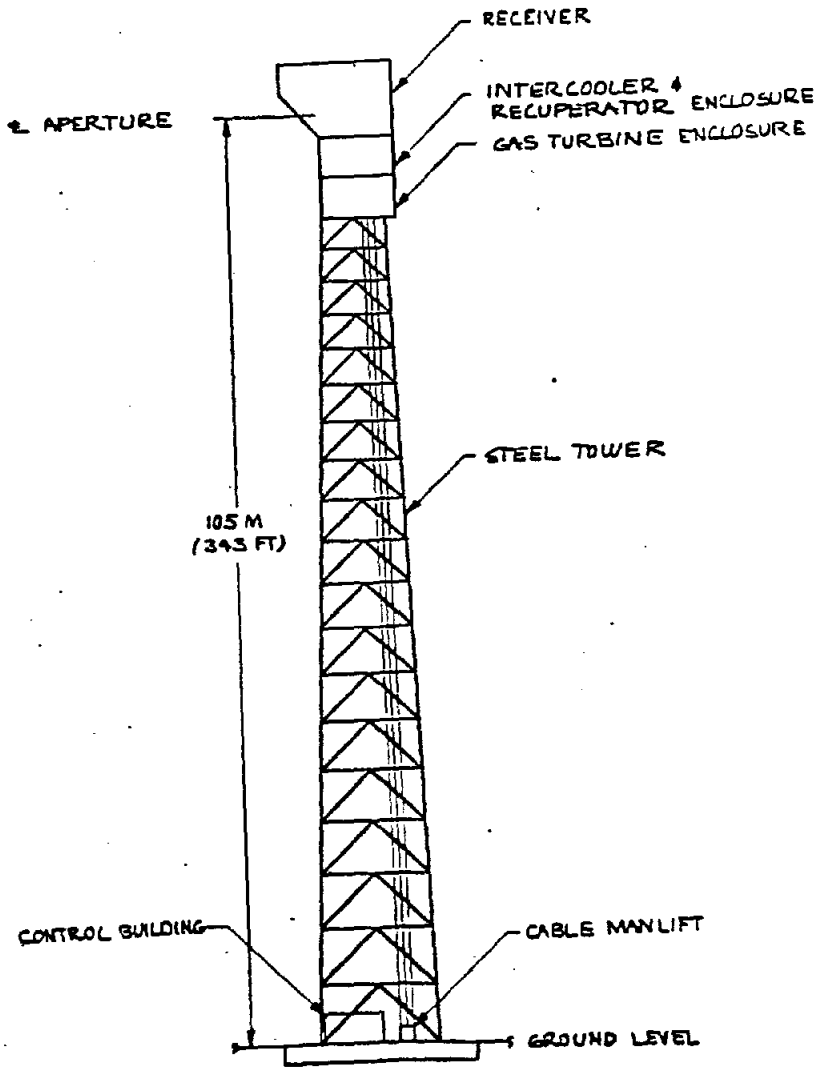

Figure 3-42. Elevation View of Receiver, Turbine Room and Tower

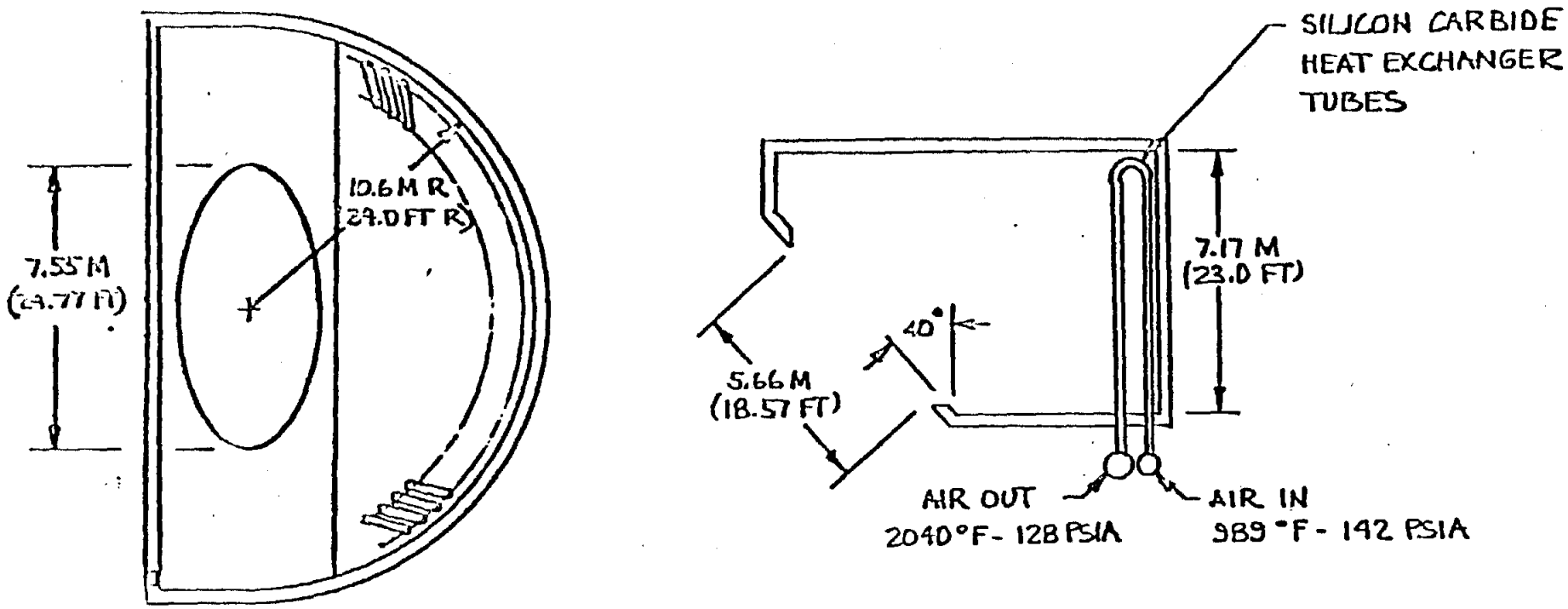

Figure 3-43. 25-MW_e Ceramic Tube Receiver

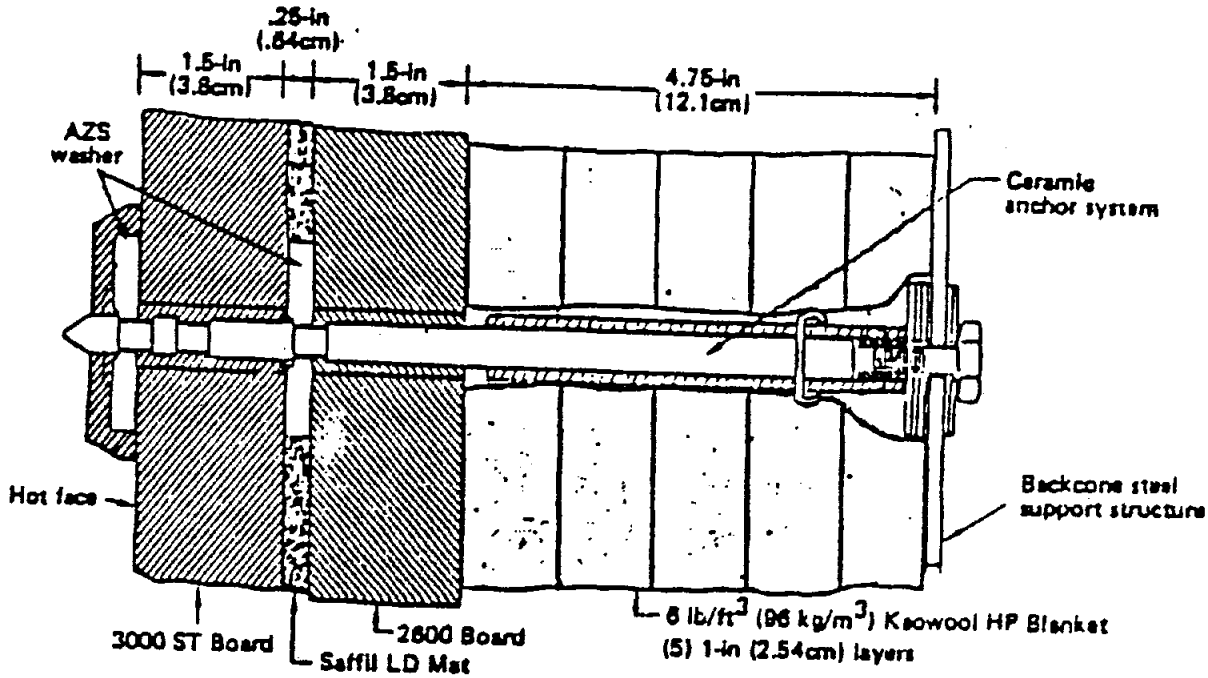

Figure 3-44. Receiver Interior Insulation Concept

Figure 3-45 shows a silicon carbide heat exchanger tube assembly. The individual silicon carbide tube elements are formed, sintered, assembled with Si-20Mo brazing compound then furnace brazed. These tube assemblies operate with the highest solar flux on the discharge side of the loop. The inlet side is nearest the receiver wall. The upper end of the loop is unsupported so that the assembly is free to elastically distort under thermal expansion. A preliminary structural analysis of the heat exchanger tube is presented in Appendix C.

Figure 3-46 shows the attachment of the silicon carbide tube flange to the manifold steel flange. The manifold elements are lined with Kaowool® insulation and a thin metallic liner. The liner and insulation reduce the operating temperature of the outside pressure tube to temperatures where carbon steel can be used. The hotter discharge manifold uses a nickel liner for 1116°C (2040°F) air. The inlet manifold uses Type 316 stainless steel for 531°C (989°F) air.

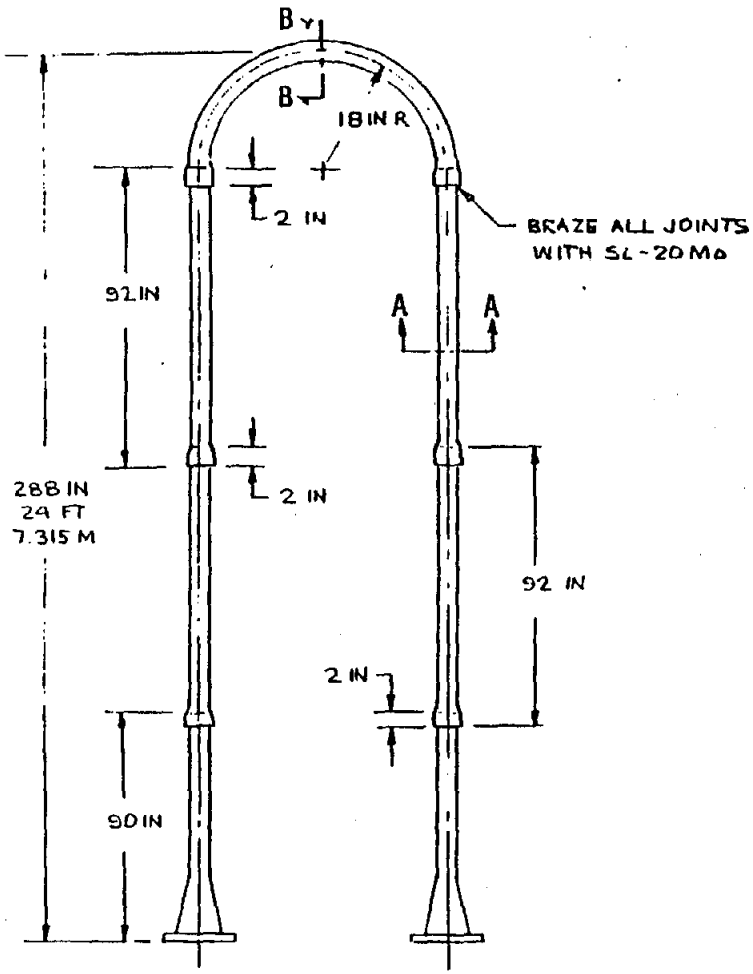

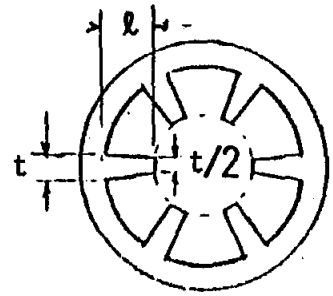

Section A-A

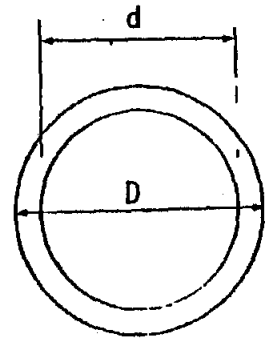

Section B-B

	Dimensions in.
d	2.50
D	3.00
t	0.25
ℓ	0.575

Figure 3-45. Heat Exchanger Tube Assembly

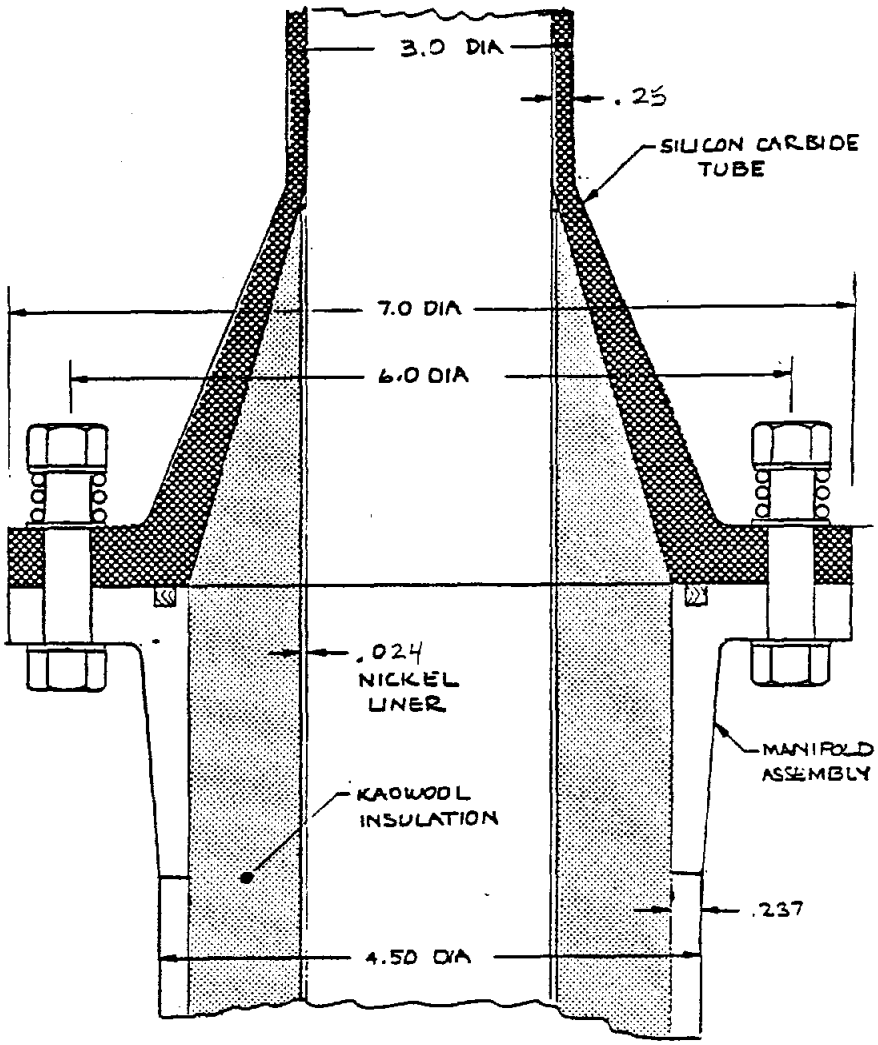

Figure 3-46. Heat Exchanger Tube-to-Manifold Assembly

Figure 3-47 shows a plan view of the manifolds and heat exchanger tubes. The manifolds are attached to the structure at the riser and the downcomer. The two manifolds are tied together at the outer ends with a leaf spring which rigidly maintains the centerline spacing of the manifolds but prevents differential twisting and allows ready expansion in a lengthwise direction.

The design of the interconnect piping between the turbine, precooler, recuperator and receiver is similar to that of the manifold. The hot piping between the receiver outlet and turbine inlet is constructed of a carbon steel outer pipe interior insulated with Kaowool® and lined with nickel. The piping between the turbine exit and the recuperator hot side inlet and between the recuperator cold side outlet and receiver inlet is exterior-insulated stainless steel. The remaining piping is exterior-insulated carbon steel. Expansion joints are included at the ends of each piping run to allow for thermal growth.

Figure 3-48 shows the steel structure for the receiver. The main frame consists of W8x24 beams. W6x15 members transmit wind and gravity loads to the frame. The entire outer surface of the receiver is lined with 0.48-cm (3/16-inch) steel sheet that provides attachment for the insulation and seals the receiver against the weather. Angle stiffeners break the skin into smaller panels to increase buckling resistance. The skins carry wind pressure loads and provide the resistance to shear.

Figure 3-49 shows the structure around the aperture and on the bottom of the receiver. Figure 3-50 shows the structural arrangement of the turbine enclosure and the intercooler/recuperator enclosure. The receiver attaches to the top. The tower attaches to the lower floor. There is a trapdoor access to the lower floor from a cable manlift. Figure 3-51 shows the dimensions of the tower and concrete base. The tower and concrete base were designed based on similar size steel towers contained in reference 73. Table 3-28 summarizes the design conditions and the quantities of material required for the tower and base. Table 3-29 summarizes the receiver subsystem design.

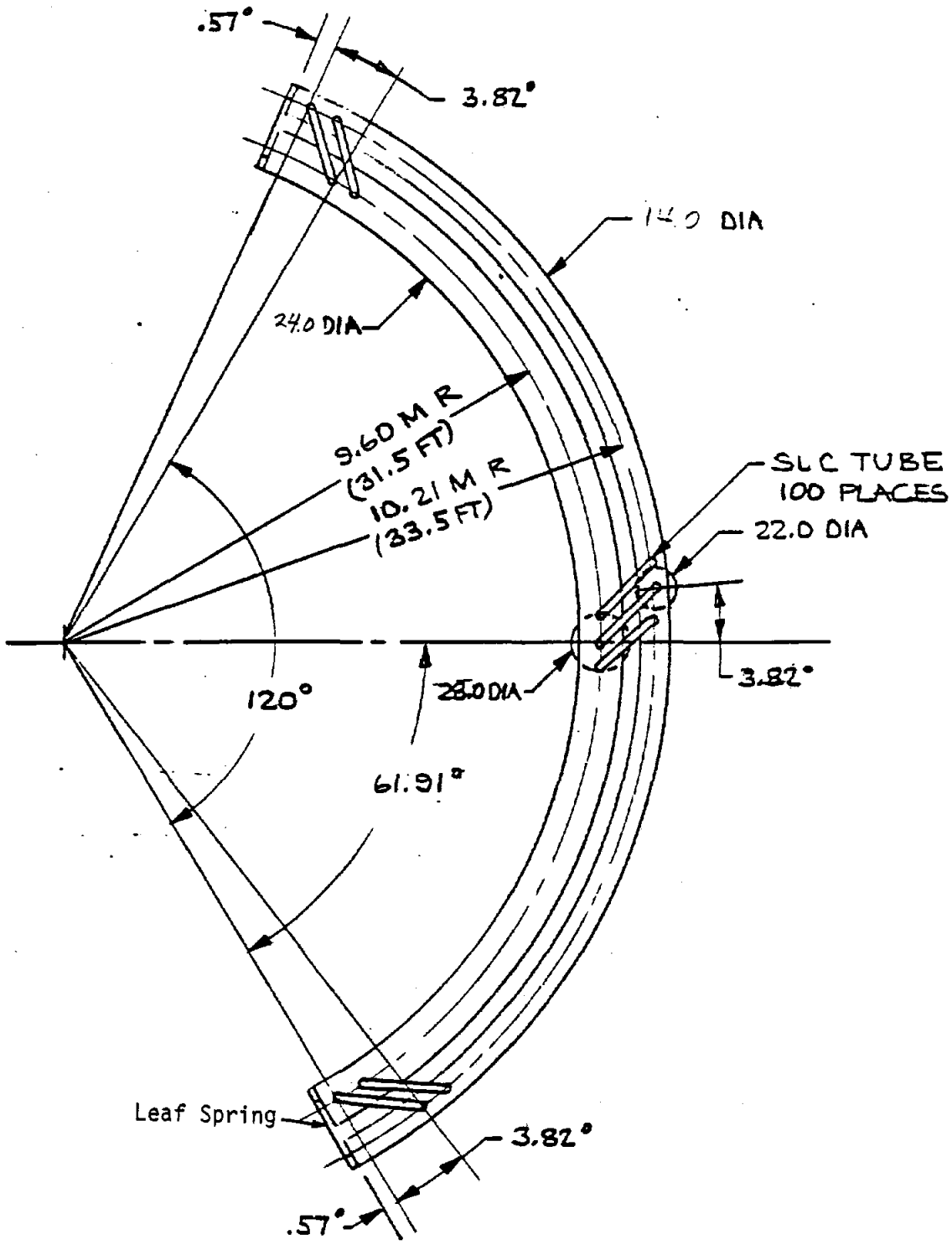

Figure 3-47. Manifold Design

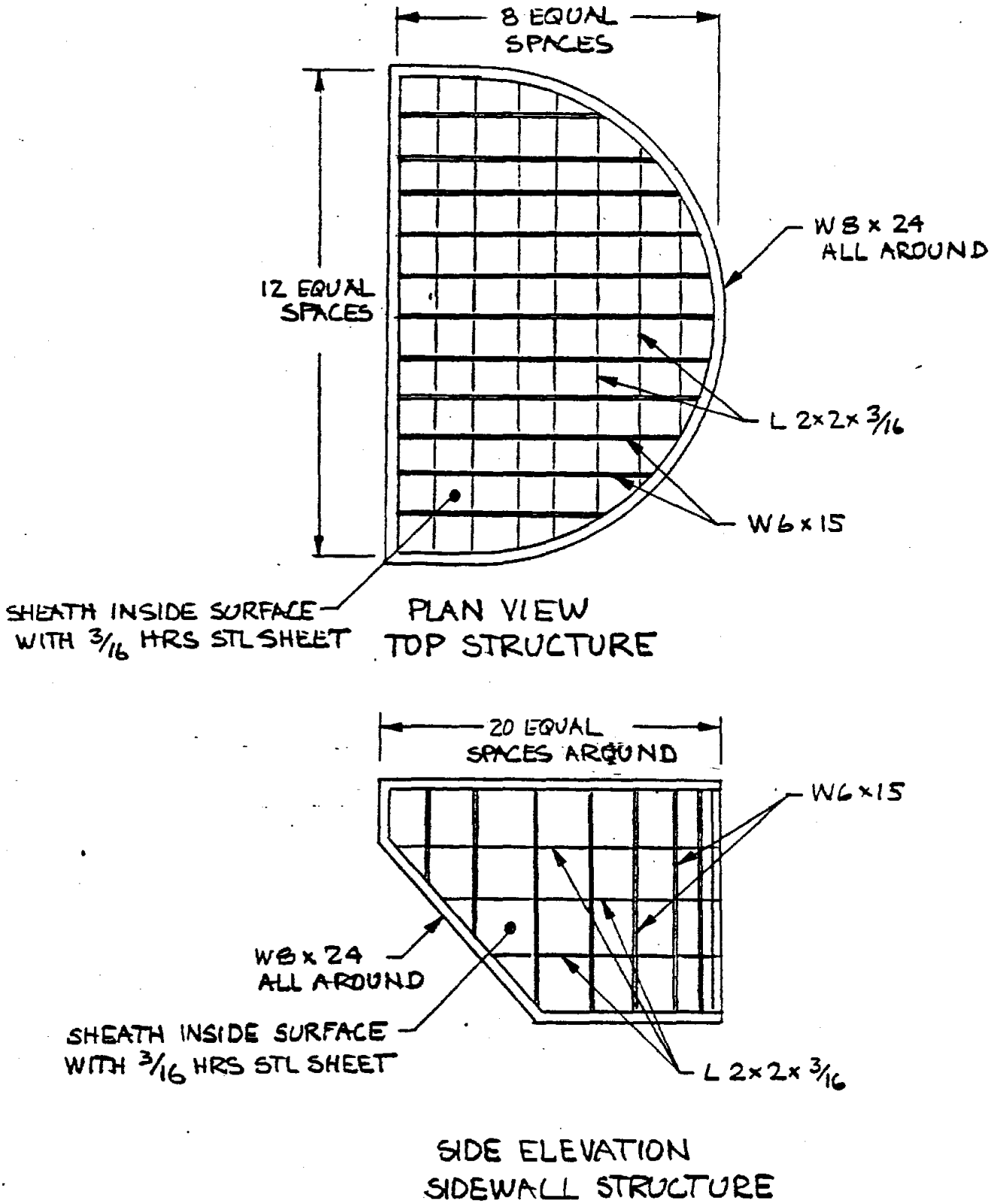

Figure 3-48. Receiver Structural Design

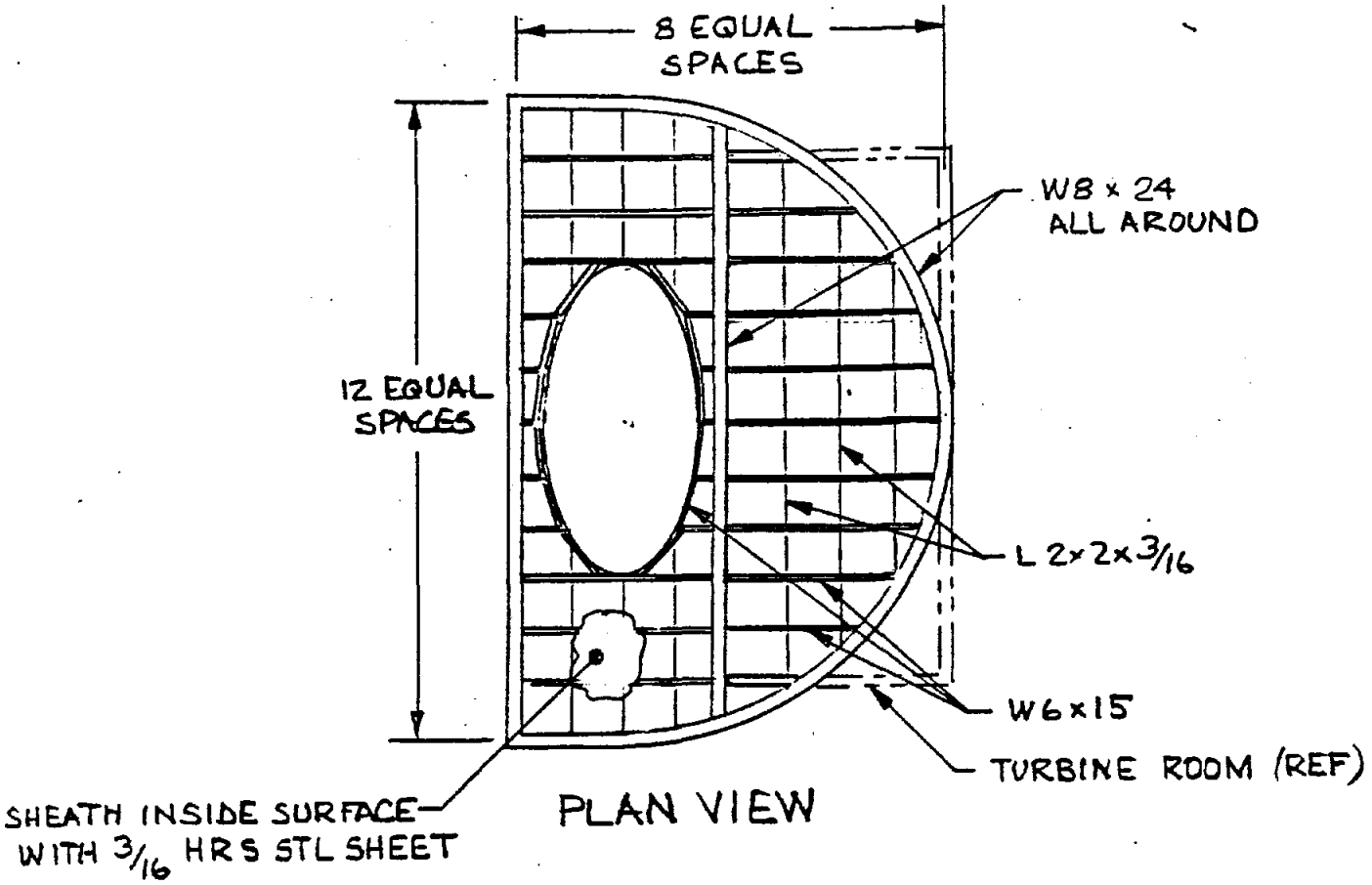

Figure 3-49. Aperture Structural Design

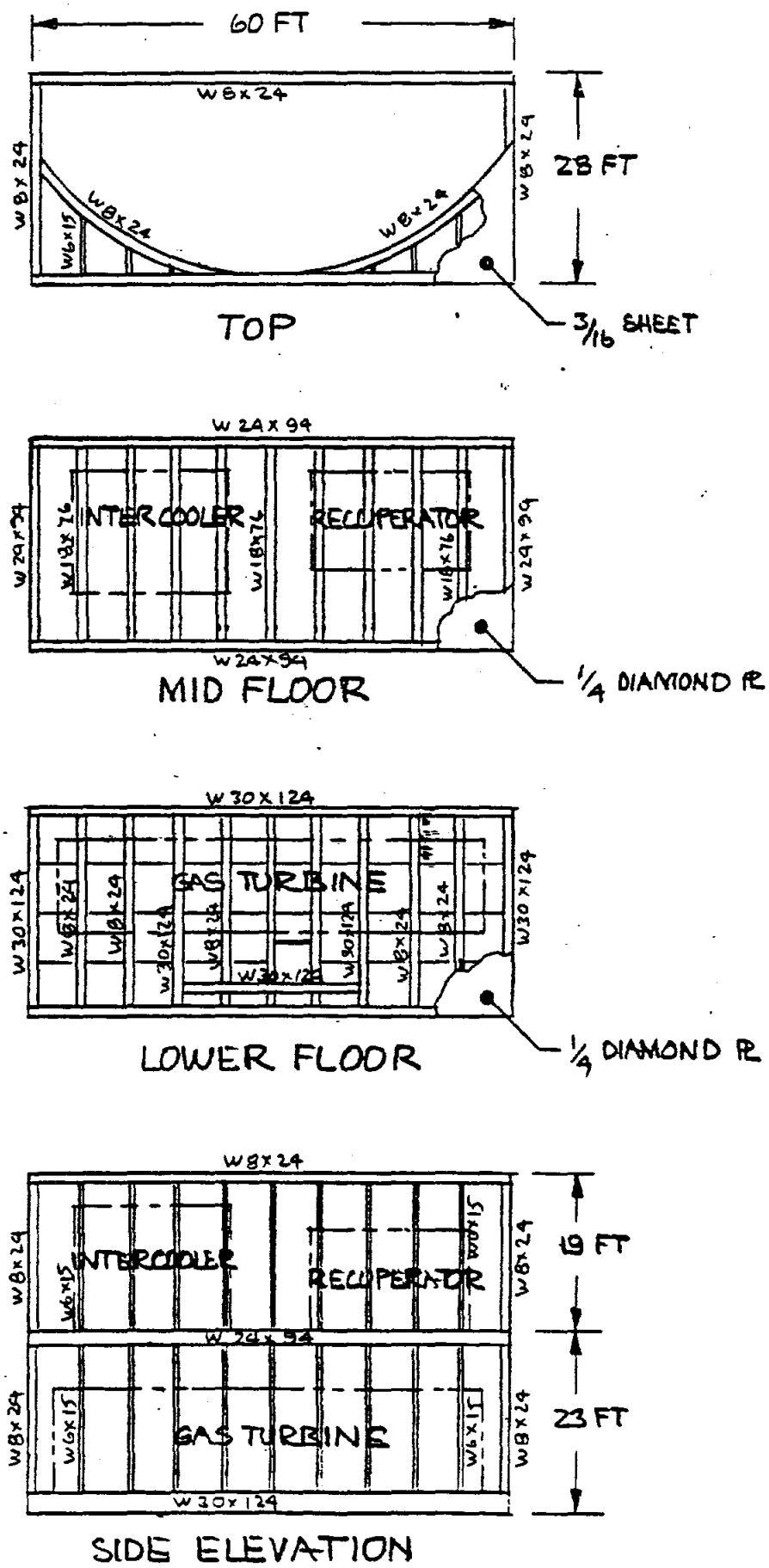

Figure 3-50. Turbine Room Structural Design

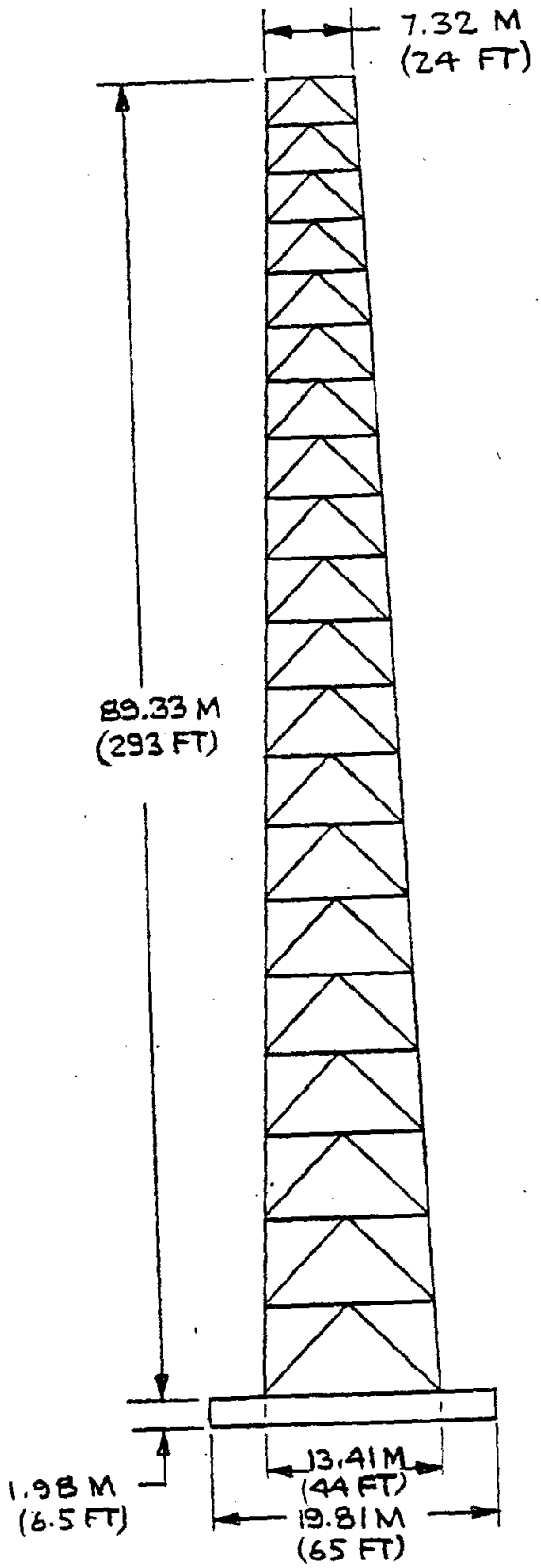

Figure 3-51. Steel Tower and Concrete Base Design

Table 3-28. 25-MW_e Steel Tower Design Summary

Receiver Wt. (10^3 lb)*	1000
Ground Accel (Gs)	.05
Wind Velocity (MPH)	120
Soil Shear Modulus (KSI)	∞
Allow, Soil Bear (KSF)	12
Tower Height (FT)	293
Diam. across Flats at Top (FT)	20
Diam. across Flats at Bot. (FT)	40
No. of Columns	4
Column Weight (Tons)	102
Column Material	A440
Vertical Bracing Weight (Tons)	87
Horizontal Bracing Weight (Tons)	28
Connection Weight (Tons)	11
Bracing and Connection Material	A36
Total Tower Weight (Tons)	228
Mat Type	Sq.
Mat Width/diameter (FT)	65
Mat Thickness (FT	6.5
Concrete f'c (KSI)	3
Concrete Volume (CY)	1017
Rebar fy (KSI)	60
Rebar Weight (Tons)	38

*Assumed to include receiver, turbine, recuperator, intercooler, and turbine room mass

Table 3-29. 25-MW_e Receiver Design Summary

Receiver cavity radius (characteristic)		10.4m (34.0 ft)		
Receiver height		7.17m (23.0 ft)		
Peak solar flux		450 kW/m^2		
Aperture shape		Elliptical		
Aperture inclination from vertical		40°		
Aperture height		5.66m (18.56 ft)		
Aperture width		7.55m (24.76 ft)		
Aperture area		33.56m^2 (361.2 ft^2)		
Number of tubes		100		
Tube outside diameter		7.62cm (3.0 in)		
Tube wall thickness		0.64cm (0.25 in)		
Tube pitch ratio		3.0		
Heated tube length		14.0m (46 ft)		
Tube material		Siliconized silicon carbide		
Manifolds:				
Outside diameter	Inlet:	35.6cm (14 in)	Outlet:	61.0cm (24 in)
Wall thickness		0.48cm (.188 in)		0.56cm (.219 in)
Wall material		A139		A53
Liner material		--		Nickel
Insulation material		Fiberglass (ext.)		Kaowool® (interior)
Insulation thickness		7.62cm (3 in)		7.62cm (3 in)
Riser/Downcomer:				
Outside diameter	Riser:	45.7cm (18 in)	Downcomer:	76.2cm (30 in)
Wall thickness		0.56cm (.219 in)		0.64cm (.25 in)
Wall material		A155		A53
Liner material		--		Nickel
Insulation material		Fiberglass (ext.)		Kaowool® (interior)
Insulation thickness		7.62cm (3 in)		7.62cm (3 in)

Pressure loss budget:

Heat exchangers	7.0%
Riser/inlet piping	0.5%
Downcomer/outlet piping	0.5%
Valving and control	2.0%
Total	10.0%

2MWe Receiver

Figure 3-52 shows an elevation view of the 2-MWe small particle receiver, turbine room and tower. Figure 3-53 shows a schematic of the small particle receiver. The receiver is a 6-m (19.58 ft) diameter spherical pressure vessel with the interior insulated with 12.7 cm (5 in) of Kaowool®. Carbon particles can be created by a number of methods including arc evaporation, pyrolysis of organic resins, and thermal composition of hydrocarbons (72). Experiments performed by Lawrence Berkeley Laboratory have shown promise for the generation of carbon particles via the pyrolysis of acetylene in an inert gas such as argon (28). The carbon particles would be injected into the compresor outlet flow. The receiver inlet air and carbon particles are distributed evenly in the cavity with a nickel diffuser. The carbon particles absorb the solar flux, heat the air and oxidize forming CO_2.

A transparent aperture window admits the solar flux while maintaining pressure in the cavity (see Figure 3-54). The window would be made of a 120° spherical segment of fused quartz. The window would be fabricated by fusing smaller window sections into the final assembly. The window-to-shell interface design is illustrated in Figure 3-55. A portion of the cooler compressor outlet flow, 406°C (763°F), would be injected around the periphery to cool the aperture window. A sliding seal will allow differential expansion between the spherical shell and the window. The arched shape of the window and the internal cavity pressure will maintain the window in compression against the seal. Retaining springs will align and retain the window during non-operating periods. Table 3-30 summarizes the receiver subsystem design.

3.5.3 Receiver Concept Performance

Table 3-31 presents a summary of the receiver performance for both plant sizes. The data are based on the cavity thermal analyses presented earlier.

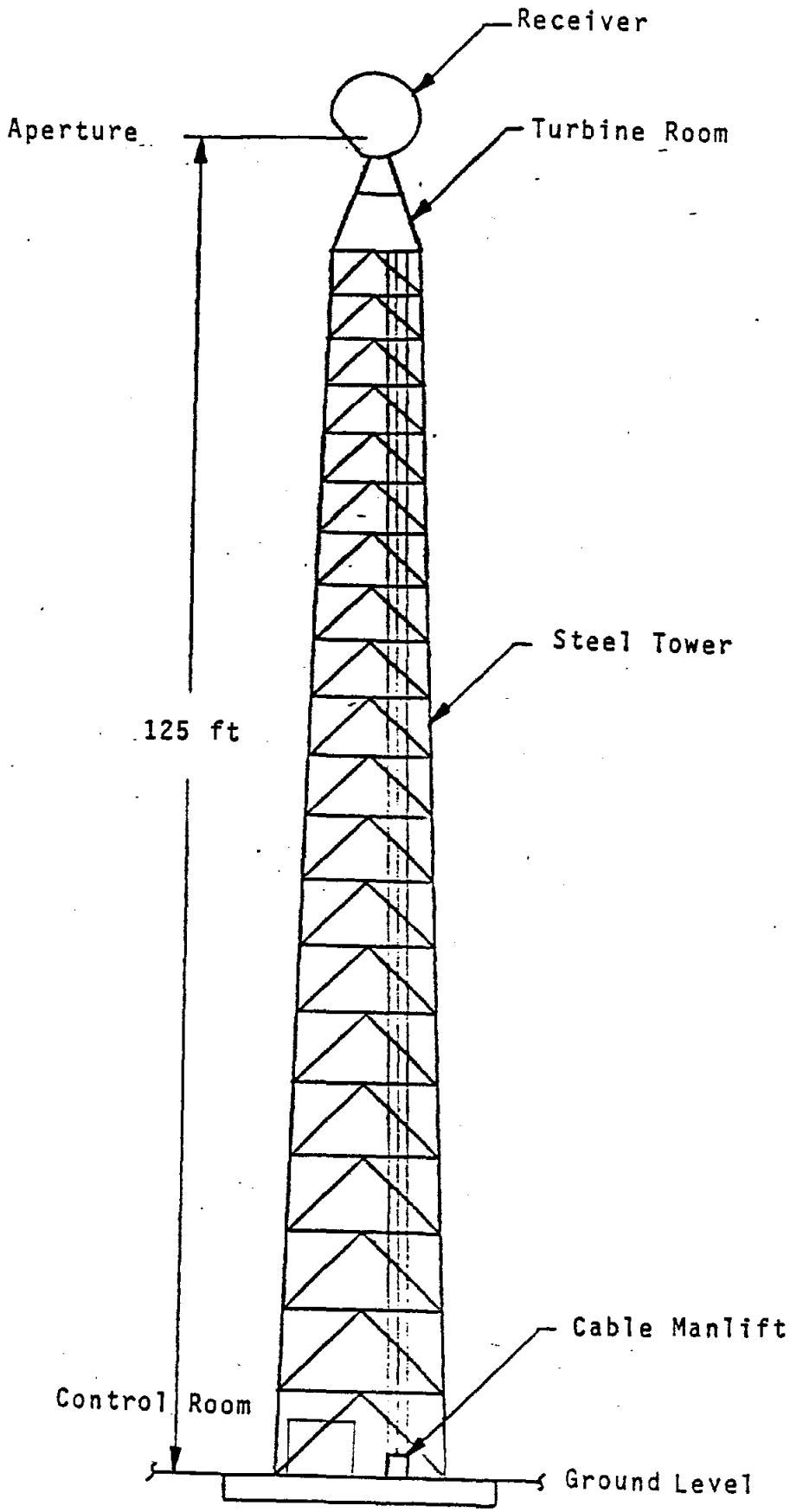

Figure 3-52. 2-MW_e Plant Tower Arrangement

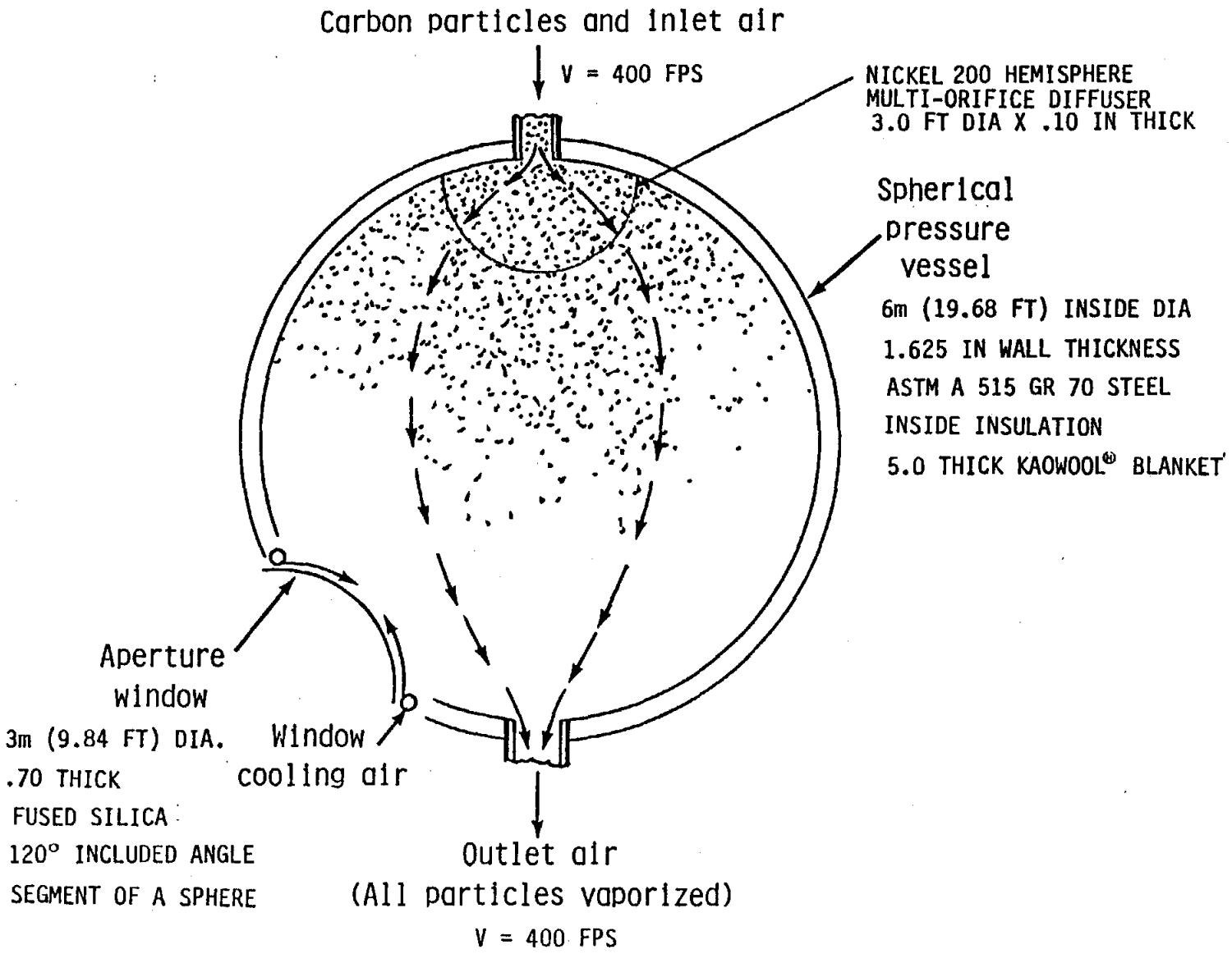

Figure 3-53. 2-MW_e Small Particle Receiver

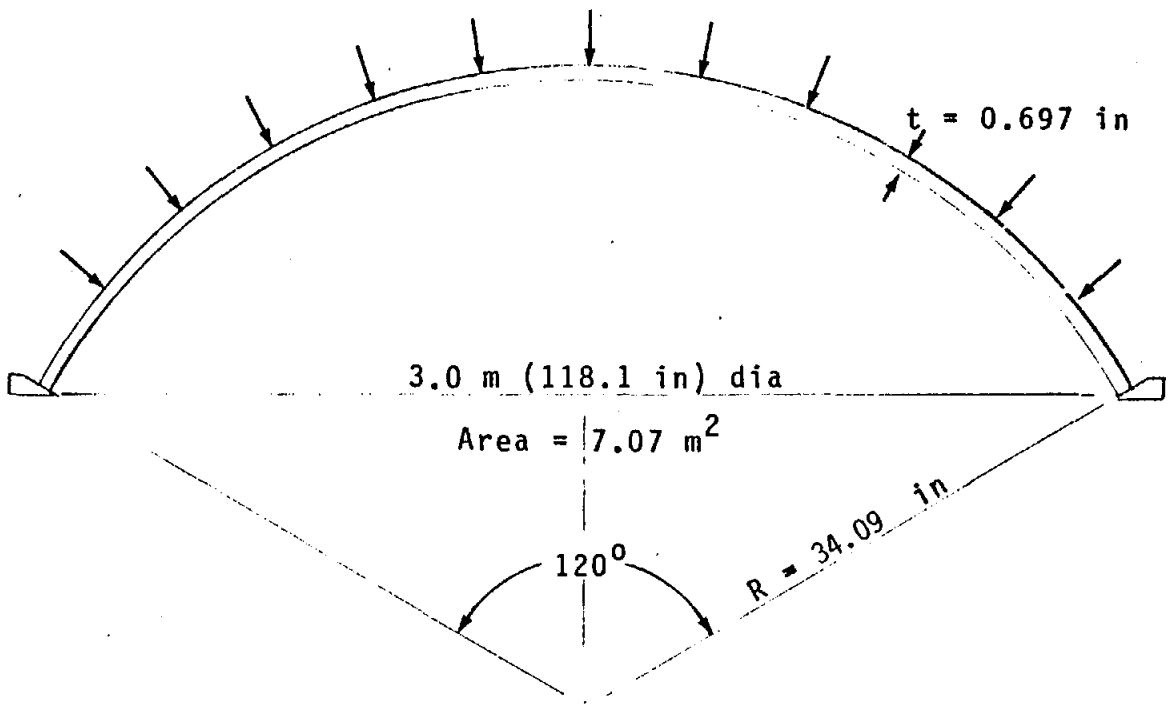

Figure 3-54. 3.0-m Diameter Fused Quartz Window Design

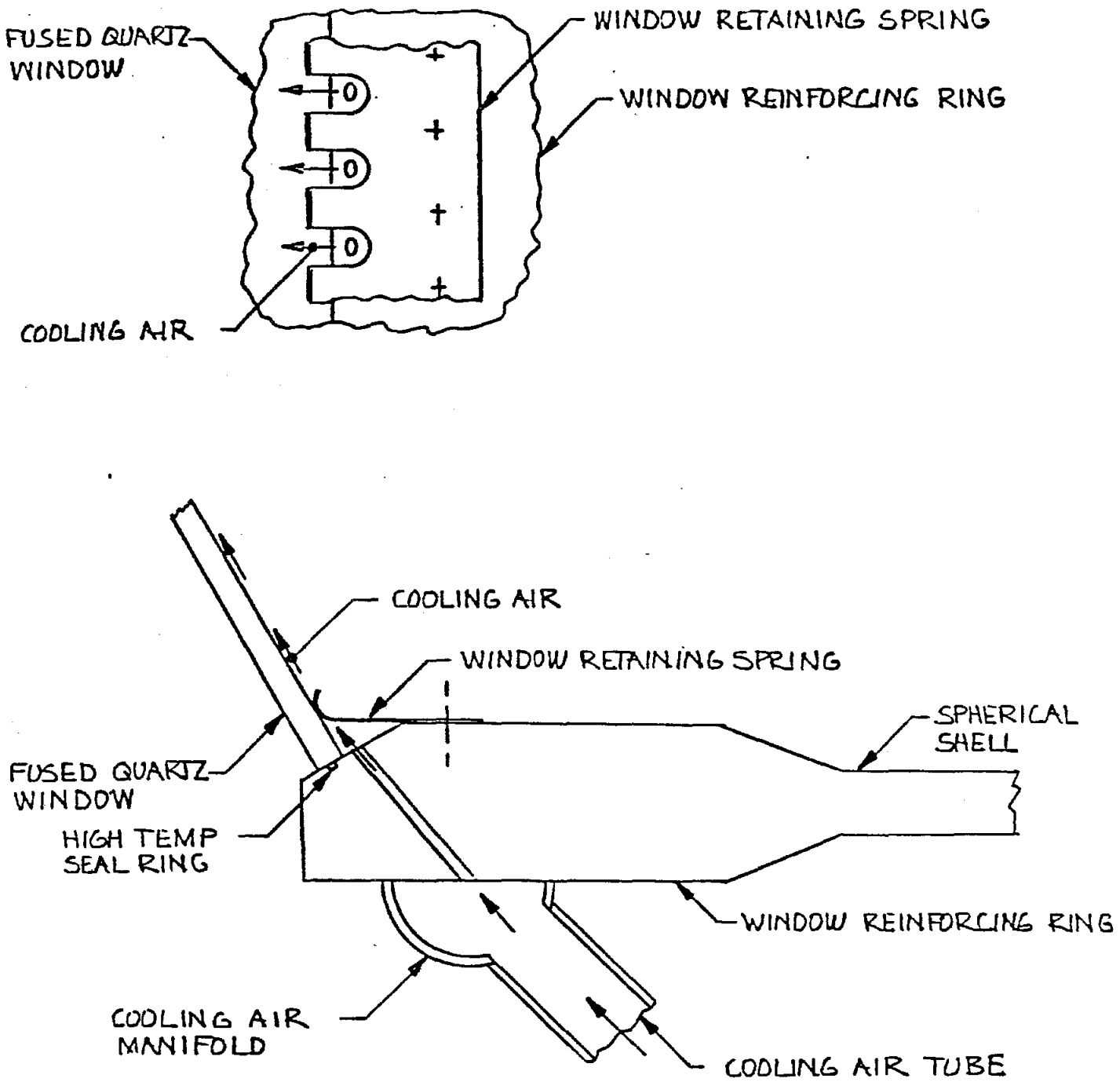

Figure 3-55. Window-to-Shell Interface Design

Table 3-30. 2-MW_e Receiver Design Summary

Receiver cavity inside diameter		5.75m (18.9 ft)	
Peak solar flux		2,000 kW/m^2	
Aperture shape		Circular	
Aperture inclination from vertical		40°	
Aperture diameter		3.0m (9.8 ft)	
Aperture area		7.07m^2 (76.1 ft^2)	
Window material		Fused quartz	
Window shape		120° spherical segment	
Window thickness		1.78cm (0.7 in)	
Window mass		367kg (810 lb)	
Pressure vessel inside diameter		6m (19.7 ft)	
Pressure vessel wall thickness		4.1cm (1.625 in)	
Pressure vessel material		ASTM A515 GR 70	
Interior insulation thickness		12.7cm (5 in)	
Insulation material		Kaowool®	
Riser/Downcomer:			
Outside diameter	Riser: 10.2cm (4 in)	Downcomer:	30.5cm (12 in)
Wall material	A53 Sch 40		A53 Sch 40
Liner material	--		Nickel
Insulation material	Fiberglass (ext)		Kaowool® (interior)
Insulation thickness	7.62cm (3 in)		7.62cm (3 in)
Pressure loss budget			
Heat exchangers		2.0%	
Riser/inlet piping		0.5%	
Downcomer/outlet piping		0.5%	
Valving and control		2.0%	
Total		5.0%	

Table 3-31. Receiver Concept Performance

Concept	25 MW_e Ceramic Tube MW	%	2 MW_e Small Particle MW	%
Reflection	2.62	4.4	0.462	6.6
Reradiation	4.11	6.9	0.322	4.6
Conduction & Convection	1.78	3.0		
Receiver	50.74	85.7	6.213	88.8
Solar Input	59.25	100.0	6.997	100.0
Pressure Loss	10%		5%	

3.5.4 Receiver Concept Cost Estimate

Receiver costs were estimated by first developing a list of materials based on the conceptual design presented in the previous section. Materials costs were estimated based on vendor contacts and BEC experience with similar components. Labor estimates and rates were based on previous BEC studies and building construction cost data. Specific data are presented in Appendix D. Table 3-32 presents a summary of the 25-MW_e receiver cost estimate. The receiver insulation and ceramic tubing are seen to be the most costly components. The cost associated with receiver insulation installation is also significant. The receiver structure and manifold costs are less significant.

Similar receiver cost summary data are presented in Table 3-33 for the 2-MW_e receiver. Details are also presented in Appendix D. The quartz window is the most expensive receiver component. The receiver structure cost is relatively more significant in small particle receiver design because the receiver cavity

Table 3-32. 25-MW_e Receiver Cost Estimate

Component		Cost
Steel work:	Material	$ 40,500
	Labor	10,463
Insulation:	Material	383,993
	Labor	325,917
Heat Exchangers	Material	512,400
	Labor	10,800
Manifolds:	Material	15,197
	Labor	21,986
TOTAL		$1,321,256

Table 3-33. 2-MW_e Receiver Cost Estimate

Component		Cost
Steel work:	Material	$42,080
	Labor	7,750
Insulation:	Material	20,834
	Labor	8,504
Window		120,000
Carbon particle generator		22,168
TOTAL		$221,336

is also a pressure vessel. Since this receiver does not require the use of a high-flux-capability cavity insulation, the insulation cost is less significant. The carbon particle generator costs were scaled from the estimates from Reference 9.

The tower and piping costs are presented in Table 3-4. The tower costs were based on the tower designs presented in reference 73 updated to 1983 unit costs. The large crane rental shown in Table 3-4 was based on recent BEC experience for the erection of large wind turbines.

Piping costs were based on vendor data and BEC experience. Costs for the nickel liner were based on discussions with Huntington Alloys.

Table 3-34. Piping and Tower Cost Estimates

		25 MW_e	2 MW_e
Tower:	Earthwork	$ 5,506	$ 2,185
	Concrete Base	200,552	12,185
	Steelwork	273,690	22,339
	Large Crane Rental	85,000	38,815
		$564,748	$75,524
Piping:	Steel Pipe	$ 13,832	$ 3,807
	Anchors, Hangers and Joints	8,545	2,495
	Nickel Liner	10,282	417
	Insulation	15,172	304
	Fabrication	34,515	4,320
		$ 82,346	$11,343

4.0 SYSTEM DESCRIPTION

The purpose of this section is to present a description of the entire small Brayton central receiver system. The results of the Brayton Cycle Configurations Study and the High-Temperature Receiver Study will be combined to produce an estimate of the cost and performance of the entire solar thermal system.

4.1 SYSTEM DESIGN DESCRIPTION

4.1.1 25-MW_e Plant

Table 4-1 presents a listing of the system design data for the 25-MW_e small Brayton solar plant. Figure 4-1 presents a schematic of the plant/tower arrangement. The plant is sited on $3.7 \times 10^5 m^2$ of land with 1591 second generation glass/metal heliostats canted at the slant range in a north, radial stagger heliostat layout pattern. A steel truss tower supports the receiver and turbogenerator. The receiver aperture is located 97.8m above plane of the heliostat pivots. The turbogenerator is close-coupled to the receiver being located just below the receiver. Both receiver and turbine room are protected from weather and stray solar flux.

The control room is located at the tower base on the tower concrete foundation. The room is depicted in Figure 4-2. The control room building structure is concrete masonry block with a steel open web joist roof system. The room includes raised computer flooring, restroom fixtures, heating, ventilating, air conditioning, electrical and halon fire suppression system. The computer control system includes control consol, displays, main computer, printer plus the sensors and instrumentation required to operate the system. The turbogenerator package will have its own control system which will allow manual operation of the turbine if desired.

Table 4-1. 25-MW_e System Definition

System:	
Power range, MW_e	25
Working fluid	air
Cycle configuration	open cycle, regenerated and intercooled
Collector Subsystem:	
Heliostat	MDC 2nd. Gen.
Field configuration	north
Field area, m^2	374,000
Mirror area, m^2	90,400
Number of heliostats	1,591
Receiver Subsystem:	
Receiver type	Cavity
Number of apertures	1
Aperture shape	Elliptical
Aperture width, m	7.55
Aperture height, m	5.66
Aperture area, m^2	33.56
Aperture inclination fm vert	40°
Cavity diameter, m	21.2
Cavity height, m	7.17
Total tube number	100
Tube outside diameter, cm	7.62
Tube length, m	14.02
Tube pitch	3.0 tube dia.
Inlet air temp, ^oC	531
Outlet air temp, ^oC	1116
Inlet pressure, MPa	0.98
Pressure loss, % of inlet	10
Tower height, m	97.8
Tower type	steel
Estimated receiver mass, kg	127,600
Electrical Power Generation Subsystem:	
Pressure ratio	10.0
Turbine inlet temp, ^oC	1116
Mass flow rate, kg/s	74.84
Cycle efficiency	49.5%
Turbomachinery location	Tower top

Table 4-1. 25-MW_e System Definition (Continued)

Turbine mass, kg	100,000
Recuperator diameter, m	3.5
Recuperator length, m	5.5
Recuperator pressure loss, %	4 (Hot side) 1 (Cold side)
Recuperator effectiveness, %	90
Recuperator mass, kg	53,000
Intercooler diameter, m	4.6
Intercooler pressure loss, %	2
Intercooler effectiveness, %	90
Intercooler mass, kg	46,000
Piping Subsystem:	
Riser flow diameter, m	0.46
Riser length, m	12.2
Riser insulation thickness, cm	7.62 (exterior)
Riser pressure loss, %	0.5
Riser heat loss (steady state), kW_{th}	34
Downcomer flow diameter, m	0.56
Downcomer length, m	12.2
Downcomer insulation thickness, cm	7.62 (interior)
Downcomer pressure loss, %	0.5
Downcomer heat loss (steady state) kW_{th}	174

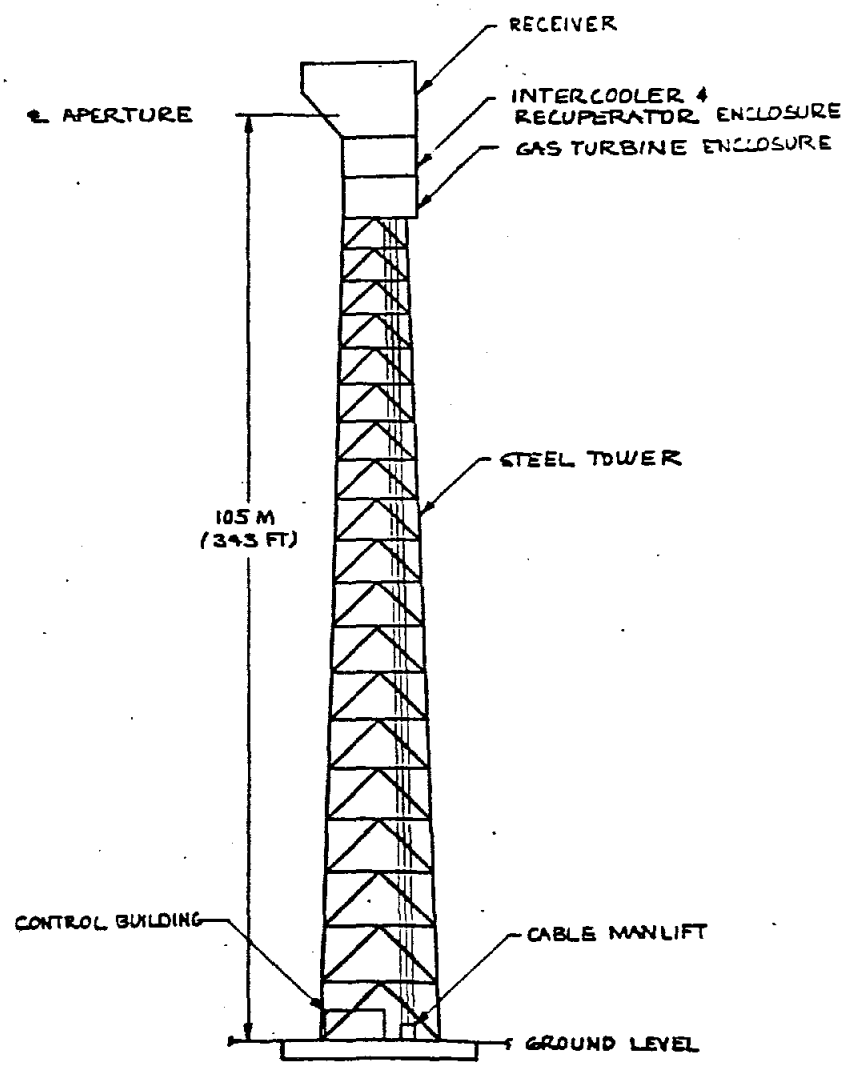

Figure 4-1. 25-MW_e Plant Tower Arrangement

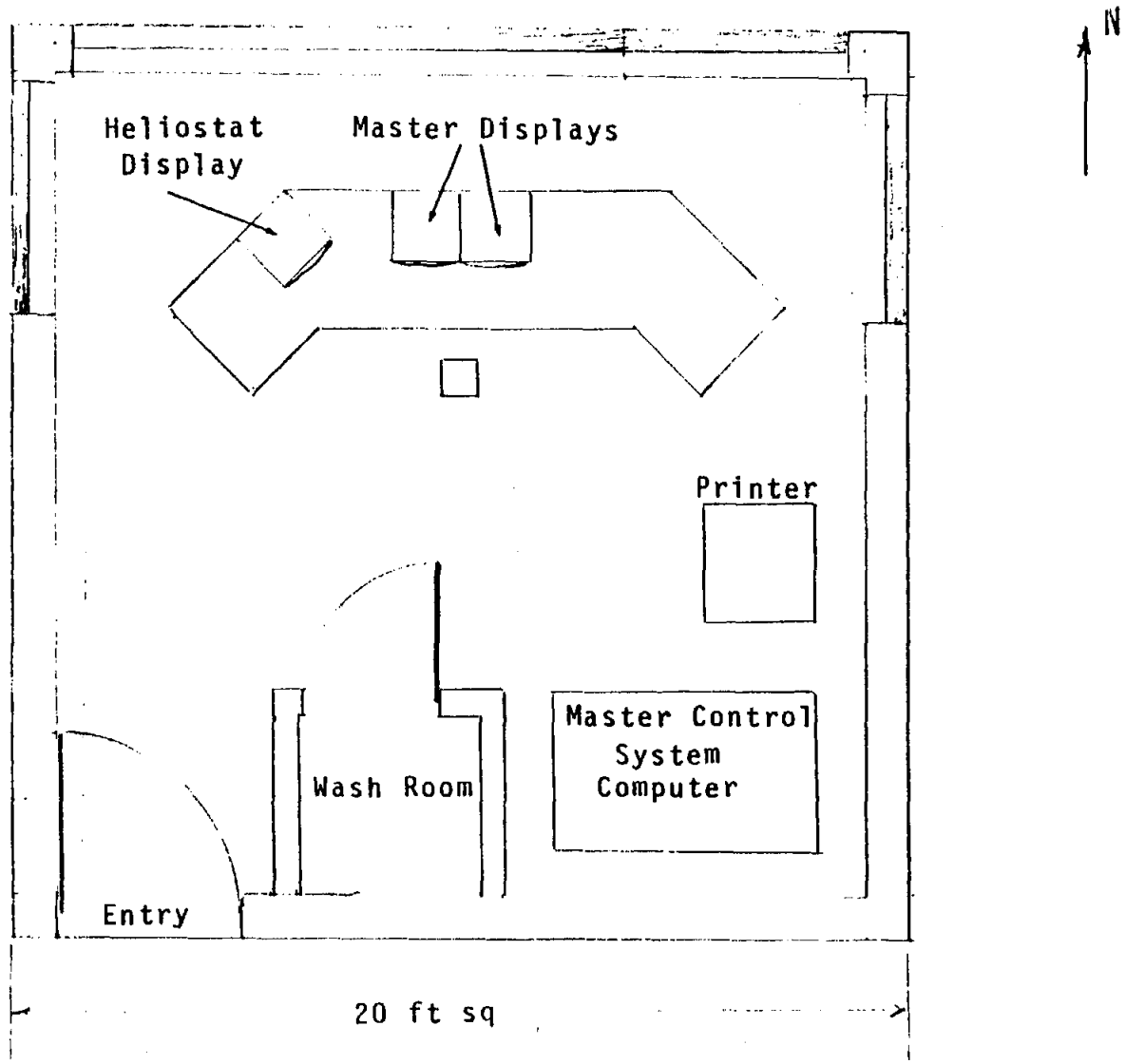

Figure 4-2. Control Room Design

4.1.2 2-MW_e Plant

Table 4-2 presents a design data summary for the 2-MW_e small Brayton solar plant. One hundred, seventy-six heliostats are located on $46x10^3m^2$ of land. A steel truss tower supports the receiver and turbogenerator. The receiver aperture is located 35m above the heliostat pivots. A control room is located on the tower base foundation.

4.2 SYSTEM PERFORMANCE

Figures 4-3 and 4-4 present the design point and annual average 25-MW_e plant performance calculated with the DELSOL 2 program (13). Similar data are presented in Figures 4-5 and 4-6 for the 2-MW_e plant.

4.3 SYSTEM COST ESTIMATES

4.3.1 Direct Capital Cost Estimates

Direct capital cost estimates by subsystem for both plant sizes are presented in Table 4-3. Land and heliostat costs are based on the data presented in Section 2.2. The turbomachinery cost estimates were derived from data in Section 2.6.2. The receiver subsystem cost details were presented in Section 3.5.4.

4.3.2 Busbar Energy Costs

Industrial Plant Application

The busbar energy costs for both plants were estimated based on the direct capital costs, system performance and the industrial plant economic factors presented in the System Requirements Definition, Table 2-1. The levelized busbar energy costs were calculated using the DELSOL2 (13) computer model methods. The results from these calculations are presented in Table 4-4. As can be seen, the 25-MW_e plant has the more attractive economics. These combine with simplicity of design, ease of operation and low maintenance.

Table 4-2. 2-MW_e System Definition

System:	
Power range, MW_e	2
Working fluid	air
Cycle configuration	open simple cycle
Collector Subsystem:	
Heliostat	MDC 2nd gen.
Field configuration	north
Field area, m^2	46,400
Mirror area, m^2	10,000
Number of heliostats	176
Receiver Subsystem:	
Receiver type	Cavity
Number of apertures	1
Aperture shape	Circular
Aperture diameter	3.0
Aperture area, m^2	7.07
Aperture inclination fm vert	40°
Cavity diameter, m	6
Inlet air temp, ^oC	405
Outlet air temp, ^oC	1116
Inlet pressure, MPa	1.52
Pressure loss, % of inlet	5
Tower height, m	35
Tower type	steel
Estimated receiver mass, kg	46,229
Electrical Power Generation Subsystem:	
Pressure ratio	15
Turbine inlet temp, ^oC	1116
Mass flowrate, kg/s	7.66
Cycle efficiency	33.6
Turbomachinery location	Tower top
Turbine mass, kg	18,150
Piping Subsystem:	
Riser outside diameter, m	0.102
Riser length,	9.1
Riser insulation thickness, cm	7.62 (exterior)
Riser pressure loss, %	0.5
Downcomer outside diameter, m	0.203
Downcomer length, m	6.1
Downcomer insulation thickness, cm	7.62 (interior)
Downcomer pressure loss, %	0.5

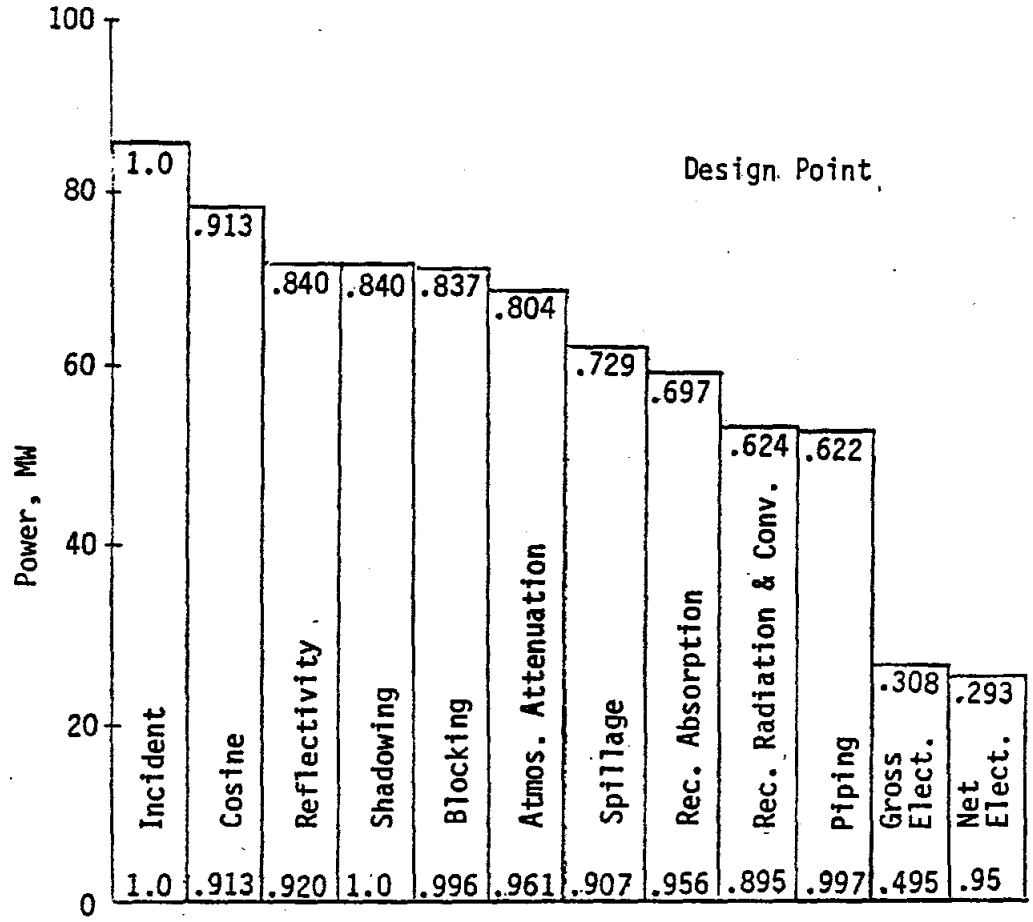

Figure 4-3. Design Point 25-MW_e Plant System Performance

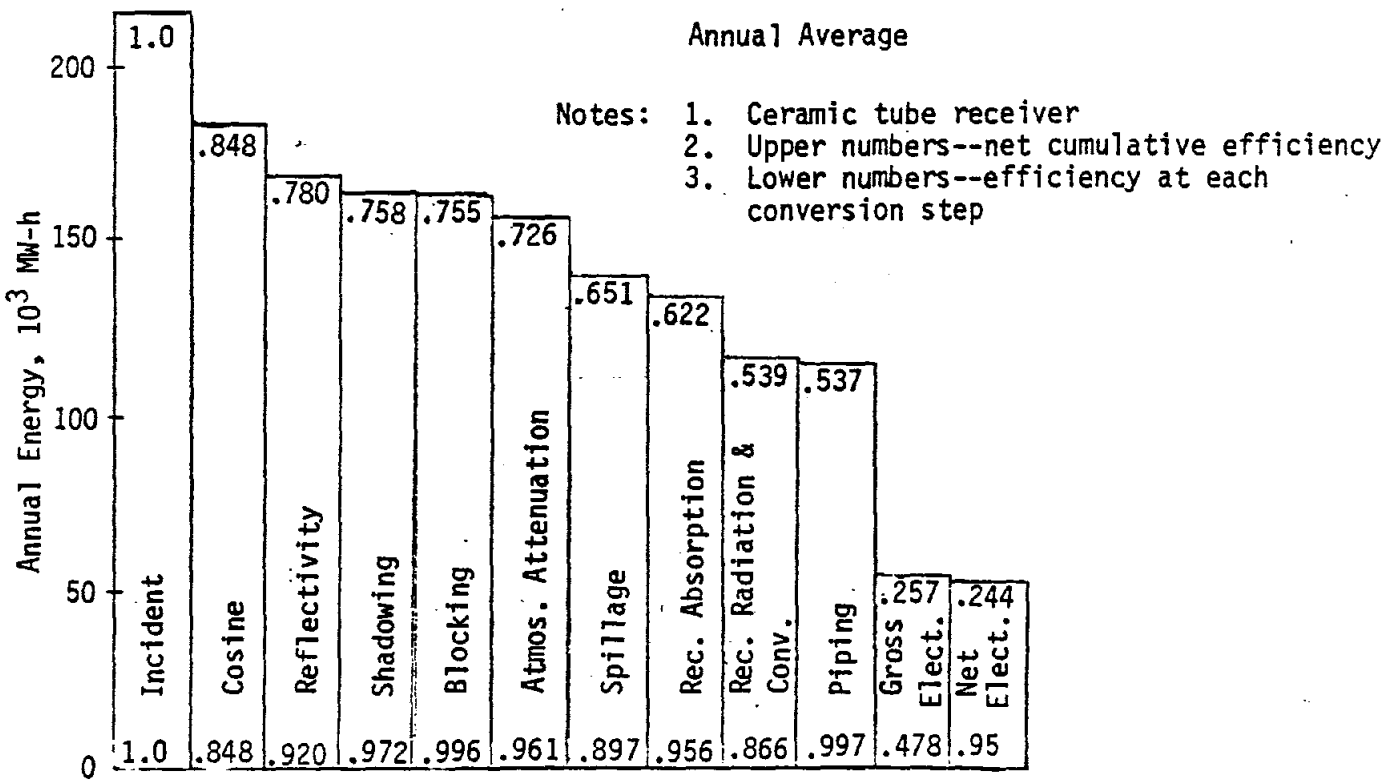

Figure 4-4. Annual Average 25-MW_e Plant System Performance

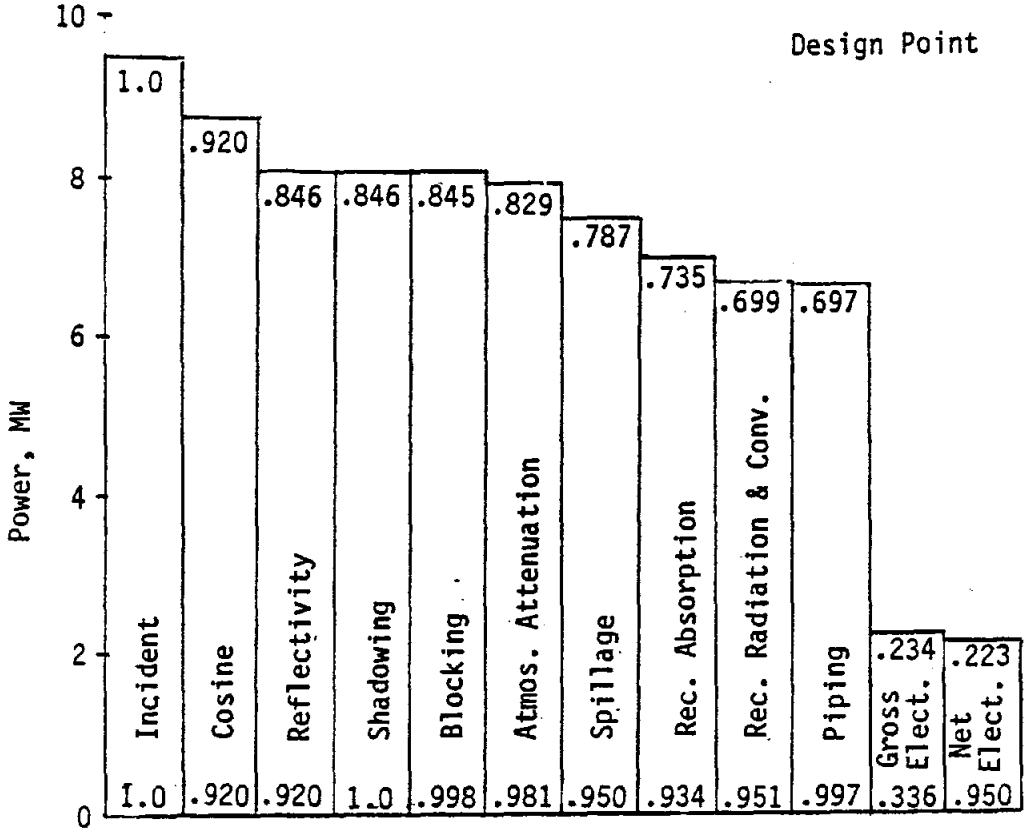

Figure 4-5. Design Point 2-MW_e Plant System Performance

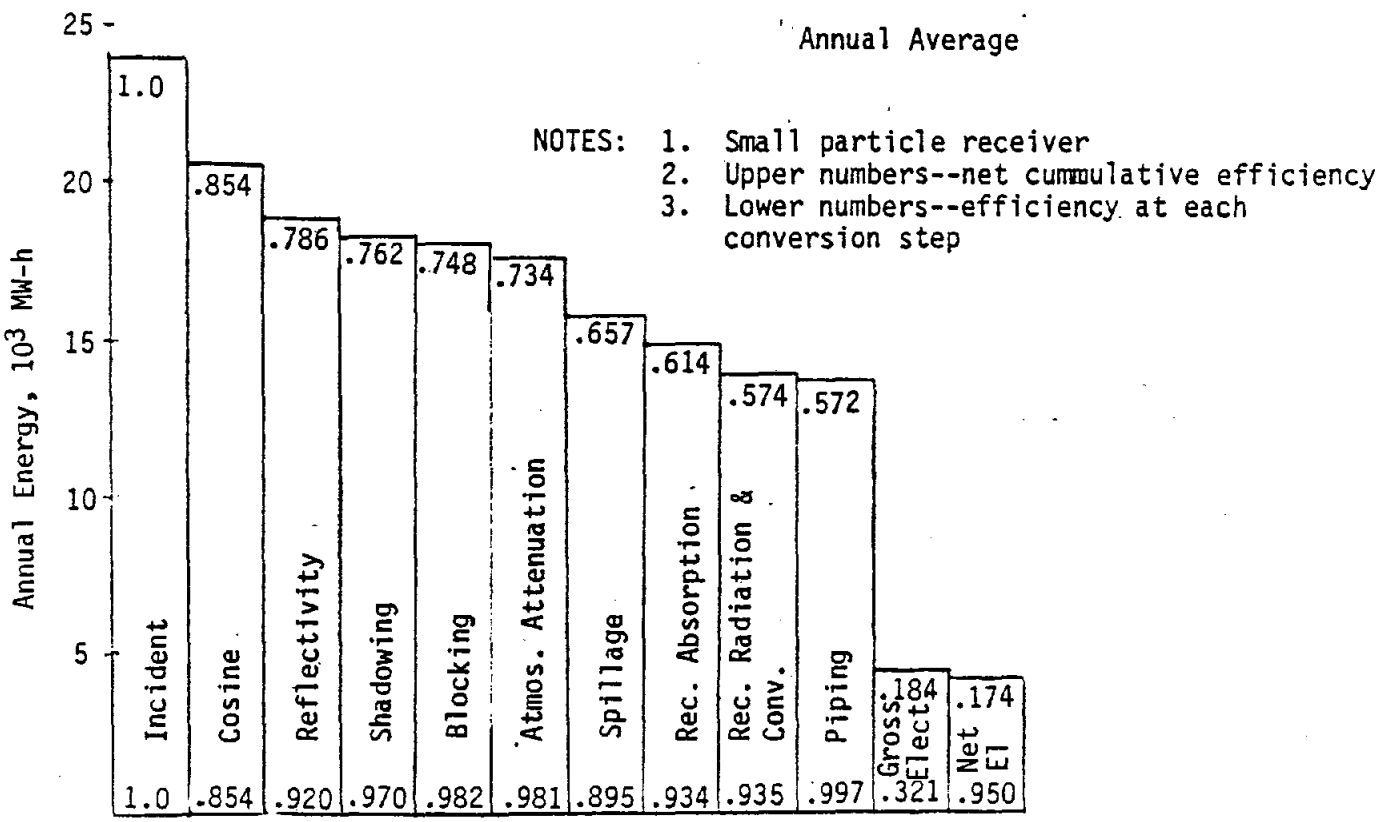

Figure 4-6. Annual Average 2-MW_e Plant System Performance

Table 4-3. System Direct Capital Cost Estimates (1983$)

Subsystem		Cost ($10^3$$) 25 MW_e	2 MW_e
Collector Field		10,235	1,132
Land		748	93
Piping		82	11
Receiver		1,321	221
Tower		565	76
Electric Power Generation:	Turbine	5,930	1,036
	Recuperator	1,000	--
	Intercooler	1,180	--
Fixed		540	285
TOTAL		21,601	2,854

Electrical Utility Application

In order to assess the effect of economic assumptions on the busbar energy costs, the final system designs were re-evaluated based on the electric utility economic factors presented in Table 4-5. These economic factors were taken from the second generation heliostat comparison (12) except evaluated in 1983$. The results are also presented in Table 4-4. The levelized busbar costs for an electrical utility application are approximately 20 mils/kWh less than the industrial application.

Table 4-4. Busbar Energy Costs (1983$)

	mils/kWh	
	25-MW_e Plant	2-MW_e Plant
Industrial Plant Application	125	209
Electrical Utility Application	103	171

Table 4-5. Alternative Economic Factors--
Electric Utility Application (12)

Cost basis	1983 dollars
Contingency	0%
Spare Parts	0%
Indirect costs	16%
Capital escalation	8%
General inflation	8%
Interest during construction	10%
Years to construction start	0
Plant lifetime	30 years
Fixed charge rate	15.9%
Discount rate	9.96%
Heliostat first year O&M	1.7%
Balance of plant first year O&M	1.5%

5.0 DEVELOPMENT PLANS

The purpose of this section is to present the critical technical problem areas for the preferred system configuration. A development plan to reduce the technical risk associated with a small Brayton power plant is also presented.

5.1 TECHNOLOGY ASSESSMENT

Off-the-shelf hardware for every system component is not available for either of the preferred small Brayton central receiver system configurations. The major technology voids exist in three areas: the turbomachinery, the piping, and the receiver. The remaining susbystems of the plant can be considered near-term technology. This subsection will discuss current technology status and trends in the three areas identified above. This will form a basis for definition of the critical technology voids as presented in Section 5.2.

5.1.1 Turbomachinery Technology Assessment

In the evaluations of this study, selection of a specific, currently available turbogenerator was avoided. Instead, performance based on mid-1980's aircraft-derivative technology projected to gas turbine electrical generating systems operating in the mid-to-late 1990's was assumed. This assumes about 10 years of development and reasonable production rates.

For the 2-MW_e plant, an open simple cycle gas turbine operating at a turbine inlet of 1116°C (2040°F) and overall pressure ratio of 15 was selected. Improved component efficiency indicated a cycle efficiency of 33% was attainable. The turbomachinery survey described in Section 2.5 determined that pressure ratios of 10 at the 2-MW_e range were available. Current turbine inlet temperatures are below the 1116°C (2040°F) level assumed, however. Improved component design will be required to reach the 33% open simple cycle projected efficiency. Overall, the 2-MW_e turbomachinery performance levels projected in this study are reasonable considering the time frame of application in the mid to late 1990's.

For the 25-MW_e plant, an open cycle regenerated and intercooled system was selected as the preferred cycle configuration. At the present, no open cycle regenerated and intercooled turbines are offered commercially. However, one notable turbine under development and potentially available in 3-4 years is the Thomassen TF10. Figure 5-1 illustrates the TF-10 gas turbine system. Table 5-1 presents the TF-10 projected performance parameters. The TF-10 will be a regenerated and intercooled, dual shaft open cycle system. Although rated at 7.5 MWe, the TF-10 performance parameters will be similar to those assumed for the 25-MWe plant. Considering again the 1990's time frame of application, the turbomachinery performance levels projected in this study are appropriate.

External firing of aircraft-derivative gas turbines remains as a development issue. As identified in the turbomachinery survey, aircraft-derivative turbines tend to the use of annular combustors located inside the turbine casing. Modifications in hardware and controls will be required to adapt these turbines to the external firing required for a solar Brayton application. Design concepts for such modifications have been started (1) but would require additional development and testing to prove the designs.

The heat exchangers (recuperator and intercooler) sized for the 25-MW_e system were based on current technology shell-and-tube designs. Recent manufacturing technology advances may produce potential reductions in size and weight while producing higher performance. The case in point is the new recuperator design available from Solar Turbines International. Figure 5-2 illustrates the relative size comparison for the new Solar recuperator against a shell-and-tube or a plate-fin recuperator. The new design uses thin sheets of high quality stainless steel folded into a corrugated pattern. Pairs of cells are joined to form air cells which are welded together. The Solar recuperator is 15-20% of the size and 1/6th the weight of conventional plate-fin and shell-and-tube recuperators. These features are combined with superior performance (heat exchange effectiveness up to 94%), lower costs and rapid equipment startup. The recuperator was also designed for long life, low

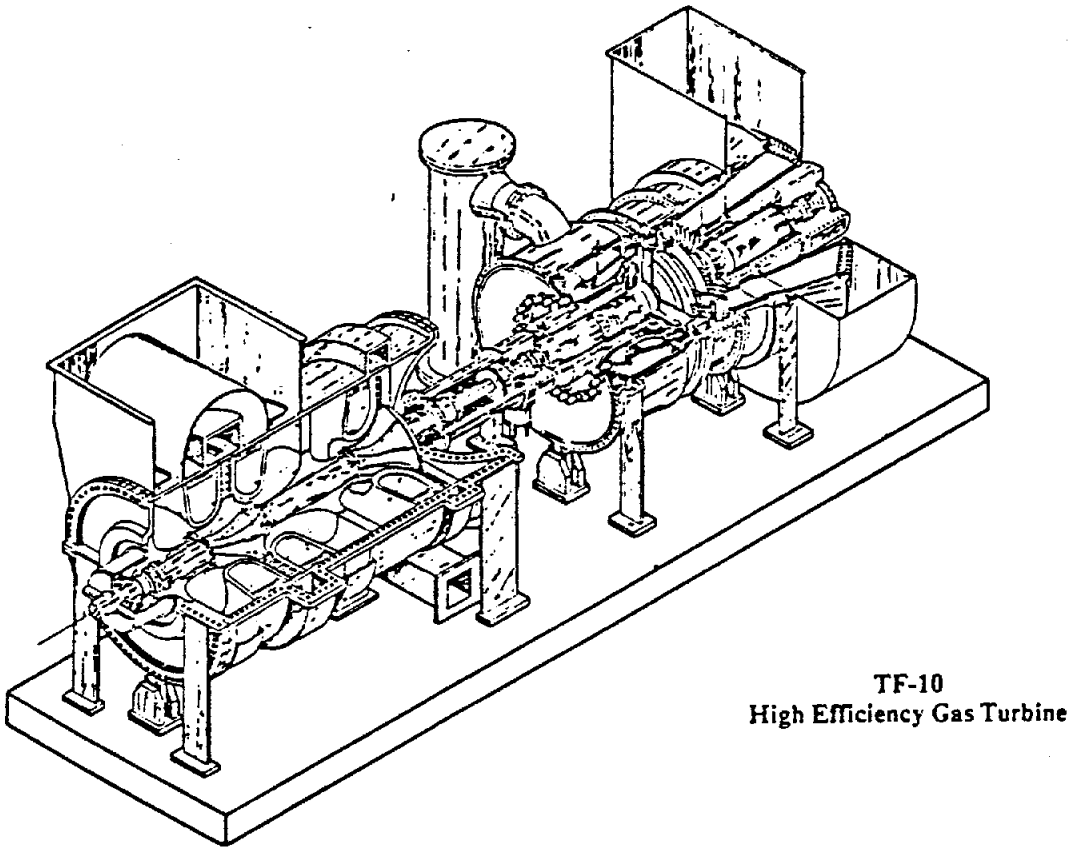

Figure 5-1. Thomassen TF-10 Gas Turbine

Table 5-1. Thomassen TF-10 Performance Data (17)
Mature Design

Shaft Horsepower	10500
Power Turbine Speed	9200
Gas Generator R.P.M.	10940
Thermal Efficiency	44%
BTU/SHP/Hr	5875
Rotor Inlet Temp. ^{o}F (R.I.T.)	2042
Exhaust Temp. ^{o}F (Reg. Inlet)	1100
Stack Temp. ^{o}F	510
Compressor Pressure Ratio	9.5
Average Compressor Efficiency	.87
Regenerator Eff. (Equal Flows)	.85
Combustor Efficiency	.995
High Pressure Turbine Efficiency	.88
Low Pressure Turbine Efficiency	.91

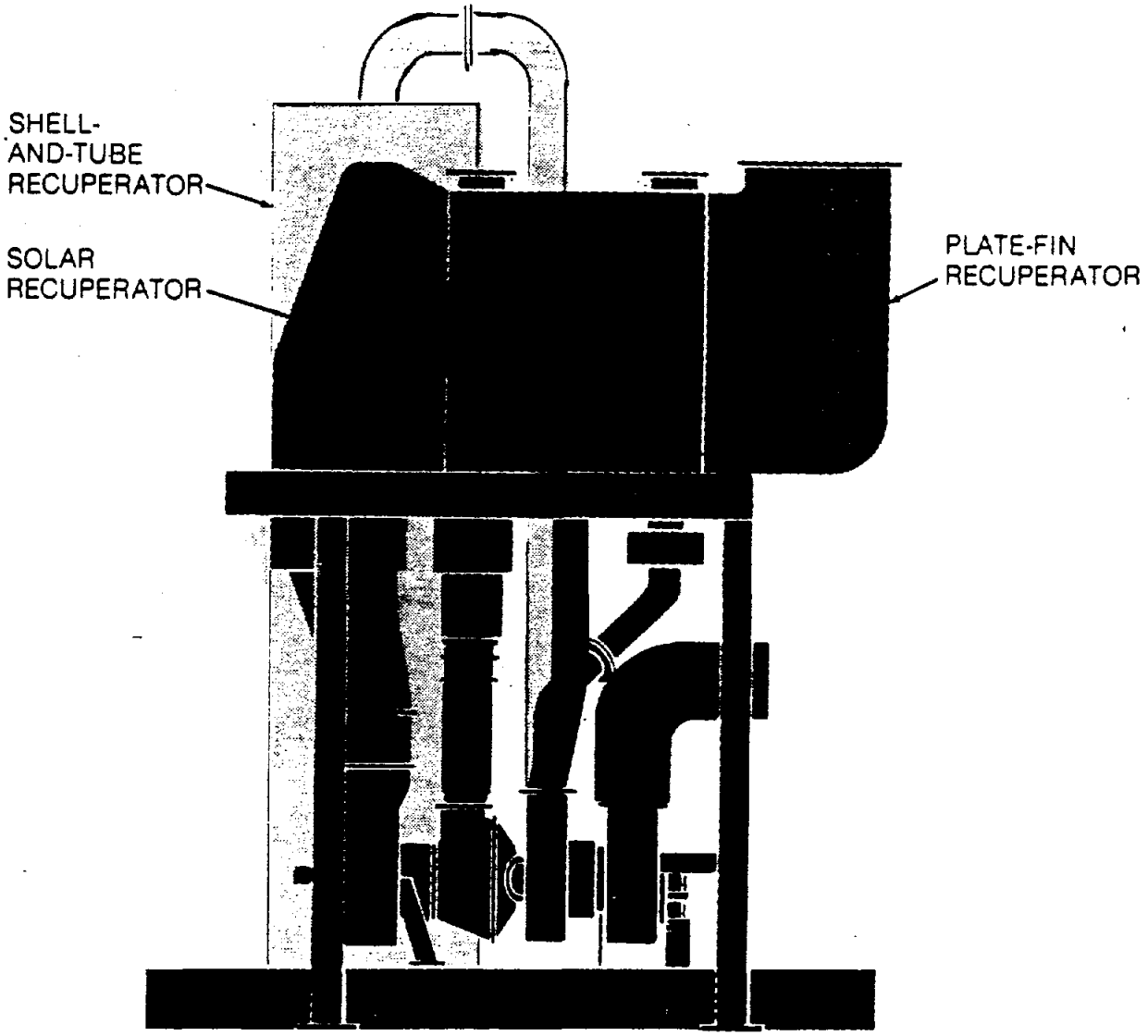

Recuperator comparisons for a Centaur turbine.

Figure 5-2. Comparison Between Recuperator Types

maintenance and ease of inspection. All of these features would make such a recuperator design attractive for a solar Brayton system and indicate future additional cost and performance benefits above those levels assumed in this study.

5.1.2 Piping Technology Assessment

An area identified as a concern in the turbomachinery survey is the ducting of high temperature air into the turbine. Also, previous studies of transporting high temperature air (11) have shown piping to be a potentially expensive item. The interior insulated piping approach described in 3.5.2 offers a solution.

The use of a nickel liner provides a means of holding the interior insulation in place while providing a smooth flow channel for the hot air. The use of cast insulation products with the interior, hot-air-side surface sprayed with a densifying ceramic layer may produce an alternative cost-effective means of insulating the pressure containing outer metal piping and turbine casing walls. The sprayed ceramic liner would produce a smooth, rigid surface to contain the air flow without allowing spalling of the cast insulation and entrainment of insulation materials in the gas flow. Although attractive in concept, this design approach has not been demonstrated in practice. Limited research and development has been performed on producing the required ceramic sprayed liners.

5.1.3 Receiver Technology Assessment

Since high-temperature receivers of the designs suggested in this study have not been demonstrated in practice, the receiver is the system design element with the greatest technical risk. This is true of all solar central receivers, but is especially true for the high-temperature (1093°C [2000°F]) receivers.

25-MW_e Ceramic Tube Receiver

The heat exchanger elements present the most severe technical challenge to the successful development of the ceramic tube receiver concept. Ceramic heat exchanger tubes of the size and quantity envisioned in this study are expected to be available in the 1990's time frame based on the expected expansion of structural ceramics into the high temperature recuperator market. Production rates of 100,000 units per year are potentially available (74), significantly above the 1000 or so units/ year required to support a solar Brayton receiver production of 4 to 5 plants per year. Design and testing experience from the larger recuperator market should be directly applicable to the solar Brayton receiver development. Many of the same development issues of concern to the solar Brayton receiver would be common with the high-temperature recuperator development: tube fabrication, joining and sealing. However, some issues or technical concerns may be unique to the solar application: high flux solar irradiation, rapid thermal cycling, and high pressure containment.

2-MW_e Small Particle Receiver Concept

The most serious technical risk area for the small particle receiver concept is the fused quartz window. Windows of the required size and shape have not been manufactured before. Smaller segments could be fabricated and fused to form an integral window with current technology. However, even at an assumed rate of 4 to 5 plants per year, each window would be fabricated as a custom item. If such windows would also be applicable to other solar applications, e.g., solar fuels and chemicals, production rates could be increased. There does not appear to be any non-solar application for such windows which would help to defray the development costs.

The carbon particle injector and its interaction with the receiver control system is a lesser technical concern. At atmospheric pressures, a prototype of such a carbon particle injector has already been demonstrated (37).

5.2 CRITICAL TECHNOLOGY ISSUES

The purpose of this subsection is to delineate the critical technology issues surrounding the small Brayton cycle solar thermal systems studied herein. Effort was concentrated on areas which are critical to the technical success of the concept. Also, emphasis was placed on the technical concerns that are unique to the solar application. For example, the technical developments necessary to produce the gas turbine component efficiencies assumed in this study were not considered. It was assumed that the gas turbine industry would continue to develop more efficient machines.

The four areas that have been identified as crucial to the success of the small Brayton central receiver concepts of this study are:

(1) High-temperature piping
(2) External firing
(3) Ceramic tube heat exchanger elements
(4) Fused quartz window assembly.

Each of these issues will be discussed briefly. A plan to reduce the technical risk in each area will be presented in the following section.

High-Temperature Piping

The 1093+°C (2000+°F) temperatures expected in this concept are beyond the structural load-bearing capabilities for even superalloy metals. An interior insulated piping system is thus required. This hot air ducting is necessary from the receiver exit manifolds through the turbine casing and ending at the turbine airfoil inlets. The piping must allow for differential thermal expansion and provide a low pressure-loss duct for the solar-heated air. The interior pipe surface must be smooth and not abrade, contaminating the air flow with particles that could damage the turbine airfoils.

External Firing

Reliable control systems and trim combustors for solar-heated, aircraft-derivative turbines have not been demonstrated in practice. Transitions between fossil fuel startup and shutdown and solar operations have been analyzed and planned for (1) but not tested experimentally. Control responses to emergency conditions, such as loss of load event, also require demonstration.

Ceramic Tube Heat Exchanger Elements

Ceramic tube elements must be fabricated, joined and sealed reliably. The assemblies must resist repeated thermal shock and cycling from ambient temperatures to peak temperatures over 1093°C (2000°F).

Fused Quartz Window Assembly

The window assembly must be fabricated to provide a leak tight pressure containing system. Allowance for thermal movement must be considered. The window material must not degrade with repeated thermal shocks and cycling.

5.3 PLAN TO REDUCE TECHNICAL RISK

This section will outline the activities needed to reduce the technical risk for the small Brayton cycle central receiver concept. Both system level and critical technology level plans will be discussed.

5.3.1 System Level Studies

At the outset, the Small Central Receiver Brayton Cycle Study was intended as a scoping study. A system level conceptual design was developed; cost and performance estimates were generated. In the current study, design point conditions were emphasized with some consideration of off-design conditions. Although appropriate for a scoping study, the resulting system design was not cost optimized.

A preliminary system design phase is appropriate next. The preliminary design process is illustrated in Figure 5-3. A systems level performance evaluation would provide a more accurate definition of the design critical performance data. Design point calculations are appropriate for an assessment of overall plant performance. However, system elements such as piping and heat exchangers are often sized at critical off-design or emergency conditions. A system level analysis would allow definition of those design critical conditions.

To support the system level preliminary design studies, subsystem performance analyses are also required. Thermal and stress analyses of the receiver would allow a better estimation of receiver efficiency. The results would also allow a more accurate sizing of system elements providing basis for more accurate receiver costs. Cost optimization of the recuperator and intercooler potentially offer reduction in size and weight plus a more accurate definition of costs. Off-design and dynamic analyses of the electrical power generation subsystem will allow definition of control strategies and critical operating conditions.

5.3.2 Critical Technology Areas

Each of the critical technology areas will require assessments in four common areas:

- Materials data
- Consultation with manufacturers
- Design analysis
- Heat transfer analysis

Each of the critical technology areas, piping, heat exchangers and windows, requires additional materials data definition. This may range from assembly of detailed materials data from vendors and manufacturers to direct measurement of critical properties from laboratory specimens. For the piping studies, required materials data would include thermal conductivity behavior with temperature, heat capacity, friction factor, resistance to spalling, and

Preliminary Design Process

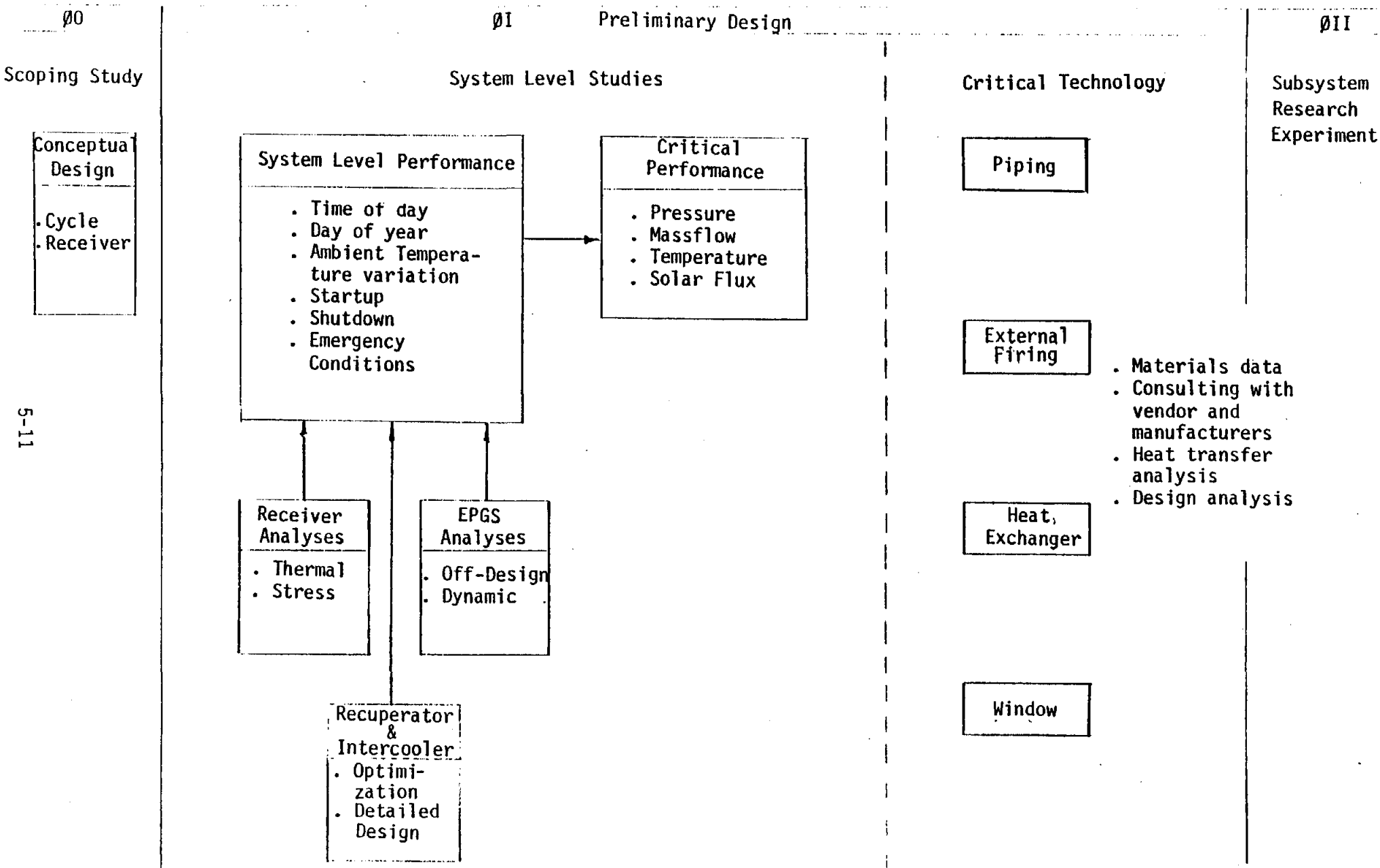

Figure 5-3. Preliminary Design Process

effect of thermal cycling. Of importance to the heat exchanger design would be thermal conductivity, repeatibility of strength data, fabrication tolerances, etc. Window design would require transmittance data, effect of thermal cycling, and thermal shock, and devitrification effects with temperature.

Consultation with materials vendors and manufacturers is expected to be an important requirement. Since the high temperature ceramics industry is in a rapid stage of growth, the ceramics manufacturers are expected to be an important source of not only materials data but new ceramic design methods too.

The results from the receiver thermal and stress analysis will allow a detailed heat transfer analysis in each of the critical technology areas. Temperature gradients through the piping insulation, heat exchanger tubing and quartz window will be important in substantiating the receiver concept technical feasibility. The detailed thermal data will also support materials thermal evaluation tests and help specify the testing conditions for a subsystem research experiment if required.

All of these data will allow a more accurate sizing of system components in the design analysis area. Refined inputs from the receiver thermal and stress analysis, manufacturers fabrication constraints, and materials property data will allow specification of a receiver design that can be tested in the subsystem research experiment phase.

The subsystem research experiment phase is a precusor to a system level experiment as shown in Figure 5-4. The subsystem research experiments could include fabrication, assembly, and testing of a critical sublement under simulated or actual conditions. For example, a section of heat exchanger tube could be fabricated from two or more attractive materials and tested in a solar simulator. Joining and sealing techniques could be explored on an assembly level. These tests could lead to the fabrication and testing of a complete heat exchanger panel at a solar test facility such as CRTF or ACTF.

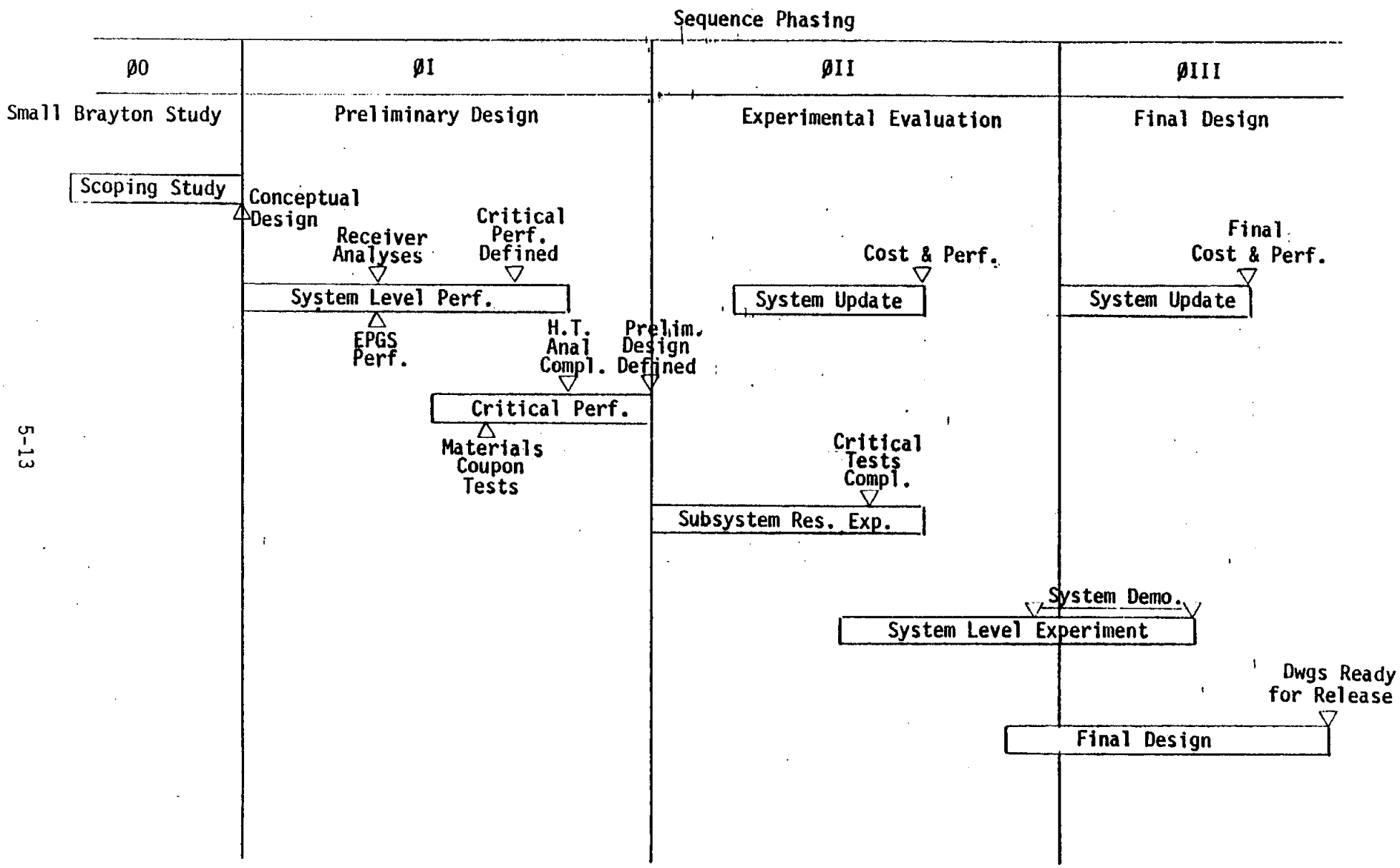

Figure 5-4. Program Development Plan

A system level test would be attempted after completion and evaluation of each of the subsystem tests. The system level test would include all the major system elements, receiver, turbine, piping, control system, in a scaled-down version. Such a test would allow a representation of an entire system with a modest investment in capital expenditures.

In parallel with these subsystem and system level tests, updates to the preliminary design would be made based on the experimental results. This process would allow the adoption of a final design which could then be offered to the commercial sector. The parallel updating tasks would allow a reassessment of the system level economic predictions as the system final design evolves.

5.3.3 Specific Plans for Preliminary Design Phase

2-MWe Plant Size

For the 2-MWe small particle receiver/open simple cycle configuration, a preliminary design phase of development would begin with system level design studies. These studies would utilize the GSA computer model described in Section 2.4.1 to consider the effects of time of day and ambient temperature. Dynamic analyses will consider startup, shutdown, and emergency conditions. Transitions between fossil fuel firing and solar operation will be considered to develop appropriate control methodologies. Consultation with turbine manufacturers will also be solicited in this regard.

Detailed thermal analysis of the receiver cavity will be performed to refine an estimate of receiver thermal performance. For the small particle receiver, areas of concern are the window and carbon particle solar absorption interaction. Temperature distributions within the cavity under varying massflow, solar insolation, and carbon particle loading will be investigated.

The results from these analyses will allow a basis for assessment in each critical technology area. Materials data will be required to support the piping and window technology areas. Coupon tests of insulation materials will determine if abrading of the interior piping insulation is a concern. The

effects of a sprayed densification layer on such insulation will also be explored. Long-term exposure to 1093°C (2000°F) temperatures will also determine insulation stability.

Coupon tests of window materials will determine optical properties such as transmittance and reflectance and mechanical properties such as compressive strengths at operating temperatures.

Close consultation with materials manufacturers and/or fabricators will be required to avoid duplication of existing data and to develop meaningful tests and realistic detailed designs.

Detailed heat transfer analyses will determine the temperature distribution within the window under varying operating conditions. These data will support window structural analyses necessary for the design studies. The design analysis will consider sealing and cooling mechanisms for the window and allowances for differential thermal expansion.

25-MWe Plant Size

Similar system level studies would be performed for the 25-MWe, ceramic tube receiver/open regenerated and intercooled cycle configuration. Again, the GSA model would be used for analysis of time of day, ambient variation, and dynamic effects. Detailed thermal analyses of the receiver cavity would be required to determine peak fluxes and temperatures. These data would allow verification of the receiver sizing and performance.

Materials coupons of ceramics materials such as siliconized silicon carbide and sintered alpha-silicon carbide would be tested in the expected solar environment.

Detailed thermal analyses would be performed on the ceramic tubing to produce temperature gradients along and through the ceramic materials. These data would support detailed stress analyses to develop designs with an acceptably low probability of failure.

6.0 REFERENCES

1. Bartlett, D.H. 1MW$_t$ Solar-Thermal Conversion Full System Experiment, Final Report, EPRI Research Project 1509, Boeing Document D277-10286-1, Boeing Engineering and Construction Company, Seattle, WA, October, 1982.

2. Bartlett, D.H., Gas Cooled Central Receiver-Closed Cycle 1MW Bench Model Testing, Vol. I-III Final Report, EPRI Research Projects 377-2 and -3, June 5, 1980, Boeing Document D277-10284-1, Boeing Engineering and Construction, Seattle, WA., August 1982.

3. Zimmerman, D.K., Solar Energy Water Desalination System Design, Vol. I-VI, Final Report, SERI Contract AF-1-9115-2, August 1981, Boeing Engineering and Construction, Seattle, WA.

4. Rubeck, M. and Beverly, W.D., "A Solar Thermal Electric Experimental Plant," Proceedings of International Solar Energy Society, Atlanta, GA, May, 1979, pp. 1125 - 1129.

5. Zimmerman, D.K., United States Gypsum Plant Solar Retrofit Program, Final Report. DOE-SF-10742-ES, July 1980, Boeing Engineering and Construction, Seattle, WA.

6. Gintz, J.R., Closed Cycle High Temperature Central Receiver Concept for Solar Electric Power, Final Report, EPRI RP-629, January, 1978, Boeing Engineering and Construction, Seattle, WA.

7. Davidson, W.S., et. al., Closed Brayton Cycle Advanced Central Receiver Solar-Electric Power system, Vol. I-III, Final Report, SAN/1726-1, November, 1978, Boeing Engineering and Construction, Seattle, WA.

8. Prieto, R., Solar Central Receiver System Integrated with a Cogeneration Facility, Final Report, DOE/SF/11533-TI (Vol. I), Gibbs and Hill, Inc., New York, NY.

9. Bird, S.P., et. al., Evaluation of Solar-Air Heating Central Receiver Concepts, PNL-4003, Sand 82-8185, Pacific Northwest Laboratory, Richland, WA, June, 1982.

10. Laity, W. W., et al., Assessment of Solar Options for Small Power System Applications, Vol. I, Executive Summary, Pacific Northwest Laboratory, Report No. PNL-4000, September, 1979.

11. DeLaquil III, P., Yang, C.L., and Noring, J.E., Solar Central Receiver High Temperature Process Air Systems, SAND 82-8254, Sandia National Laboratories, Livermore, CA, February, 1983.

12. Second Generation Heliostat Conference, Albuquerque, NM, September 30 - October 1, 1981.

13. Dellin, T.A., Fish, M.J., and Yang, C.L. A User's Manual for DELSOL2: A Computer Code for Calculating the Optical Performance and Optimal System Design for Solar Thermal Central Receiver Plants, SAND81-8237, Sandia National Laboratories, Livermore, CA, August, 1981.

14. Ashleman, R.H. Jr. and Matson, G.S. GSA User Reference - A Guide to the Steady State Computer Simulation of Gas Turbine Propulsion Engines, Boeing Document D6-46953, April 1981, The Boeing Company, Seattle, WA.

15. Solar-Powered Electric Power Generation Systems Utilizing Closed-Cycle Air Turbines, Final Technical Report, R78-954142, United Technologies Research Center, East Hartford, Connecticut, November, 1978.

16. Gas Turbine World Handbook, Vol. 6 1981-1982

17. "High-Efficiency Gas Turbine System Under Development," Turbomachinery International, May/June, 1980.

18. Gas Turbine World Handbook, Vol. 5 1980-1981

19. Gas Turbine World Handbook, Vol. 7 1982-1983

20. Provenzale, G.E. "State-of-the-Art Review of Closed Cycle Gas Turbines Burining Dirty Fuels," ASME paper 83-GT-159, 1983.

21. Donovan, M.T., Service Experience on Gas Turbine Engines - Marine and Aircraft, Boeing Document D321-13005, July 17, 1975, The Boeing Company, Seattle, WA

22. Liebenberg, J.W., "Tower Costs for Solar Central Receivers," Sandia memo, January 7, 1980.

23. Lee, J.C., Campbell, J., and Wright, D.E., "Closed-Cycle Gas Turbine Working Fluids," J. of Engineering for Power, Transactions of the ASME, V. 103, January, 1981, pp 220-228.

24. Pierce, B.L., "The Influence of Recent Heat Transfer Data on Gas Mixtures (He-Ar, H_2-CO_2) on Closed Cycle Gas Turbines," J. of Engineering for Power, Transactions of the ASME, V. 103, January, 1981, pp 114-117.

25. Serksnis, A.W., Taylor, M.F., and McEligot, D.M., "Heat Transfer to Turbulent Flow of Hydrogen-Carbon Dioxide Mixtures," Proceedings, 6th International Heat Transfer Conference, Toronto, Canada, August 7-11, 1978, pp 163-168.

26. Pickett, P.E., Taylor, M.F., McEligot, D.M., "Heated Turbulent Flow of Helium-Argon Mixtures in Tubes," Int'l. J. Heat Mass Transfer, V.22, 1979, pp 705-719.

27. Black and Veatch Consulting Engineers, Solar Thermal Conversion to Electricity Utilizing a Central Receiver, Open Cycle Gas Turbine, ER-652, EPRI, Palo Alto, CA, 1978.

28. Hunt, A.J., "Solar Radiant Heating of Small Particle Suspensions," 1982 Winter Annual Meeting of AICHE, Orlando, FL, Feb 26-Mar 1, 1982.

29. Bachovchin, D.M., "Development and Testing of a Fluidized Bed Solar Thermal Receiver," Proceeding of AS of ISES Annual Meeting, Philadelphia, PA, May, 1980.

30. Martin, J. and Vitko, J., ASCUAS: A Solar Central Receiver Utilizing a Solid Thermal Carrier, SAND 82-8203, Sandia National Laboratories, Livermore, CA, January, 1982.

31. Shaw, D., Bruckner, A.P., and Hertzberg, A., "A New Method of Efficient Heat Transfer and Storage at Very High Temperatures," 15th IECEC, Seattle, WA, p. 125

32. Copeland, R.J., "High-Temperature Molten Salt Solar Thermal Systems," 17th IECEC, Los Angeles, CA 1982, p. 2032.

33. Garden City Fans (Air Equipment Engineering, Seattle, Wa.).

34. Private communication with Mr. Curtis McMinn, Reynolds Aluminum, August 19, 1982.

35. Shannon, R.L., Radiation Simulation Program--A User's Guide to RADSIM, Boeing Document D2-121352-1, December, 1979, The Boeing Company, Seattle, WA.

36. Gintz, J. R., Technical and Economic Assessment of Phase Change and Thermochemical Advanced Thermal Energy Storage (TES) Systems, Final Report, EPRI EM-256, December, 1976, Boeing Engineering and Construction Co., Seattle, WA.

37. Dr. A. J. Hunt, Lawrence Berkeley Laboratory, private communication.

38. Ewing, J. and Zwissler, J., Performance Prediction Evaluation of Ceramic Materials in Point-Focussing Solar Receivers, DOE/JPL Report No. 1060-23 June 1979.

39. W. D. Kingery, H. K. Bowen, and D. R. Uhlmann, Introduction to Ceramics, 2nd Edition, 1976, John Wiley & Sons, N.Y., pp. 822ff.

40. Pietsch, A., et al, "Advanced Ceramic Combustor/Heat Exchange Engine System", Proceedings of the Workshop on Ceramics for Advanced Heat Engines, Orlando, FL, January 1977.

41. Rorabaugh and Mann, D. L., "Advanced SiC Heat Exchanger Materials", SAMPE Quart., April 1978.

42. Deininger, W. D. and Kupperman, D. S., "IR Techniques for the Evaluation of SiC Heat Tubing," Jnal. Test & Eval., January 1980.

43. Coombs, M., et al, High Temperature ceramic Heat Exchanger, EPRI Report No. FP-1127, July 1979.

44. Lucek, J. W., et al, "Cast Densified SiCs," SAE Technical Paper Number 790253, February 1979.

45. Myers, B., et al, "Adabatic Coal-Fired 1350°C Expander," Proceedings of the Workshop on Ceramics for Advanced Heat Engines, Orlando, FL, January 1977.

46. Grosskreutz, J., Solar-Thermal Conversion to Electricity Utilizing a Central Receiver, Open Cycle Gas Turbine Design, EPRI Report No. ER-652.

47. Wei, G.C., et al, Evaluation of Tubular Ceramic Heat Exchanger Materials in Residual Oil Combustion Environment, Oak Ridge Nat. Lab. Report No. ORNL TM-7578, March 1981.

48. Roy, D., et al, "Development of Cost-Effective Ceramic Tube Process for High Temperature Heat Recovery Systems," paper presented at the 7th Annual Conference on Composites and Advanced Ceramic Materials, Cocoa Beach, FL, January 1983.

49. Torti, M. L., "Silicon Nitride and Silicon Carbide - A Manufacturer's Perspective," Proceedings of the Workshop on Ceramics for Advanced Heat Engines, Orlando, FL, January 1977.

50. Robertson, C. S., et al, A Conceptual Design Study of a High-Temperature Solar Thermal Receiver, NASA Report No. CR-163944, November 1980.

51. Roy, D. and Hastert, J. L., "Evaluation of Coors CD-1 Coordierite as a Radome Material," Proceedings of the 16th Symposium on Electromagnetic Windows, Atlanta, GA, June 1982.

52. Rauch, H. W., et al, Improved Ceramic Heat Exchanger Materials, NASA Report No. CR-159678, December 1980.

53. Mehan, R, "Characteristics and Properties of a Si/SiC Ceramic Composite," Proc. of the Workshop on Ceramics for Advanced Heat Engines, Orlando, FL, January 1977.

54. Warren, J. W., "Carbon Fiber Reinforced Si/SiC Composites," Ibid

55. Anon', Engineering Property Data on Selected Ceramics " Vols. I, II, and III, MCIC Publication No. MCIC-HB-07, March 1976-July 1981.

56. Govila, R. K., "Uniaxial Tensile and Flexural Stress Rupture Strength of Hot-Presed Si_3N_4," Jnal. Amer. Cer. Soc., Vol. 65, No. 1, January 1982.

57. Trantina, J., "Fracture Strength of Sintered and Siliconized SiC and SiC Joints," Cer. Bull, Vol. 61, No. 5, 1982.

58. Manufacturer's Data: Asahi Glass Company, Norton Company, Pure Carbon Company Kyocera International Inc., National Beryllia Corporation, Coors Porcelain Company, Ceramic Products, Inc. and Bolt Technical Ceramics.

59. Bartlett, D., Knutson, B., Zentner, R., and Bigger, J., "Solar Receiver Cavity Insulation Evaluation," Ceramic Engineering and Science Proceedings, September-October 1982, pp. 810-819.

60. Fisk, W. J., et al, Performance Analysis of a Windowed High Temperature Gas Receiver Using a Suspension of Ultrafine Carbon Particles as the Absorber, Lawrence Berkeley Lab. Report No. LBL-10100, April 1980.

61. Bomar, S. and Elfe, T.B., "Design of Transparent Windows for Direct Flux Reactors," paper presented at the 7th Annual Conference on Composites and Advanced Ceramic Materials, Cocoa Beach, FL, January 1983.

62. Roy, D. and Hastert, J. L., "Polycrystalline $MgAl_2O_4$ Spinel for High Temperature Windows," paper presented at the 7th Annual Conference on Composites and Advanced Ceramic Materials, Cocoa Beach, FL, January 1983.

63. Personal Communictaions, J. Verzemnieks and Dr. J. I. Mueller.

64. Bakker, W. T. and Kotchick, D.: "Materials Requirements for High Pressure Ceramic Heat Exchangers," Proc. 6th Annual Conference on Composites and Advanced Ceramic Materials, Cocoa Beach, FL, January 1982 pp. 793-819.

65. Coombs, M., Kotchick, D., and Warren, K.: High Temperature Ceramic Heat Exchanger, EPRI Report No. FP-1127, July 1979.

66. Stanley, R., Fessler, H. and Sivill, A.P.: "An Engineer's Approach to the Prediction of Failure Probability of Brittle Components," Basic Science Portion of the Convention Ceramics for Turbines and Other High Temperature Engineering Applications, Cambridge, UK, July, 1972.

67. Rufin, A. C., Samos, D. R., and Bollard, R. J. H.: "A Comparative Study of Statistical Failure Prediction Models for Brittle Materials," to be published in AIAA Journal.

68. Batdorf, S.B. and Heinisch, H.K., Jr.: "Fracture Statistics of Brittle Materials with Surface Cracks," Eng. Fr. Mech. Vol. 10 (1978).

69. Manufacturer's Data: Corning Glass Works, Coors.

70. Personal Communication, J. Verzemnieks and Bob Post of MTC, Dallas, TX.

71. Personal Communication, J. Verzemnieks and A. C. Schaffhauser, Oak Ridge National Lab.

72. Hunt, Arlon J., "Development of a New High Temperature Gas Receiver Utilizing Small Particles", Systemes Solaires Thermodynamiques, No. 306, pp. 417-421.

73. Tower Cost Data for Solar Central Receiver Studies, Stearns-Rogers Engineering Co., SAND 78-8185, 1978.

74. Personal communication, J. Verzemnieks and Dr. J. Hannoosh, Norton Company, Worchester, Ma.

Appendix A: Turbomachinery Survey Cost Data Base.

The turbomachinery cost data assembled to support the discussion of Section 2.5.2 is presented in Table A-1.

Table A-1

BID PRICES AND WORK SCOPES FOR GAS TURBINE INSTALLATIONS

SOURCE: GAS TURBINE WORLD HANDBOOK: 1980-81; 1981-2; 1982-3

JOB	BID 1982$/kW AVG	STD DEV	WIN	MW ISO	DATE A AWARD B BID	REGENERATOR	TRANSFORMERS	SWITCH GEAR	FUEL STORE & HANDLE	TURBINE HOUSE	CIVIL WORKS	TURNKEY	SPARES	GAS COMPRESSOR	DUAL FUEL	COMB CYCLE PROV.	CLUTCH	COMB. CYCLE	USED EQUIPMENT	MAINTENANCE BLDG.	DEMOLITION
20	801	162			B Mar 82			X	X										X		
19	491	84	358	374	A Jun 82			X	X		X				X				X		
28	399	88	396	800	A Jul 79						X										
13	346	39		300	B Oct 80				X		X										
1	329	48	312	98	A Mar 81	X		X		X				X			X				
11	317	39	278	101	A Jun 81	X	X				X			X							
29	317	35	270	84	A Jan 81						X				X						
27	311	39	285	100	A Feb 80				X		X			X							
21	297	57	263	50	A Jun 82	X			X		X								X	X	
16	285	33	261	100	B Oct 81		X	X			X		X	X							
18	282	40	251	50	A Sep 81	X	X			X											
17	281	52	261	100	A Sep 81	X		X													
22	276	29	265	36	A Dec 81			X				X									
26	242	35		70	B Jun 80																
9	231	42	195	23.5	A Mar 81									X							
2	229	34	179	43	A Apr 81						X	X									
3	229	36	176	43	A Apr 81						X	X									
6	228	30	180	22	A Apr 81						X	X									
5	225	34	178	43	A Apr 81						X	X.									
4	223	35	174	43	A Apr 81						X	X									
7	217	18		110	B Jun 81	X	X	X			X										
10	215	31		50	B Jun 81	X		X													
25	214	44	166	54	A Apr 80																
12	192	39	201	52.5	A Dec 80							X				X					
8	182	22	162	72.9										X	X						
23	181	32		300	Dec 80																
24	170	24		300							X										
15	151	22	98	104	A Dec 81						X										
14	104	9	98	104	A Dec 81						X							X			

Table A-1 (cont'd)

Job No.	Plant Location	Data Source		Description
1	Al Fujairah UAE	1981-82 GTW	p. 12	12 bids, 7 bidders
2-6	CADAFE Venezuela		p. 13	9 or 10 bids, 9 bidders
7	ELECTROLIMA Peru		p. 14	4 bids, 4 bidders
8-9	ENELVEN Venezuela		p. 15	
10	Empresa Electrica Guatamala 2 sites		p. 16	9 bidders
11	Interonexion Electrica Columbia		p. 17	8 bidders
12	Port Elizabeth South Africa		p. 18	7 bidders
13	Trinidad & Togago Electric		p. 19	3 bidders combined cycle
14-15	City of Springfield, Missouri	1982-83 GTW	p. 12	7 bidders
16	Egypt Electricity Authority		p. 13	
17	Electrico Saudi Jizan		p. 14	6 bids, 5 bidders
18	MEW Ajman UAE		p. 16	9 bids, 8 bidders
19	SCECO South		p. 17	
20	Tabouk Electric		p. 18	6 bids, 5 bidders
21	Trinidad & Tobago Electric		p. 20	5 bids, 4 bidders
22	WED Abu Dhabai		p. 21	5 bids
23-24	CFE Mexico	1980-81 GTW	p. 11	simple equipment only
25	Capetown, South Africa		p. 14	
26	Empresa Electrica Guatemala		p. 15	10 bids, 8 bidders
27	Kuwait Electricity		p. 16	
28	Riyadh Electric		p. 18	
29	Sri Lanka Electricity		p. 19	

Appendix B: Receiver, Recuperator, Intercooler, and Precooler Thermal Scale Methods.

This appendix describes the thermal scale modeling relationships and methodology performed in support of the evaluations of the Task 2, Brayton Cycle Configuration Study.

Fluid flow and thermal scale modeling techniques have been successfully utilized at Boeing for the design of spacecraft (see Reference B-1) and solar central receivers (see Reference B-2).

Fluid flow and thermal scale modeling can provide limited extrapolations of a well characterized design over a range of operating conditions and dimensions. The application of thermal and fluid flow modeling criteria results in the formulation of governing equations. These equations provide valued insight into the sensitivity of critical parameters such as tube temperature and pressure drop to the other indepndent variables such as system operating pressure and receiver inlet and outlet temperatures. Advantages to be gained by variation of tube dimensions, spacing, and other dependent variables also become clear to the designer.

Receiver

Receivers for each cycle configuration alternative were scaled from the baseline receiver designs described in Section 2.5.2. The effects of thermal scale modeling from that design can be expressed as:

$$\dot{m}\, N\, C_p\, (T_{in} - T_{out}) = h\, A_w\, (T_t - T_b) \qquad (1)$$

making the following substitutions:

$$h = k\, Nu/D \qquad (2)$$

$$\dot{m} = Re \cdot \mu\, D\, \pi/4$$

Equation (1) becomes:

$$\frac{Re\ Pr}{Nu}\ \frac{\Delta T_g}{L}\ \frac{D}{4} = \Delta T_e$$

or:

$$\Delta T_e{}^* = \frac{Re^*\ Pr^*\ \Delta T_g{}^*\ D^*}{Nu^*\ L^*} \qquad (3)$$

where:

$$(\ )^* = \frac{(\ )_{new\ value}}{(\ )_{old\ value}}$$

The pressure loss is calculated from:

$$\alpha = \frac{\Delta P}{P} = \frac{\frac{1}{2}\ \rho\ v^2}{P}\ \beta \qquad (4)$$

where:

$$\beta = f\ (L/D + K) \qquad (5)$$

The factor K is used to account for non-friction pressure losses such as bends and valves. These pressure losses are often expresed in terms of effective L/D's. For a constant friction factor, f, β is a function only of L/D.

Making the following substitutions:

$$v = \dot{m}/(\rho A_f) \qquad N = W/D\Gamma \tag{6}$$

$$\dot{m} = M/N \qquad \rho = P/(R\ T)$$

Equation (4) becomes:

$$\alpha^* = \frac{M^{*2}\ T^*\ L^*\ \Gamma^{*2}}{P^{*2}\ D^{*3}\ W^{*2}} \tag{7}$$

Solving for D* and substituting in Equation (3) yields:

$$\Delta T_e^* = \frac{Re^*\ Pr^*\ \Delta T_g^*}{Nu^*\ L^*} \left\{ \frac{M^{*2}\ T^*\ L^*\ \Gamma^{*2}}{P^{*2}\ \alpha^*\ W^{*2}} \right\}^{1/3} \tag{8}$$

Assuming the heat transfer can be related by:

$$Nu^* = Re^{*0.8}\ Pr^{*0.6} \tag{9}$$

then $\Delta T_e{}^*$ becomes:

$$\Delta T_e{}^* = \frac{Re^{*0.2}\ Pr^{*0.4}\ \Delta T_g{}^*}{L^*} \left\{ \frac{M^{*2}\ T^*\ L^*\ \Gamma^{*2}}{P^{*2}\ \alpha^*\ W^{*2}} \right\}^{1/3} \tag{10}$$

Experience has shown the $Pr^{*0.4}$ dependence to be very slight for gas-cooled heat exchangers and can be ignored. Also, Re* can be expressed as:

$$Re^* = M^*/(N^*\ D^*) = M^*\ \Gamma^*/W^* \tag{11}$$

Substitution and rearrangement yields:

$$L^{*0.67} = \frac{1}{W^{*0.87}} \frac{\Delta T_g{}^*}{\Delta T_e{}^*} \frac{M^{*0.87}\ \Gamma^{*0.87}\ T^{*0.33}}{P^{*0.67}\ \alpha^{*0.33}} \tag{12}$$

The sensitivity of the non-dimensional heat exchanger length, L*, to the other non-demensional parameters is illustrated in Figure B-1. Increases in system pressure, p, while preserving all other parameters allows a decrease in panel, and hence cavity, size. For a constant pressure loss fraction, increasing pressure allows larger absolute pressure drop. This in turn allows smaller diameter tubes and higher Reynolds numbers. The increased heat transfer coefficient and smaller tubing dimensions cause decreases in panel size. This

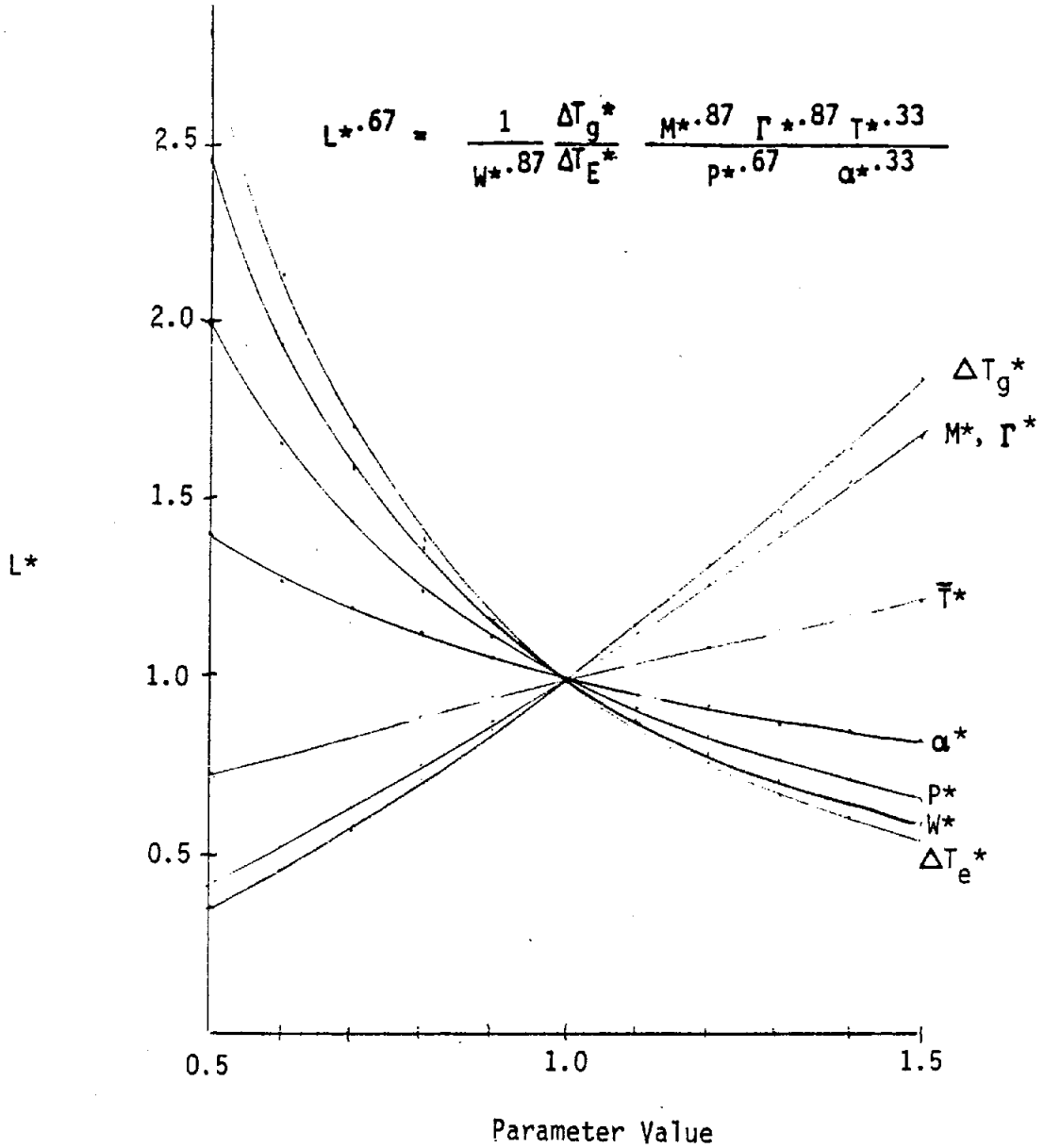

Figure B-1. Sensitivity of Heat Exchange Length to Changes In in Design and Operating Condition Parameters

trend favorably affects heat exchanger designs at high system pressures such as closed cycle or higher pressure ratio open cycle turbomachinery. Other parameter changes are seen to produce different changes in panel size. The most sensitive parameters are the difference between fluid inlet and outlet temperatures and the difference between tube wall and gas temperatures.

The use of the thermal scale modeling technique is illustrated by the following. Table B-1 presents data for the 25-MW_e baseline reeiver from Section 2.5.2. Also presented are the known data for the receiver operating in an open simple cycle (OS) configuration. The non-dimensional parameters can be formed and substituted into the relations shown above resulting in the determined values of Table B-1. The heat exchanger length values are used to calculate the receiver cavity area shown in Table 2-9. Similar calculations were made for all the 25-MW_e and 2-MW_e cycle configurations.

The power of the thermal scale modeling concept is that the designer can develop simple relationships that allow rapid sizing of conceptual designs. The acccuracy of the scaling method depends on the magnitude of the parameter change and the similarity between the two designs. Order of magnitude changes in parameters and use of vastly different tubing concepts (e.g., straight vs. bent tubes) would most likely invalidate the scaling process. However, detailed designs are believed to be scalable to similar configurations to within a factor of 2-4 from the original design.

Heat Exchanger Sizing

Similar thermal scale modeling techniques were employed to size the recuperator, precooler, and intercooler for the cycle configurations as required. A detailed recuperator design from the BEC/DOE Advanced Central Receiver Program (B-3) was used as the base design. The heat exchangers were modeled as shell-and-tube, counterflow, air-to-air designs as illustrated in Figure B-2.

TABLE B-1: Receiver Thermal Scale Modeling Example Data
25-MW_e, Ceramic Tube Receiver

Parameter	Units	Baseline Design	OS Configuration	Non-Dimensional Value
P	psia	246.6	294	1.192
$\dot{m}$	lb/s	159.7	186.3	1.167
W	ft	23.2	20.74	0.894
L	ft	36	32.9*	0.914*
D	in	.656	.670*	1.022*
N	-	141	123*	0.874*
Γ	-	3.0	3.0	1.0
α	-	0.10	0.10	1.0
T	°R	1950.5	1899.2	0.974
T_{in}	°F	781	838.4	N/A
T_{out}	°F	2200	2040	N/A
T_{tube}	°F	2300	2140	N/A
ΔT_e	°F	100	100	1.0
ΔT_g	°F	1419	1201.6	.847

* Determined from scaling relationships.

Figure B-2. HEAT EXCHANGER SIZING

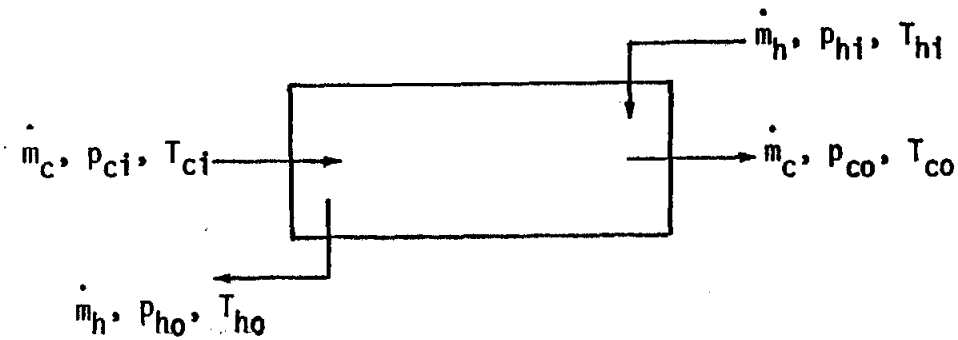

- Shell and tube
- Counterflow
- Air to air
- scale from detailed recuperator design for ACR program

Heat Exchanger Effectiveness

$$\epsilon = \frac{\dot{m}_h C_{ph}}{\dot{m}_c C_{pc}} \frac{(T_{hi} - T_{ho})}{(T_{hi} - T_{ci})}$$

$$= fn(\dot{m}, C_p, NTU)$$

$$NTU = \frac{U A}{\dot{m}_c C_{pc}}$$

Using a NTU-design method where:

$$NTU = \frac{U\ A_w}{(\dot{m}\ C_p)_{min}} \tag{13}$$

the heat exhchanger effectiveness for a counterflow arrangement is given by (B-4).

$$\varepsilon = \frac{1 - \exp\left[-NTU\ (1 - \frac{C_{min}}{C_{max}})\right]}{1 - \frac{C_{min}}{C_{max}} \exp\left[-NTU\ (1 - \frac{C_{min}}{C_{max}})\right]} \tag{14}$$

$$C_{min} = \text{Capacity Rate} = \dot{m}_{min}\ C_{p\ min}$$

$$\varepsilon = \frac{C_h\ (T_{hi} - T_{ho})}{C_{min}(T_{hi} - T_{ci})} \quad \text{for } C_{min} = C_c \tag{15}$$

$$\varepsilon = \frac{C_c\ (T_{co} - T_{ci})}{C_{min}(T_{co} - T_{hi})} \quad \text{for } C_{min} = C_h \tag{16}$$

For an air-to-air heat exchanger where hot side and cold side pressure losses are chosen to correspond to the system pressure ratio, the hot side and cold side heat transfer coefficients are approximately equal. Assuming:

$$U^* = h^*$$

where

$$(\ )^* = \frac{(\ )_{\text{new value}}}{(\ )_{\text{old value}}}$$

and assuming turbulent flow:

$$U^* = \frac{k^* \, Nu^*}{d^*} = \frac{k^* \, Re^{*0.8} \, Pr^{*0.6}}{d^*} \qquad (17)$$

$$= \frac{k^* \, \dot{m}^{*0.8} \, Pr^{*0.6}}{d^{*1.8} \, \mu^{*0.8}} \qquad (18)$$

Assuming pressure loss calculations from equations (4) and (5) above, the tube diameter is given by:

$$d^* = \left\{ \frac{T^* \, \dot{m}^{*2} \, L^*}{P^{*2} \, \alpha^*} \right\}^{1/5} \qquad (19)$$

Substituting (19) into (18) yields:

$$U^* = \xi(T) \frac{\dot{m}^{*0.02} \; p^{*0.72} \; \alpha^{*0.36}}{L^{*0.36}} \tag{20}$$

where:

$$\xi(T) = \frac{k^{*0.4} \; C_p^{*0.6}}{\mu^{*0.2} \; T^{*0.36}} \tag{21}$$

is a function of average fluid temperature only.

The sensitivity of U* to changes in massflow, pressure loss fraction, and heat exchanger length is illustrated in Figure B-3. Increases in presure and presure loss fraction increase the overall heat transfer, whereas increases in massflow have minimal effects.

Table B-2 presents data for the ACR recuperator and for the 25-MW_e, closed cycle (CR) configuration recuperator. Substitution into equations (20) and (21) yields an overall heat transfer coefficient of 55.5 BTU/hr-ft^2-°F. Assuming a heat exchanger effectiveness of 0.9, the required NTU value of 7.3 can be calculated from equations (14).

These data can be used to calculate the recuperator heat exchange area, A, required from equation (13). Table 2-11 presented earlier shows 30,532 ft^2 of area is required for the CR recuperator. Similar calculations were performed for the other heat exchangers.

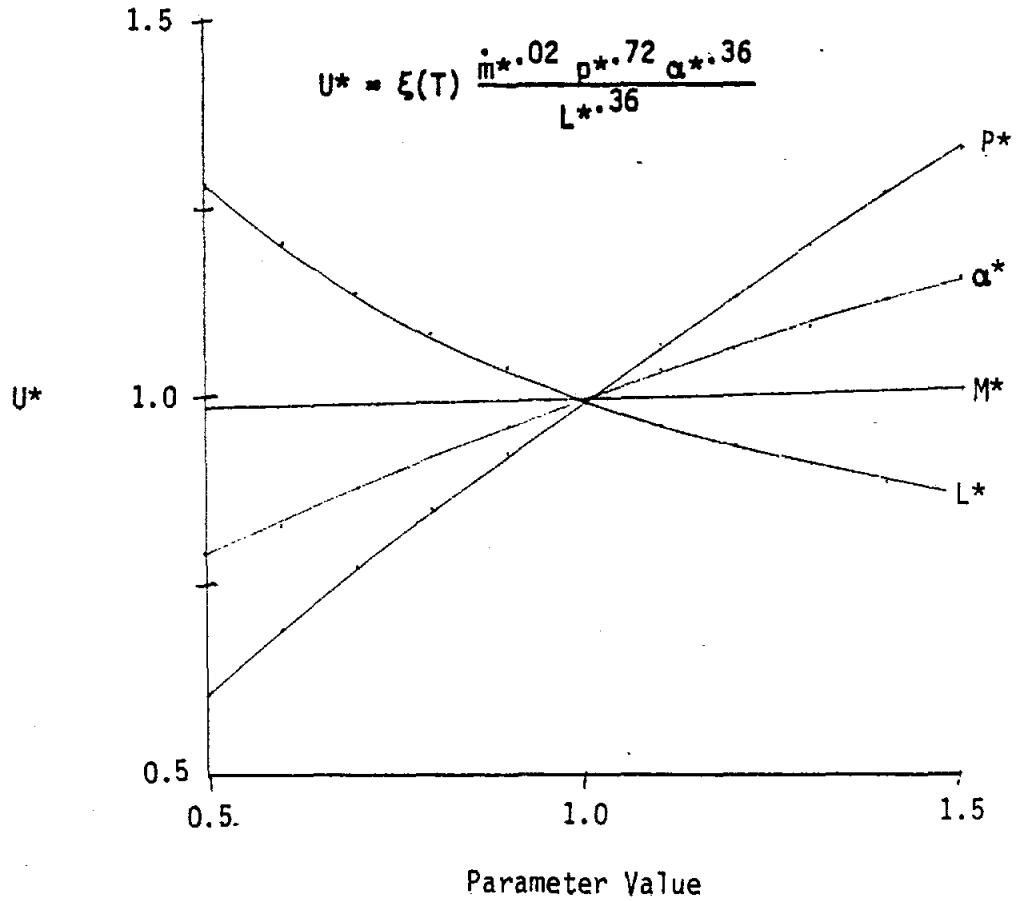

Figure B-3. Sensitivity of Heat Transfer Coefficient to Changes in Design and Operating Condition Parameters

TABLE B-2: Recuperator Thermal Scale Modeling Example Data

Parameter	Units	ACR Recuperator	CR Recuperator	Non-Dimensional Value
$\dot{m}_c$	lb/s	991.6	249.9	0.252
T_{ci}	°F	258.2	486.0	N/A
T_{co}	°F	871.3	1239.0	N/A
T_{hi}	°F	937.9	1319.5	N/A
T_{ho}	°F	333.6	608.3	N/A
Pi_c	psia	528.9	500	0.945
α_c	-	0.0072	0.01	1.389
L	ft	57.6	25	0.434
μ_e	10^{-5} lbm/s-ft	2.03	2.34	1.153
k_c	B/h-ft-°F	0.0247	0.0296	1.198
C_{pc}	B/lbm-°F	0.249	0.258	1.036
T_c	°R	1024.8	1322.5	1.291
$\xi(T_c)$	-	-	-	0.973
U	B/h-ft^2-°F	40.19	55.50*	1.381*

* Determined from scaling relationships.

Nomenclature

A_f	Tube cross-sectional area = $\pi D^2/4$
Aw	Tube interior wall area = $N\pi DL$
Cp	Working fluid heat capacity
D,d	Tube inside diameter
K	Pressure loss coefficient for valves, bends, etc
L	Panel tube length
M	Panel mass flow
N	Number of tubes per panel
Nu	Nusselt number = hD/k
NTU	Number of thermal units = $UA/\dot{m}Cp$
Pr	Prandtl number = $\mu Cp/k$
R	Gas constant
Re	Reynolds number = $\rho v A/\mu = 4 \dot{m}/(\mu\pi D)$
Tin	Inlet gas temperature
Tout	Outlet gas temperature
Tb	Bulk gas temperature
Tt	Tube wall temperature
T	Average gas temperature = (Tin - Tout)/2
ΔTg	Gas temperature rise = (Tout - Tin)/2
ΔTe	Excess temperature, (Tt - Tb)/2
U	Overall heat transfer coefficient
W	Panel width
f	Friction factor
h	Convective heat transfer coefficient
k	Gas thermal conductivity
ℓ	Distance between tubing centerlines
m	Tube mass flow
p	System pressure
Δp	Pressure drop across panel
v	Gas velocity
Γ	Heat exchanger pitch - ℓ/D
α	Pressure drop fraction = $\Delta p/p$
ε	Heat exchange effectiveness
ρ	Gas density
μ	Gas viscosity

References

B-1 MacGregor, R.K., Limitations in Thermal Similitude , Final Report, Boeing Document D2-121352-1, December, 1969, The Boeing Company, Seattle, Wa.

B-2 Zentner, R. C. and Shannon, R. L., "Thermal Scale Modeling of the Central Receiver of a Helium Brayton Cycle Solar Power Plant", IECEC, Washington, D.C., 1977, pp 179-186.

B-3 Davidson, W. S., et al, Closed Brayton Cycle Advanced Central Receiver Solar-Electric Power System, Vol. I-III, Final Report, SAN/1726-1, Nov. 1978, Boeing Engineering and Construction, Seattle, Wa.

B-4 Kakac, S., Bergles, A. E., and Maxinger, F., Heat Exchangers, Thermal-Hydraulic Fundamentals and Design, McGraw Hill, NY, 1981, p. 439.

Appendix C. Preliminary Structural Analysis of the 25-MW_e Ceramic Tube Receiver

The structural reliability of the heat exchanger tube array was checked by analysing the response of individual tubes to a number of representative steady state and transient thermal and mechanical load conditions. A "worst case" scenario was then constructed by linear superposition, and the corresponding probability of failure estimates for the tube and the tube array were found.

Considered in the present study were stresses arising from:

- Internal pressure
- Tube weight
- Axial temperature gradients
- Radial temperature gradients
- Earthquake loads

Table C-1 lists the parameters defining these conditions for the tube quantities (a) and (b) shown in Figure C-1. The materials evaluated here were siliconized silicon carbide (SSC) and sintered alpha-silicon carbide (SASC). Other candidate materials were dropped primarily because of fabrication and size constraints. SSC and SASC material properties are shown in Table C-2.

A listing of the estimated maximum tube tensile stresses generated by the load conditions indicated above is provided in Table C-3. Individual tube probabilities of failure were calculated by the Weibul/Principle of independent Action method (C-1), which can be stated as follows:

$$P_f = 1 - \exp\left\{-\iiint_V \left[\left(\frac{\sigma_1}{\sigma_0}\right)^m + \left(\frac{\sigma_2}{\sigma_0}\right)^m + \left(\frac{\sigma_3}{\sigma_0}\right)^m\right] dV\right\}$$

Table C-1. Load Configurations Used in the Structural Analysis of the 25 MW_e Receiver Heat Exchanger Tubes

Load Condition	Load Magnitudes
1. Internal Pressure	142 psia, uniform
2. Tube weight	$\rho g \cdot$ volume (distr. vertical load)
3. Axial temperature gradient	Assume: . Uniform temp. on straight segment (upcom.) = 1230°F . Uniform temp. on straight segment (downcom.) = 1800°F . Uniform temp. on semicircular segment = 1450°F
4. Radial temperature gradient	+30°F temperature gradient between inside and outside of tubes, uniform.
5. Earthquake	0.35 $\rho g \cdot$ volume (distributed side load)

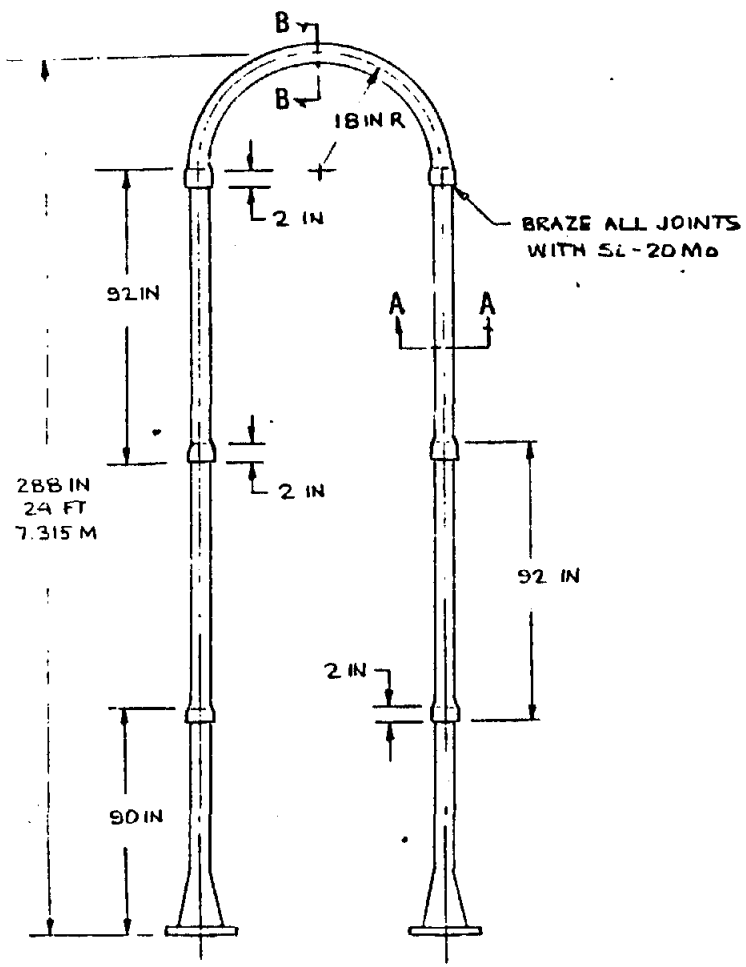

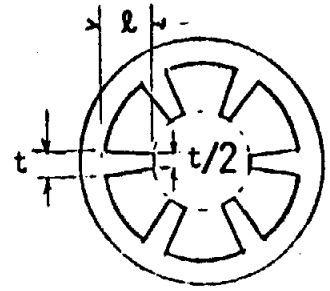

Section A-A

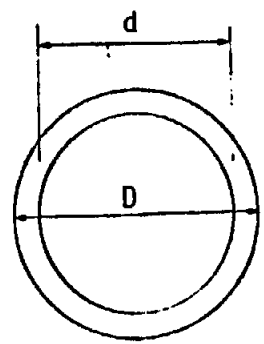

Section B-B

	Dimensions (in.)	
Case	a	b
d	2.067	2.000
D	2.375	2.500
t	0.154	0.250
ℓ	0.460	0.460

Figure C-1. Tube Geometries

Table C-2. SSC and SASC Properties Used in the Heat Exchanger Tube Structural Analysis

Property	SSC	SASC
Density (lb/in^3)	0.036	0.036
Young's modulus (Msi)	45	60
Poisson's Ratio	0.20	0.20
Thermal Expansion Coefficient (10^{-6} in/in-°F)	2.4	2.4
Thermal conductivity (Btu/hr-°F-ft)	30	24
Weibull modulus	8	8
Weibull distribution scaling factor, σ_o (ksi · $[in.]^{0.125}$)	13	22

Table C-3. Maximum Tube Tensile Stresses

	Straight tubes	Semicircular Tube
Axial Stress (psi)	$430 + (2950-14x+ +7.22\cdot10^{-3}x^2)\cos\phi$ (a)	$460+(6900-7650\cos\phi- -250\sin\theta)\cos\phi$ (a)
	$240+(2800-12x+ +7.40\cdot10^{-3}x^2)\cos\phi$ (b)	$270+(5350-4450\cos - -190\sin\theta)\cos\phi$ (b)
Circumferential Stress (psi)	26400r-28200 (a) SSC	26400r-28200 (a) SSC
	35100r-37900 (a) SASC	35100r-37900 (a) SASC
	16250r-17600 (b) SSC	16250r-17600 (b) SSC
	21600r-23650 (b) SASC	21600r-23650 (b) SASC

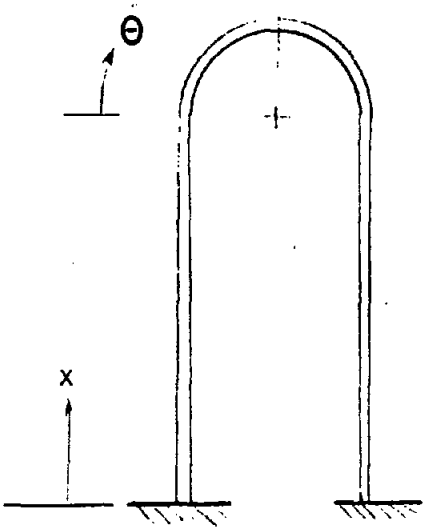

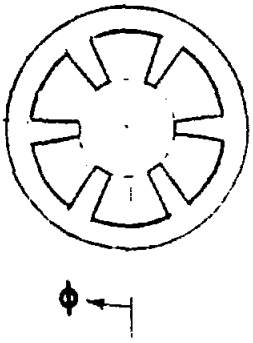

Where P_f = Probabilitiy of failure

V = Tube volume

$\sigma_1, \sigma_2, \sigma_3$ = Principal stresses (functions of position)

σ_0 = Distribution scaling factor

and m = Weibull modulus (a reciprocal function of the degree of strength variability)

Other currently available analytical failure prediction models have been shown to lead to more accurate probability of failure estimates (C-2 and C-3), but could not be readily applied here. Results for the individual tubes and the tube array are listed in Table C-4.

Checks on the magnitudes of the compressive loads acting on the tubes rule out the possibility of collapse under compression. The structural analysis results can be summarized as follows:

- Tube geometry (a) produces unacceptably high probability of failure estimates for both SSC and SASC.

- From a structural standpoint, configuration (b) for SASC tubes appears to perform satisfactorily. However, it has been shown that the average strength and Weibull moduli of SASC tubes can be significantly lower than for the same parameter values derived from tests on small SASC components (see References C-4 and C-5). This problem has been attributed to SASC processing limitations and cannot be accounted for by the analytical failure model used above. On the other hand, the individual tube probability of failure for the SSC tubes in configuration (b) are also quite low, and could be further reduced in practice to acceptable levels by prestressing or proof testing techniques (C-6). These techniques could make the cheaper and technologically more advanced SSC tubes to become an attractive candidate for the present application. Consequently, a safe material choice at this time would be SSC (with provisions for component proof testing). SASC could still become a viable material if SASC tube properties were to improve to the levels obtained for smaller components.

Table C-4. Structural Analysis Results

Geometry (Per Fig. C-1)	Material	Probability of Failure (Tube)	Probability of Failure (Array)*
(a)	SSC	0.3	1.0
	SASC	$6 \cdot 10^{-3}$	0.4
(b)	SSC	0.03	0.95
	SASC	$4 \cdot 10^{-4}$	0.04

*Probability of Failure (array) = 1- [1-Probability of failure (tube)]^n

n = 100 tubes

- A final structural design should be accompanied by a more detailed stress analysis, with emphasis on critical areas, such as joints and which in addition to the load geometrics described above would address:

    - Other thermal load cases (e.g., front-to-back thermal gradients).

    - Fatigue, creep and subcritical crack growth.

    - Loads arising from tube header system motion, caused by pressure and thermal expansion.

Use of improved probability of failure models (such as the ones described in references C-2 and C-3) would also be recommended.

Note: Late in the study, the 25-MW_e ceramic tube diameter (d in Figure C-1) was increased to 2.50 inches to reduce pressure losses. It was not possible to reevaluate the stresses for the larger diameter tube.

References

C-1 Stanley, R. H., Fessler and A. P. Sivill, "An Engineer's Approach to the Prediction of Failure Probability of Brittle Components," Basic Science Portion of the Convention Ceramics for Turbines and Other High-Temperature Applications, Cambridge (UK), July 1972.

C-2 Giovan, M. N. and G. Sines, "Biaxial and Unixial Data for Statistical Comparisons of a Ceramic's Strength," Jnl. Amer. Cer., Sec. 1, Vol. 62, Nos. 9-10 (1979), pp 510-515.

C-3 Rufin, A. C., R. J. Bollard and D. R. Samos, "A Comparative Study of Statistical Failure Prediction Models for Brittle Materials," to be published in the AIAA Journal.

C-4 Coombs, M., D. Kotchick and H. Warren, High-Temperature Ceramic Heat Exchanger, EPRI Report No. FP-1127, July 1979.

C-5 Ward, M. E., et al, Development of a Ceramic Tube Heat Exchanger with Relaxing Joint, Final Report, January 1977 - June 1980, DOE Report FR-2556-30, (Solar Report No. SR-80-R-4553-30).

C-6 Trantina, G. G.: "Strengthening and Proof Testing of Siliconized SiC", Jnl. Mat. Science, (17), 1982, pp 1487-1492.

Appendix D. Detailed Receiver Subsystem Cost Data.

This appendix presents the cost data basis for the summary receiver subsystem costs presented in Section 3.5.4. These data presented in this appendix are based on the conceptual receiver designs developed in this study and presented earlier in Section 3.5. Unit costs were based on vendor contacts and BEC experience and engineering estimates. Because of the scoping nature of this study, firm quotes were not secured for each component. Due to the level of maturity of these designs, the reader is cautioned against use of these data beyond the conceptual level intended for this study.

25-MW_e Receiver Subsystem

A list of materials for the 25-MW_e receiver is presented in Table D-1. Receiver cavity insulation cost details are presented in Table D-2. The insulation product costs were developed from 1980 quotes from Babcock and Wilcox and presented in BEC/EPRI report No. AP-2436, Solar Central Receiver Cavity Insulation Evaluation. Two insulation designs are considered. For directly solar irradiated cavity wall areas, the layered board product approach depicted earlier in Figure 3-44 was used. For the indirectly solar irradiated cavity walls, six inches of Kaowool® were used. The directly irradiated cavity area was 2847 ft^2, and the indirectly irradiated area was 6317 ft^2. The 1980 dollar costs were escalated to 1983 dollars assuming 6% inflation/year, i.e., $(1.06)^3 = 1.19$.

Manifold cost data are presented in Table D-3. Quantities, unit cost and total costs are presented. The receiver cost summary is presented in Table D-4. Similar data for the tower and piping are presented in Tables D-5 and D-6 respectively.

2-MW_e Receiver Subsystem

A list of materials for the 2-MW_e receiver is presented in Table D-7. The receiver cost summary is presented in Table D-8. Tower and piping costs are summarized in Tables D-9 and D-10 respectively.

TABLE D-1: 25-MW_e RECEIVER LIST OF MATERIALS

ITEM	QUANTITY	DESCRIPTION	LB/ UNIT	TOTAL LB	$/LB
1	25 ft	Tube 32.0 in dia x .06 Wall ASTM A53	20.3	503	.38
2	2	90° Weld Ell 32 dia x .06 Wall ASTM A53	108	206	1.75
3	2	Corrugated Flex Joint 32 dia x 32 long	60	120	2.00
4	2	Flanges 35 OD x 32 ID x .25	111	22	1.50
5	2	Hangers	55	110	1.00
6	20 ft	Tube 24.0 dia x .06 WASS ASTM A53	15.2	304	.38
7	4	90° Weld Ell 29 dia. x .06 Wall ASTM A53	60	240	1.75
8	2	Corrugated Flex Joint 24 dia. x 24 long	61	122	2.00
9	2	Flanges 28 OD x 24 ID x .25	8.5	17	1.50
10	2	Hangers	50	100	.38
11	35 ft	Tube 20 dia. x .06 Wall ASTM A53	12.7	445	.38
12	4	90° Weld Ell 20 dia. x .06 Wall ASTM A53	41.5	166	1.75
13	2	Corrugated Flex Joint 20' dia. x 20" long	42	84	2.00
14	2	Flanges 23 OD x 20 ID x .25	7.0	14	1.50
15	2	Hangers	48.5	97	.38
16	25 ft	Tube 3.5 dia. x .083 Wall ASTM A53	3.07	77	.38
17	2	90° Weld Ell 3.5 dia. x .083 Wall	1.76	4	1.75
18	2	Corrugated Flex Joint	2	4	2.00
19	2	Flanges 6.5 OD x 3.5 ID x .25	2	4	1.50
20	2	Hangers	39	78	.38
21	25 ft	Tube 12.0 dia. x .172 Wall A53	21.8	545	.38
22	4	90° Weld Ell 12.0 dia x .172 Wall A53	43	172	1.75
23	2	Corrugated Flex Joint 12 dia x 12 long A53	44	88	2.00
24	2	Flange 15 OD x 12 ID x .38	7	14	1.50
25	2	Hanger	43	86	1.00
26	30 ft	Tube 18.0 dia. x .219 Wall A155	42	1,260	.45
27	4	90° Weld Ell 18.0 dia. x .210 Wall A155	122	488	1.85
28	2	Corrugated Flex Joint	126	252	2.10
29	3	Flange 21 OD x 18 ID x .38	10	20	1.60
30	2	Hanger	45	90	1.10
31	65 ft	Tube 30 OD x .250 Wall A53	79	5,135	.38
32	65 ft	Tube 24 OD x .024 Wall Nickel	7	455	10.00
33	5	90° Weld Ell 30 OD x .250 Wall A53	335	1,675	1.75
34	5	90° Weld Ell 24 OD x .024 Wall Nickel	27	135	11.00

TABLE D-1: 25-MW_e RECEIVER LIST OF MATERIALS

ITEM	QUANTITY	DESCRIPTION	LB/ UNIT	TOTAL LB	$/LB
35	2	Corrugated Flex Joint A53	297	594	2.00
36	2	Corrugated Flex Joint Nickel	28	56	15.00
37	3	Flange 33 OD x .30 ID x .50	21	62	1.50
38	5	Hanger	53	265	1.00
39	9 ft	Tube 34 OD x .25 Wall A53	90	810	.38
40	9 ft	Tube 32 OD x .024 Wall Nickel	9.3	84	10.00
41	2	90° Weld Ell 34 OD x .25 Wall A53	498	996	1.75
42	2	90° Weld Ell 32 OD x .024 Wall Nickel	48.4	97	11.00
43	2	Corrugated Flex Joint A53	508	1,016	2.00
44	2	Corrugated Flex Joint Nickel	50	100	15.00
45	2	Flange 37 OD x 34 ID x .50	23.5	47	1.50
46	1	Hanger	58	58	.38
47	35	Tube 54 OD x .06 Wall A155	34.2	1,197	.45
48	3	90° Weld Ell A155	302	906	1.85
49	2	Corrugated Flex Joint A155	308	616	2.10
50	2	Flange 57 OD x 54 ID x .25	18.3	37	1.60
51	4	Hanger	71.0	284	1.00
52	10 ft	Tube 42 OD x .06 Wall A53	26.6	266	.38
53	2	90° Weld Ell 42 OD x .06 Wall A53	182.5	365	1.75
54	1	Corrugated Flex Joint	186	186	2.00
55	1	Flange	14	14	1.50
56	2	Hanger	63	126	1.00
57					
58	200	Flanged Lwr Tube - SiC - 3.00 OD X .250 t	27.4	5,477	30.0
59	400	Tube - SiC - 3.00 OD x .250 t	24.89	9,955	30.0
60	100	"U" Tube - SiC - 3.00 OD x .250 t 18" Bend R.	16.48	1,648	30.0
61	200	Weld Flange 7.0 OD X 4 in Pipe (Manifold)	6.51	1,302	1.50
62	200	4.5 Pipe Sched 40 x 10.0 in long (Manifold)	9.00	1,800	.38
63	74 ft	Pipe 14.0 OD x .188 t ASTM A139 (Manifold)	27.80	2,057	.45
64	70 ft	Pipe 24.0 OD x .219 t ASTM A53 (Manifold)	55.3	3,869	.38
65	100	Flared Tube 2.5 dia x .024 x 17.5 Nickel 200 (Manifold)	.90	90	10.00
66	70 ft	Tube - 18.0 dia x .024 Nickel 200 (Manifold)	5.21	365	10.00

TABLE D-1: 25-MW_e RECEIVER LIST OF MATERIALS

ITEM	QUANTITY	DESCRIPTION		LB/ UNIT	TOTAL LB	$/LB
67	1	TEE 18.0 dia x 24.0 dia x .024 Nickel 200	(Manifold)	26	26	15.00
68	1	TEE 24.0 dia x 30.0 dia x .250 A53	(Manifold)	347	347	.38
69	100	Retaining Disc 6" OD x 3.0" ID X .024 Nickel 200	(Manifold)	.30	30	10.00
70	1	TEE 14.0 dia x 18.0 dia x .219 A53	(Manfiold)	124	124	.38
71	25 ft^2	End Blockers and Tie Plates 1/4" PL	(Manifold)	10	250	.38
72	as required	Support Steel	(Manfiold)		1,000	.38
73	9164 ft^2	3/16 t HRS Sht ASTM A635	(Receiver)	7.65	70,105	.38
74	3686 ft^2	3/16 t HRS Sht ASTM A635	(Turbine Room)	7.65	28,198	.38
75	1904 f^2	1/4 t Diamond Deck PL	(Turbine Room)	10.2	19,421	.38
76	442 ft	W 8 x 24 ASTM A36	(Receiver)	24	10,608	.38
77	432 ft	W 8 x 24 ASTM A36	(Turbine Room)	24	10,368	.38
78	1600 ft	W 6 x 15 ASTM A36	(Receiver)	15	24,000	.38
79	480 ft	W 6 x 15 ASTM A36	(Turbine Room)	15	7,200	.38
80	234 ft	W 30 x 124 ASTM A36	(Turbine Room)	124	29,016	.38
81	1428 ft	L 2 x 2 x 3/16 ASTM A36	(Receiver)	2.44	3,484	.38
82	384 ft	L 2 x 2 x 3/16 ASTM A36	(Turbine Room)	2.44	937	.38
83	2040 ft^2	3" Thick Fiberglass Mat Insulation	(Piping)			.81/ft^2
84	2040 ft^2	3" Thick Kawool Mat Insulation	(Piping)			5.91/ft^2
85	15348 ft	4" Wide 6OZ Fiberglass Tape	(Piping)			.085/ft
86	518 ft^2	3" Thick Kaowool Mat Insulation	(Manifold)			5.91/ft^2

TABLE D-2: 25-MW_e Receiver Cavity Insulation Costs

Materials Costs

- Directly Irradiated Area

Product*	$/ft^2 (1980 $)
3000 ST Board (1.5" Thick)	23.04
Saffil LD Mat (0.25" Thick)	10.63
2600 Board (1.5" Thick)	10.66
Kaowool HP Blanket (5" Thick)	11.26
Anchor	4.50
Cement	.75
Total =	60.84 x 1.19
=	72.40 (1983 $)

- Indirectly Irradiated Area

Kaowool (6" Thick)	13.51
Anchor	4.50
Total =	18.51 x 1.19
=	22.03 (1983 $)

Labor Costs

- Directly Irradiated Area
  2.9 hr/ft^2 x 21.86 $/hr = 63.394 $/ft^2

- Indirectly Irradiated Area
  1.0 hr/ft^2 x 21.86 $/hr = 21.86 $/ft^2

Total Costs

	Quantity (ft^2)	Unit Cost ($/ft^2)	Cost ($)	Total ($)
Materials -				
. Directly Irradiated	2,847	72.40	206,123	
. Indirectly Irradiated	6,317	22.03	139,163	
				345,286
Labor -				
. Directly Irradiated	2,847	63.39	180,483	
. Indirectly Irradiated	6,317	21.86	138.089	
				318,572
			Total	$663,858

* Babcock and Wilcox insulation products.

TABLE D-3: 25-MW_e Receiver Manifold Costs

Cost Category	Item	Quantity	Unit Cost	Cost ($)	Total ($)
Materials	A53 Steel Tube	5,669 lb	.38 $/lb	2,154	
	A139 Steel Tube	2,057 lb	.45 $/lb	926	
	A36 Tie & Support	1,250 lb	.38 $/lb	475	
	A53 Flanges	1,302 lb	1.50 $/lb	1,953	
	A53 Tees	471 lb	1.75 $/lb	824	
	Nickel 200 Liner	485 lb	10.00 $/lb	4,850	
	Nickel 200 Tees	26 lb	15.00 $/lb	390	
	Kaowool Blanket	518 ft^2	5.91 $/ft^2$	3,061	
	Fiberglass Blanket	427 ft^2	.81 $/ft^2$	346	
	Fiberglass Tape	2,562 ft	.085 $/ft	218	
					15,197
Labor	Fabrication	638 hr	27 $/hr	17,226	
	Installation	80 hr	27 $/hr	2,160	
	Insulation	104 hr	25 $/hr	2,600	
					21,986
				Total	37,183

Table D-4: 25-MW_e Receiver Cost Summary

Component	Cost Category	Quantity	Unit Cost	Cost ($)
Steelwork	Material	54 tons	750 $/ton	40,500
	Labor	432 hrs	24.22 $/hr	10,463
Insulation	Material (outside)	1680 ft^2	23.04 $/$ft^2$	38,707
	Material (inside)	--	--	345,286
	Labor (outside)	336 hrs	21.86 $/hr	7,345
	Labor (inside)	--	--	318,572
Heat Exchangers	Material	17,080 lb	30 $/lb	512,400
	Labor	400 hrs	27 $/hr	10,800
Manifolds	Material	--	--	15,197
	Labor	--	--	21,986
			Total	$1,321,256

Table D-5: 25-MW_e Tower Cost Summary

Component	Cost Category	Quantity	Unit Cost	Cost ($)
Earthwork	Material & Labor	2185 cu yd	2.52 $/cu yd	5,506
Concrete Base	Material	1017 cu yd	94.50 $/cu yd	96,106
	Labor	5085 hrs	20.54 $/hr	104,446
Steelwork				
(Tower)	Material	228 tons	750 $/ton	171,000
	Labor	1824 hrs	24.22 $/hr	44,177
(Turbine Room)	Material	62 tons	750 $/ton	46,500
	Labor	496 hrs	24.22 $/hr	12,013
Large Crane Rental				85,000
				$564,748

Table D-6: 25-MW_e Piping Cost Summary

Cost Category	Component	Item	Quantity	Unit Cost	Cost ($)	Total ($)
Materials	Steel Pipe	A53 Tube	8085 lb	.38 $/lb	3,072	
		A155 Tube	2457 lb	.45 $/lb	1,106	
		A53 90° ell	3824 lb	1.75 $/lb	6,692	
		A155 90° ell	1394 lb	1.85 $/lb	2,579	
		A53 Flanges	194 lb	1.50 $/lb	291	
		A155 Flanges	57 lb	1.60 $/lb	92	13,832
	Anchors, Hangers and Joints	A53 Joint	2214 lb	2.00 $/lb	4,428	
		A155 Joint	868 lb	2.10 $/lb	1,823	
		Hangers	2294 lb	1.00 $/lb	2,294	8,545
	Nickel Liner	Tube	539 lb	10.00/lb	5,390	
		90° ell	232 lb	11.00/lb	2,552	
		Joint	156 lb	15.00/lb	2,340	10,282
	Insulation	Kaowool Mat	2040 ft^2	5.91 $/$ft^2$	12,056	
		Fiberglass Mat	2040 ft^2	.81 $/$ft^2$	1,652	
		Fiberglass Tape	15348 ft	.085 $/ft	1,304	
		Resin	5 gal	32 $/gal	160	15,172
Labor	Fabrication		575 hr	27 $/hr	15,525	
	Installation		120 hr	27 $/hr	3,240	
	Insulation		630 hr	25 $/hr	15,750	34,515
				Total		$82,346

TABLE D-7: 2-MW_e RECEIVER LIST OF MATERIALS

ITEM	QUANTITY	DESCRIPTION	LB/ UNIT	TOTAL LB	$/LB
1	96 ft	Square Tube 8 X 8 X .37	37.69	3618	.38
2	248 ft	Square Tube 4 x 4 x .1875	9.42	2336	.38
3	140 ft	L 6 x 6 x 5/16	12.4	1736	.38
4	386 ft	W 6 x 15	15.0	5790	.38
5	240 ft	L 2 x 2 x 3/16	2.44	586	.38
6	104 ft	W 29 x 94	94	9776	.38
7	140 ft	W 8 x 24	24	3360	.38
8	1696 ft^2	1/8 thick hrs sht ASTM A635	5.04	8548	.38
9	640	1/4 thick Diamond Deck PL	10.2	6528	.38
10	12 ft	10" dia x .06 Wall Tube ASTM A53	6.3	75.6	.38
11	2	90° Ell 10" dia x .06 Wall	10.3	20.6	1.75
12	1	Flange 14 O.D. x 10 I.D. x .19 t	4.0	4.0	1.50
13	12 ft	3" Pipe Sched 40 ASTM A53	7.4	88.8	.38
14	2	90° Ell 3" dia x .216 t	7.3	14.6	1.75
15	2	Flange 6 OD x 3 I.D. x .31	1.8	3.6	1.50
16	30 ft	4" Pipe Sched 40 ASTM A53	10.79	323.7	.38
17	4	90° Ell 4" dia x .237 t	14.1	56.4	1.75
18	2	Flange 7" OD x 4" I.D. x .38	2.8	5.6	1.50
19	20 ft	12" Pipe Sched 40 ASTM A53	43.8	876.0	.38
20	2	90° Ell 12" dia .330 Wall	114.	228.	1.75
21	2	Flange 15" OD x 12" ID x .45	8.39	16.8	1.50
22	10 ft	16.5 dia x .06 Wall Tube ASTM A53	10.47	104.5	.38
23	2	90° Ell 16.5 dia x .06 Wall	56	112	1.75
24	2	Flange 19.5 OD x 16.5 ID x .19	4.5	9	1.50
25	as required	Pipe Hangars 20% Piping Weight		250	.38
26	20	6" OD Tube X .02 Wall Nickel 200	1.4	28	10.00
27	2	90° Ell 6" dia x .02 Wall Nickel 200	2.8	5.6	11.00
28	40 ft^2	3" Thick Kaowool Insulation			5.91/ft^2
29	36 ft^2	3" Thick Fiberglass Insulation			.81/ft^2
30	456	4" Fiberglass Tape			.085/ft^2
31	1	6 Meter ID Sphere 1.625 Wall ASTM A515 6R 70	79,721	79,721	.45
32	1217 ft^2	5" Thick Kaowool Insulation			9.85/ft^2

Table D-8: 2-MW_e Receiver Cost Summary

Component	Cost Category	Quantity	Unit Cost	Cost ($)
Steelwork	Material	40 tons	1052$/ton	$ 42,080
	Labor	320 hrs	24.22/hr	7,750
Insulation	Material (outside)	384 ft^2	23.04$/$ft^2$	8,847
	Material (inside)	1217 ft^2	9.85$/$ft^2$	11,987
	Labor (outside)	80 hr	21.86$/hr	1,749
	Labor (inside)	309 hr	21.86$/hr	6,755
Window	Materials & Labor			120,000
Carbon Particle Generator	Materials & Labor			22,168
			Total =	$221,336

Table D-9: 25-MW_e Tower Cost Summary

Component	Cost Category	Quantity	Unit Cost	Cost ($)
Earthwork	Materials & Labor	867 cu yd	2.52$/cu yd	$ 2,185
Concrete Base	Material	62 cu yd	94.50$/cu yd	5,859
	Labor	308 hrs	20.54$/hr	6,326
Steelwork				
(Tower)	Material	20 ton	750$/ton	15,000
	Labor	161 hrs	24.22$/hr	3,899
(Turbine Room)	Material	3.65 ton	750$/ton	2,738
	Labor	29 hr	24.22$/hr	702
Large Crane Rental				38,815
			Total =	$ 75,524

TABLE D-10: 2-MW_e Piping Cost Summary

Cost Category	Item	Quantity	Unit Cost	Cost ($)	Total ($)
Materials	Steel Pipe				
	A53 Tube	1469 lb	0.38$/lb	558	
	A53 Ell	1823 lb	1.75$/lb	3190	
	A53 Flange	39 lb	1.50$/lb	59	$ 3,807
	Anchors, Hangers, and Joints				
	A53 Joint	1200 lb	2.00$/lb	2400	
	Hangers	250 lb	0.38$/lb	95	2,495
	Nickel Liner				
	Tube	28 lb	10.00$/lb	280	
	Ell	5.6 lb	11$/lb	62	
	Joint	5.0 lb	15$/lb	75	417
	Insulation				
	Kaowool Mat	40 ft^2	5.91$/$ft^2$	236	
	Fiberglass Mat	36 ft^2	.81$/$ft^2$	29	
	Fiberglass Tape	456 ft	.085$/ft	39	304
Labor	Fabrication	80 hr	27$/hr	2,160	
	Installation	40 hr	27$/hr	1,080	
	Insulation	40 hr	27$/hr	1,080	4,320
				Total =	$11,343

UNLIMITED RELEASE
INITIAL DISTRIBUTION

U.S Department of Energy (6)
Forrestal Building
1000 Independence Avenue, S.W.
Washington, D.C. 20585
Attn: H. Coleman
C. Carwile
C. Mangold
F. Morse
M. Scheve
F. Wilkins

U.S. Department of Energy (2)
1333 Broadway
Oakland, CA 94612
Attn: R. W. Hughey
M. Lopez

U. S. Department of Energy
Albuquerque Operations Office
P.O. Box 5800
Albuquerque, NM 87115
Attn: J. Weisiger

Arco Power Systems
7061 S. University, Suite 300
Littletonn, CO 80122
Attn: F. A. Blake

Arco Power Systems
302 Nichols Drive
Hutchins, TX 75141
Attn: R. L. Henry

Arizona Public Service Company
P.O. Box 21666
Phoenix, AZ 85036
Attn: E. Weber

Arizona Solar Energy Commission
1700 W. Washington, Suite 502
Phoenix, AZ 85007
Attn: R. L. Sears

Babcock and Wilcox (3)
91 Stirling Avenue
Barberton, OH 44203
Attn: G. Grant
M. Seale
D. Smith

Battelle Pacific Northwest Laboratories (3)
P.O. Box 999
Richland, WA 99352
Attn: K. Drumheller
T. A. Williams
J. A. Dirks

Bechtel Group, Inc.
P.O. Box 3965
San Francisco, CA 94119
Attn: Dr. S. Fleming

Black and Veatch Consulting Engineers (2)
P.O. Box 8405
Kansas City, MO 64114
Attn: J. C. Grosskreutz
S. L. Levy

Boeing Aerospace Company (6)
Energy Systems
P.O. Box 3999, MS87-63
Seattle, WA 98124
Attn: W. D. Beverly

Bureau of Reclamation
Code 1500E
Denver Federal Center
P.O. Box 25007
Denver, CO 80225
Attn: S. Hightower

California Energy Commission
1516 North St. M/S 40
Sacramento, CA 95814
Attn: A. Jenkins

Combustion Engineering, Inc.
1000 Prospect Hill Road
Windsor, CT 06095
Attn: C. R. Buzzuto

Department of Natural Resources
Energy Alternatives Administration
1302 State Office Building
Baltimore, MD 21201
Attn: R. S. Nietubicz

Department of Planning and Economic Development
P.O. Box 2359
Honolulu, HI 96804
Attn: E. Grabbe

Edison Electric Institute
1111 - 19th Street, N.W.
Washington, D.C. 20036
Attn: G. H. Lovin

El Paso Electric Company (2)
P.O. Box 982
El Paso, TX 79946
Attn. J. E. Brown
E. Wall

Electric Power Research Institute (3)
P.O. Box 10412
Palo Alto, CA 94303
Attn: J. Bigger
J. Cummings
E. DeMeo

Fluor Corporation
3333 Michelson Drive
Irvine, CA 92730
Attn: J. W. Mohlman

Foster Wheeler Development Corporation (2)
12 Peach Tree Hill Road
Livingston, NJ 07039
Attn: S. F. Wu
R. J. Zoschak

Garrett-AiResearch
402 S. 36th Street
Phoenix, AZ 85253
Attn: L. Six

G. A. Technologies
2021 K. Streen, N.W.
Washington, D.C. 20006
Attn: L. Green, Jr.

Georgia Institute of Technology (4)
Atlanta, GA 30332
Attn: C. Thomas Brown
D. H. Neale
N. Poulos
R. Williams

Gibbs and Hill, Inc. (2)
393 Seventh Avenue
New York, NY 10001
Attn: R. Prieto
G. Stern

Honeywell Energy Research Center
2600 Ridgway Parkway
Minneapolis, MN 55413

Institute of Gas Technology
IIT Center
3424 South State Street
Chicago, IL 60616
Attn: F. L. Kester

Jet Propulsion Laboratory
4800 Oak Grove Drive
Pasadena, CA 91103
Attn: M. Alper

Lawrence Berkeley National Laboratory (5)
University of California
Berkeley, CA 94720
Attn: R. Bailey
D. B. Evans
A. J. Hunt
M. Wahlig
R. Wolgast

Los Angeles Department of Water and Power
111 North Hope St.
Los Angeles, CA 90051
Attn: D. Chu

Martin Marietta Aerospace
P.O. Box 179, MS L0450
Denver, CO 80201
Attn: H. C. Wroton

McDonnell Douglas Astronatics Company (3)
5301 Bolsa Avenue
Huntington Beach, CA 92647
Attn: R. L. Gervais
J. Reatz
R. Riedesel

Modern Alloys, Inc. (4)
11172 Western Avenue
Stanton, CA 92669
Attn: J. E. Dressel
R. B. Grey
C. R. Mitchell
A. M. Peterson

National Bureau of Standards
Thermal Engineering Section
Washington, D.C. 20234
Attn: M. McCabe

New Mexico University
P.O. Box 3450
Las Cruces, NM 88003

Ohio Department of Energy
30 East Broad
Columbus, OH 43215
Attn: A. Rahim

Olin Chemical Co.
Metals Research Laboratory
91 Shelton Avenue
New Haven, CT 06511
Attn: E. F. Smith

Olin Chemical Company (2)
120 Long Ridge Road
Stamford, CT 06904
Attn: F. N. Christopher
L. C. Fioruccio

Pacific Gas and Electric Company
77 Beale Street
San Francisco, CA 94105
Attn: R. E. Price

Pacific Gas and Electric Company (2)
3400 Crow Canyon Road
San Ramon, CA 94526
Attn: C. Weinberg
G. Braun

The Ralph M. Parsons Company
100 West St.
Pasadena, CA 91124
Attn: N. W. Snyder

PFR Energy Systems, Inc.
P. O. Box 91890
Los Angeles, CA 90045
Attn: T. Rosenman

PRC Energy Analysis Company
7600 Old Springhouse Road
McLean, VA 22102
Attn: E. F. Shaver

Polydyne, Inc. (2)
1900 S. Norfolk St., Suite 209
San Mateo, CA 94403
Attn: P. B. Bos
J. M. Weingart

Rockwell International
Energy Systems Group
8900 De Soto Avenue
Canoga Park, CA 91304
Attn: T. Springer

Rockwell International
Rocketdyne Division
6633 Canoga Avenue
Canoga Park, CA 91304
Attn: J. M. Friefeld

San Diego Gas and Electric Company
Mechanical Engineering
P.O. Box 1831
San Diego, CA 92112
Attn: R. E. Potthoff

Solar Energy Industries Association
1140 19th St., N.W.
Suite 600
Washington, D.C. 20036
Attn: C. LaPorta

Solar Energy Research Institute (4)
1617 Cole Boulevard
Golden, CO 80401
Attn: B. Gupta
F. Krawiec
L. Murphy
J. Thorton

Southern California Edison
P.O. Box 325
Daggett, CA 92327
Attn: C. Lopez

Southern California Edison (2)
P.O. Box 800
Rosemead, CA 92807
Attn: J. N. Reeves
P. Skvarna

Standard Oil of California (2)
555 Market Street, Room 1104
San Francisco, CA 94119
Attn: S. G. Gibb
E. D. Lewis

Stanford University (3)
Department of Mechanical Engineering
Stanford, CA 94305
Attn: J. A. Erickson
J. P. Johnston
R. J. Moffat

Stearns Catalytic Corp.
P.O. Box 5888
Denver, CO 80217
Attn: W. R. Lang

United States Congress
Office of Technical Assessment
Washington, D.C. 20510
Attn: J. Furber

University of Houston (2)
Solar Energy Laboratory
3801 Cullen Blvd.
Houston, TX 77004
Attn: A. F. Hildebrandt
L. Vant-Hull

University of Illinois/EPRI
1206 W. Green Street
Urbana, IL 61820
Attn: A. M. Clausing

E. H. Beckner, 6000; Attn: V. Dugan, 6200
D. G. Schueler, 6220
J. V. Otts, 6222
E. C. Boes, 6226
J. A. Leonard, 6227

B. Granoff, 6254; Attn: J. D. Fish, 6254
D. C. Hawn, 6254
R. S. Claassen, 8000; Attn: D. M. Olson, 8100
A. N. Blackwell, 8200
D. L. Hartley, 8300
C. S. Selvage, 8000A
C. Hartwig, 8244
M. E. John, 8245
R. C. Wayne, 8400; Attn: L. D. Bertholf, 8430
H. Hanser, 8440
R. L. Rinne, 8470
A. C. Skinrood, 8471 (25)
J. C. Swearengen, 8473
R. L. Rinne, 8475 (Actg.)

Publications Division 8265, for TIC (30)
Publications Division 8265/Technical Library Processes Division, 3141
Technical Library Processes Division, 3141 (3)
M. A. Pound, 8024, for Central Technical Files (3)

Org.	Bldg.	Name	Rec'd by	Org.	Bldg.	Name	Rec'd by

Sandia National Laboratories